
# HYBRID MATERIALS: DISCOVERING PROPERTIES AND MECHANISMS

**Dana Georgiana Crivoi**

UNIVERSITAT ROVIRA I VIRGILI
HYBRID MATERIALS: DISCOVERING PROPERTIES AND MECHANISMS
Dana Georgiana Crivoi

HYBRID MATERIALS: DISCOVERING PROPERTIES AND MECHANISMS

Dana-Georgiana Crivoi

Dana-Georgiana Crivoi

Doctoral Thesis 2016

# Hybrid Materials: Discovering Properties And Mechanisms

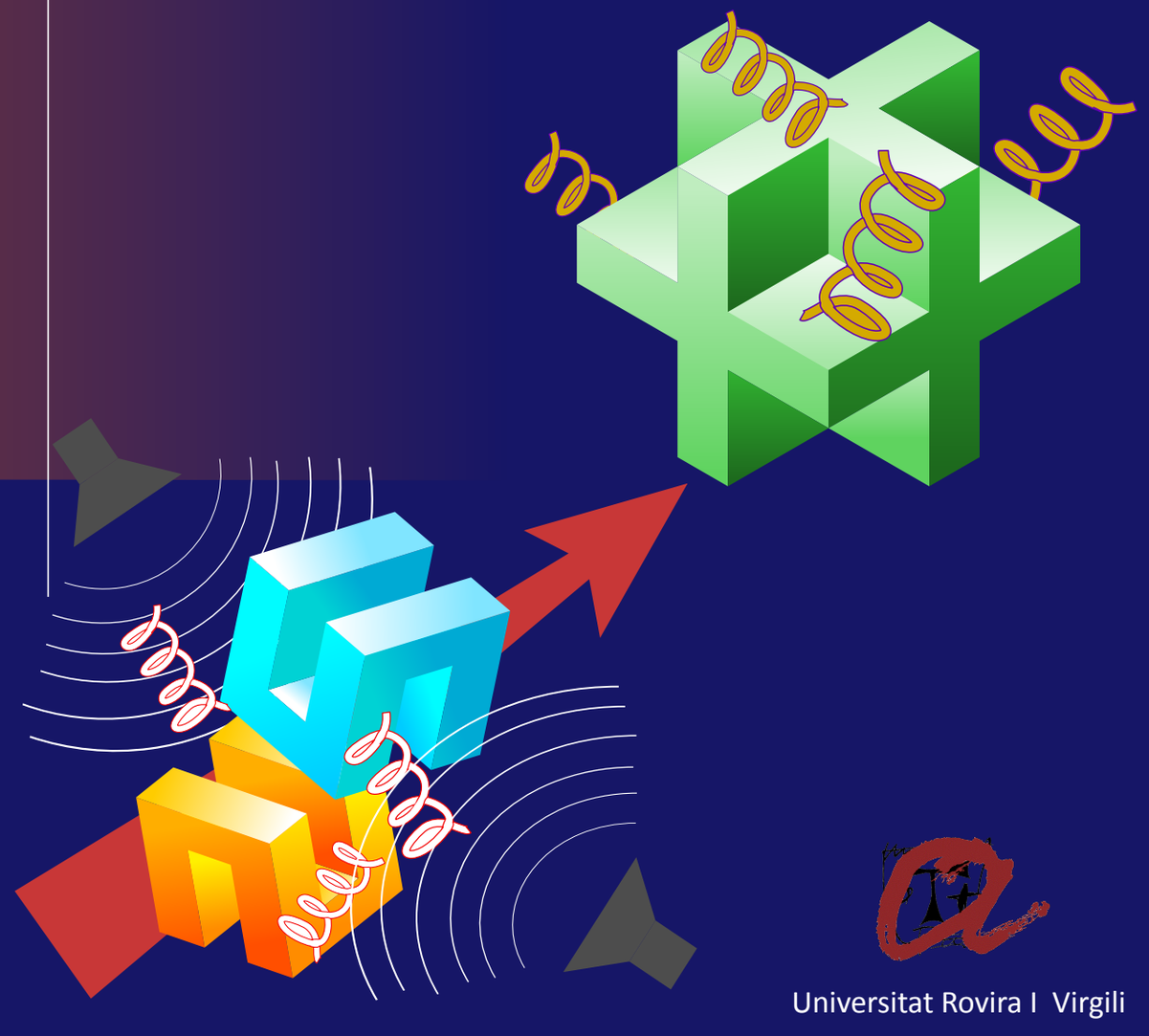

Universitat Rovira I Virgili

Dana-Georgiana Crivoi

UNIVERSITAT ROVIRA I VIRGILI
HYBRID MATERIALS: DISCOVERING PROPERTIES AND MECHANISMS
Dana Georgiana Crivoi

UNIVERSITAT ROVIRA I VIRGILI
HYBRID MATERIALS: DISCOVERING PROPERTIES AND MECHANISMS
Dana Georgiana Crivoi

DANA-GEORGIANA CRIVOI

# Hybrid Materials: Discovering Properties and Mechanisms

Doctoral Thesis

Supervised by:

**Dr. Francisco Medina Cabello**

**Dr. Anna Maria Segarra Gonzalez**

Departament d'Enginyería Química

UNIVERSITAT ROVIRA i VIRGILI

**Tarragona**

**2016**

UNIVERSITAT ROVIRA I VIRGILI
HYBRID MATERIALS: DISCOVERING PROPERTIES AND MECHANISMS
Dana Georgiana Crivoi

UNIVERSITAT ROVIRA I VIRGILI
ESCOLA TÈCNICA SUPERIOR D'ENGINYERIA QUÍMICA
DEPARTAMENT D'ENGINYERIA QUÍMICA

Av. dels Països Catàlans, 26
43007, Tarragona (Spain)
Tel. +34 977 55 96 03 / 04
Fax +34 977 55 96 21
e-mail: secdeq@etseq.urv.es
http://www.etseq.urv.es/DEQ/

Prof. Dr. Francisco Medina Cabello and Dr. Anna Maria Segarra Gonzalez,

CERTIFY:

That the present study, entitled "Hybrid Materials: Discovering Properties and Mechanisms", presented by Dana-Georgiana Crivoi for the award of the degree of Doctor, has been carried out under our supervision at the Chemical Engineering Department of this university, and that it fulfils all the requirements to obtain the degree of Doctor in Chemical, Environmental, and Process Engineering.

Tarragona, 8th of March 2016

Doctoral Thesis Supervisors

Prof. Dr. Francisco Medina Cabello

Dr. Anna Maria Segarra Gonzalez

UNIVERSITAT ROVIRA I VIRGILI
HYBRID MATERIALS: DISCOVERING PROPERTIES AND MECHANISMS
Dana Georgiana Crivoi

"Ask and it will be given to you;
Seek and you will find;
Knock and the door will be opened to you.
For everyone who asks receives;
The one who seeks finds;
And to the one who knocks, the door will be opened."

Matthew 7:7-8

UNIVERSITAT ROVIRA I VIRGILI
HYBRID MATERIALS: DISCOVERING PROPERTIES AND MECHANISMS
Dana Georgiana Crivoi

# ACKNOWLEDGEMENTS

Finally, this is it, the result of one of the most challenging, interesting and life-changing experience of my life till now. I have always believed that, although we are guided by a superior force (God, Buddha, Allah, whatever you believe in), we have the ability to choose our paths in life. Each person with whom you interact and each event in your life happen for a reason and not by chance. No matter if this sounds like a cliché, looking back over the last 4 years I can definitely attest this! During this period, I wondered many times how my life would have been if I had chosen another path. And every time I answered myself "probably easier, but I would have not been the person that I am now", as all the struggle, all the sorrow, all the bad and happy events, all the wonderful people I met along my way had an impact over me. As Newton's third law states "For every action there is an equal and opposite re-action", the whole thing made me stronger, tougher and, why not, brighter.

Everything could not have happened without the help of my supervisor, Dr. Francisco Medina – the head leader of Heterogeneous Catalysis Group (CatHeter). I am very grateful for giving me the freedom of exploration and I am hoping that the final result not only met, but exceeded the targeted requirement.

A PhD thesis could not have been done without a financial aid; therefore, I would like to thank "Rovira i Virgili" University (URV) for my first year' scholarship and Spanish Ministry of Education, Culture and Sports (Ministerio de Educación, Cultura y Deporte) for my last 3 years' scholarship.

My next thoughts go to the technical support from Servei de Recursos Cienifics i Téchincs, mainly Irene Maijó Ferré, Ramon Guerrero Grueso, Rita Marimon Picó and Francesc Gispert i Guirado.

I would never forget the help (both personal and professional) given by Sandra Ramos and Vanessa Torné. The time spent listening to my problems, your kind words, sharing your experience with me, all together helped me fight on towards my goal.

The work in the lab could not have been possible without a good technician; thus, I would like to deeply thank Susana Dominguez (aka "nena") for all the help given: passing "pedidos" faster than normal, struggling to find all the things that I needed, and, the most important of all, the nice times we spent together.

Special thanks go to Anton Dafinov for his assistance and for many discussions about my thesis, science in general and unrelated topics. It was a pleasure to collaborate with you!

Another person with whom was a pleasure to collaborate with, was Mayra García. Thus, I would like to present my sincere gratitude to her and her husband, Enrique Nieto (aka "Kike")

not only for the scientific discussions, but also for the nice time spent together, for showing me interesting parts of Spain and for trusting me in taking care of their beautiful and fluffy cats (Gibbs, King and Lola).

Next thoughts go to all my former labmates (Oscar Osegueda, Alexander Miranda, Luis Iglesia and so many others) and current ones (Verónica Pinos, Shailesh Sable, Pallavi Ghute, Llorenç Gavilà, Ana Antolin and many others) and all those who intersected with CatHeter (e.g. Mariá Alba). Of course I cannot forget my newest PhD colleague Abel Toscano – good luck in your new position!

My sincere thanks go to Dr. Mark Rutland and Dr. Deborah Wakeham for introducing me in the world of QCM-D, for accepting me in their group and for all the nice moments spent together.

My gratitude is also extended to Dr. Atsushi Urakawa who, although I was not one of his PhD students, offered me support and guidance.

I cannot forget all my friends from ICIQ (Institut Català d'Investogació Quómica) with whom I spent (and I still do) so many great moments, parties, shared our fears and disappointments, but also shared our knowledge: Sérgio Lima, Luis Bobadilla, Sergio Roso (aka "Pequeño"), Atul Bansode, Aurora Càceres, Dina Fakhrnasova, Muralidhar Chourashiya, Yi Zhang, Andrea Alvarez, Rohit Gaikwad, Jordi Ampurdanés, Marta Borges, Antonio Bazzo (aka "Xut") and all their new colleagues. I could have not forgotten Tsuyoshi Hyakutake (aka "Dr. Tsu") with his beautiful wife, Yoko Hyakutake and adorable daughter Toyo; we have spent so many happy afternoons / evenings together!

Le port o deosebita stimă, reunoștinţă și respect domnilor profesori Anca și George Marton și domnului Constantin Drăghici. Cunoștinţele acumulate sub supravegherea dănșilor, sfaturile primite și nenumăratele disuţii atăt pe teme de ştiinţă cât și de viaţă au fost pietrele de temelie ale acestei teze.

Nu aș putea să nu le mulţumesc Simonei și lui Dan Libotean, alaturi de copiii lor superbi Ana și bebelușul Victor (care nu mai este de mult atât de micuţ). Ei mi-au fost alături în toate momentele grele, m-au încurajat și mi-au împărtășit din experienţa lor. Cu ajutorul lor am descoperit zone minunate în Spania, am mers la meciuri și, desigur, ne-am distrat împreună la numeroasele concerte rock din Barcelona!

Nu aș fi devenit omul care sunt astăzi fără suportul necontenit al părinţilor mei, Doina și Dan Crivoi. Vă mulţumesc pentru tot!

Dragoș, îţi mulţumesc că ai fost alături de mine, la bine și la greu, pe parcursul acestor ani. Nu cred că aș fi putut rezista fără suportul și dragostea ta nemărginită. Îţi mulţumesc! ☺

UNIVERSITAT ROVIRA I VIRGILI
HYBRID MATERIALS: DISCOVERING PROPERTIES AND MECHANISMS
Dana Georgiana Crivoi

UNIVERSITAT ROVIRA I VIRGILI
HYBRID MATERIALS: DISCOVERING PROPERTIES AND MECHANISMS
Dana Georgiana Crivoi

# TABLE OF CONTENTS

# 1 Introduction

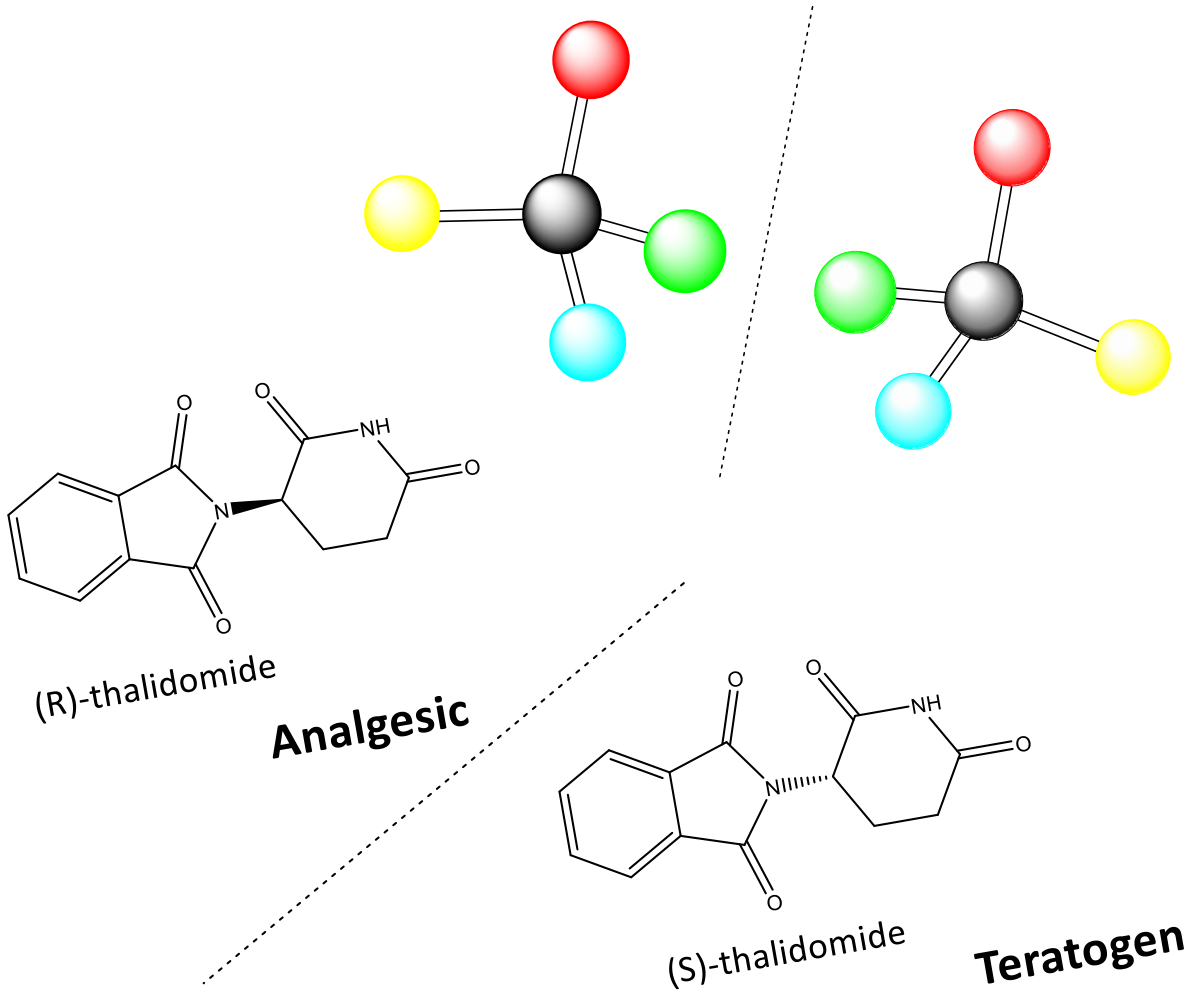

# 1.1 The Concept of Chirality

## 1.1.1 A Brief Historical Overview

Everything around us is chiral, thus, one of the most important properties which underlies the drug disposition and action is given by the chirality of the active substance. Consequently, stereochemistry represents an active, changing, and challenging field which combines different disciplines of natural sciences that lead to the most spectacular findings.

Stereochemistry was first mentioned in 1801 when the French crystallographer R.H. Haüy detected the phenomenon of hemidrism of a quartz crystal [1]. He observed that the hexagonal symmetry of this crystal can be reduced to very small hemihedral facet faces which, present at alternate corners of the crystal, eliminate the apparent symmetry of quartz. Moreover, this new finding indicated the presence of two non-superimposable mirror image forms, chiral and enantiomorphic (opposite forms).

Later, the mathematician-physician F. Arago discovered optical activity [2] which led J. B. Biot in 1812 [3] to observe that two pieces of natural quartz can rotate the plane of the polarized light in different directions. The connection between the optical rotation and the two hemihedral forms of quartz was identified in 1822 by J. W. F. Herschel [4]. These findings made Biot to extend his search to solutions like turpentine, sucrose, camphor, and tartaric acid, observing in all the cases the same phenomenon of rotation of the plane of polarized light.

In fact, the molecular chirality was revealed in 1848 by the French chemist and microbiologist Louis Pasteur, a student of J.B. Biot [5]. In one of his experiments, Pasteur was growing crystals of sodium ammonium salts of natural occurring tartaric acid when he noticed that two different mirror crystals were formed (Figure 1.1). He separated the crystals by hand, dissolved them in water and discovered that the solutions rotated the plane of polarized light in equal and opposite directions, leading to the conclusion that the molecules making up the salt were of two types: one “right-handed” and the other “left-handed”.

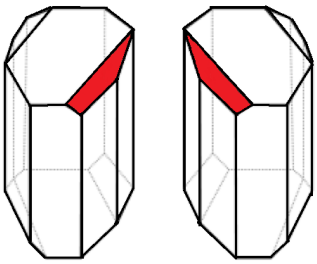

**Figure 1.1** Crystals of sodium ammonium tartrate. Left (-)-enantiomer and right (+)-enantiomer, hemihedral faces marked with red.

Even though Pasteur recognized the importance of the three dimensional structure of a molecule in establishing its symmetry, he did not have the necessary tools to determine the structure of tartaric acid. The basic chemical structure of this acid was elaborated in 1867 by W. H. Perkin who discovered that tartaric acid was composed of a four-carbon chain containing two hydroxyl groups and two carboxylic groups [6]. Seven years later, Le Bel [7] and J. H. van't Hoff [8] independently observed that the four bonds of a carbon atom are arranged in such a manner that a tetrahedral geometry is obtained. The initial structure of tartaric acid was confirmed for the first time by X-ray crystallography in 1923 by Astbury [9], but the absolute configuration of the chiral centres was finally resolved in 1951 by von Bommel *et al.* [10].

A substance containing a carbon atom bearing four different substituents can be arranged in two ways (Figure 1.2), resulting in the formation of two non-superimposable mirror image structures. This carbon atom is known as chiral centre (or asymmetric centre) and the resulting structures are known as enantiomers. For n chiral centres there are $2^n$ possible optic isomers known as diastereoisomers.

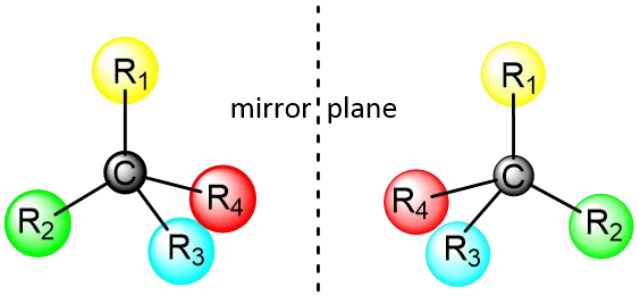


**Figure 1.2** An $sp^3$ C having four different substituents forming two asymmetric mirror image molecules

## 1.1.2 Importance of Chirality

The origin of life on Earth has been linked to the origin of enantiomerically pure compounds, even though there is a lot of debate on this subject [11]. From the discovery of chirality, scientists have been fascinating with trying to understand why almost all the important molecules in the cells are chiral, why L-amino acids are preferred to D-amino acids, etc.

It is generally accepted that two enantiomers have the same chemical and physical properties (except the optical activity) in an achiral environment. But, when the environment is changed and another chiral molecule (e.g. human receptors, enzymes) is present, their chemical activity will be strongly related to their absolute configuration (Table 1.1).

## 1 Introduction

**Table 1.1** Enantiomers of selected chiral molecules which have different properties in a chiral environment like human body

| Entry | (R) - Enantiomer | (S)-Enantiomer | Chemical name | References |
|---|---|---|---|---|
| 1 | 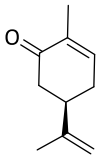 | 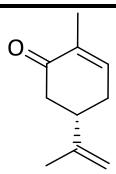 | Carvone | [12-14] |
| 2 | 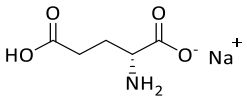 | 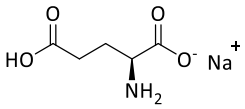 | Monosodium glutamate | [15] |
| 3 | 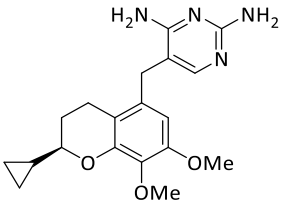 | 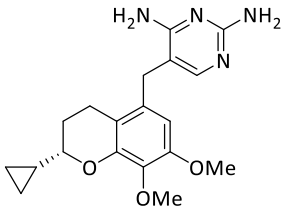 | Iclaprim | [16] |
| 4 | 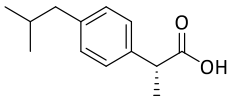 | 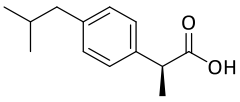 | Ibuprofen | [17] |
| 5 | 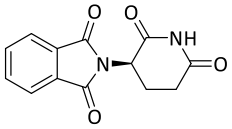 | 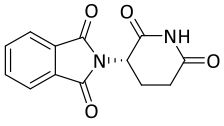 | Thalidomide | [17] |

One of the first examples of such compounds are (R)- carvone and (S)-carvone (entry 1, Table 1.1) that have identical physical properties, but are perceived totally different by human beings. The R-enantiomer smells like the spearmint leaves while the S-isomer has a caraway smell [12-14]. As in the case of smell, taste can be sensitive to chirality. For example, the R-isomer of monosodium glutamate is tasteless while the S-one has an umami taste (entry 2, Table 1.1). The umami taste is relatively new to the Western world, but was known in Japan from the early 1900s and it is used to describe an “aged cheese” taste typical to the S-monosodium glutamate, discovered by Kikunae Ikeda [15].

Chirality does not only have an effect on senses, but also on biological processes where the presence of one of the enantiomers can have similar effects as the other one, or can make the difference between life and death. Iclaprim (entry 3, Table 1.1), a substance used in the treatment of bacterial infections, belongs to the first category where both R and S isomers have the similar activity against the dihydrofolate reductase enzyme [16]. In the same way, ibuprofen (entry 4, Table 1.1) is generally found as a racemic mixture, even though the S-isomer is more active. The presence of 2-arylpropionyl-CoA epimerase in the human body interconverts the less active enantiomer into the desired one, thus, no side effects were observed when the R-enantiomer was ingested [17]. Unfortunately, this was not the case for thalidomide (entry 5,

Table 1.1) which caused one of the biggest tragedy of the 20th century [17]. In the 50s-60s the drug was sold as a racemic mixture to treat the morning sickness of pregnant women, but it caused more than 10,000 birth defects. After an in depth study, researchers discovered that only the R-enantiomer had analgesic properties while the other one was a teratogen, thus the production was focused on the R-thalidomide. It turned out that under physiological conditions fast racemization took place, so the drug was completely removed from the market.

Nowadays, researchers and drug companies are well aware of the relationship between chiral drugs, their biological activity and the importance of selective production of only one enantiomer. Consequently, the development of production and separation of a single enantiomer has rapidly evolved in the last decade, at the moment about 60-70% of the pharmaceuticals being chiral drugs [18].

### 1.1.3 Methods to Produce Enantiopure Compounds

As mentioned above, it is of great interest to have clear and well established procedures to obtain enantiopure compounds. In the early 1980s, Dieter Seebach introduced the term "EPC-synthesis" (synthesis of enantiomerically pure compounds) to define all the processes required to prepare enantiopure compounds and included three main approaches: chiral pool, resolution of racemates and asymmetric synthesis [19].

#### *1.1.3.1 Resolution of Racemates*

Resolution of racemates represents the separation of a racemic mixture into the pure enantiomers and it is considered one of the most challenging processes as the two optical isomers (R- and S- enantiomers) have identical chemical and physical properties, thus conventional separation methods cannot be used. Chiral separation procedures fall broadly into the following classes: crystallization method, liquid and gas chromatographic methods, capillary electrophoresis and kinetic resolutions.

Preferential crystallization or resolution of the enantiomer implies that each enantiomer crystallize in mirror-image crystals, known as conglomerates. In spite of the simplicity of this method, the procedure can be applied only to very few cases representing between 5 to 10% of all the crystalline racemates [19]. This drawback was overcome using a method that relies on the different physical properties of diastereomers. Mainly, the racemic mixture is treated with a chiral compound to form a pair of diastereoisomers which can be separated easily by crystallization due to difference in solubility. The method was first used to separate enantiomers in 1848 by Pasteur [5] who manually separated the two kinds of crystals of racemic tartaric acid salts.

Kinetic resolution of racemates represents an alternative to crystallization. In this case the separation is based on the fact that one enantiomer reacts faster with a certain reactant than the other. Even if both enantiomers can be produce from the same racemic mixture, the maximum theoretical yield obtained through this procedure cannot overcome 50%. To allow the total conversion of a racemic mixture to the desired enantiomer, dynamic kinetic resolution can be used. This process can be efficient only if the kinetic resolution used is irreversible and no spontaneous reaction of the substrate enantiomers and racemization of the product are present.

Chromatography represents a key technique for chiral separation, being widely used in the pharmaceutical, food, and beverage industries. This separation method implies the continuously passing of a mobile phase through a column containing a chiral stationary phase. The mobile phase, which can be either liquid or gaseous, contains the enantiomers which are separated inside the column based on their different interactions with the chiral stationary phase. The intermolecular forces that are involved in the chiral recognition are polar and ionic interactions, hydrophobic effects, hydrogen bonding and π-π interactions. Chiral chromatography is one of the most used techniques due to its versatility (a large number of chiral stationary phases are available on the market) and the fast method development (an analytical method is rapidly established with the suitable column) [20].

If the species are charged, the separation is done using an external electrical field. The capillary electrophoresis is based on the formation of diastereomeric complexes between the optical isomer and a chiral selector. The separation is done based on different equilibrium constants of complex formation. As in the case of chiral chromatography, there is a large number of chiral selectors available, making capillary electrophoresis one of the most efficient separation techniques [21].

#### *1.1.3.2 Chiral Pool*

Nature itself is a master in producing enantiopure substances and scientists have managed to separate these substances to further synthesized optically active compounds. The chiral pool strategy has been used starting from simpler molecules like e.g. amino acids (AA), up to carbohydrates, terpenes, and alkaloids. The huge development of fermentation processes led to the production of various acids like lactic acid, α-amino acids, and penicillin [21]. This approach is very attractive when the starting material is abundant and can be converted into the desired product in only few steps. However, this method can be applied to a very selective class of substances as there are few natural occurring compounds matching the stereo-structure to that of targeted compounds.

### *1.1.3.3 Stereoselective Synthesis*

When the chiral pool is not an option to obtain the desired enantiopure substance, the conversion of a prochiral compound into a chiral one seems to be the best alternative. This procedure involves the introduction of one or more elements of chirality (known as chiral auxiliary) in a substrate, producing stereoisomeric products. The main drawbacks of this method (often equimolar amounts of the auxiliary are needed and their reusability might be limited) [19] made scientists to divert their attention towards asymmetric catalysis. Depending on the nature of the catalyst, these new reactions can be classified as follows: organometallic catalysis, biocatalysis and organocatalysis.

The tragic events that took place in the 50-60's led to a dramatic increase in research of new methods for the preparation of chiral compounds. Tremendous achievements have been accomplished in the last 50 years in the field of organometallic asymmetric catalysis, fact demonstrated by the 2001 Noble Prize in Chemistry awarded to Sharpless, Knowles and Noyori for their contribution in this particular field [22]. The success of asymmetric organometallic catalysis is due to the affinity of metals to complexes bearing different functional groups and the efficient asymmetric induction of the well-defined metal-organic chiral ligand structure. An effective chiral ligand should meet several conditions, like: (i) the coordination process should be done in the same time as the chiral centre on the substrate is created, (ii) chemical modifications of the ligand structure should be possible, (iii) the synthesis of the ligand should be cheap and relatively easy, and (iv) the catalytic activity should be better relative to the achiral catalyst [23]. Although this domain has been developing continuously (reaching the point of combining the advantages of both homogeneous and heterogeneous catalysis by immobilizing the metal-ligand on a solid support), metal leaching represents an important drawback regarding the use of such chiral catalysts in drug or agro-alimentary industry.

Environmental and health regulations strongly restrict the use of toxic chemical processes, thus industry and academia are focusing more and more on greener catalytic reactions. Once again Nature proves its greatness through its powerful enantioselective catalysts which selectively produce only one of the enantiomers. Biocatalysis represents the use of enzymes to accelerate different process and due to their complex three-dimensional structure, they are involved in highly chemo-, regio-, diastereo-, and enantioselective processes. From ancient times humans have been using enzyme to produce and preserve food by means of fermentation, but Louis Pasteur was the one who established the basis of biocatalysis by using the mold *Penicillium glaucum* to enrich the (-) enantiomer of the tartaric acid ammonium salt [24]. From that moment till now this field has grown tremendously, being widely used in the manufacture of a large variety of chemical substances used in medicine, biodiesel, food additives, etc. In 2010

the industrial biocatalyst market was estimated to be 3.3 billion $, reaching ca. 4.4 billion $ in 2015 [25]. Even though biocatalytic reactions can be carried out under very mild conditions, enzymes are easily susceptible to degeneration, hence efforts have been made to improve the enzyme structure and develop novel biocatalysts.

The first organic molecule used as a catalyst dates from 1860, when Justus von Liebig [26] accidently observed that acetaldehyde speeds up the synthesis of oxamide from dicyan – milestone moment for organocatalysis. The knowledge assimilated from asymmetric organometallic catalysis and biocatalysis emerged into a new filed where the catalysts are chiral organic molecules. Even if their mode of action is similar to that of chiral auxiliaries, asymmetric organocatalysts are used in very small amounts, interact only temporary with the substrates and are release when the product is formed. The first asymmetric organocatalytic reaction was done in the early 1900s when Bredig and Fiske [27] studied the addition of HCN to benzaldehyde in the presence of alkaloids such as quinine (Scheme 1.1). Despite the low enantioselectivity (<10%) this work was considered ground-breaking.

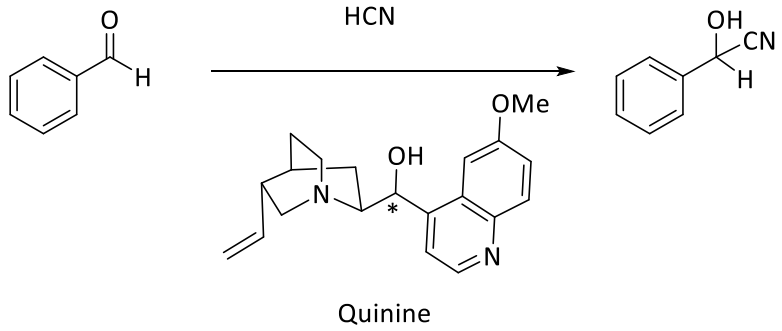


**Scheme 1.1** Alkaloid-catalysed addition of HCN to benzaldehyde

The asymmetric organocatalysis regained interests in the 60s-70s when two pharmaceutical companies (Hoffmann-La Roche and Schering AG) used for the first time proline to obtained optically active bicyclic ketol, reaction known nowadays as Hajos–Parrish–Eder–Sauer–Wiechert reaction (Scheme 1.2). After 1980, the first examples of phase transfer catalysis [28] and activation through hydrogen interactions [29] appeared, culminating in 2000s with the work of Barbas III [30] - who used amino acids to catalyse reactions promoted until then by bigger molecules - and MacMillan [31] - who developed the first asymmetric Dies-Alder reaction catalysed by secondary chiral amines.

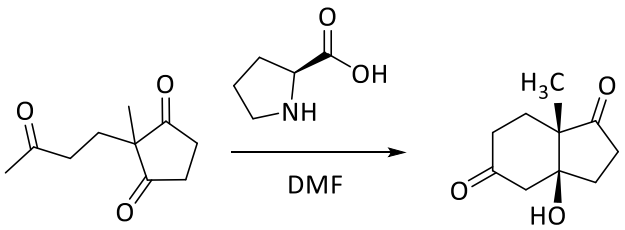


**Scheme 1.2** The Hajos–Parrish–Eder–Sauer–Wiechert reaction

Chiral organocatalysts present several advantages, the most important one being their resistance towards humidity, meaning that they can be used in any conditions. Moreover, Nature provides plenty of chiral compounds that can be directly used as catalysts. Despite all of these, their use in industrial synthesis [32-34], nanotechnology [35] or medicinal chemistry [36] is still limited, due to the their possible toxic effects, complicated separation protocols from the reaction products, and their incompatibility with continuous processes.

At a glance, the use of catalysts based on chiral organic molecules, Nature-inspired, supported on different materials appears quite attractive in terms of application and reusability.

## 1.2 Hybrid and Bio-nanohybrid Materials

The word “hybrid” is defined in the Oxford Dictionary as “a thing made by combining two different elements” and has been continuously used in material science and engineering. In most of the cases the term “hybrid” has not been clearly defined being generally confused with the term “composite”. Thus, a brief definition of concepts and material classes is required.

When an organic compound is combined with an inorganic host, an organic-inorganic material is formed, considered to be a “hybrid material” (Figure 1.3) only when the modification occurs at the molecular level, e.g. at the nanoscale [37, 38]. This material can exhibit new properties which can be unrelated to the individual components. On the contrary, composite materials are formed through the dispersion of one material into a second one and their properties are those of the two (or more) components added up.

## 1 Introduction

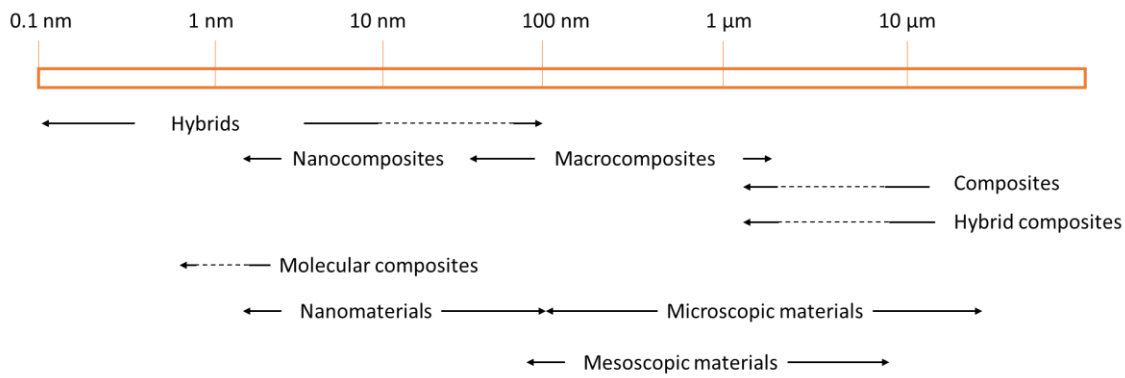


**Figure 1.3** Classification of materials at different scale levels

Scientists have been trying to classify hybrid materials in different manners. For example, Makishima categorized hybrid materials in four main groups:

- *composites* – mixture of materials consisting of matrix and micron-level dispersion;
- *nanocomposites* – sub-micron level mixture of similar kinds of materials
- *hybrids* – sub-micron level mixture of different kinds of materials
- *nanohybrids* – atomic or molecular level mixture of different materials with chemical-bonds between their components [37], explaining that there is no obvious difference between the two latter groups.

A more basic classification of the organic-inorganic hybrid materials is: *(i) intercalation compounds*, *(ii) organic derivatives of inorganic solids,* and *(iii) sol-gel hybrid materials.* Type *(i)* hybrids describe materials obtained through the intracrystalline insertion of organic compounds inside the layers of 2D and 3D lamellar solids, like clay minerals, graphite oxide, layer double hydroxides (LDH), etc. The second type of hybrids imply the grafting of organic groups into inorganic surfaces though covalent bonds, typical anchoring groups on e.g. siliceous host materials bearing silanol groups (Si-OH). Organometallic compounds based on alkoxydes of silicon, titanium, tin, aluminium or zirconium act as precursors for the third class of hybrids due to the presence of -M-O-R metal-organic bonds in the metal oxo-network. One of the most important group of this class is represented by organopholysiloxane materials.

Another more general classification of organic-inorganic hybrid materials is based on the bond between the two components which can be noncovalent (*Class I* - linked by hydrogen bonds, electrostatic forces or van der Waals forces) or covalent (*Class II*).

When the organic part of these hybrid materials is substituted with biological species or bio-inspired ones, a new class emerges – *biohybrid* or *bio-nanohybrid* materials [38]. This represents an important breakthrough in science as the unlimited possible combinations of bio-molecules and inorganic hosts might produce materials with vast functionalities, often beyond the man-

made synthetic systems. Important examples of such materials are the ones based on anionic biomolecules intercalated in layered double hydroxides used to deliver drugs [39] or on layered perovskite mixed oxides assembled with gelatine with high dielectric permittivity [40].

The stability of the bio-nanohybrid materials resulted from the affinity between the bio-organic guest and the inorganic host depends on the interaction mechanism which governs the immobilization process. If the inorganic solid is layered, the intercalation of the molecules may involve several simultaneously mechanisms based on hydrogen bonds, ionic bonds or even covalent bonds, the only requirement being the thermodynamic behaviour and the geometrical impediment of the host-guest affinity. Hence, in a 2D lamellar solid three types of molecules can be intercalated: neutral, anionic or cationic molecules.

### 1.2.1 Inorganic Host Materials

Before proceeding towards a detailed analysis of the forces and/or bonds that govern the bio-nanohybrid materials, it is compulsory to define the term “clay” and “clay mineral”. While the first one refers to small inorganic particles (< 2 µm) of a soil fraction without taking into consideration its composition of crystallinity, the latter one defines layered silicates [41]. Nowadays the terms “clay” and “clay mineral” are interchangeable and also term other layered-materials than silicates.

A typical layer of clay mineral (layered silicates) consists of cations tetrahedrally and octahedrally coordinated to oxygen atoms, designated as tetrahedral (T) and octahedral (O) [42]. Each tetrahedron is linked together at the apical oxygen to give the tetrahedral sheet, as can be seen in Figure 1.4 a. On the other hand, in the octahedral sheet the basic unit is composed of a cation (e.g. $Al^{3+}$, $Mg^{2+}$, $Fe^{2+}$ but not $Ca^{2+}$, $Na^{+}$ and $K^{+}$) surrounded by 6 oxygen or hydroxyl atoms (Figure 1.4 b).

## 1 Introduction

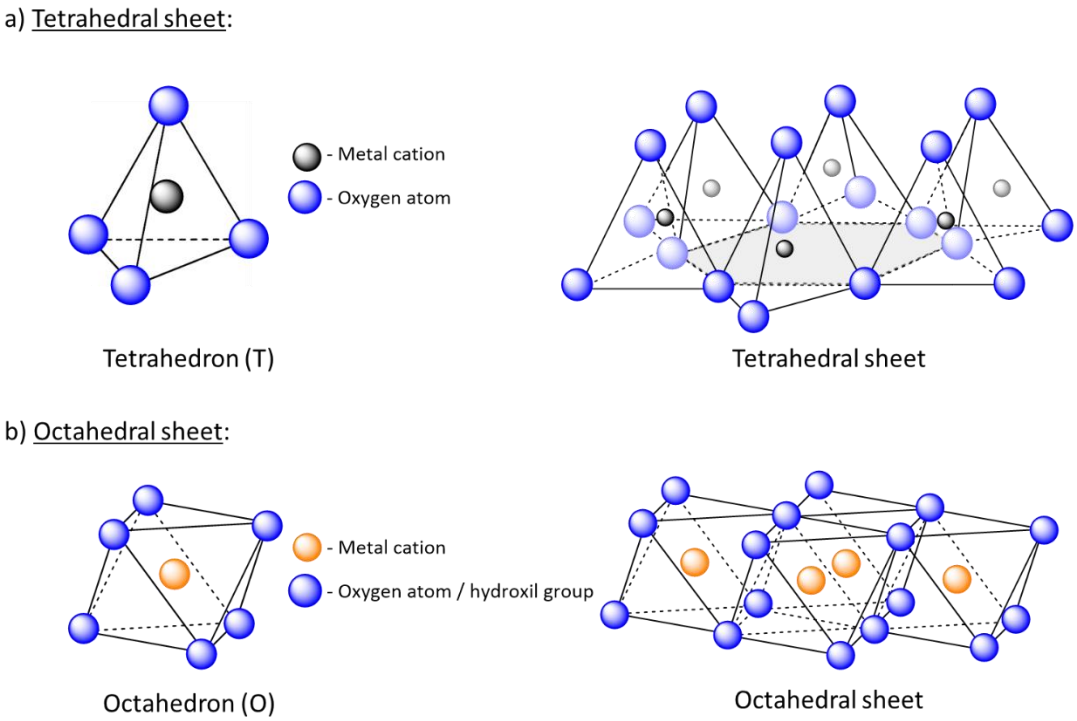


**Figure 1.4** Basic building blocks of a clay mineral: a) tetrahedral sheet- the grey area represents the link between the apical oxygens; b) octahedral sheet.

Tetrahedral sheets do not exist by themselves and are always associated with the octahedral sheets, either in the ratio 1:1 or 2 tetrahedral sheets and 1 octahedral one, resulting in structures that can be either neutral or negatively charged. In the first case (Figure 1.5 A), the layer structure consists of a repetition of one tetrahedral and one octahedral sheet, where one surface of the layer consists of oxygen atoms from the T form and the other surface of oxygen atoms or -OH groups from the O form. In the 2:1 structure (Figure 1.5 B), the O sheet is found between the two Ts forming a sandwich structure, both surfaces consisting of tetrahedral basal oxygen atoms [43]. The charge variability between the layers make clay mineral susceptible to accommodate molecules in the interlayer space.

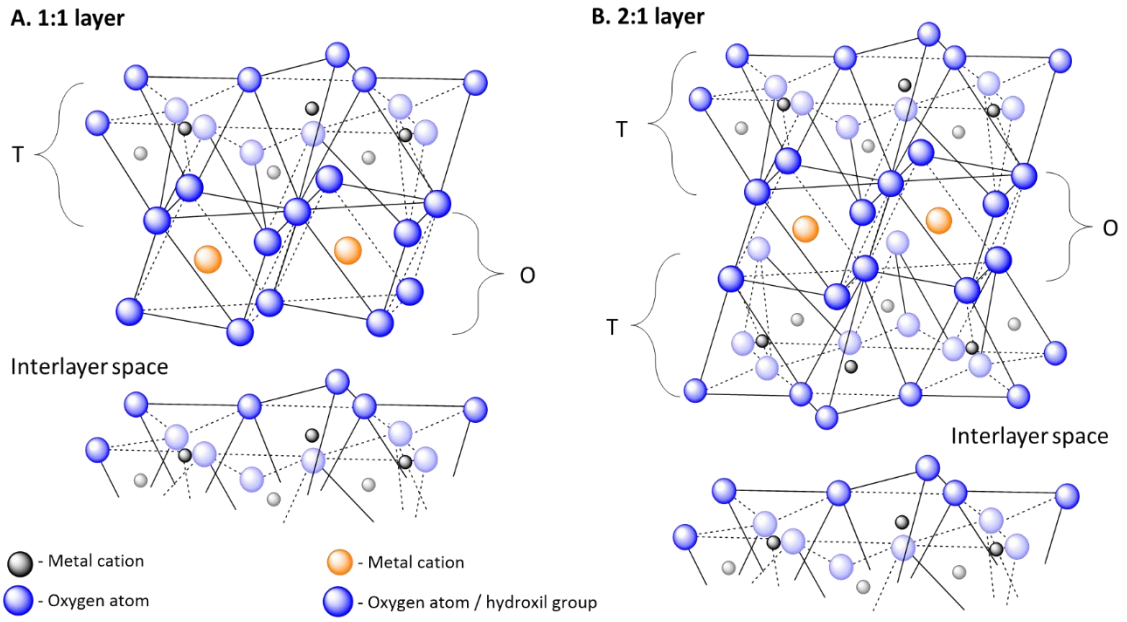


**Figure 1.5** Different layer structures: A. 1:1 layer; B. 2:1 layer. T – tetrahedral sheet, O - octahedral sheet

## 1.2.2 Guest-Host Interactions

Neutral species penetrate the interlayer space of a clay-type material only when the energy released in the absorption process overcomes the attraction forces between the layers, resulting in an increase of the basal spacing, easily detected during XRD measurements. The intercalation mechanism is directly related to the polarity of the guest molecule and can be governed by: van der Waals forces, hydrogen bonding and water bridges, ion-dipole and coordination, proton or electron transfer.

For example, van der Waals forces are important when alkylammonium species are introduced in the interlayer space of the clay. The hydrocarbon tail can be found perpendicularly directed with respect to the layer or can lie flat into the lamellar space. In the first case the interactions between the neighbouring groups are important while in the second case the van der Waals forces are established between the oxygen atoms of the inorganic sheets and the methyl or methylene groups in the chain.

If the interlayer environment has an acidic character, the interaction with a basic molecule will produce a proton transfer, generating an organic cation which will balance the electrical charge of the inorganic host. Additional, electron transfer mechanisms were observed when organometallic species were introduced into various 2D solids.

The group of phyllosilicates bear a framework charge deficiency which is compensated by interlamellar cations, through electrostatic interactions. These cations can be easily exchanged by the treatment of the inorganic solid with a salt solution. As in the case of neutral species,

after the interlamellar sorption the interlayer distance is increased, depending also on the molecular size of the guest molecule.

If the layers of the inorganic host are positively charged (as in the case of layered double hydroxides), the interlamellar species will bear a negative charge, which can be easily interchanged by either inorganic or organic anions.

### 1.2.3 Hydrotalcites

As mentioned in the previous section, the layers of clay minerals can be neutral or have a negative or positive charge. Layered double hydroxides (LDHs) or hydrotalcites (HT) represent the family of natural and artificial minerals that have positively charged layers with compensating anions in the interlayer space.

The natural mineral hydrotalcite was firstly discovered around 1842 in Sweden [44], but its chemical formula - $Mg_6Al_2(OH)_{16}CO_3.4H_2O$ (magnesium aluminium hydroxycarbonate) - was discovered in 1915 by Manasse. The first synthetic LDH was prepared in the '30-'40s by Feitknecht, who mixed dilute aqueous metal salt solutions with a base, but its first detailed structure was not discovered until the '60s by Allmann and Taylor independently one of each other [45].

#### *1.2.3.1 Structure*

The structure of LDH resembles to that of brucite, $Mg(OH)_2$. In a single unit of a brucite layer the $Mg^{2+}$ is octahedrally surrounded by 6 $OH^-$ and when several units are in a close proximity the octahedra share edges to form an infinite 2D layer (Figure 1.6 A). The layers are stacked on top of each other and are held together by hydrogen bonds between the hydroxyl groups. These brucite-like layers will gain a positive charge if some of the $Mg^{2+}$ ions are replaced with a trivalent one with a similar radius (such as $Al^{3+}$). This positive charge is compensated by anions and water of crystallization that lie in the interlayer space (Figure 1.6 B). Water and anions are randomly located and they move freely by breaking and forming new bonds continuously.

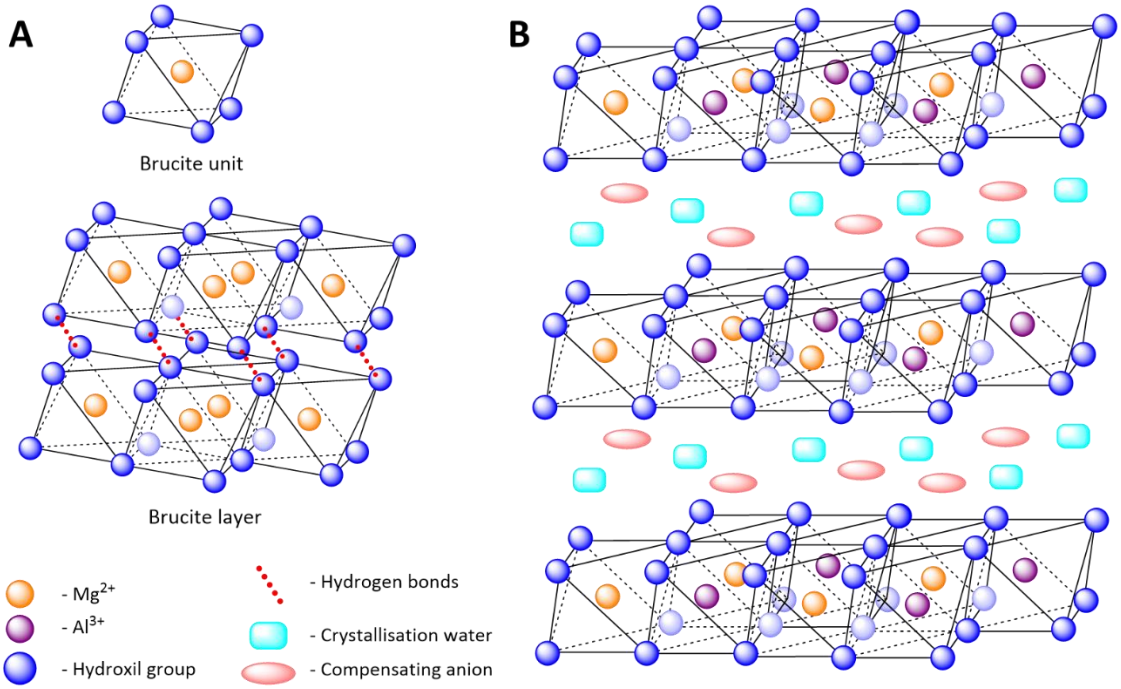


**Figure 1.6** Bucite lattice (A), HTs lattice(B)

Although the ideal structure of a HT is similar to the one shown in Figure 1.6 B, the layers of LDH can be stacked in different ways, producing a variety of polytype structures (which differ only in one of the dimensions of the unit cell). The classification was not established until 1993 by Bookin and Drits [46, 47] based on the number of layers stacked on the *c*-axis of the unit cell, the symmetry of the stacking sequence, and the arrangement of the hydroxyl groups of adjacent layers. Typically, a number of 2 or 3 layers can be stacked on the *c*-axis, having a rhombohedral (R) or a hexagonal (H) symmetry. If the opposite OH groups of adjacent layers lie vertical above one another a trigonal prismatic arrangement occurs (denoted with 1) and when they are offset, then an octahedral arrangement is obtained (denoted with 2). For example, a notation of $3R_1$ denotes a 3-layer stacking having a rhombohedral symmetry and a trigonal prismatic arrangement of OH groups.

The identity of the polytype can be determined from the powder XRD, but only if the hydrotalcite-type material has a high crystallinity. The HTs present three XRD reflections groups [48]:

(i) Strong (0 0 *l*) reflections found at low angles that determine the interlayer distance *d* (or the thickness of one layer plus one interlayer space); further, the unit cell parameter *c* can be obtained using the formula *c=nd*, where *n* – represents the number of HT layers;

(ii) (1 1 0) reflection at a high angle which is used to compute the lattice parameter $a_0 = 2d_{1\,1\,0}$. The lattice parameter is important as it corresponds to the inter-cation distance in the hydroxide layer;

(iii) (0 1 *l*) and/or (1 0 *l*) reflections found at intermediate angles used to determine the polytype of the LDH.

The chemical composition of a HT-like material is $M(II)_{1-x}M(III)_x(OH)_2(A^{-n})_{x/n}*yH_2O$, where M(II) represents the divalent cation, M(III) the trivalent cation, A the interlayer anion, -n the charge on interlayer ion and *x* and *y* fraction constants [49]. As previously mentioned, the combination of divalent and trivalent cations can vary as long as they have similar radii as $Mg^{2+}$ and $Al^{3+}$, although there are cases when larger ions are used (such as $Mn^{2+}$, $Ca^{2+}$ or $Pd^{2+}$) leading to a partially distortion of the close packing configuration of the LDH.

The fraction constant *x* can vary between 0.1 and 0.5, but the pure LDHs are obtained in the range 0.2-0.33. Due to the electrostatic repulsions between the positive charges, the trivalent cations should be as far as possible, thus *x* should not be higher than 0.33. If the value of *x* is too low, the density of divalent cations in the layer will be higher than normal, so less anions will be found in the interlayer, resulting in the formation of hydroxides of M(II).

If the nature of cations is limited, the type of anions that can be found in the interlayer structure of a LDH material is unlimited, varying from inorganic anions (e.g. halides, $CO_3^{2-}$, $NO_3^-$) to organic anions (e.g. carboxylates, organic dyes), complex anions (e.g. $NiCl_4^{2-}$), etc. The most important feature of the anions is that they are orientated in such a manner to maximize the interaction with their surroundings. Besides anions, water molecules can be found in the interlayer space that is not occupied by the anions, held through hydrogen bonds between them and the -OH and/or other anion.

### *1.2.3.2 Synthesis*

The best method to obtain LDHs with a high chemical homogeneity is the coprecipitation method at constant pH obtained by the simultaneous addition of a base solution and a mixed metal solution. Both pH and the concentration of the mixed metal solution have a crucial effect on the chemical, structural and textural properties of the final product. The precipitate obtained under low supersaturation conditions is more crystalline (the rate of nucleation is higher than the rate of crystal growth) than under high supersaturation conditions. The main drawback of this method is that it might be limited by possible competitive reactions like precipitation of a metal salt or complexation of the metal cation.

Besides pH and concentration, the type of solvent used during coprecipitation influences the properties of the LDH. The specific surface area (SSA) of the material is increased if ethylene

glycol is used, while water pools give rise to dispersed solids. A smaller sized LDH can be synthesized using colloid mill processes or narrow channel reactors.

Large platelets of well-crystallized LDHs with a hexagonal shape can be obtained by using urea as a base retardant. Its role is to separate the nucleation step from the particle growth, preventing the aging process from the beginning.

Another interesting way to synthesize HTs is based on using insoluble metal oxides or hydroxides. By adding them to an acidic solution of another metal a buffer medium is obtained, favouring the precipitation of the LDH.

A newer method of synthesis was developed by Lopez *et al.* in 1996 [50] and it is based on the sol-gel process which produced HTs with a very high thermal stability and enhanced specific surface area.

New HTs can be obtained from "as-prepared" samples using microwave, ultrasounds or hydrothermal treatments. The use of microwaves during the synthesis will accelerate the growing and aging steps, prolong exposure leading to a high SSA and high porosity. Large particles size is obtained when ultrasound treatment is used during coprecipitation treatment or when high temperatures are used during the synthesis process.

Compared to other materials, LDHs have the ability to exchange the anions found inside their layers. The anionic exchange process depends mainly on the electrostatic interactions between the positively charged layers and the exchanging anion. The equilibrium constant of this process increases when the radius of the bare anion decreases, thus the order of affinity of LDH for monovalent anions decreases in the order $OH^->F^->Cl^->Br^->NO_3^->I^-$ and for the divalent anions in the order: $CO_3^{2-}>C_{10}H_4N_2O_8S^{2-}>SO_4^{2-}$ [49, 51].

The structural memory effect of these materials can be widely use to synthesize new LDHs and is based on a calcination/reconstruction process. In the first step, the volatile anion found in the interlayer space is removed during calcination resulting in the formation of mixed oxides. Next, the intercalation is done by rehydrating the mixed oxides in an aqueous solution containing the desired anion. Important parameters in determining the degree of recovery and the success of the reconstruction method are temperature of calcination and the M(II)-M(III) combinations.

### 1.2.4 Nanohybrid Materials Based on HTs and Amino Acids

Intercalating biological active substances is a simple and effective tool to modify and tune the physical and chemical properties of HTs. Being amphoteric, amino acids (AAs) are perfect molecules to be immobilized in the interlayer space of LDHs either by coprecipitation, anionic

exchange or reconstruction method. These molecules can be immobilized both in the zwitterion form or the anion form depending on the pH used and the $pKa_x$ of the AA.

#### *1.2.4.1 Coprecipitation Method*

As mentioned in the previous subsection (Section 1.2.3.2), the coprecipitation method consists in the nucleation and growth of the M(II) and M(III) hydroxide layers from an aqueous solution containing the anion that is going to be incorporated inside the layers. This anion has to have a high affinity for the hydroxide layers, otherwise the counter anion of the metal salts might be incorporated, thus metal nitrates and chlorides are generally used in this method.

In 1997, Whilton *et al.* intercalated negatively charged amino acids (aspartic acid and glutamic acid) in the gallery spaces of LDHs (Mg:Al molar ratio 2) using the coprecipitation method at a pH of 12. The XRD patterns of the carbonate-LDH showed an interlayer spacing of 7.6 Å while the aspartate- and glutamate-LDHs presented broad (*0 0 3*) diffraction peaks of 11.1 and 11.9 Å, consistent with the intercalation of the organic anions. The galleries spacing of the amino acid-LDHs were of 6.3 and 7.1 Å, respectively, suggesting a monolayer arrangement of the organic molecules with the carboxylates of individual molecules bridging adjacent LDH layers. The study showed that the amount of organic and inorganic anions incorporated is stoichiometrically related to the net positive charge generated by the Al substitution in the layer [52].

For a better understanding of the coprecipitation process, Aisawa *et al.* used phenylalanine (Phe) as the guest molecule and different M(II)-M(III) materials. Phenylalanine was chosen due to the nonpolar side chain which simplifies the interactions between the amino acid and the hydroxide layers of the host materials. They discovered that the degree of precipitation of the AA was affected by both pH and the nature of HT, decreasing in the following order: Ni-Al > Zn-Al > Mn-Al > Zn-Cr > Mg-Al [53]. The AA was introduced in the amphoteric form for all the HT materials, except the Mg-Al one. In the latter case, the intercalation proceeds slowly, initial intercalation being done through the ion-exchange reaction between the Phe and the $NO_3^-$ and/or $OH^-$. The AA is temporarily oriented vertically with respect to the basal layer and in time is rearranging leading to a final horizontal intercalation in the interlayer space (Figure 1.7).

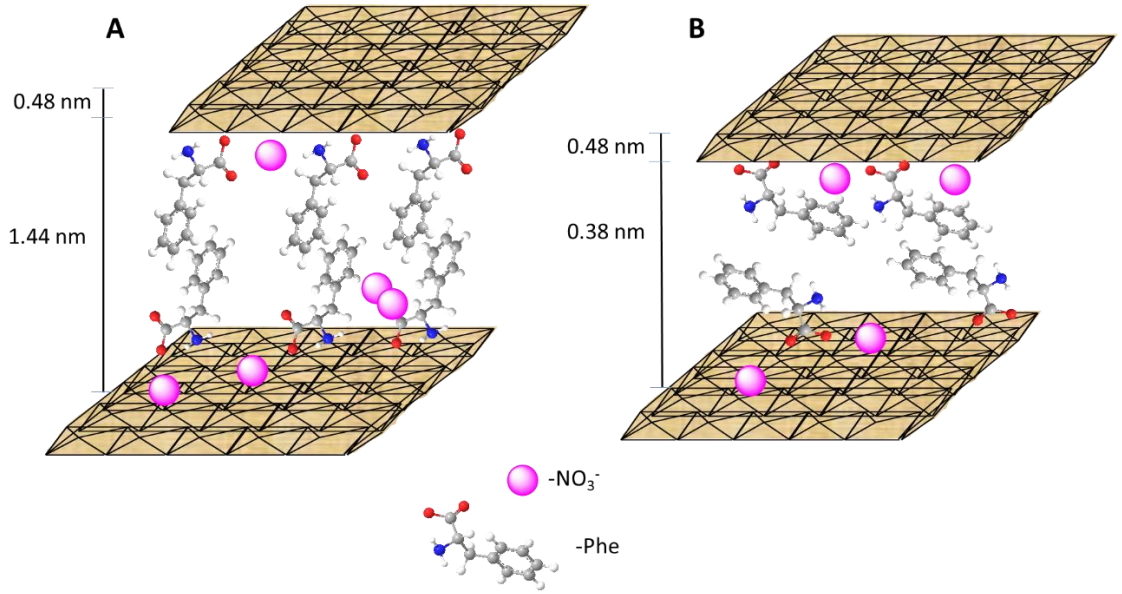


**Figure 1.7** Schematic model for the formation process of Phe/Mg-Al LDH, pH = 10: A – initial stage; B – final stage

L-proline/LDH materials were prepared by coprecipitation by Choudary *et al.* who observed that the $d_{003}$ basal spacing of the support did not changed, indicating that proline was located at the edge of the layer and not inside [54]. Hibino studied the incorporation through precipitation of 14 different AAs into Mg:Al 3:1 materials and observed that the ones having aromatic or acidic side chains were highly intercalated and were oriented in a vertical monolayer or bilayer position in the interlayers. The low basal spacings of the nanohybrid materials formed from HT and the other AAs suggested that these molecules were horizontally oriented in the interlayers [55].

Based on the molecular dynamic calculations provided by Newman *et al.* [56] who concluded that the guest interacts with the LDH host layers by hydrogen bonding, Duan *et al.* [57, 58] studied the *in-situ* thermolysis of L-aspartic acid/LDH and came to the conclusion that this AA is accommodated in the interlayer region as a monolayer with the two carboxylic groups electrostatically attracted to both the upper and lower hydroxide layers and with hydrogen-bonding network existing between the water, the guest anions and the host layers. The same researchers studied the intercalation of L-tyrosine in the interlayer space of Ni-Al, Zn-Al and Mg-Al HTs, all 2:1 molar ratios [59]. They observed that this AA is found as a bilayer arrangement, with the phenyl groups in the centre of the galleries and the contact with the layers being done through the oxygen atoms of the carboxylate group. These oxygen atoms along with the interlayer water molecules form an oxygen monolayer on the surfaces of the hydroxide layers having the hydrogen bonding of 0.22 nm (Figure 1.8). As the coprecipitation was done at a pH < pKa phenolic, the AA was present as a monovalent ion. In addition, the presence of the nitrate

ions in the galleries demonstrate the incomplete intercalation of L-Tyr, phenomenon previously reported.

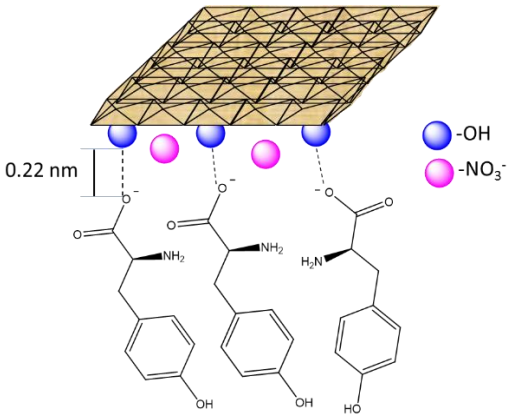


**Figure 1.8** The oxygen monolayer having a hydrogen bond of 0.22 nm

The similar incomplete intercalation was observed also in the case of L-cysteine and L-cystine [60-62]. In the first case, the coprecipitation pH was 10.5, thus, according to the pKa of this AA, L-cysteine exists mainly as a divalent anion. The thickness of the LDH hydroxide basal layer was found to be 0.48 nm while the $d_{003}$ of the nanohybrid material of 1.03 nm, demonstrating that the gallery height was close to the height of a molecule of cysteine. Thus, the molecule is accommodated vertically as a monolayer, with the two negative groups of individual anions attracted electrostatically to upper and lower hydroxide layer, as depicted in Figure 1.9 A. In the second case, the cystine was present also in the divalent anion form, accommodated approximatively vertically, the two negative groups being connected to the inorganic layers (Figure 1.9 B).

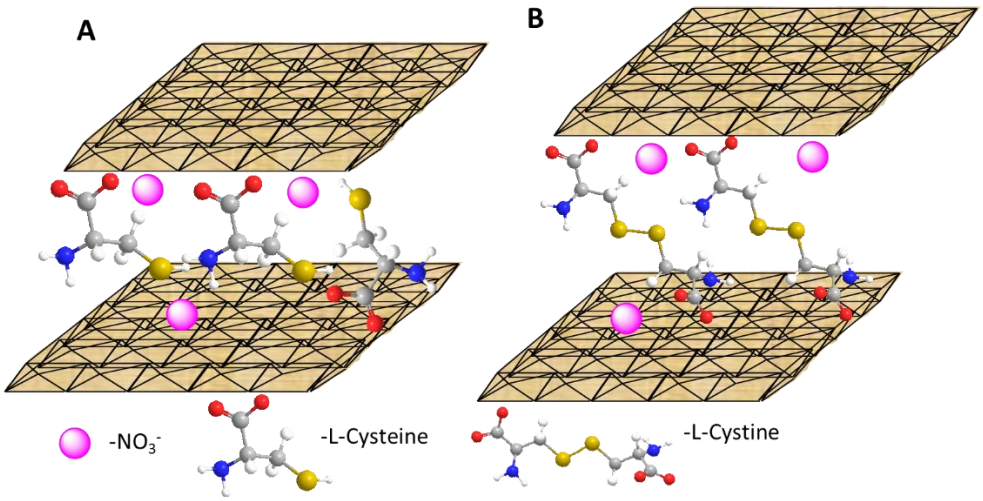


**Figure 1.9** Schematic representation of possible arrangements for A Cysteine/LDH and B Cystine/LDH

Reinholdt *et al.* used different techniques to analyse the glutamate (Glu) interactions with Mg-Al HTs and observed that the nanohybrid materials synthesized at pH between 8.0 and 12.1 contained substantial amount of the AA. The highest amount of glutamic acid was incorporated at pH 10 (data observed from XRD) at temperatures between 50 ° and 70 °C, while substantial amount of the HT structural charge was compensated by small inorganic anions. At pH lower than 10, the interlayer space is filled with $NO_3^-$ while at pH > 10 by $CO_3^{2-}$ and $OH^-$ [63]. In a second study, isotopically enriched HT was used to investigate the proportion of glutamate anions with different charges absorbed or intercalated. At pH 10.0 and 11.0 the ratio of $Glu^-/Glu^{2-}$ was higher than expected, demonstrating that the H-bond networking inside the galleries favours the absorption of the positively charged $-NH_3^+$ instead of the $-NH_2$, phenomenon known as pKa shift [64].

Two newer works investigated the interaction of the amino acids/HT prepared by coprecipitation with either silicone [65] or a vanadium complex [66]. While in the first case no interesting interaction is observed, being more focused on the exfoliation of the bioinorganic host, in the latter one it was observed that the electrostatic interaction of brucite-like structure with the AAs decreased in the order: L-serine > L-alanine > L-glutamate.

#### *1.2.4.2 Anionic Exchange Method*

The most used method in synthesizing organo-LDHs is the anionic exchange method, but there are far less examples employing the use of AAs than in the case of the coprecipitation method. Fudala *et al.* immobilized L-tyrosine and L-phenylalanine in a Zn-Al HT and observed the shifting of the basal spacing of HT from 0.85 nm to 1.75 nm in the case of L-Tyr and to 1.80 nm in the case of L-Phe. The two amino acids were immobilized in the anionic form in a bilayer arrangement with the aromatic side chain towards the centre of the galleries (Figure 1.10 A and B) [67-69]. On the contrary, Choudary *et al.* did not observe any increase in the $d_{003}$ when L-proline was used, demonstrating that during anionic exchange process this amino acid got immobilized at the edges of the HTs [54].

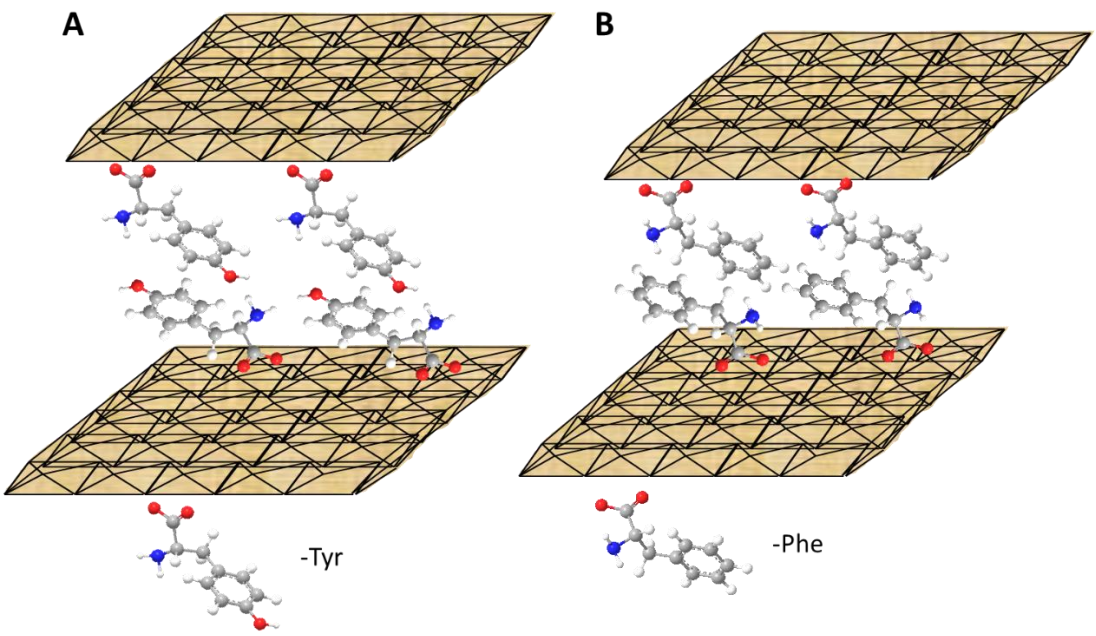


**Figure 1.10** Schematic representation of possible arrangements for A Tyr/LDH and B Phe/LDH obtained by anionic exchange method

Duan *et al.* immobilized L-cysteine into Mg-Al HT using an amino acid solution of pH = 8.5, thus the AA existed mainly as a monovalent anion. The XRD pattern of the nanohybrid material showed the gallery height was twice as high as a molecule of monovalent L-cysteine, demonstrating that the organic molecule was immobilized in a bilayer arrangement with the carboxyl group of individual molecules attaching alternatively to the upper and lower inorganic layer. The authors also suggested that the -SH groups of adjacent molecules might be involved in hydrogen bonding (Figure 1.11) [61].

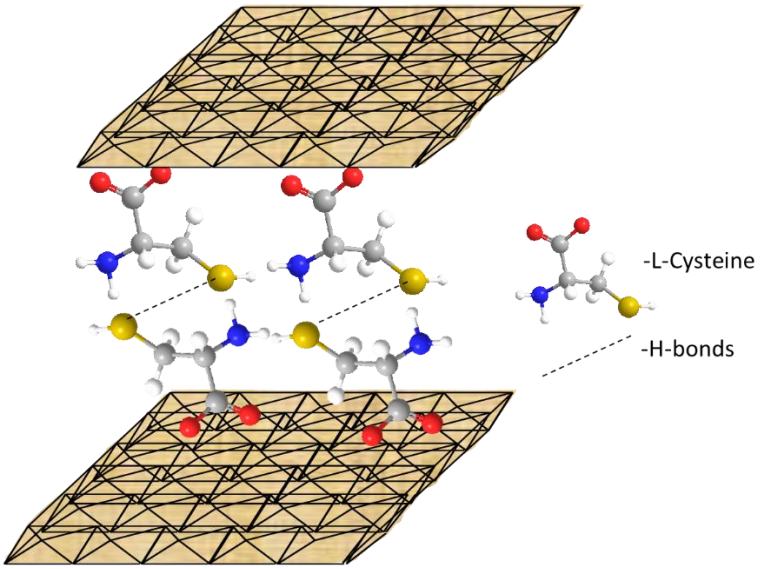


**Figure 1.11** Schematic representation of possible arrangement of L-Cys/HT obtained by anionic exchange method

Recently, Miranda *et al.* studied the anionic exchange immobilization of L-leucine using two methods: one involving stirring at room temperature for 30 minutes and the other one stirring for 3h at 80 °C. In the first case, the basal distance of the hybrid material did not change, demonstrating that the entire amount of L-leucine was immobilized on the edges of the HT. When temperature was used, the $d_{003}$ increased to 11.7 Å, proving that the AA was found in the interlayer space of the HT. In both cases, the AA was mainly found in the anionic form [70].

#### *1.2.4.3 Reconstruction Method*

The *memory-effect* property of HTs can be used to introduce organic molecules between their layers by calcination and rehydration in an aqueous solution containing the desired anion (a more detailed description can be found in Section 1.2.3.2). Compared to the coprecipitation method, the present one was rarely used in literature.

Nakayama *et al.* studied the immobilization of several AAs in Mg-Al HT by reconstruction method. It was observed that in the case of Gly, Ala, Ser, Thr, Pro, Asn, Gln, Asp, and Glu no expansion was observed, while for the Val, Ile, Phe, Trp, Cys, Met, Leu, and His, the intercalation is accompanied by an expansion of the interlayer distance of the solid product. In the former case, the long axis of the amino acid seems to be parallel with the layer, thus intercalation can occur without expansion. If the long axis of the AA is increasing, an increase in the interlayer distance of the nanohybrid material is observed, giving rise to a bilayer structure in the galleries of the HTs, behaviour already reported in Section 1.2.4.1. Besides the use of reconstruction method, Nakayama *et al.* explained for the first time the possibility of L-leucine to be intercalated in both ionic and zwitterionic from, no matter if the aqueous solution used had a pH = 10. If the AA is found in the zwitterion form in the interlayer space of HT, then the material requires another anion ($OH^-$ or $CO_3^{2-}$) for cointercalation. In this case, the AA interacts with the inorganic layer through hydrogen-bonds and not by Coulomb forces [71].

Using Zn-Al HT, Aisawa *et al.* found that the intercalation of Phe was influenced by the solution pH, indicating that the intercalated Phe has a vertically orientation if the solution is alkaline and a horizontally one if the solution is neutral. Moreover, it was shown that the amino acids possessing a hydrophobic or negative-charged side chain are preferentially intercalated in the HTs galleries [72].

An *et al.* intercalated L-Proline in HT Mg-Al 3:1 and observed that the interlayer gallery size was equal to the thickness of the AA, suggesting the organic molecule has a horizontal orientation compared to the inorganic layer. The FTIR analysis showed the AA is found as an anion, thus, due to spatial restriction, this anion cannot counteract the LDH charge. Using these findings, they proposed a model where the AA is found horizontally, with the carboxyl group

attached to the hydroxide layers and surrounded by four additional water molecules and one carbonate molecule (Figure 1.12) [73].

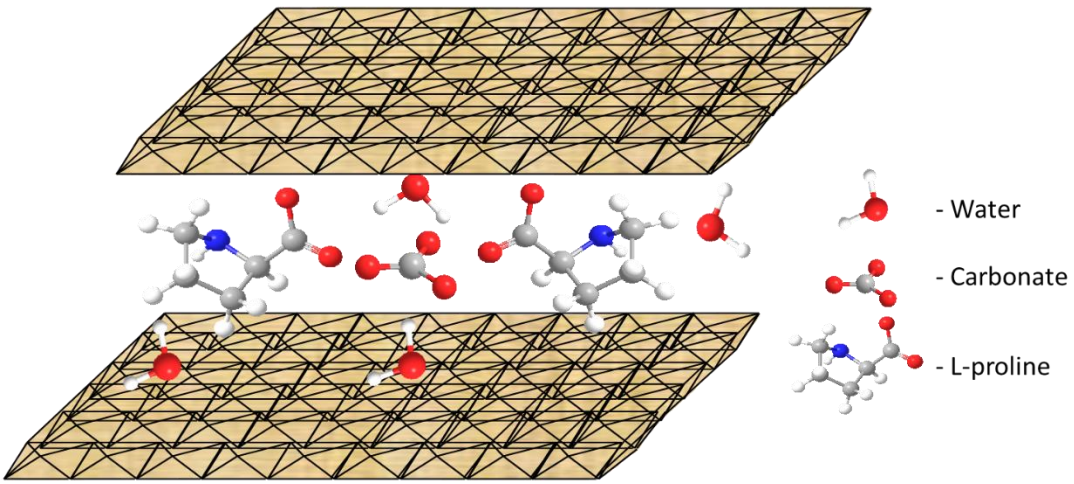


**Figure 1.12** The schematic model of L-Pro/LDH

Vijaikumar *et al.* immobilized L-proline in the HTs using reconstruction method for catalytic purposes, without focusing on the structure of these nanohybrid materials [74].

All of the methods presented in this subsection have their advantages and disadvantages depending on the future use of the synthesized nanohybrids. The materials obtained by coprecipitation cannot be calcined, as the AA will be lost, thus, their basicity will be very low. Nanohybrid materials obtained through anionic exchange and reconstruction methods seem to be suitable for different application, but care should be taken in the synthesis process not to introduce carbonates in the interlayer space – generally avoided by using decarbonated solutions and/or inert atmosphere.

## 1.2.5 Nanohybrid Materials Based on HTs and Oligomers / Poly-Amino Acids

Oligomers and poly-amino acids (PAAs) containing at least one -COOH end are suitable to be incorporated in the interlayer space of LDHs, although few papers exist on this topic.

### *1.2.5.1 Thermal Condensation Method*

Whilton *et al.* are pioneers in immobilizing not only amino acids, but also poly-amino acids into LDH, being the first ones to use the *in-situ* thermal polycondensation of an aspartate-containing LDH. The procedure used was similar to the thermal condensation of aspartic acid and consisted in heating a dried aspartate-LDH sample at 220 °C for 24 h, followed by a slow cooling, dispersion in a NaOH solution at pH = 11.0 and neutralization with HCl. The XRD patterns of the material before treatment with NaOH presented a decrease in the $d_{003}$ to 9.0 Å compared to the 11.1 Å of the initial material, attributed to the loss of intercalated water molecules and

the polycondensation of the monomers in the galleries of the inorganic host. Interestingly, the basal space increased to 12.2 Å after the treatment with the aqueous base solution, demonstrating that the initial heating starts the *in-situ* polymerization of the aspartate monomer producing the intercalated polyimides which subsequently undergoes ring-opening by hydrolysis (Scheme 1.3) [52]. The main disadvantage of this method is the facile exchange of nitrates with the carbonates found in the aqueous solutions.

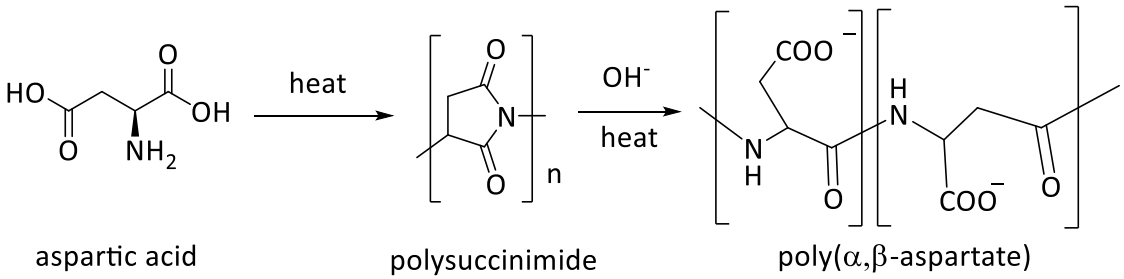


**Scheme 1.3** Thermal polycondensation of aspartic acid to poly(α,β-aspartate)

### *1.2.5.2 Coprecipitation Method*

When the poly-aspartic acid was immobilized by coprecipitation method, Whilton *et al.* observed that the distance of the interlayer space increased to 15.1 Å and the elemental and FTIR analysis indicated that the charge balancing species are the single charged aspartate side residues of the polyaspartate and no other counter anion was observed. Compared to the materials obtained by thermal polycondensation, the present ones consisted of irregularly shaped aggregates of plate-like particles with very smooth surface textures [52].

Using Zn and Al nitrates precursors, Aisawa *et al.* immobilized four different oligomers: Phe-Phe, Gly-Phe, Gly-Gly and Gly-Gly-Gly. In the first case, it was observed that the nitrates and water molecules were hardly intercalated in the gallery space of the LDH as this space becomes smaller and more hydrophobic. Moreover, the Phe-Phe molecules are arranged vertically with phenyl groups overlapped due to hydrophobic interactions (Figure 1.13 A). The coprecipitation of the Gly-Phe was lower compared to the Phe-Phe at the same pH due to a reduce number of phenyl groups which facilitated the introduction of nitrates anion. The XRD pattern showed that the dimer Gly-Phe was oriented horizontal to the LDH basal layer. Interestingly, the amount of Gly-Gly and Gly-Gly-Gly (Figure 1.13 B) intercalated did not change with increasing the peptide bonds and neither the interlayer distance, suggesting that the dimer and trimer are oriented horizontal to the LDH layer. It was concluded that the intercalated amount of oligomers decreased in the order: Phe-Phe > Gly-Phe > Gly-Gly-Gly > Gly-Gly [75].

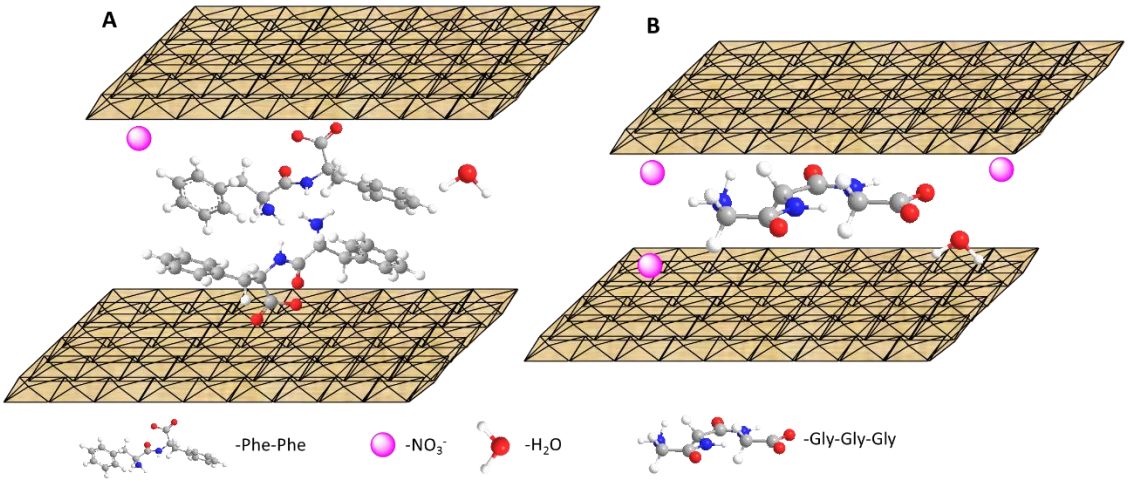


**Figure 1.13.** Schematic representation of A Phe-Phe/LDH orientation vertical and B Gly-Gly-Gly/LDH orientation horizontal.

### *1.2.5.3 Anionic Exchange Method*

Miranda *et al.* studied the anionic exchange method in the immobilization of commercial and synthesized poly-L-leucine (PLL) into Mg-Al HTs 2:1 using three different conditions: i) stirring for 2 days at 80 °C in water or 60 °C in THF, ii) stirring at room temperature in water for 1 h, and iii) using ultrasounds for 30 minutes. The commercial poly-L-leucine did not contain a -COOH end, thus, in all the three cases a very small amount of polymer was immobilized inside the galleries of the LDH, probably through hydrogen bonds formed between the carbonyl group of an leucine residue and the -OH groups found between the layers. The highest amount of synthesized poly-L-leucine (containing both a -COOH and a $-NH_2$ ends) immobilized into HT was obtained under sonication in water medium. This was explained by the fact that the sonication and rehydration treatments maximize the accessibility and utility of the -OH groups [76], thus favouring the anionic exchange with the polymer [77].

Later, the same group studied the nature of the PLL immobilized in HT and observed that the α-helical form of the polymer is not destabilized after immobilization. It was also detected that a very small amount of cyclic polymer was immobilized due to the nucleophilic attack of the -OH groups found inside the galleries on the NCA end group of the PLL (Figure 1.14) [78].

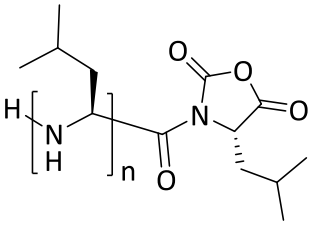

**Figure 1.14** PLL with a NCA end group

In a more recent work, Wang *et al.* studied the immobilization of glutathione (GSH) into Mg-Al HT 2:1 by anionic exchange method at different temperatures and concluded that increasing the temperature favours the immobilization. Using DFT calculations, a reaction pathway for the intercalation of GSH in the galleries was proposed. The process proceeds through a hydrogen transfer from the carboxyl group to the neighbouring amino group, a fundamental mechanical process that occurs in solutions that contain zwitterion molecules (Figure 1.15). The new molecule, bearing both positive and negative charges, is unstable, so it will quickly immobilize into HT by exchanging the nitrate anions. A higher temperature will increase the amount of nitrates interchanged [79].

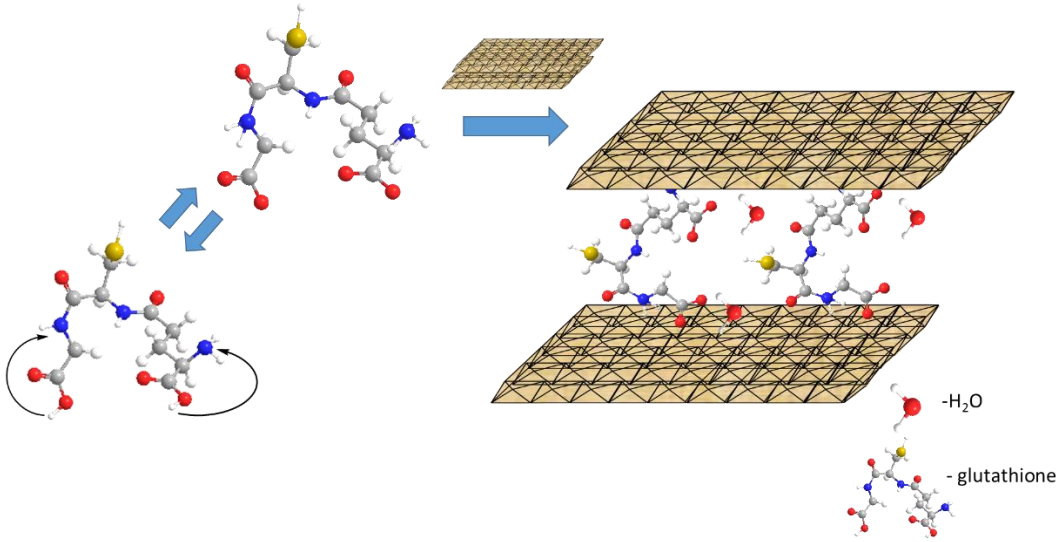


**Figure 1.15** Reaction pathway of immobilization of glutathione into LDHs

### *1.2.5.4 Reconstruction Method*

The only paper presenting the use of reconstruction method in the peptide immobilization into LDHs is that of Nakayama *et al.* who studied aspartame (composed of Asp and a methyl ester of Phe), dipeptide, tripeptide, and tetrapeptide of Gly. As in the case of hydrophobic amino acids, the intercalation of aspartame led to an expansion of the interlayer distance of HTs, due to the presence of the aromatic ring from Phe. In the other 3 cases no change in the interlayer distance was observed, as the oligomers have a parallel arrangement of the long axis of the molecule. It is very difficult to estimate the ionic state of an oligomer or a poly-amino acid, but the authors manage to demonstrate that the Gly-Gly could be found in both anionic and zwitterion form [71].

More information regarding the properties of the common amino acids can be found in Appendix I.

## 1.3 Different Asymmetric Reactions

This section is design to present a general overview on two asymmetric reactions (aldol addition and Juliá-Colonna epoxidation reactions), focusing in the end on those reactions catalysed by nanohybrid materials based on AA and PAA and HT.

### 1.3.1 Aldol Addition Reaction

The reaction of carbonyl enolates with aldehydes and ketones to form β-hydroxyl carbonyl compounds is known as aldol reaction (the term "*aldol*" is an abbreviation of *ald*ehyde and alcoh*ol*). As the reaction can take place in either acidic or basic media, HTs materials seem to be good candidates, but their lack of chirality will lead to an achiral product. In this context, AAs (like L-proline [30], L-t-leucine [80], etc.) were intensively used to afford enantioselective aldol addition products.

In the basic medium (Scheme 1.4), the base extracts a hydrogen from the α position to afford the corresponding enolate **(1)**. Next, the enolate anion (which represent the attacking nucleophile) will attack a second carbonyl molecule **(2)**, to afford the desired aldol product **(3)**.

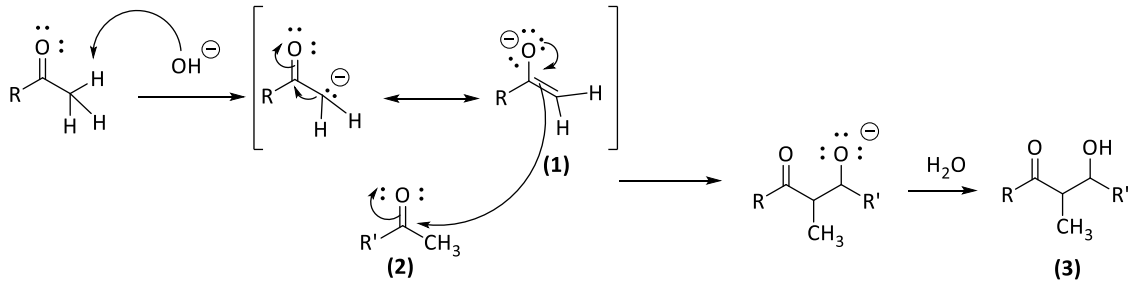


**Scheme 1.4** Base catalysed aldol addition mechanism

In the second case (Scheme 1.5), the carbonyl oxygen atom of the two carbonyl compounds will be protonated, increasing the carbonyl carbon's electrophilicity so that it can be attacked by the enol. In general, aldol addition reactions are favoured by a basic medium and not an acidic one.

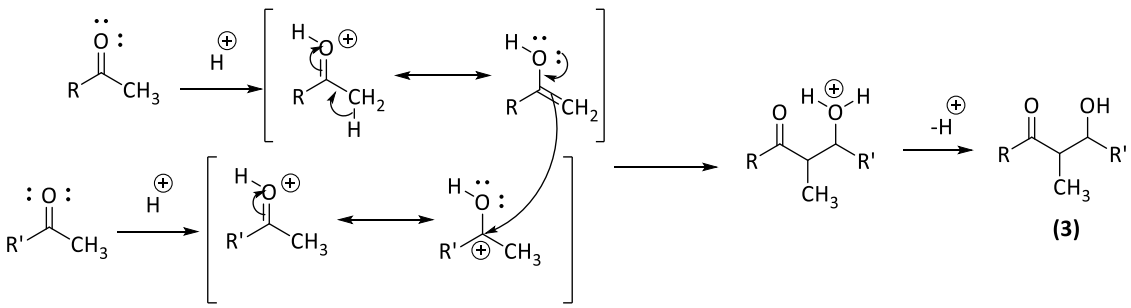


**Scheme 1.5** Acid catalysed aldol addition mechanism

## 1.3.2 Juliá-Colonna Epoxidation Reaction

When an α,β-unsaturated carbonyl compound is treated with hydrogen peroxide in basic medium, the double bond is transformed into an epoxide, which, depending on the substituents connected to the C atoms, can be chiral. Juliá-Colonna epoxidation reaction (Scheme 1.6) was discovered in 1983 by Colonna *et al.* who introduced a triphasic catalytic system based on water-inorganic solvent-poly-amino acids to afford optical active epoxides [81]. The potential use of chiral epoxides in pharmaceutical industry, made Roberts *et al.* [82] and Geller *et al.* [83] to improve the reaction conditions by either developing a biphasic system composed of urea-hydrogen peroxide and PAA or using a phase transfer co-catalysts like tetrabutylammonium bromide (TBAB).

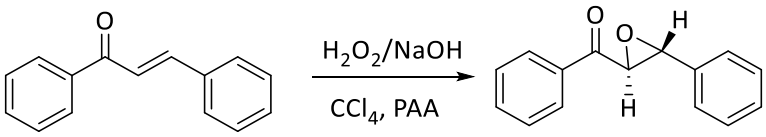


**Scheme 1.6** The Juliá-Colonna epoxidation reaction

### *1.3.2.1 Mechanism of Reaction*

The first mechanistic studies of the Juliá-Colonna epoxidation reaction showed that the reaction proceeds via a fast reversible addition of hydroperoxide, followed by a slow, intramolecular nucleophilic displacement of the hydroperoxide [84].

The role of PAA in the Juliá-Colonna epoxidation reaction has also been intensively studied, and the results showed that, from the entire pool of possible PAAs, poly-L-leucine is the best catalyst for this reaction. Okuyama *et al.* showed that leucine has close to the highest helix propensity of all natural amino acids, thus its oligomers and polymers will show an α-helical conformer [85]. Berkessel [86] and Roberts [87] demonstrated that the catalytic site of poly-L-leucine is found at the N-end of the polymer, where the last 4 N-H groups are not involved in the helix hydrogen bonding, thus creating a perfect oxoanion hole available to interact with the substrates (Figure 1.16 A) [88].The kinetic models postulated that Juliá-Colonna epoxidation reaction proceeds through the formation of a hydroperoxy enolate complex through two possible pathways: I) $HOO^-$ binds first or II) chalcone binds first (Figure 1.16 B) [89]. Despite all the information found in the literature, there is scant information on the preferred pathway.

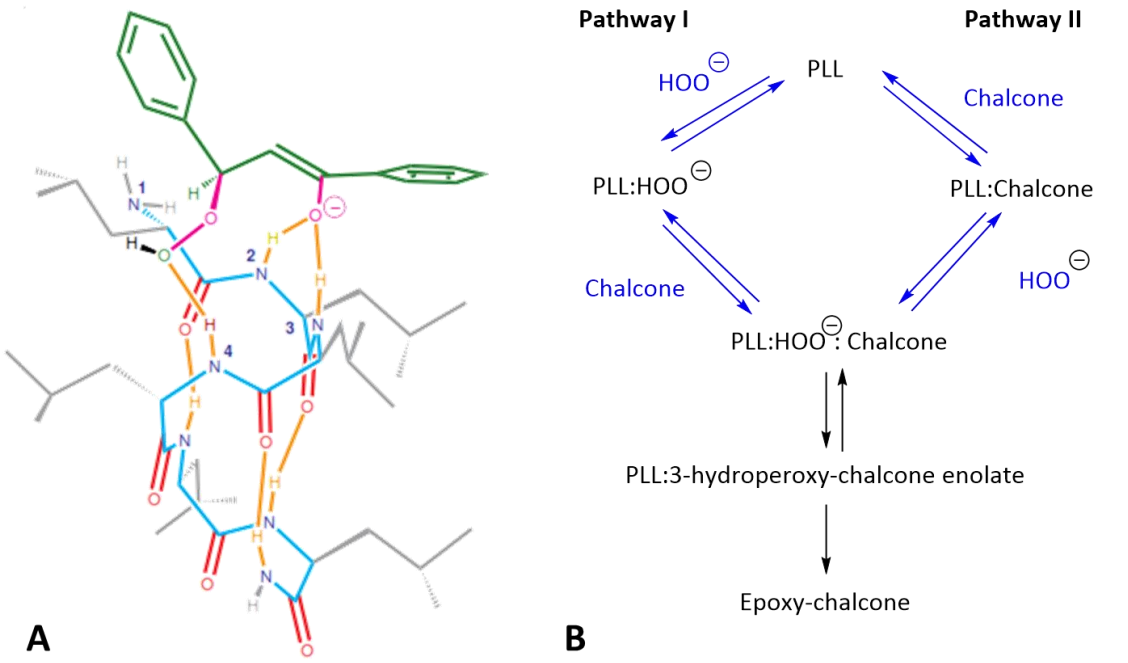


**Figure 1.16 A** – Stick bond depiction of a structure close to the transition state for epoxide formation taken from [88] and **B** – Kinetic scheme for chalcone epoxidation taken from [89].

### *1.3.2.2 One-pot Claisen-Schmidt Condensation / Juliá-Colonna Epoxidation Reaction*

The α,β-unsaturated ketones, the substrates for the Juliá-Colonna epoxidation reaction, can be easily obtained using Claisen-Schmidt condensation reaction in either acidic or basic medium; thus, a combination of these two reactions seems viable from the industrial point of view. Briefly, Claisen-Schmidt condensation reaction is a sequel of the aldol addition reaction presented in Section 1.3.1 when the aldol product is dehydrated to obtain the corresponding unsaturated ketone.

Although literature presents only six catalytic systems active in the one-pot Claisen-Schmidt condensation/Juliá-Colonna epoxidation reaction, only two of them are heterogeneous systems. The first catalytic system for this one-pot reaction was reported in 2004 by Choudary *et al.* who used a bifunctional nanomagnesium oxide, but the conversion and enantioselectivity were moderate [90]. Later, Wang *et al.* proposed a homogeneous system where the aldehyde and ketone were treated with an aqueous potassium hydroxide solution to yield the corresponding enone, and then a quaternary ammonium salt and trichloroisocyanuric acid were added to afford the corresponding epoxy ketone [91]. Dai *et al.* used a two-step homogeneous system: in the first case the condensation reaction was carried out in MeOH and aqueous NaOH and afterwards $H_2O_2$ was added and the epoxidation reaction was performed at 0 °C. The obtain yields were good, but the enantioselectivity was not studied [92].

Good to moderate yields were obtained by Li *et al.* who used ultrasound irradiation to obtain the corresponding epoxy ketones [93]. Liu *et al.* carried out the first part of the reaction in homogeneous medium and added afterwards poly-L-leucine for the asymmetric epoxidation. Though the polymer was recycled, the system is not completely heterogeneous and the process requires longer reaction time [94]. The most recent study was done by Ngo *et al.* who carried out the condensation reaction in methanol and aqueous NaOH and the epoxidation reaction at 0 °C and 30 % $H_2O_2$ [95].

### 1.3.3 Catalysis of Nanohybrid Materials Based on AA/HT & PAA/HT

Despite the widely use of hydrotalcite-like materials and of amino acids and poly-amino acids in catalysis, the nanohybrid materials based on these components did not receive too much attention. Choudary *et al.* used L-proline immobilized into HT (by either anionic exchange or coprecipitation method) in different asymmetric C-C bond formation reactions: aldol condensation, Henry reaction, Michael reaction, and cyanosilylation. In the first case (Scheme 1.7 (a)), they studied the reactivity of acetone with different aldehydes (both aromatic and aliphatic) and observed that although high yields were obtained after 24 h, the enantioselectivity was very law. Similar results were achieved when the materials were used in the Henry reaction – a carbonyl group reacts with a nitro group to give a nitro alcohol (Scheme 1.7 (b)) - and in the Michael reaction (Scheme 1.7 (c)) – the nucleophilic addition of a carbanion to an α,β-unsaturated carbonyl compound. Total conversion but poor enantioselectivity was obtained in the reaction between *p*-nitro benzaldehyde with trimethylsilylcyanide (Scheme 1.7 (d)) [54].

## 1 Introduction

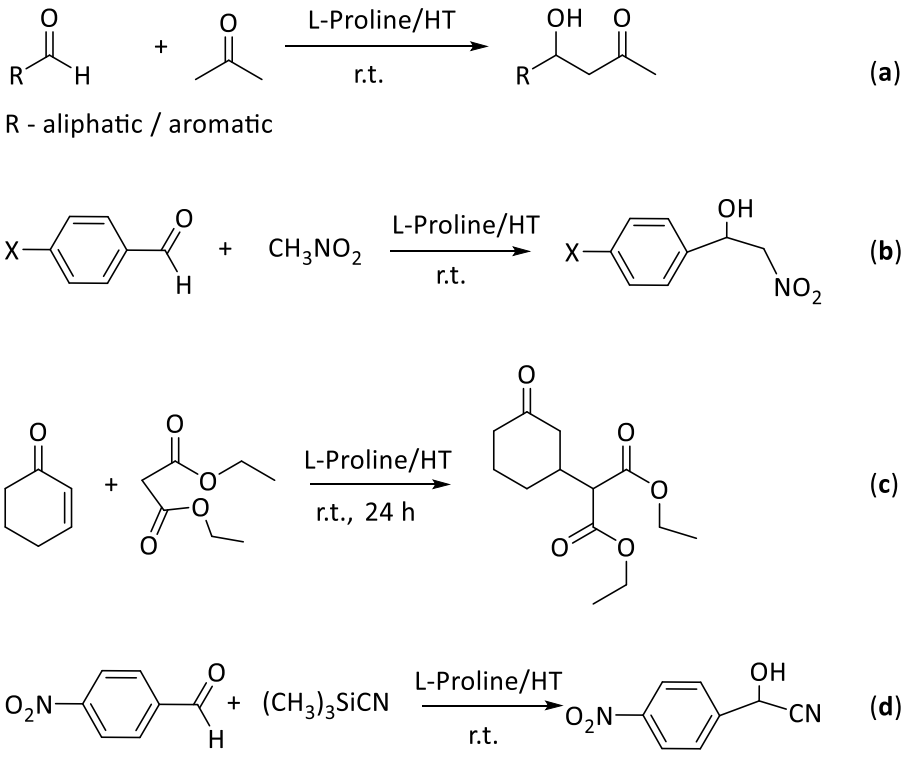


**Scheme 1.7** Asymmetric C-C bond-forming reactions catalysed by L-proline/HT

Better results (up to 89% yield and 94% ee) in the aldol condensation reaction between benzaldehyde and acetone were obtained by An *et al.* who used a catalyst based on L-proline immobilized into HT Mg-Al 3:1 by reconstruction method. The proposed mechanism starts with the diffusion of the reagents into the interlayer space of the nanohybrid, where they interact with the L-proline anions. The entire catalytic process takes place inside the interlayer space and the enantioselectivity of the final product was explained by a metal-free version of the Zimmerman-Traxler transition state (Figure 1.17) [73].

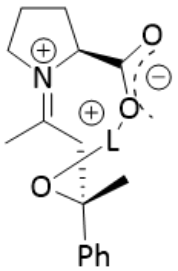


**Figure 1.17** Metal-free version of the Zimmerman-Traxler transition state

A similar material was used by Vijaikumar *et al.* in the Michael addition reaction between β-nitrostyrene and acetone and the reaction between nitromethane and benzylideneacetone, obtaining good conversions and moderate to good enantioselectivities. Compared to previous studies, a more detailed explanation on the mechanism of reaction was given; for example, the

reaction between β-nitrostyrene and acetone is governed by an enamine-type catalysis, while the second reaction by an iminium-type catalysis (Figure 1.18) [74].

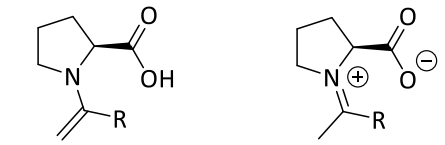


**Figure 1.18** Modes of action in proline-catalysis

L-leucine immobilized into HT Mg-Al 2:1 through anionic exchange method was used by Miranda *et al.* in the Juliá-Colonna epoxidation reaction of chalcone (Scheme 1.8), in a typical triphasic system: co-catalysts (tetrabutylammonium bromide -TBAB), catalyst and $HOO^-$. Even though a low enantioselectivity was achieved, it was reported that the ee% is directly related to the L-leucine/$Al^{3+}$ molar ratio, the best results being obtained when the AA was found in the interlayer of the AA at 1.9 molar ratio L-leucine/$Al^{3+}$ [70].

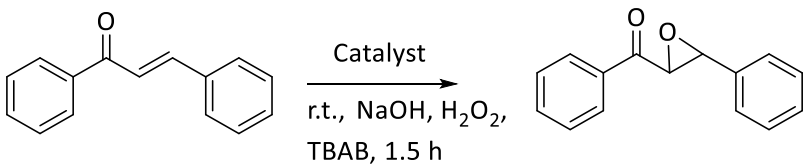


**Scheme 1.8** Juliá-Colonna epoxidation of chalcone

Until the present moment, there was only one work focused on the use of poly-L-leucine immobilized into HT in catalysis. Miranda *et al.* studied this catalyst in the Juliá-Colonna epoxidation of different α,β-unsaturated carbonyl compounds and attained very good yields and moderate to good enantioselectivities. The materials proved to be very stable after 5 consecutive runs, without any apparent deactivation [77].

## 1.4 Green Chemistry

Over decades, chemistry and chemical engineering have been developed and optimized to assure the best time-space yield. Starting with the 90's, sustainable or green chemistry has been emerging as a new branch of chemistry, with the recognition that the production, processing, use, and eventual disposal of chemical products may cause harm to both people and environment.

Paul Anastas, the director of the US EPA and John C. Warner, from Polaroid Corporation have published in 1998 a set of 12 principles which represent the foundation stone of what we know today as Green Chemistry [96]:

**1. Prevention** - It is better to prevent waste than to treat or clean up waste after it is formed.

**2. Atom Economy** - Synthetic methods should be designed to maximize the incorporation of all materials used in the process into the final product.

**3. Less Hazardous Chemical Synthesis** - Whenever practicable, synthetic methodologies should be designed to use and generate substances that possess little or no toxicity to human health and the environment.

**4. Designing Safer Chemicals** - Chemical products should be designed to preserve efficacy of the function while reducing toxicity.

**5. Safer Solvents and Auxiliaries** - The use of auxiliary substances (solvents, separation agents, etc.) should be made unnecessary whenever possible and, when used, innocuous.

**6. Design for Energy Efficiency** - Energy requirements should be recognized for their environmental and economic impacts and should be minimized. Synthetic methods should be conducted at ambient temperature and pressure.

**7. Use of Renewable Feedstocks -** A raw material or feedstock should be renewable rather than depleting whenever technically and economically practical.

**8. Reduce Derivatives** - Unnecessary derivatization (blocking group, protection/ deprotection, temporary modification of physical/chemical processes) should be avoided whenever possible.

**9. Catalysis -** Catalytic reagents (as selective as possible) are superior to stoichiometric reagents.

**10. Design for Degradation** - Chemical products should be designed so that at the end of their function they do not persist in the environment and instead break down into innocuous degradation products.

**11. Real-time Analysis for Pollution Prevention** - Analytical methodologies need to be further developed to allow for real-time in-process monitoring and control prior to the formation of hazardous substances.

**12. Inherently Safer Chemistry for Accident Prevention** - Substance and the form of a substance used in a chemical process should be chosen so as to minimize the potential for chemical accidents, including releases, explosions, and fires.

No matter the reaction under study, the development of green methods is focused on three main aspects: the choice of solvent, eliminating any corrosive/harming reagents, and the development of new greener catalysts, active in multistep reactions.

The solvent of choice for green chemistry is water which is non-toxic, but which limits the chemical compatibility. Although there are a huge number of chemical reactions that can be carried out in water [97], many reactants are still incompatible with water (e.g. Organometallic compounds). A better alternative is the use of neat conditions [98] or supercritical $CO_2$ [99].

Eliminating reagents might be a very difficult process, thus scientists have focused on producing them *in-situ*, avoiding exposure to any extra hazards. One important example is the direct production of $H_2O_2$ via the anthraquinone route, formic acid or from $H_2$ and $O_2$ over Pd or Pd-Au catalysts [100]. Even though the large-scale application of hydrogen peroxide direct production from $H_2$ and $O_2$ is still limited, the process presents obvious advantages like: no intermediate purification, no separation steps, reduction of operational costs, etc.

In the end, it is important to underline that a suitable catalyst for green chemistry has to satisfy the following properties: non-toxic, easily recovered, reusable, no leaching and last but not the least, economical in terms of both production and usage.

## 1.5 Aim of the Thesis

Despite the large number of articles published in the field of asymmetric heterogeneous catalysis, there are still reactions to be studied, catalysts to be developed, and mechanisms to be revealed.

In this context, the objectives of the present thesis can be summarized as it follows: i) the development of new catalytic systems for the production of chiral substances with potential applications in pharmaceutics and/or perfumery, ii) the understanding of the subsequent reaction mechanisms, and iii) the design of greener sustainable processes.

The hybrid catalyst based on L-leucine immobilized into hydrotalcites proved to be more active in the aldol addition reaction of cyclohexanone with aromatic aldehydes than the corresponding constituents. Section 2 provides information on how diastereoselectivity and enantioselectivity of the aldol product can be modulated using different synthesis protocols and different reactions conditions. Moreover, the mechanism of reaction discloses a simultaneous activity of the two parts of the catalyst: the hydrotalcite and the immobilized L-Leu. If, in general, the free amino acid favours the formation of the *anti*-isomer, the presence of the basic HT leads to the formation of the *syn*-isomer.

Section 3 focuses on the one-pot Claisen-Schmidt condensation/Juliá-Colonna epoxidation reaction catalysed by poly-L-leucine immobilized into rehydrated hydrotalcites. This catalytic system did not require any pre-activation and was easily recovered and recycled for four consecutive runs without losing its catalytic efficiency in terms of conversion, total selectivity towards the corresponding epoxy-chalcones and excellent enantioselectivity.

In the last decade, quartz crystal microbalance with dissipation (QCM-D) has been successfully used to study polymers behaviour at various solid/liquid interfaces. This analysis provides important information not only on the variations in mass, thickness, and rigidity of the

polymer, but also on its viscoelastic properties. Section 4 presents the use of QCM-D for the *in-situ* monitoring of Juliá-Colonna epoxidation reaction, offering an alternative rationalization for the viability of the preferred catalytic pathway.

A sustainable and green process implies not only the elimination of any hazardous reagent, but also the *in-situ* production of any of the reaction intermediates. One of these reagents is hydrogen peroxide, known as an extremely aggressive oxidizer which can corrode many materials (including skin), frequently used in the Juliá-Colonna epoxidation reaction. Section 5 demonstrates that the *in-situ* produced $H_2O_2$ from $H_2$ and $O_2$ can be used in chalcone epoxidation reaction.

Last but not the least, Section 6 summarizes the main results of the thesis along with an outlook on the use of graphene-hydrotalcite based catalysts in the Claisen-Schmidt condensation, Juliá-Colonna epoxidation, and *in-situ* production of $H_2O_2$.

# Bibliography

[1] A. Guijarro, M. Yus, *The Origin of Chirality in the Molecules of Life : A Revision from Awareness to the Current Theories and Perspectives of this Unsolved Problem*, RSC Publishing **2008**.

[2] D.F. Arago, *Mémoires de l'Institut National des Sciences Mathématiques et Physiques*, **1**, 93-134, **1811**.

[3] J.B. Biot, *Bulletin de la Société Philomathique de Paris*, **5**, 190-192, **1815**.

[4] J.W.F. Herschel, *Transactions of the Cambridge Philosophical Society*, **1**, 43-50, **1822**.

[5] R.A. Hegstrom, D.K. Kondepudi, *Scientific American*, 108-115, **1990**.

[6] W.H. Perkin, *Journal of the Chemical Society*, **20**, 138-160, **1867**.

[7] J.A. LeBel, *Bulletin de la Societe Chimique de France*, **22**, 337-347, **1874**.

[8] J.H.v.t. Hoff, *Archives Neerlandaises des Sciences Exactes et Naturelles*, **9**, 445-454, **1874**.

[9] W.T. Astbury, *Proceedings of the Royal Society of London Series A*, **102**, 506-530, **1923**.

[10] J.M. Bijvoet, A.F. Peerdeman, A.J.v. Bommel, *Nature*, **168**, 271-272, **1951**.

[11] M. Avalos, R. Babiano, P. Cintas, J.L. Jiménez, J.C. Palacios, *Chemical Communications (Cambridge)*, 887-892, **2000**.

[12] T.J. Leitereg, D.G. Guadagni, J. Harris, T.R. Mon, R. Teranishi, *Journal of Agricultural and Food Chemistry*, **19**, 785-787, **1971**.

[13] L. Friedman, J.G. Miller, *Science*, **172**, 1044-1046, **1971**.

[14] G.F. Russell, J.I. Hills, *Science*, **172**, 1043-1044, **1971**.

[15] K. Ikeda, *Journal of the Chemical Society of Tokyo*, **30**, 820-836, **1909**.

[16] S.A. Kohlhoff, R. Sharma, *Expert Opinion on Investigational Drugs*, **16**, 1441-1448, **2007**.

[17] J.R. Cossy, *1.1 Introduction: The Importance of Chirality in Drugs and Agrochemicals*, in: Comprehensive Chirality, Elsevier 1-7, **2012**.

[18] B. Sharma, *Journal of Xenobiotics*, **4**, 2272-2291, **2014**.

[19] C. Arróniz, C. Escolano, *Strategies for the synthesis of enantiopure compounds focused on organocatalysis*, in: Recent Advances in Pharmaceutical Sciences 115-134, **2012**.

[20] B. Schuur, A.B.d. Haan, M. Kaspereit, M. Leeman, *2.52 – Chiral Separations*, in: M. Moo-Young (Ed.) Comprehensive Biotechnology, 737–751, **2011**.

[21] V. Andrushko, N. Andrushko, *Stereoselective synthesis of drugs and natural products*, **2013**.

[22] R. Noyori, *Angewandte Chemie International Edition*, **41**, 2008-2022, **2002**.

[23] H.B. Kagan, *Chiral ligands for asymmetrie catalysis*, in: J.D. Morrison (Ed.) Asymmetric synthesis, 1-3, **1985**.

[24] M.T. Reetz, *Journal of American Chemical Society*, **135**, 12480−12496, **2013**.

[25] L.M. Pera, M.D. Baigori, A. Pandey, G.R. Castro, *Biocatalysis*, in: Industrial biorefineries and white biotechnology, Elsevier, 391-408, **2015**.

[26] J.v. Liebig, *Justus Liebigs Annalen der Chemie*, **113**, 246-247, **1860**.

[27] G. Bredig, W.S. Fiske, *Biochemische Zeitschrift*, **46**, 7-23, **1912**.

[28] U.-H. Dolling, P. Davis, E.J.J. Grabowski, *Journal of American Chemical Society*, **106**, 446-447, **1984**.

[29] M.S. Sigman, E.N. Jacobsen, *Journal of American Chemical Society*, **120**, 4901-4902, **1998**.

[30] B. List, R.A. Lerner, C.F.B. III, *Journal of American Chemical Society*, **122**, 2395-2396, **2000**.

[31] K.A. Ahrendt, C.J. Borths, D.W.C. MacMillan, *Journal of American Chemical Society*, **122**, 4243-4244, **2000**.

[32] H.U. Blaser, E. Schmidt, *Asymmetric Catalysis on Industrial Scale: Challenges, Approaches and Solutions*, Wiley-VCH Verlag GmbH & Co. KGaA, **2004**.

[33] H. Gröger, in: Ernst Schering Foundation Symposium Proceedings ''Organocatalysis'', 227-258, **2007**.

[34] C.A. Busacca, D.R. Fandrick, J.J. Song, C.H. Senanayake, *Advanced Synthesis & Catalysis*, **353**, 1825-1864, **2011**.

[35] V. Blanco, A. Carlone, K.D. Hänni, D.A. Leigh, *Angewandte Chemie International Edition*, **51**, 5166-5169, **2012**.

[36] J. Alemán, S. Cabrera, *Chemical Society Reviews*, **42**, 774-793, **2013**.

[37] M. Nanko, *Advances in Technology of Materials and Materials Processing*, **11**, 1-8, **2009**.

[38] E. Ruiz-Hitzky, M. Darder, P. Aranda, *An Introduction to Bio-nanohybrid Materials*, in: Bio-inorganic Hybrid Nanomaterials, WILEY-VCH Verlag GmbH & Co. KGaA, **2008**.

[39] J.-H. Choy, S.-J. Choi, J.-M. Oh, T. Park, *Applied Clay Science*, **36**, 122–132, **2007**.

[40] A.I. Ruiz, M. Darder, P. Aranda, R. Jiménez, H.V. Damme, E. Ruiz-Hitzky, *Journal of Nanoscience and Nanotechnology*, **6**, 1602-1610, **2006**.

[41] K.A. Carrado, *Introduction: Clay Structure, Surface Acidity, and Catalysis*, in: Handbook of Layered Materials, Marcel Dekker, Inc, **2004**.

[42] M.F. Brigatti, E. Galan, B.K.G. Theng, *Structures and minerology of clay minerals*, in: Handbook of clay ccience, 19-86, **2006**.

[43] E. Ruiz-Hitzky, P. Aranda, M. Darder, *Hybrid and biohybrid Materials based on layered clays*, in: Tailored organic–inorganic materials, John Wiley & Sons, 245-297, **2015**.

[44] U. Costantino, M. Nocchetti, G. Gorrasi, L. Tammaro, *Hydrotalcites in nanobiocomposites*, in: J. Lagarón (Ed.) Multifunctional and Nanoreinforced Polymers for Food Packaging, Woodhead Publishing, 44-85, **2011**.

[45] S.P. Newman, W. Jones, *New Journal of Chemistry*, 105-115, **1998**.

[46] A.S. Bookin, V.A. Drits, *Clays and Clay Minerals*, **41**, 551-557, **1993**.

[47] A.S. Bookin, V.I. Cherkashin, V.A. Drits, *Clays and Clay Minerals*, **41**, 558-564, **1993**.

[48] P.S. Braterman, Z.P. Xu, F. Yarberry, *Layered double hydroxides* in: Handbook of layered materials Marcel Dekker, Inc., **2004**.

[49] F. Cavani, F. Trifirò, A. Vaccari, *Catalysis Today*, **11**, 173-301, **1991**.

[50] T. Lopez, P. Bosch, E. Ramos, R. Gomez, O. Novaro, D. Acosta, F. Figueras, *Langmuir*, **12**, 189-192, **1996**.

[51] C. Forano, U. Costantino, V. Prévot, C.T. Gueho, *Layered double hydroxides (LDH)*, in: Handbook of Clay Science, 745-782, **2013**.

[52] N.T. Whilton, P.J. Vickers, S. Mann, *Journal of Materials Chemistry*, **7**, 1623–1629, **1997**.

[53] S. Aisawa, S. Takahashi, W. Ogasawara, Y. Umetsu, E. Narita, *Journal of Solid State Chemistry*, **162**, 52-62 **2001**.

[54] B.M. Choudary, B. Kavita, N.S. Chowdari, B. Sreedhar, M.L. Kantam, *Catalysis Letters*, **78**, 373-377, **2002**.

[55] T. Hibino, *Chemistry of Materials*, **16**, 5482-5488, **2004**.

[56] S.P. Newman, T.D. Cristina, P.V. Coveney, *Langmuir*, **18**, 2933-2939, **2002**.

[57] Q. Yuan, M. Wei, D.G. Evans, X. Duan, *Journal of Physical Chemistry B*, **108**, 12381-12387, **2004**.

[58] Q. Yuan, M. Wei, Z. Wang, G. Wang, X. Duan, *Clays and Clay Minerals*, **52**, 40–46, **2004**.

[59] M. Wei, Q. Yuan, D.G. Evans, Z. Wang, X. Duan, *Journal of Materials Chemistry*, **15**, 1197-1203, **2005**.

[60] M. Wei, Z. Shi, D.G. Evans, X. Duan, *Journal of Materials Chemistry*, **16**, 2102-2109, **2006**.

[61] M. Wei, J. Guo, Z. Shi, Q. Yuan, M. Pu, G. Rao, X. Duan, *Journal of Materials Science*, **42**, 2684-2689, **2007**.

[62] Q. Chen, S. Shi, X. Liu, L. Jin, M. Wei, *Chemical Engineering Journal*, **153**, 175-182, **2009**.

[63] M.X. Reinholdt, R.J. Kirkpatrick, *Chemistry of Materials*, **18**, 2567-2576, **2006**.

[64] M.X. Reinholdt, P.K. Babu, R.J. Kirkpatrick, *The Journal of Physical Chemistry C*, **113**, 3378–3381, **2009**.

[65] J.F.N. Filho, F. Leroux, V. Verney, J.B. Valim, *Applied Clay Science*, **55**, 88-93, **2012**.

[66] H. Liu, L. Zhao, J. Wang, J. He, *Journal of Catalysis*, **298**, 70-76, **2013**.

[67] Å. Fudala, I. Pálinkó, B. Hrivnák, I. Kiricsi, *Journal of Thermal Analysis and Calorimetry*, **56**, 317-322, **1999**.

[68] Á. Fudala, I. Pálinkó, I. Kiricsi, *Journal of Molecular Structure*, **482-483**, 33-37, **1999**.

[69] Á. Fudala, I. Pálinkó, I. Kiricsi, *Inorganic Chemistry*, **38**, 4653-4658, **1999**.

[70] R.-A. Miranda, J. Llorca, E. Finocchio, G. Ramis, F. Medina, J.E. Sueiras, A.M. Segarra, *Catalysis Today*, **177**, 48-52, **2011**.

[71] H. Nakayama, N. Wada, M. Tsuhako, *International Journal of Pharmaceutics*, **269**, 469–478, **2004**.

[72] S. Aisawa, H. Kudo, T. Hoshi, S. Takahashi, H. Hirahara, Y. Umetsu, E. Narita, *Journal of Solid State Chemistry*, **177**, 3987–3994, **2004**.

[73] Z. An, W. Zhang, H. Shi, J. He, *Journal of Catalysis*, **241**, 319-327, **2006**.

[74] S. Vijaikumar, A. Dhakshinamoorthy, K. Pitchumani, *Applied Catalysis A: General*, **340**, 25–32, **2008**.

[75] S. Aisawa, S. Sasaki, S. Takahashi, H. Hirahara, H. Nakayama, E. Narita, *Journal of Physics and Chemistry of Solids*, **67**, 920–925, **2006**.

[76] R.J. Chimentão, S. Abelló, F. Medina, J. Llorca, J.E. Sueiras, Y. Cesteros, P. Salagre, *Journal of Catalysis*, **252**, 249–257, **2007**.

[77] R.-A. Miranda, J. Llorca, F. Medina, J.E. Sueiras, A.M. Segarra, *Journal of Catalysis*, **282**, 65-73, **2011**.

[78] R.-A. Miranda, E. Finocchio, J. Llorca, F. Medina, G. Ramis, J.E. Sueiras, A.M. Segarra, *Physical Chemistry Chemical Physics*, **15**, 15645-15659, **2013**.

[79] Y. Wang, P. Wu, Y. Li, N. Zhu, Z. Dang, *Journal of Colloid and Interface Science*, **394**, 564-572, **2013**.

[80] T. Kanemitsu, A. Umehara, M. Miyazaki, K. Nagata, T. Itoh, *European Journal of Organic Chemistry*, 993–997, **2011**.

[81] S. Colonna, H. Molinari, S. Banfi, S. Juliá, J. Masana, A. Alvarez, *Tetrahedron*, **39**, 1635-1641, **1983**.

[82] T. Geller, S.M. Roberts, *Journal of the Chemical Society, Perkin Transactions 1*, 1397-1398, **1999**.

[83] T. Geller, A. Gerlach, C.M. Krüger, H.-C. Militzer, *Journal of Molecular Catalysis A: Chemical*, **251**, 71-77, **2006**.

[84] D.R. Kelly, E. Caroff, R.W. Flood, W. Heal, S.M. Roberts, *Chemical Communications*, 2016-2017, **2004**.

[85] K. Okuyama, N. Tanaka, M. Doi, M. Narita, *The Bulletin of the Chemical Society of Japan*, **61**, 3115-3120, **1988**.

[86] A. Berkessel, N. Gasch, K. Glaubitz, C. Koch, *Organic Letters*, **3**, 3839-3842, **2001**.

[87] D.R. Kelly, S.M. Roberts, *Biopolymers (Peptide Science)*, **84**, 74-89, **2006**.

[88] G. Carrea, S. Colonna, D.R. Kelly, A. Lazcano, G. Ottolina, S.M. Roberts, *Trends in Biotechnology*, **23**, 507-513, **2005**.

[89] S.P. Mathew, S. Gunathilagan, S.M. Roberts, D.G. Blackmond, *Organic Letters*, **7**, 4847-4850, **2005**.

[90] B.M. Choudary, M.L. Kantam, K.V.S. Ranganath, K. Mahendar, B. Sreedhar, *Journal of American Chemical Society*, **126**, 3396-3397, **2004**.

[91] Y. Wang, J. Ye, X. Liang, *Advanced Synthesis & Catalysis*, **349**, 1033-1036, **2007**.

[92] L.-Z. Dai, M. Shi, *Tetrahedron Letters*, **50**, 651-655, **2009**.

[93] J.-T. Li, Y. Yin, M.-X. Sun, *Ultrasonics Sonochemistry*, **17**, 363-366, **2010**.

[94] W. Luo, Z. Yu, W. Qiu, F. Yang, X. Liu, J. Tang, *Tetrahedron*, **67**, 5289-5292, **2011**.

[95] D. Ngo, M. Kalala, V. Hogan, R. Manchanayakage, *Tetrahedron Letters*, **55**, 4496-4500, **2014**.

[96] P. Anastas, J. Warner, *Green chemistry: Theory and practice*, Oxford University Press, Oxford, UK, **2000**.

[97] M. Raj, V.K. Singh, *Chemical Communications (Cambridge)*, 6687-6703, **2009**.

[98] N. Shapiro, M. Kramer, I. Goldberg, A. Vigalok, *Green Chemistry*, **12**, 582-584, **2010**.

[99] S. Mayadevi, *Inidan Journal of Chemistry*, **51A**, 1298-1305, **2012**.

[100] B. Puértolas, A.K. Hill, T. García, B. Solsona, L. Torrente-Murciano, *Catalysis Today*, **248**, 115-127, **2015**.

# 1 Introduction

# 2 Bio-nanohybrid Catalysts Based on L-leucine Immobilized in Hydrotalcite and Their Activity in Aldol Reaction

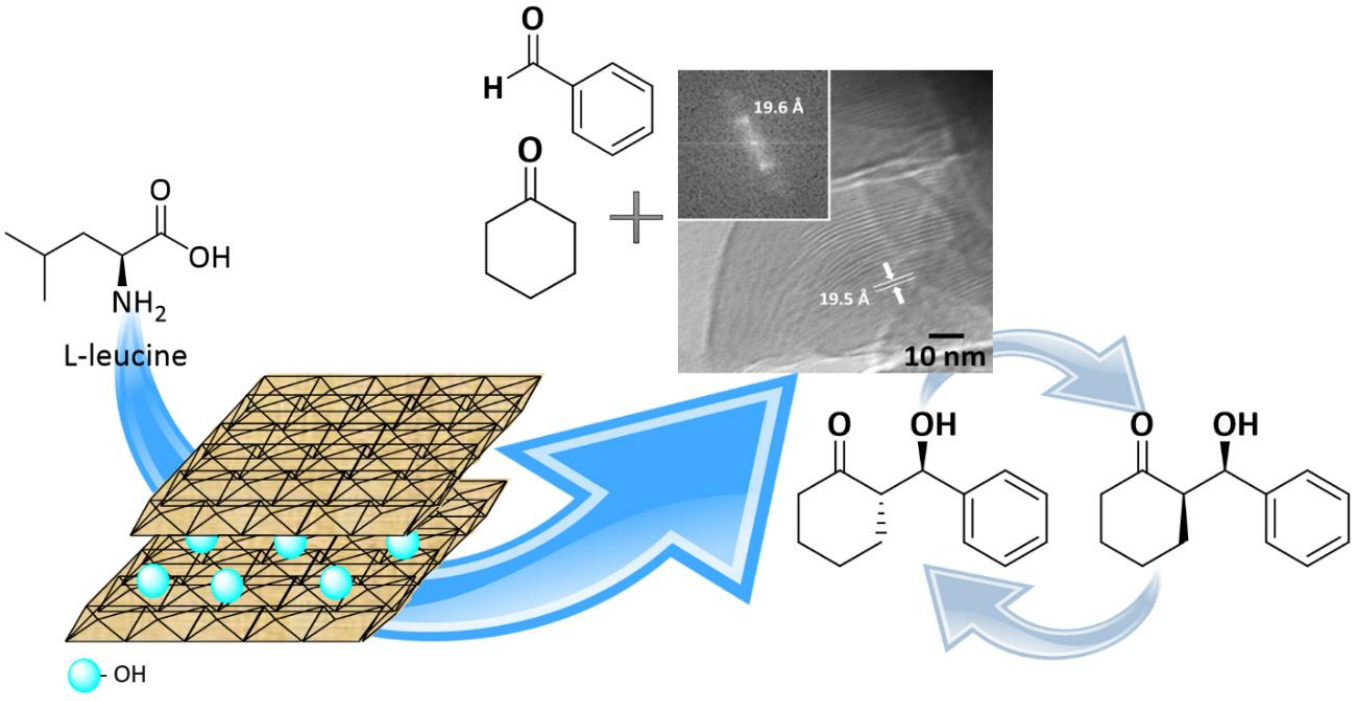


Dana-Georgiana Crivoi, Ronald-Alexander Miranda, Elisabetta Finocchio, Jordi Llorca, Gianguido Ramis, Jesús E. Sueiras, Anna M. Segarra and Francisco Medina, *Applied Catalysis A: General*, **2016**, 519, 116-129

## 2.1 Introduction

Nowadays, considerable attention is focused on the synthesis of nanohybrid materials, which exhibit new and better properties than the corresponding constituent materials. Research into and understanding the organic/inorganic interaction between bioactive molecules and the surface of inorganic materials have led to their use in many biochemical applications [1] or as catalysts [2] and drug delivery carriers [3], although these interactions remain only partially understood. Many bioactive molecules (e.g. peptides, amino acids, proteins, etc.) are anions under neutral and basic pH, so they can easily be immobilized in positively charged solids. Examples of such solids are the hydrotalcites (HTs), a family of naturally occurring layered clays with low or null toxicity, good biocompatibility and a high anion swelling capacity. These properties make HTs interesting materials for applications in the pharmaceutical field [4], cosmetics [5], catalysis [6] or even medical field [7].

The anionic exchange properties of HTs transform these materials in excellent candidates for the immobilization of amino acids (AAs). Starting with 1997 when Whilton *et al.* studied the immobilization of aspartic and glutamic acid in the interlayer space of layered double hydroxides through coprecipitation method [8], a series AAs have been immobilized into HT materials by means of three general methods: coprecipitation [9-12], anionic exchange [12-15] and reconstruction method [16, 17]. Regarding the nature of the interaction, it is now clear that the immobilization of AAs in HTs structures is pH-dependent, although other factors should be taken into account: the kind of HT, the synthesis and the physical and chemical properties of the AAs.

AAs are organocatalysts which display several advantages such as non-toxicity, easy manipulation and stability and have been widely used in the asymmetric aldol reaction [18]. For example, Córdova *et al*. obtained *anti* diastereoselectivity in a direct asymmetric aldol reaction between cyclohexanone and *p*-$NO_2$-benzaldehyde using a series of AAs [19]. Wu *et al.* used a threonine derivative in the aldol addition reaction, producing the *anti*-diastereomer when cyclohexanone was the substrate and *syn*-isomer in the case of hydroxyacetone [20]. Similar results were obtained by Barbas [21], Lu [22] and Gong [23]. Itoh *et al*. observed that in the presence of L-*t*-Leu compounds with *syn* diastereoselectivity were obtained in the case of cyclopentanone, cycloheptanone and cyclooctanone and with *anti* diastereoselectivity when cyclohexanone was used [24]. Thus, obtaining the *syn*-product when cyclohexanone is used as substrate seems to be a challenge. Moreover, AAs used in their natural form can react with aromatic aldehydes to form the corresponding immonium salts which, by decarboxylation, will form a stable side-product [24, 25].

In this study, we present the synthesis of nanohybrid materials based on L-Leu immobilized in HTs. We studied different synthetic procedures and their effects on the nature of the inorganic/organic interaction in order to evaluate: i) the role of the immobilization time on one hand, and the relationship between the immobilization speed and the strength and kind of basic centres in the HT on the other hand; ii) the role of the HT precursor in the immobilization process and iii) the nature of the AA structure in the immobilization process. To achieve this goal, the nanohybrid materials were synthesized using the anion-exchange and reconstruction method and the organic/inorganic interactions were investigated by EA, ICP, XRD, FT-IR, Raman, $^{13}C$, $^{27}Al$ MAS NMR and thermal evolution using TG/DTA analyses.

The new nanohybrid materials were tested in the aldol addition reaction of cyclohexanone with different aromatic aldehydes. The synergistic effect between the bio-organic guest (L-Leu) and the inorganic host (HTs) proved to play an important role in modulating both the diastereoselectivity and enantioselectivity of the final product. Herein, we report that the *anti-syn* selectivity depends not only on the nature of the catalyst but also on the solvent used.

## 2.2 Materials and Methods

### 2.2.1 General

All chemicals and solvents were commercially available (Aldrich Chemical, Fluka) and used without further purification/drying unless otherwise mentioned.

Molecular formulae were calculated from the results of elemental analyses (EA) and inductively coupled plasma analyses (ICP). EA were performed using an elemental analyser EA-1108 C.E. instrument from Thermo Fisher Scientific with a Mattler Toledo MX5 microbalance. The analyses were carried out using atropine as a standard and vanadium as an additive to facilitate combustion. ICP analyses were performed in an ICP-OES Spectro Arcos FHS16 Instrument.

The $N_2$-physisorption analysis of BET surface areas and average pore diameters were performed in a QuadStar Quantachrome surface analyser at 77 K. Before analysis all the samples were degassed in vacuum at 393 K for 12 h.

Powder X-ray diffraction (XRD) patterns of the samples were performed on a Bruker-AXS D8-Discover diffractometer with a 2θ angle ranging from 3° to 70°. The samples were dispersed onto a low background Si (510) sampler holder. The data were collected with an angular step of 0.03° at 5s per step and sample rotation. CuKα radiation (λ = 1.54056 Å) was obtained from a copper X-ray tube operated at 40 kV and 40 mA. The crystalline phases were identified using

JCPDS files. The interlayered spaces were analysed with the reflection bands of the (*003*) and (*006*) and calculated using the Bragg law.

Fourier transform infrared spectra (FT-IR) were recorded with Nicolet Nexus Fourier Transform instrument equipped with a DTGS KBr detector. Each analysis was performed using 100 scans in the range 4000 – 400 $cm^{-1}$. Pure powders diluted in KBr pressed disks (about 1% w/w) were used for the analysis of skeletal vibrations. OMNIC software provided by ThermoElectron Corporation was used for spectra analysis.

Raman spectra were obtained using a Renishaw Raman via reflex instrument. The polarized radiation (λ = 785 nm) of a Ranishaw diode laser of 500 mW was used. A Laica DM2500 optical microscope was used to determine the part of the sample analysed. The RamaScope was calibrated using a silicon wafer. The focus (maximum opening 100%) and power (50%) were carefully optimized in order not to alter the sample during measurement. The spectral resolution was 2 $cm^{-1}$ with an exposure time of 10 s and 5 accumulations for each run.

$^{13}C$ and $^{27}Al$ Magic Angle Spinning-Nuclear Magnetic Resonance (MAS-NMR) spectra were obtained on a Varian Mercury VXR-400S spectrometer operating at 104.2 MHz with a pulse width of 1 ms. A total of 4,000 scans were collected with a sweep width of 100 kHz and an acquisition time of 0.2 s. An acquisition delay of 1 s between successive accumulations was selected to avoid saturation effects. $^{13}C$-MAS NMR spectra were recollected using tetramethylsilane (TMS) as reference.

High-resolution transmission electron microscopy (HRTEM) was performed with a JEOL 2010F instrument equipped with a field emission source, working at an acceleration voltage of 200 kV. The point-to-point resolution of the microscope was 0.19 nm, and the resolution between lines was 0.14 nm.

Thermogravimetric Analyses and Differential Thermal Analyses (TGA/DTA) were measured on a TGA7 instrument from Perkin Elmer. The analyses were carried out using a sample amount of 10 mg in an $N_2$ atmosphere. The heating rate was 10 °C.$min^{-1}$ within the range 30 - 900 °C.

The products were characterized by $^{1}H$-NMR and $^{13}C$-NMR using a Varian NMR System 400 MHz and HPLC-DAD (Diode Array Detector G1315D) Agilent Technologies and HPLC-RID 10A (Refractive Index Detector) Shimadzu using CHIRALPACK IA column (250*4.6 mm ID).

### 2.2.2 Synthesis of Hydrotalcite Materials (HTs)

Mg-Al HTs (Mg/Al molar ratio 2) containing nitrates and chloride anions were synthesized by the coprecipitation method (using as starting materials the corresponding salts precursors) at room temperature and pH = 10. The materials obtained were named $HT_{NO3}$ and $HT_{Cl}$ respectively. After the drying process, $HT_{Cl}$ was sonicated for 1 hour, while $HT_{NO3}$ was decomposed by

calcination at 450 °C overnight in air. The calcined HT ($HT_{cc}$) was rehydrated in an inert atmosphere using decarbonated water and ultrasound treatment for 1 hour. The materials obtained were named $HT_{Clus}$ and $HT_{rus}$ respectively.

## 2.2.3 Synthesis of LL/HT Materials

### *2.2.3.1 Anionic Exchange Method (Method A)*

Two procedures were used to synthesize LL/$HT_x$-Ay materials, where x is the type of HT used ($HT_{rus}$ or $HT_{Clus}$) and y indicates the procedure followed. In the first case, 500 mg of HT was added to a solution containing 320 or 160 mg (2.4 or 1.2 mmol, respectively) of L-Leu. The mixture was stirred for 30 minutes at room temperature (method A1). In the second case, 500 mg of HT was added to a solution containing 840.4 mg (6.4 mmol) of L-Leu. The mixture was stirred for 3 hours at 80 °C (method A2). An Ar atmosphere and deionized-decarbonated water were used in all cases. Materials synthesized by the anionic exchange method were named LL/$HT_{rus}$-A1, LL/$HT_{Clus}$-A1, LL/$HT_{rus}$-A2 and LL/$HT_{Clus}$-A2.

### *2.2.3.2 Reconstruction Method (Method R)*

Two procedures were used to synthesize LL/$HT_x$-Ry materials (where x is the type of HT and y indicates the procedure followed), in both cases using 250 mg of $HT_{cc}$ added to a solution containing 736.9 mg (5.6 mmol) of L-Leu. In the first procedure, L-Leu-$HT_{cc}$ mixture was first treated by sonication for 1 hour and then the slurry was stirred for another 3 hours at 80 °C. The material obtained was named LL/$HT_{rus}$-R1 (method R1). Alternatively, $HT_{cc}$-L-Leu mixture was stirred for 3 hours at 80 °C (method R2). The material obtained was named LL/$HT_r$-R2. Table 2.1 summarizes the synthetic methods used in the present article.

**Table 2.1** Summary of the synthesis methods

| Method | Variations | Material |
|---|---|---|
| **Anionic exchange (A)**<br>*500 mg HT*<br>*L-Leu*<br>*HT = $HT_{rus}$ or $HT_{Cl}$* | A1<br>*30 min, r.t.*<br>*2.4 mmol L-Leu* | LL/$HT_{rus}$-A1<br>LL/$HT_{Clus}$-A1 |
| | A2<br>*3 h; 80 °C*<br>*6.4 mmol L-Leu* | LL/$HT_{rus}$-A2<br>LL/$HT_{Clus}$-A2 |
| **Reconstruction (R)**<br>*250 mg $HT_{cc}$*<br>*6.4 mmol L-Leu*<br>*80 °C, 3 h* | R1<br>*(previous sonication 1h)* | LL/$HT_{rus}$-R1 |
| | R2 | LL/$HT_r$-R2 |

### 2.2.4 Typical Procedure for the Aldol Reaction of Cyclohexanone

$H_2O$ (25 mmol) and cyclohexanone (1.5 mmol) were added to a mixture containing aldehyde (0.5 mmol), catalyst (2.5 mol % L-Leucine with respect to ketone) in DMSO (2 ml) or Toluene (2 ml) and the resulting mixture was stirred at room temperature. Due to its high boiling point, DMSO cannot be removed by vacuum distillation. In this context, DMSO was diluted by adding brine solution (NaCl solution) to: (i) facilitate the separation of aqueous and organic phases after adding $CH_2Cl_2$ and (ii) destroy any emulsion that might be formed during the extraction process. After a defined period of time, brine was added and the reaction mixture was extracted several times with $CH_2Cl_2$. The organic layer was dried with $MgSO_4$ and concentrated under vacuum. The reaction mixture was purified by column chromatography using silica gel and hexane/ethyl acetate 3/1 as eluent. The conversion was determined by either isolation or $^1$H-NMR analysis and the enantiomeric excess by HPLC analysis.

## 2.3 Results and Discussion

### 2.3.1 Catalyst Characterization

#### *2.3.1.1 Textural Properties of HT and LL/HT Materials*

Nanohybrid materials based on L-Leu and HTs were synthesized by two methods (anion-exchange and reconstruction) to understand the nature of immobilized L-Leu in the HT structure: the location and ionic state of this AA. Table 2.2 shows the L-Leu/Al molar ratio, BET surface area and interlayer space of the different HTs and nanohybrid materials synthesized.

**Table 2.2** Characterization data of HT and LL/HT materials

| Entry | Material | L-Leu/Al molar ratio[a] | Interlayer space $d_{003}$ (Å)[b] | Gallery height (Å)[c] | BET surface area ($m^2/g$) |
|---|---|---|---|---|---|
| **1** | $HT_{NO3}$ | - | 8.4 | 3.6 | 56 |
| **2** | $HT_{cc}$ | - | - | - | 188 |
| **3** | $HT_{rus}$ | - | 7.7 | 2.9 | 40 |
| **4** | $HT_{Clus}$ | - | 7.9 | 3.1 | 55 |
| **5** | LL/$HT_{rus}$-A1 | 0.44 | 7.7 | 2.9 | 12 |
| **6** | LL/$HT_{Clus}$-A1 | 0.04 | 7.9 | 3.1 | 43 |
| **7** | LL/$HT_{rus}$-A2 | 1.09 | 19.5 | 14.3 | 14 |
| **8** | LL/$HT_{Clus}$-A2 | 0.16 | 7.9 | 3.1 | 30 |
| **9** | LL/$HT_{rus}$-R1 | 0.95 | 20.0 | 15.2 | 10 |
| **10** | LL/$HT_r$-R2 | 0.92 | 21.2 | 16.4 | 8 |

[a]Calculated by EA and ICP analysis. [b]In all cases, the materials obtained exhibit the characteristic diffraction peaks of the meixnerite structure (JCPDS 35-0965).[c]Gallery height was calculated on the basis of Aisawa *et al.* calculations [9] where the Mg/Al layer has a total height of 4.8 Å.

Cavani *et al.* explained that the introduction of large anionic species in the interlayer space of a hydrotalcite material, either by anionic exchange method or reconstruction method, will be reflected in an increase in the interlayer space of the HT [26]. In accordance with Cavani's findings, we have observed an increase in the HT's gallery height in all the materials where the L-Leu was immobilized inside the hydrotalcite (entries 7, 9 and 10, Table 2.2). When the anionic exchange method was used at room temperature for 30 minutes (LL/$HT_{rus}$-A1 material) no increase in the gallery height of the support was observed, even though a ratio of 0.44 L-Leu/$Al^{3+}$ was obtained (entry 5, Table 2.2). This demonstrates that the AA was preferably immobilized on the edges of the $HT_{rus}$ layers. An increase in the amount of immobilized AA will produce a loss of crystallinity, observed in the XRD patterns presented in the Appendix B – Figure B.1.

Increasing the time and temperature of synthesis to obtain LL/$HT_{rus}$-A2 increased the amount of immobilized L-Leu to 1.09 mol L-Leu/mol $Al^{3+}$, producing an interlayer space to 19.5 Å (entry 7, Table 2.2). This finding shows that both time and temperature have an effect on the swelling of the HT structure, allowing the immobilization of L-Leu molecules in its interlayer space. The loss of crystallinity in all nanohybrid materials was due to the decrease of the layers' lengths by the ultrasound effect.

The same conclusions can be withdrawn from the HRTEM images of the precursor and the nanohybrid materials. In the case of $HT_{rus}$, the image shows aggregated layers up to about 100 nm in length, with an interlayer space around 7.6 Å as deduced by FT analysis (Figure 2.1-A). The LL/$HT_{rus}$-A1 material (Figure 2.1-B) has a similar morphology as the $HT_{rus}$, demonstrating once again that using method A1 the L-Leu is not found inside the HT layers, but on the edges. The distinctive morphology observed in the case of LL/$HT_{rus}$-A2 (Figure 2.1-C) compared to that of $HT_{rus}$ proves the intercalation of the LL inside the layers and not on the edges of the material.

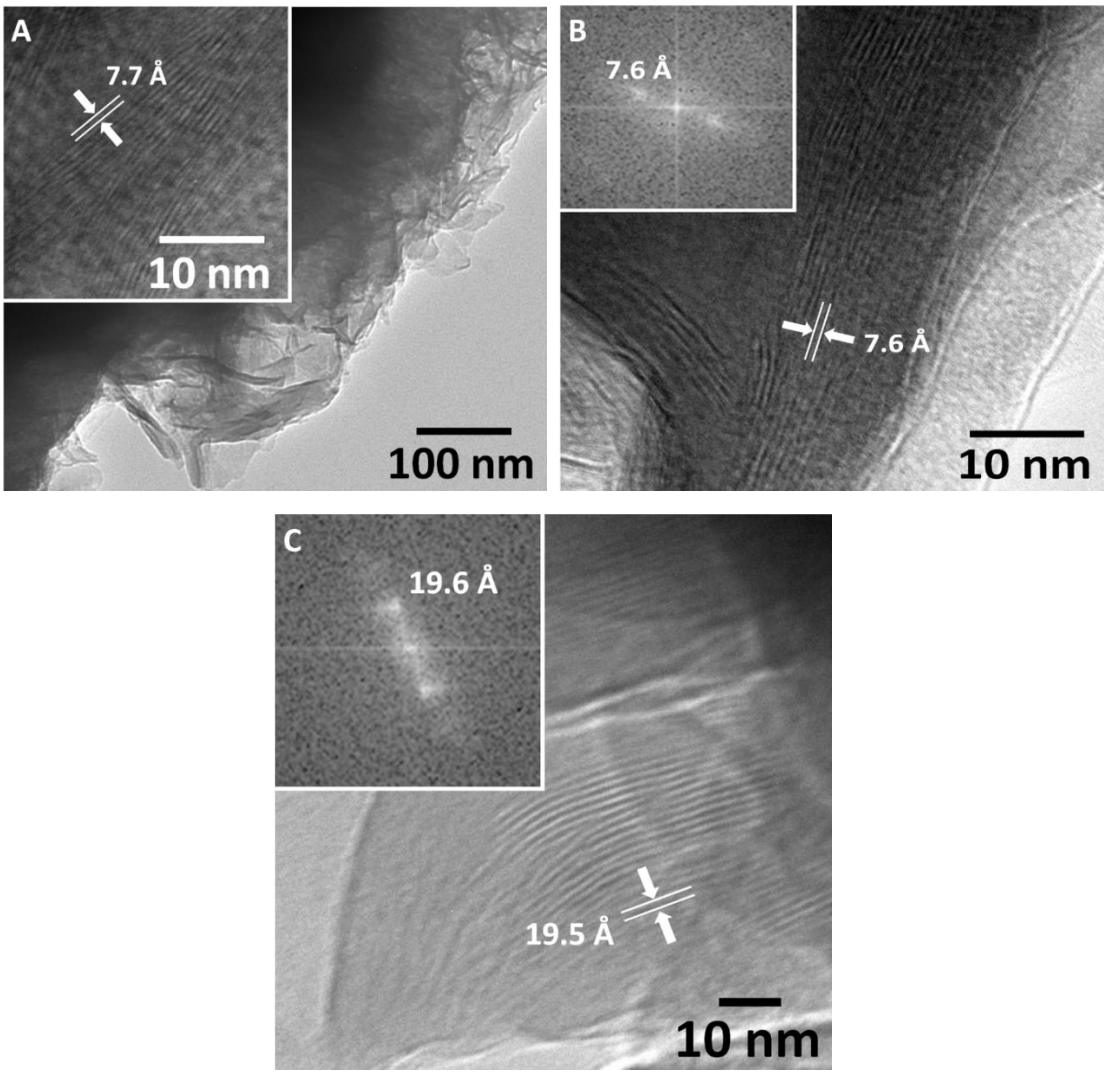


**Figure 2.1** HRTEM images of the nanohybrids synthesized by anionic-exchange method: A) $HT_{rus}$, B) LL/$HT_{rus}$-A1 and C) LL/$HT_{rus}$-A2.

To sustain our previous findings, we have conducted several control experiments using hydrotalcites containing $Cl^-$; these HTs have a lower basicity than the $HT_{rus}$ [27] and do not favour the immobilization of hydrophobic amino acids through anionic exchange method [17]. Indeed, in both cases (LL/$HT_{Clus}$-A1 and LL/$HT_{Clus}$-A2) no increase in the interlayer space was observe, demonstrating that the AA did not exchange the chloride ions (entries 6 and 8, Table 2.2). Moreover, the very low amount of L-Leu computed by EA and ICP analysis suggest that the $HT_{Clus}$ surface is not basic enough to immobilize a larger amount of amino acid.

Materials synthesized by reconstruction method (LL/$HT_{rus}$-R1 and LL/$HT_r$-R2) exhibited a significant shift in the $d_{003}$ peak position compared with the $HT_{rus}$ XRD pattern (Figure B.1 – Appendix B). Furthermore, the interlayer space of these nanohybrid materials increased to around 20 Å (entries 9 and 10, Table 2.2). The HRTEM images (Figure 2.2) do not conserve the layer morphology of their HT precursor and revealed interlayer spacing at 22.5-22.6 Å, indicating

that the immobilization of L-Leu molecules occurs in the interlayer space of the HT. In addition to the basal planes at 22.5-22.6 Å, both LL/$HT_{rus}$-R1 and LL/$HT_r$-R2 materials present lattice fringes at 14.8-14.9 Å.

Nakayama *et al.* [17] immobilized L-leucine into HT using a reconstruction method and observed an increase in the gallery height of 9.8 Å corresponding to the thickness of two L-leucine molecules arranged in a bilayer structure. The material LL/$HT_{rus}$-A1 presented a similar gallery height as the normal HT which demonstrate that the immobilized L-leucine is found at the edges of the HT in a horizontal position with respect the HT layer. On the other hand, the material LL/$HT_{rus}$-A2 has a gallery height of 14.3 Å. The approximate length of a L-leucine molecule is of 7.109 Å, thus the interlayer distance observed for L/$HT_{rus}$-A2 can be explained by a bilayer structure of L-leucine oriented in a vertical position with respect to the HT layer.

The high gallery heights observed in the case of nanohybrids synthesized using reconstruction method suggest that the bilayer structure of L-leucine contains the amino acids in both vertical and oblique orientation with respect to the HT layer.

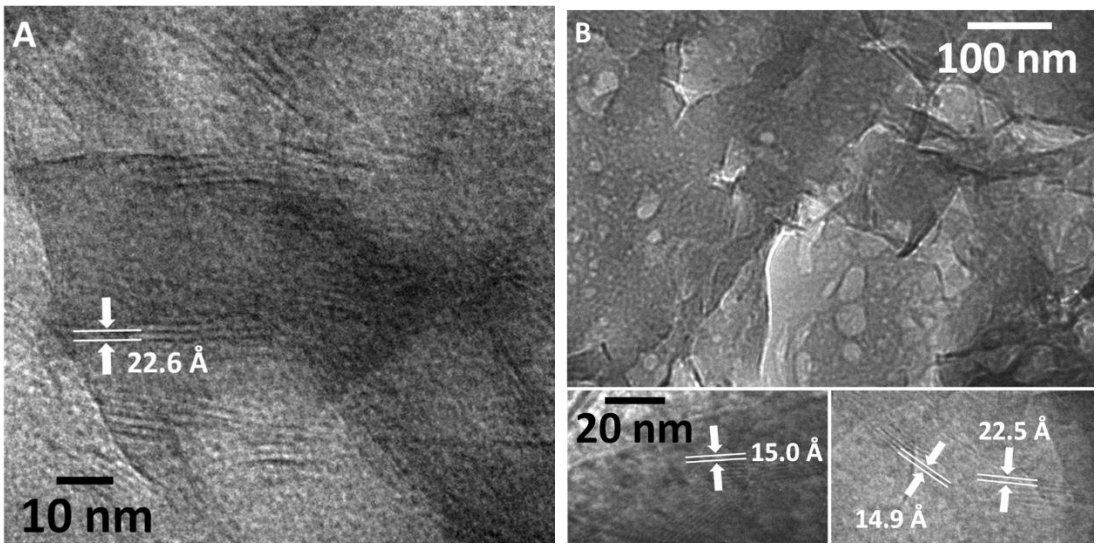


**Figure 2.2 HRTE**M images of the nanohybrids synthesized by the reconstruction method: A) LL/$HT_{rus}$-R1 and B) LL/$HT_r$-R2.

BET surface area results (found in Table 2.2) are in agreement with the previous discussion: when L-Leu is immobilized inside the HT-structure the surface area decreases considerably compared to the parent material. The LL/$HT_{rus}$-R1 and LL/$HT_r$-R2 materials presented a more significant decrease in surface area loss than the ones by A1 and A2 method. This suggests that the AA is found within the aggregates formed by the disordering of the layers (during ultrasound treatment) and their position hinders the adsorption of $N_2$, reducing the available surface area of the materials (see the $N_2$ adsorption-desorption isotherms – Figures B.2 and B.3 - Appendix B).

### 2.3.1.2 FT-IR and RAMAN Spectroscopy

Skeletal FT-IR and Raman spectra of L-Leu, $HT_{Clus}$ and $HT_{rus}$ can be found in Appendix B (Figure B.4) along with the detailed explanations of the specific bands of each parent material. Moreover, the thermal decomposition curves of the nanohybrid precursors can be found in Appendix B (Figures B.7 - B.9).

***Nanohybrids synthesized by the anionic exchange method***

To better understand and evaluate the interaction of L-Leu with the HT surface, we used the control materials based on $HT_{Clus}$. The FT-IR (left) and Raman (right) spectra of LL/$HT_{Clus}$-A1 and LL/$HT_{Clus}$-A2 do not present strong evidence of immobilized L-Leu (Figure 2.3-a and 2.3-b, respectively). In the case of the LL/$HT_{Clus}$-A1, it is difficult to draw conclusions because of the very low content of L-Leu present in the sample (entry 6, Table 2.2). The FT-IR spectrum of LL/$HT_{Clus}$-A2 material showed some differences compared to its HT precursor. At high frequency, two bands at 2957 and 1581 $cm^{-1}$ can be observed due to the small amount of L-Leu molecules interacting with HT material. At low frequency, the differences in the bands at 970, 790 and 553 $cm^{-1}$ compared to the spectrum of the HT precursor suggest changes in the Al-OH species. These changes could result from the presence of a higher amount of $OH^-$ anions and to some L-Leu molecules immobilized in the HT structure. However, the Raman spectrum of LL/$HT_{Clus}$-A2 does not present any evidence of immobilized L-Leu (Figure 2.3-b, right).

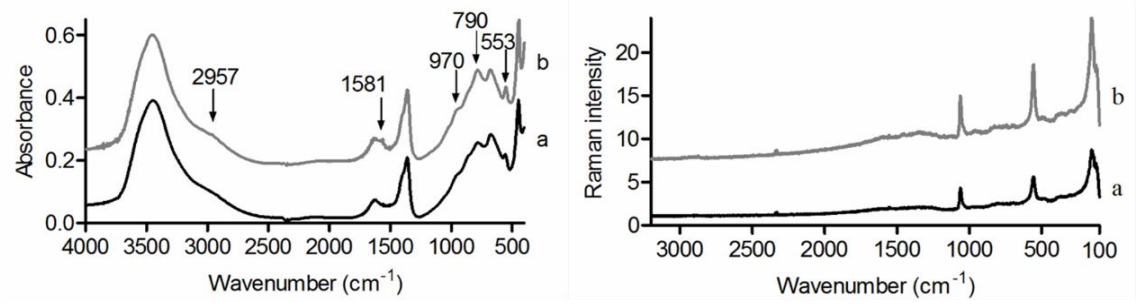


**Figure 2.3** Skeletal FT-IR (left) and Raman (right) spectra of a) LL/$HT_{Clus}$-A1, b) LL/$HT_{Clus}$-A2.

The FT-IR spectra of nanohybrid materials (Figure 2.4 left) synthesized using $HT_{rus}$ material showed, besides the vibration bands due to the HT precursor, some sharp components attributable to the L-Leu, demonstrating that the AA was successfully immobilized. LL/$HT_{rus}$-A1 and LL/$HT_{rus}$-A2 spectra exhibit the bands corresponding to the C-H stretching mode at 2975 ($\nu_{CH}$) and 2870 $cm^{-1}$ ($\nu_{CH3}$), slightly shifted with respect to the bands of pure Leu, confirming the immobilization of the L-Leu. The FT-IR spectrum of LL/$HT_{rus}$-A1 material exhibits the $\nu_{a(COO-)}$ and $\nu_{s(COO-)}$ stretching at 1560 and 1407 $cm^{-1}$ respectively, while bands attributable to the $NH_3^+$ group were not clearly detected (Figure 2.4-a left). These findings, together with the XRD and HRTEM

prove that the immobilization process was mainly caused by an anionic exchange between anionic L-Leu and the $OH^-$ groups located on the HT edges. Similarly, in the FT-IR spectrum of LL/$HT_{rus}$-A2 material, the $\nu_{a(COO-)}$ stretching at 1560 $cm^{-1}$ indicates the presence of the anionic L-Leu (Figure 2.4-b left). An exhaustive study of this spectrum also shows small bands at 1581, 1610 and 1516 $cm^{-1}$ due to $COO^-$ and $NH_3^+$ groups of the zwitterionic L-Leu. The decrease in intensity of the broad band specific to water OH stretching mode and of the band ascribed to $CO_3^{2-}$ species at 1384 $cm^{-1}$ in both LL/$HT_{rus}$-A1 and LL/$HT_{rus}$-A2 materials suggests that the incorporation of the L-Leu in the materials causes the displacement of physisorbed water and the competition with the adsorption of $CO_3^{2-}$ anions [28, 29].

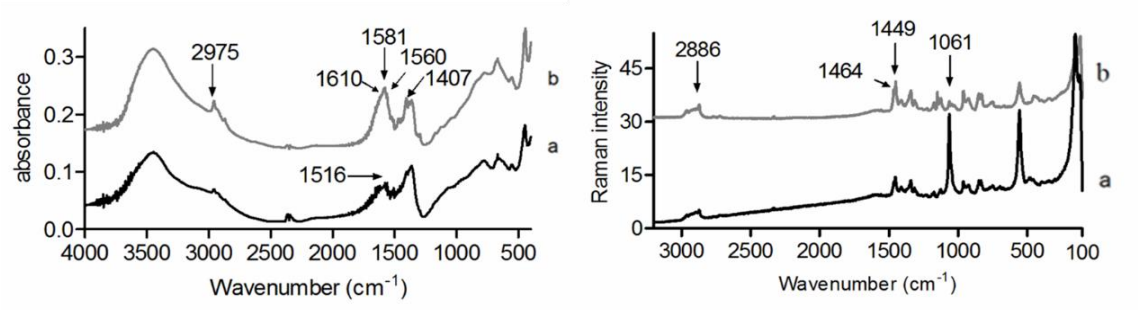


**Figure 2.4** Skeletal FT-IR (left) and Raman (right) spectra of a) LL/$HT_{rus}$-A1 and b) LL/$HT_{rus}$-A2

The Raman spectra of LL/$HT_{rus}$-A1 and LL/$HT_{rus}$-A2 materials present bands at 2886, 1227 and 835 $cm^{-1}$ due to CH stretching modes (Figure 2.4-a and 2.4-b right, respectively). The form in which L-Leu is found in the LL/$HT_{rus}$-A1 is difficult to be identified due to the low intensities of the RAMAN bands (Figure 2.4-a right). In the LL/$HT_{rus}$-A2 Raman spectrum, the bands at 1471 and 1455 $cm^{-1}$ attributable to the $COO^-$ group in pure L-Leu shifted to 1464 and 1449 $cm^{-1}$ respectively (Figure 2.4-b right). In addition, the relative intensity of both bands changes after immobilization, suggesting the presence of two kinds of $COO^-$ groups in L-Leu: anionic and zwitterionic. Changes in their relative intensity also indicate that both $COO^-$ are interacting with the HT structure, anions located in the interlayer space and/or other L-Leu molecules. Moreover, the relative intensity of the band at 1061 $cm^{-1}$ due to $CO_3^{2-}$ species decreased after L-Leu immobilization, confirming the reduced incorporation of atmospheric $CO_2$ in the HT structure.

In general, the FT-IR and Raman spectra of nanohybrid materials synthesized by anion exchange method show that the immobilization process cannot occur on the surface of the HT material. In addition, the high basicity of the $HT_{rus}$ can favour the immobilization of L-Leu in its anionic form until the accessible $OH^-$ groups in the HT edges are compensated. This interaction protects the material from $CO_3^{2-}$ incorporation. Nevertheless, the decrease in the strong basic centres in the material causes the formation of zwitterionic AA (L-Leu detected through

diagnostic bands ascribed to $NH_3^+$) which could interact with Al-OH species, structural water, $OH^-$ groups still available in the material or other zwitterionic L-Leu molecules.

### *Nanohybrids synthesized by the reconstruction method*

The FT-IR (left) and Raman (right) spectra of nanohybrid materials synthesized by the reconstruction method are presented in Figure 2.5. The FT-IR spectrum of LL/$HT_r$-R2 (Figure 2.5-b left) presents broad bands at 3064 $cm^{-1}$ and around 2700 $cm^{-1}$ assigned to vibration modes of the $NH_3^+$ group. In addition, the band at 2130 $cm^{-1}$ is also due to a combination of asymmetric deformation and hindered rotation of $NH_3^+$ groups [30]. The relative intensity of all the bands assigned to the $NH_3^+$ group decreased following immobilization, in comparison to the spectrum of the pure Leu, probably due to H-bonds between the $NH_3^+$ group and the oxygen atoms of the HT layers. Bands due to $\nu_{a(COO-)}$ and $\nu_{s(COO-)}$ stretching were also detected as in pure L-Leu. Although the intercalation of some anionic L-Leu cannot be completely ruled out, immobilized L-Leu using $HT_{cc}$ without ultrasound treatment clearly occurs mostly in its zwitterionic form.

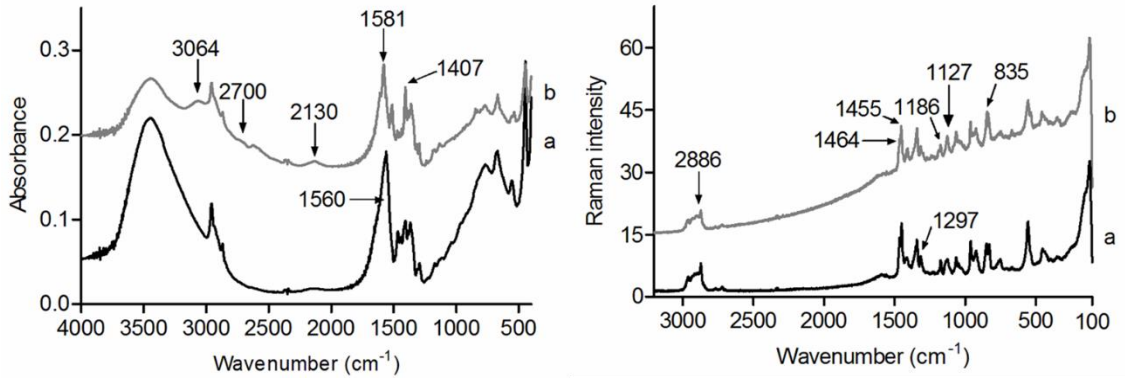


**Figure 2.5** Skeletal FT-IR (left) and Raman (right) spectra of a) LL/$HT_{rus}$-R1 and b) LL/$HT_r$-R2.

The Raman spectrum of LL/$HT_r$-R2 material presents bands at 2886, 1227 and 835 $cm^{-1}$ attributable to CH and CC stretching modes (see Figure 2.5-b right). The band at 1455 $cm^{-1}$ due to the $COO^-$ group in pure L-Leu spectrum remains unchanged after the immobilization process, while the band at 1471 $cm^{-1}$ shifted to 1464 $cm^{-1}$ after immobilization. Moreover, the detection of weak and broad band at 1186 $cm^{-1}$ and shifted band at 1125 $cm^{-1}$ due to $NH_3^+$ group demonstrated the immobilization of both zwitterionic and anionic L-Leu molecules.

FT-IR and Raman spectra of LL/$HT_{rus}$-R1 presented no significant differences compared to LL/$HT_{rus}$-A2 (see Figure 2.5-a and Figure 2.4-b, respectively). The band due to $\nu_{a(COO-)}$ stretching shifted to lower frequencies from 1581 to 1560 $cm^{-1}$, while the bands corresponding to $NH_3^+$ stretching vibrations were not detected. This suggests that the immobilization of the L-Leu occurs in its anionic form, in agreement with Aisawa *et al.* findings [9]. Only two differences in

the Raman spectrum of LL/$HT_{rus}$-R1 were detected in comparison with the LL/$HT_{rus}$-A2 spectrum: the band at 1297 $cm^{-1}$ due to the deformation mode of the -OH in plane and the band at 1187 $cm^{-1}$ due to the $NH_3^+$ group were not detected. This indicated that the immobilization mainly occurred in an anionic form.

In conclusion, the FT-IR and Raman spectra of the nanohybrid materials synthesized using the reconstruction method show that using ultrasound treatment during the synthesis, L-Leu molecules are immobilized in their anionic form.

All the information extracted from the Raman and FT-IR analysis of the nanohybrid materials is summarized in Table 2.3.

**Table 2.3** Summary of characterization data for the LL/HT materials

| Material | Method | Location [a] | $\nu_{a(COO-)}$ [b] | $\nu_{s(COO-)}$ [b] | $\Delta\nu$ [c] | Structure [d] | Interaction [e] |
|---|---|---|---|---|---|---|---|
| L-Leu | - | - | 1581 | 1407 | 174 | Z | - |
| LL/$HT_{Clus}$-A1 [f] | A1 | - | - | - | - | - | - |
| LL/$HT_{Clus}$-A2 [f] | A2 | - | - | - | - | - | - |
| LL/$HT_{rus}$-A1 | A1 | Edges | 1560 | 1408 | 152 | A | Bridging |
| LL/$HT_{rus}$-A2 | A2 | Interlayer space | 1560 | 1408 | 152 | A | Bridging |
| | | | 1581 | 1408 | 173 | Z | H-bonding |
| LL/$HT_{rus}$-R1 | R1 | Interlayer space | 1560 | 1407 | 153 | A | Bridging |
| LL/$HT_r$-R2 | R2 | Interlayer space | 1581 | 1407 | 174 | Z | H-bonding |

[a]AA location in HT determined by XRD analysis. [b]Determined directly from the FT-IR spectra. [c]$\Delta\nu = \nu_{a(COO-)} - \nu_{s(COO-)}$. [d]Structure of AA based on the presence of $NH_3^+$ group by FT-IR. Z= zwitterionic and A= Anionic. [e]Host-guest interaction based on the FTIR spectra: $\Delta\nu L_{-Leu} > \Delta\nu_{nanohyb.}$ = bidentate interaction; $\Delta\nu_{L-Leu} < \Delta\nu_{nanohyb.}$ = bridging interaction. According to Nakamoto [31]. [f]Undetected immobilized L-Leu

### *2.3.1.3 MAS NMR Spectroscopy*

To investigate the nature of the interaction between L-Leu and the HTs using MAS NMR spectroscopy, we have chosen the nanohybrid materials that contained the highest L-Leu/Al molar ratio: LL/$HT_{rus}$-A2, LL/$HT_{rus}$-R1 and LL/$HT_r$-R2.

The typical $^{27}$Al MAS-NMR spectrum of $HT_{rus}$ presents an important signal at 9 ppm due to the octahedral coordinated Al and two small signals at 105 and 81 ppm attributable to extra framework tetrahedral Al atoms still present after rehydration process (see Figure B.5 – Appendix B) [32-34]. Because none of the nanohybrid materials $^{27}$Al MAS-NMR spectra had the signal at 9 pm sifted, demonstrates that the interaction of the immobilized L-Leu with the HT does not involve the Al atoms (entries 2, 3 and 4, Table 2.4).

The $^{13}C$ MAS-NMR spectrum of the pure L-Leu exhibits the typical signals of the zwitterionic form, mainly: a signal at 176 ppm due to the carboxylate group, signals at 55 and 44 pm corresponding to $C_\alpha$ and $C_\beta$ respectively and a broad band at 26 ppm assigned to the $C_\gamma$ and $C_\delta$ (entry 1, Table 2.4). The shifting of the carboxylate group signal from 176 ppm to 186 ppm in the case of LL/$HT_{rus}$-A2 and LL/$HT_{rus}$-R1 spectra (entries 2 and 3, Table 2.4) confirm that L-Leu was immobilized in the anionic form [16]. The $^{13}C$ MAS-NMR spectrum of the LL/$HT_{rus}$-A2 material presented also a less intense signal at 176 ppm, suggesting that some of the L-Leu is found in a zwitterion form (Appendix B – Figure B.6).

**Table 2.4** $^{27}Al$-MAS and $^{13}C$ MAS NMR characterization of LL/HT nanohybrid materials

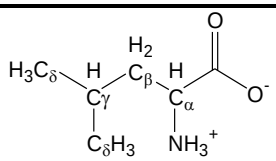


| Entry | Material | $Al_{oh}$ | $COO^-$ | $C_\alpha$ | $C_\beta$ | $C_\gamma$ | $C_\delta$ |
|---|---|---|---|---|---|---|---|
| **1** | L-Leu | - | 176 | 55 | 44 | 26 | 26 |
| **2** | LL/$HT_{rus}$-A2 | 9 | 186<br>177[a] | 56 | 48 | 27 | 24 |
| **3** | LL/$HT_{rus}$-R1 | 9 | 186 | 58 | 49 | 27 | 25 |
| **4** | LL/$HT_r$-R2 | 9 | 177<br>186[a] | 56 | 48 | 27 | 25 |

[a]Less intense signal

The same two signals were also observed in the case of LL/$HT_r$-R2 material (entry 4, Table 2.4), but the intensities were inversed, demonstrating that the L-Leu was immobilized mainly under the zwitterionic form.

## 2.3.2 Nature of the Organic/Inorganic Interaction

The extensive and detailed characterization presented in the above section revealed that variations in the immobilization methods led to materials with different characteristics, as it is summarized in Scheme 2.1.

Briefly, when the starting material was $HT_{cc}$, the L-Leu immobilization took place in the same time as the rearrangement of the HT. Ultrasound treatment (in the case of LL/$HT_{rus}$-R1 material) breaks the HT layers creating more basic sites, which, in the presence of water and L-Leu facilitate the immobilization process. The L-Leu is found in the anionic form between the HT layers. When the hybrid was synthesised without ultrasounds (LL/$HT_r$-R2 material), the L-Leu

was immobilized in the interlayer space in both anionic and zwitterionic form, producing a catalyst with a higher crystallinity. Our results indicate that immobilization of the anionic L-Leu occurs by compensating the $OH^-$ groups found in the HT interlayer space. The immobilization of zwitterionic L-Leu occurs by H-bonding between the $-NH_3^+$ group of the L-Leu with water and/or $OH^-$ groups in the HT layers.

When the synthesis started with $HT_{rus}$, the temperature used was the crucial parameter. Thus, the synthesis carried out at 80 °C (material LL/$HT_{rus}$-A2) favoured the immobilization of L-Leu in the interlayer space by anionic exchange until all accessible centres were compensated, then the immobilization occurred by interactions between the zwitterionic L-Leu with water or $OH^-$ anions located in the interlayer space. When the $HT_{rus}$ was simply stirred in the presence of L-Leu (LL/$HT_{rus}$-A1), immobilization occurred by anionic exchange of the $OH^-$ anions located on the edge of the HT with the anionic L-Leu.

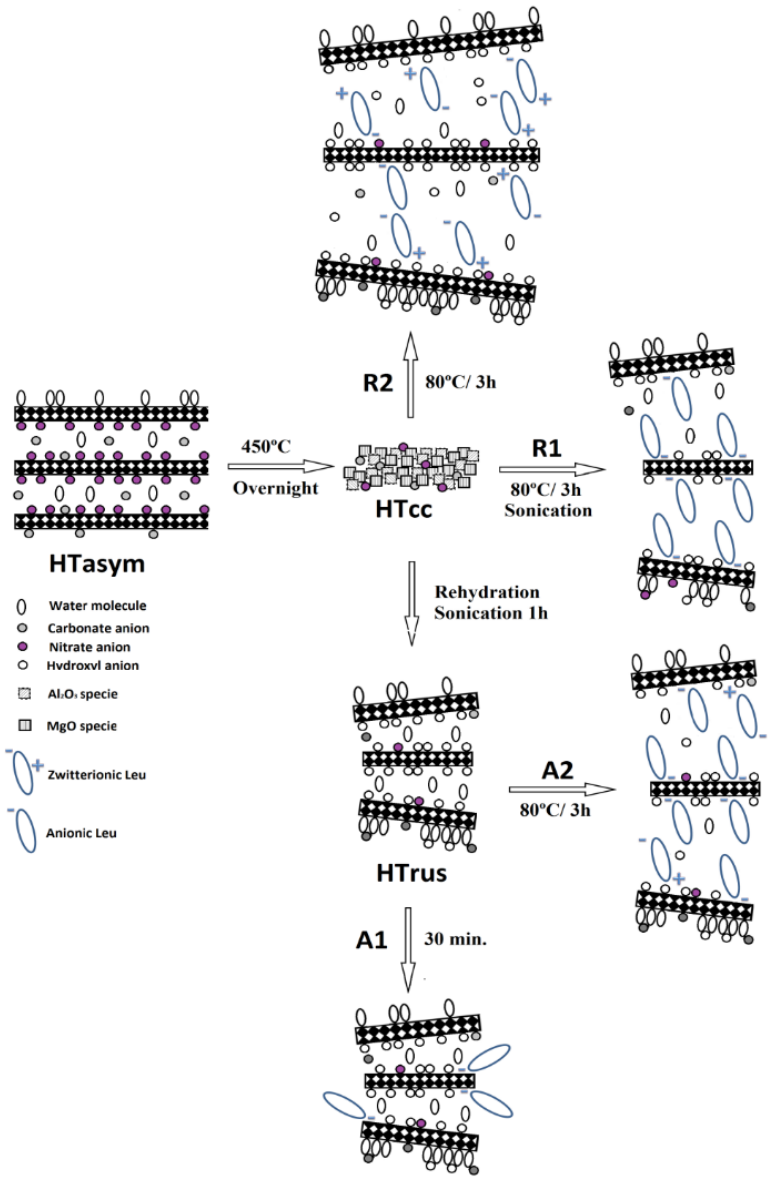


**Scheme 2.1** Schematic representation of the LL/HT materials obtained by the different protocols. L-Leu is immobilized in both zwitterion and anionic form in method A2 and only in anionic form in method R1.

## 2.3.3 Asymmetric Aldol Reaction of Cyclohexanone

T. Itoh *et al.* [24] reported the low activity of L-Leu in the aldol reaction of *p*-nitrobenzaldehyde with cyclohexanone in the presence of DMSO and water for seven days. Under these conditions, the reaction gave the corresponding β-ketoalcohol with a very low yield, moderate *anti* diastereoselectivity and high enantioselectivity towards the (2S,1'R)-aldol compound (entry 1, Table 2.5). The low activity is attributable to the cyclization of the imine intermediate (formed in the reaction between the amino acid and the aldehyde) followed by a decarboxylation, resulting in a stable 1,3-oxazolidine compound [25].

Rehydrated hydrotalcites have proven to possess high activity in several reactions, due to the presence of a large number of –OH groups which act as Brönsted basic sites and are presumed to be responsible for the catalytic activity of these materials. On this basis, the $HT_{rus}$ was tested in the aldol reaction of different benzaldehyde-like compounds with cyclohexanone using the conditions mentioned by T. Itoh *et al.* [24] (Table 2.5). The $HT_{rus}$ afforded high yields and efficiently controlled *syn*-selectivity when substituted aromatic aldehydes were used (entries 2, 5 and 8, Table 2.5), while the *anti*-selectivity was preferred in the case of benzaldehyde (entry 11, Table 2.5).

**Table 2.5** Asymmetric Aldol Reaction of Cyclohexanone

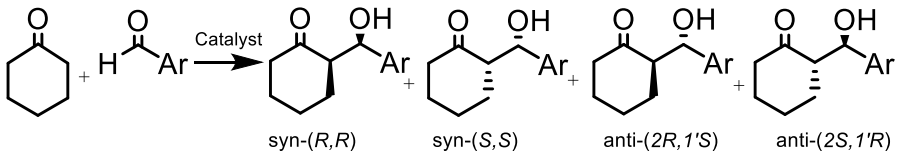


| Entry[a] | Ar | Catalyst | Yield [%][b] | *dr*[b] (*syn/anti*) | *ee* syn[c] [%] | *ee* anti[c] [%] |
|---|---|---|---|---|---|---|
| **1**[d] | 4-$NO_2C_6H_4$ | L-Leu | 16 | 1:3.4 | N.D. | 82 [d] |
| **2** | | $HT_{rus}$ | 99 | 64:36 | - | - |
| **3** | | LL/$HT_{rus}$-R1 | 99 | 58:42 | 90 | 60 |
| **4** | | LL/$HT_{rus}$-A2 | 94 | 61:39 | 71 | 74 |
| **5** | 2-$NO_2C_6H_4$ | $HT_{rus}$ | 96 | 63:37 | - | - |
| **6** | | LL/$HT_{rus}$-R1 | 80 | 53:47 | 60 | 98 |
| **7** | | LL/$HT_{rus}$-A2 | 91 | 56:44 | 36 | 91 |
| **8** | 4-$ClC_6H_4$ | $HT_{rus}$ | 97 | 53:47 | - | - |
| **9** | | LL/$HT_{rus}$-R1 | 80 | 56:44 | 49 | 86 |
| **10** | | LL/$HT_{rus}$-A2 | 80 | 59:41 | 38 | 87 |
| **11** | $C_6H_5$ | $HT_{rus}$ | 99 | 44:56 | - | - |
| **12** | | LL/$HT_{rus}$-R1 | 99 | 54:46 | 50 | 74 |
| **13** | | LL/$HT_{rus}$-A2 | 94 | 43:57 | 5 * | 0 |
| **14** | | $HT_{cc}$ + LL | 85 | 46:54 | 10 | 28 |
| **15** | | $HT_{rus}$ + LL | 99 | 48:52 | 27* | 38 |

[a]Standard conditions: corresponding benzaldehyde (0.5 mmol), cyclohexanone (1.5 mmol), catalyst (2.5 mol % L-Leucine with respect to ketone) in DMSO (2 ml) and $H_2O$ (25 mmol) for 7 days. Brine was added over the reaction mixture and the organic layer was extracted with dichloromethane. [b]Determined by either isolation or $^1H$ NMR based on ref [24, 35].[c]Determined by HPLC based on ref.[35-37].[d]From ref. [24] *The other *syn*-enantiomer was obtained.

Using the same conditions, we tested L-Leu/$HT_{rus}$ materials in the aldol reaction of the four chosen aromatic aldehydes. We used LL/$HT_{rus}$-R1 and LL/$HT_{rus}$-A2 as model catalysts due to the nature of AA immobilized (as mentioned in the previous section, in the R1 the L-Leu is present in the anionic form while in A2 in both zwitterion and anionic form). The manner in which the catalyst was prepared turned out to be crucially important in the reaction efficiency. Both catalysts yield good conversions in the reaction of 4-nitrobenzaldehyde (entries 3 and 4, Table 2.5) compared to the case when free L-Leu was used (entry 1, Table 2.5). Even though *syn* diastereoselectivity was preferred, the form in which L-Leu was immobilized greatly influenced the enantioselectivity. Thus, when L-Leu was present in the anionic form - LL/$HT_{rus}$-R1 – 90% ee for the *syn*-diastereoisomer was obtain and only 60% ee for the *anti*. When L-Leu was present in both anionic and zwitterion form, the ee % of the *syn*-diastereoisomer decreased to 71% while the ee% for *anti*-increased to 74%. In the case of 2-nitrobenzaldehyde the reaction done in the presence of LL/$HT_{rus}$-R1 afforded also the *syn*-diastereoisomer, but enantioselectivity was higher towards *anti*-diastereoisomer (entry 6, Table 2.5). This shows that the steric hindrance of the nitric group found in *ortho* position and the anionic form of L-Leu play an important part in determining the enantioselectivity. A similar trend was observed when LL/$HT_{rus}$-A2 was used, exhibiting a lower stereoselectivity for the *syn*-diastereoisomer. The second para-substituted aldehyde used in this study showed similar trends in both cases, but with a slighter increase in ee% for the *syn* isomer (entries 9 and 10, Table 2.5). A totally different behaviour was observed in the case of benzaldehyde: LL/$HT_{rus}$-R1 favoured the formation of the *syn*-diastereoisomer, with good to moderate enantioselectivity for both diastereoisomers, while the LL/$HT_{rus}$-A2 favoured the *anti*-diastereoisomer, but with practical no enantioselectivity and reverse ee % for the *syn* (entries 12 and 13, Table 2.5). All these results clearly show that both LL/$HT_{rus}$-R1 and LL/$HT_{rus}$-A2 are far better catalysts than pure L-Leu, employing the same conditions as T. Itoh *et al.* [24].

As control experiments, we have studied the catalytic activity of the physical mixture between L-Leu and the corresponding HT (calcined or rehydrated) for the aldol reaction between benzaldehyde and cyclohexanone (entries 14 and 15, Table 2.5). High conversions were obtained in both cases and the diastereoselectivity is similar to the one obtained with LL/$HT_{rus}$-A2. This catalytic behaviour indicates that part of the $HT_{cc}$ is rehydrated in the reaction medium favouring the intercalation of the L-Leu to give the LL/$HT_{rus}$-A2 material. The XRD diffractograms of the physical mixture of $HT_{cc}$ and L-Leu before and after the reaction, along with the XRD pattern of the LL/$HT_{rus}$-A2 can be found in Appendix B. Interestingly, the trends of the ee% for *syn* and *anti* are similar to that of the corresponding catalysts, slightly higher in the case of $HT_{rus}$ + LL and lower for the other physical mixture.

To evaluate the reusability and stability of the catalysts, we chose as substrate benzaldehyde, due to its unique behaviour in terms of diastereoselectivity and enantioselectivity. When LL/$HT_{rus}$-A2 was used and under the conditions proposed by T. Itoh *et al.* [24] the catalyst lost its activity after the first run (entry 1, Table 2.6). In the LL/$HT_{rus}$-A2 material, L-Leu is found in both zwitterion and anionic form and due to the exothermic reaction that takes place during work-up (adding brine over reaction mixture) the amino acid is removed from the HT, decreasing thus the activity of the catalyst (Figure B.11 – Appendix B). Moreover, the $Cl^-$ anions found in the brine solution are able to replace the vacant zones of the HT interlamellar space, leading to the formation of an inactive catalyst. The amino acid which is now free in solution will react with benzaldehyde leading to the formation of the corresponding 1,3-oxazolidine (Figure B.12– Appendix B). The catalyst LL/$HT_{rus}$-R1 presented slightly higher activity in the second run compared to the other case, suggesting a stronger interaction between the anionic form of the amino acid and the HT interlamellar space than in the case of LL/$HT_{rus}$-A2 (entry 2, Table 2.6).

To avoid the use of NaCl, we repeated the reactions using toluene as solvent (entries 3 and 4, Table 2.6). In this case, two different behaviours were observed depending on the nature of the catalyst: when LL/$HT_{rus}$-A2 was used, an increase towards the *anti*-diastereoisomer can be observed over the three runs while, in the other case (LL/$HT_{rus}$-R1), an increase of the *syn*-diastereoisomer is observed. In terms of enantioselectivity, a slightly increase in ee% is detected for both isomers over the three runs, in the case of LL/$HT_{rus}$-A2, while when LL/$HT_{rus}$-R1 is used, a change in enantioselectivity is observed for the *syn*-diastereoisomer. These preliminary results suggest that the solvent plays an important part in the reaction pathway and might have an effect on the reaction enantioselectivity.

**Table 2.6** Stability and Reusability of the Heterogeneous Catalyst in Asymmetric Aldol Reaction of Benzaldehyde with Cyclohexanone

| Entry | Solvent | Catalyst | Run | Yield [%][c] | *dr*[c] (*syn/anti*) | *ee* syn[d] [%] | *ee* anti[d] [%] |
|---|---|---|---|---|---|---|---|
| **1** | DMSO[a] | L-Leu/$HT_{rus}$-A2 | 1 | 94 | 43:57 | 5* | 0.4 |
| | | | 2 | - | - | - | - |
| | | | 3 | - | - | - | - |
| **2** | DMSO[a] | L-Leu/$HT_{rus}$-R1 | 1 | 93 | 47:53 | 50 | 74 |
| | | | 2 | 99 | 32:68 | 83 | 13 |
| | | | 3 | - | - | - | - |
| **3** | Toluene[b] | L-Leu/$HT_{rus}$-A2 | 1 | 99 | 43:57 | 10* | 22 |
| | | | 2 | 97 | 41:59 | 18* | 32 |
| | | | 3 | 99 | 40:60 | 33* | 46 |
| **4** | Toluene[b] | L-Leu/$HT_{rus}$-R1 | 1 | 86 | 37:63 | 15* | 18 |
| | | | 2 | 84 | 40:60 | 7* | 22 |
| | | | 3 | 99 | 45:55 | 8* | 17 |

[a]Reaction conditions: benzaldehyde (0.5 mmol), cyclohexanone (1.5 mmol), catalyst (2.5 mol % L-Leucine with respect to ketone) in DMSO (2 ml) and $H_2O$ (25 mmol) for 7 days. Brine was added over the reaction mixture and the organic layer was extracted with dichloromethane. [b]Reaction conditions: benzaldehyde (0.5 mmol), cyclohexanone (1.5 mmol), catalyst (2.5 mol % L-Leucine with respect to ketone) in Toluene (2 ml) ;[c] Determined by either isolation or $^1$H NMR based on ref [24, 35].[d]Determined by HPLC based on ref. [35-37] *The other *syn*-enantiomer was obtained.

For an in-depth study of this process and to understand the reaction profile, we performed a 4 h kinetic study of the aldol reaction between cyclohexanone and benzaldehyde under all the conditions mentioned above (catalysed by $HT_{rus}$, mechanical mixture between L-Leu and HT, LL/$HT_{rus}$-A2 and LL/$HT_{rus}$-R1 and the conditions mentioned by T. Itoh *et al.* [24]).

The first study was done using $HT_{rus}$ as catalyst. (Figure 2.6). It is intriguing to note that, although the reaction was complete after only 1 h, there is a continuous interchanging between the *syn* and the *anti*-diastereoisomers. Miller *et al.* discovered a stereoisomeric system in which spontaneous enantiomeric enrichment occurred in a homogeneous mixture. They observed an amide isomerization proportional to the fluctuation of each diastereoisomer's enantiomeric ratio as the *cis-trans* equilibration occurred [38].

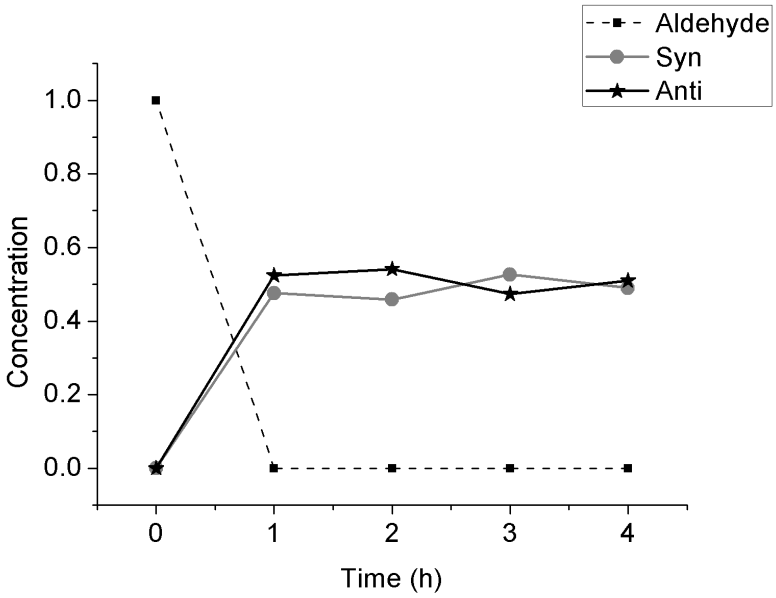


**Figure 2.6** First 4 h of reaction: Reaction conditions: benzaldehyde (0.5 mmol), cyclohexanone (1.5 mmol), catalyst $HT_{rus}$ in DMSO (2 ml) and $H_2O$ (25 mmol); results obtained from $^1$H-NMR spectra.

To explain the observed behaviour, we have to take into account the strong basic sites present in the $HT_{rus}$ which can promote the reaction by extracting an H atom in the α-position of the ketone compound [39]. Scheme 2.2 presents a possible mechanism of the *syn-anti* isomerization, where the cyclohexanone (**1**) will be in equilibrium with the enol form (**2**) in aqueous solvent and will react further with the benzaldehyde to give the corresponding aldol product (**4**). Due to the presence of the interlayer –OH groups and the water medium, H-bonds play an important role in stereoselectivity, favouring the *syn-an*ti inversion [40].

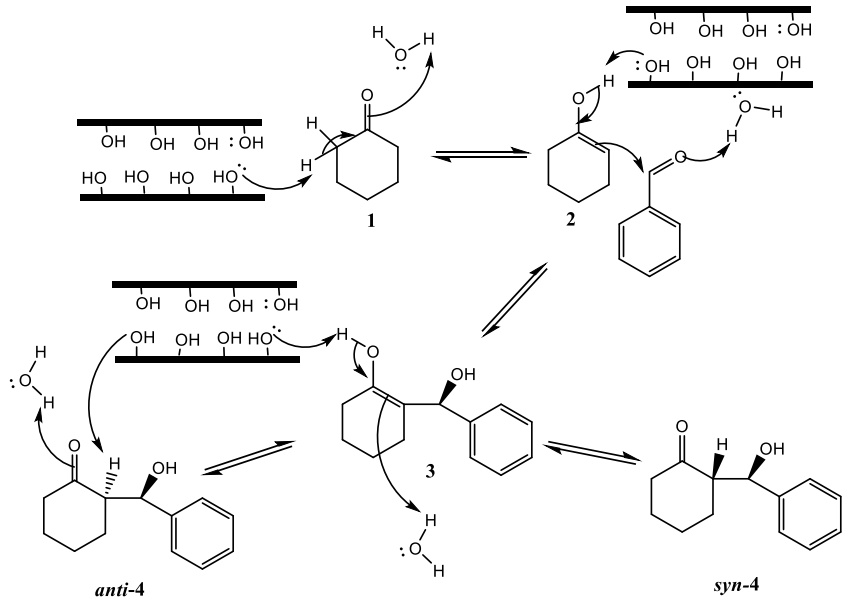


**Scheme 2.2** Possible mechanism for the *syn-anti* isomerization

A different behaviour is observed when the reaction is carried out using the corresponding HT mixed with L-Leu. In the first case (Figure 2.7-A), two different catalysts are present in the reaction mixture: $HT_{cc}$ and L-Leu. As $HT_{cc}$ has lower basic sites than $HT_{rus}$, the aldol reaction will require longer time for completion. Additionally, the quantity of water present in the medium is able to rehydrate the HT material and thus, proceeding in the formation of LL/$HT_{rus}$-A2. The free amino acid is involved in three competitive processes: catalysing the formation of 1,3-oxazolidine compound, catalysing the aldol reaction and being involved in the immobilization process. At this point is difficult to know which form of L-Leucine is active in this experiment. Surprising, along the 4 h a slowly decrease in the enantioselectivity of the reverse *anti*-diastereoisomer is observed.

Furthermore, the system $HT_{rus}$ + L-Leu is much more active giving a higher selectivity towards the aldol products (Figure 2.7-B). In this case, three processes may occur simultaneously: formation of the 1,3 – oxazolidine, aldol reaction and immobilization of the AA. From all of them, the reaction system favours the immobilization of L-Leu on the $HT_{rus}$ and thus, only a small portion of the L-leucine will be involved in the formation of 1,3-oxazolidine compound and of the *anti* –aldol product (Figure 2.7-B – values in brackets). After 2 hours of reaction, the catalyst LL/$HT_{rus}$-A2 is already formed.

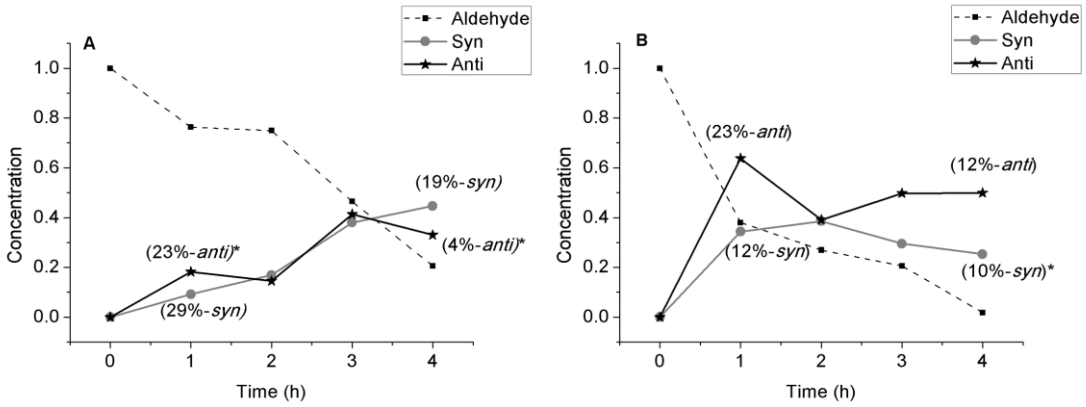


**Figure 2.7** First 4 h of reaction: A) – $HT_{cc}$+ L-Leu ; B) - $HT_{rus}$ + L-Leu. Reaction conditions: benzaldehyde (0.5 mmol), cyclohexanone (1.5 mmol), catalyst (2.5 mol % L-Leucine with respect to ketone) in DMSO (2 ml) and $H_2O$ (25 mmol); results obtained from $^1$H-NMR spectra. *The other enantiomer was obtained.

The degree of interchanging between *syn* and *anti*-isomers depends on the nature of the catalyst: in the case of LL/$HT_{rus}$-A2 during the first hour the *syn*-diastereoisomer is present in a higher concentration than the *anti*, but in time its concentration decrease as it can be seen in Figure 2.8-A; on the other hand, when LL/$HT_{rus}$-R1 was used, the *anti*-diastereoisomer is in excess from the beginning, and after 3 h the conversion towards the *syn*-diastereoisomer increases, as observed in Figure 2.8-B. Regarding the enantioselectivity, during the first 3 hours

of reaction in the presence of LL/HT$_{rus}$-R1 the ee% remains constant for the *anti*-isomer (Figure 2.8-B – values in brackets) while there is no enantioselectivity for the *syn*-diastereoisomer. In the case of LL/HT$_{rus}$-A2 a change in stereoselectivity is observed for the *syn*-diastereomer and a slightly increase in enantioselectivity for the *anti* (Figure 2.8-A – values in brackets).

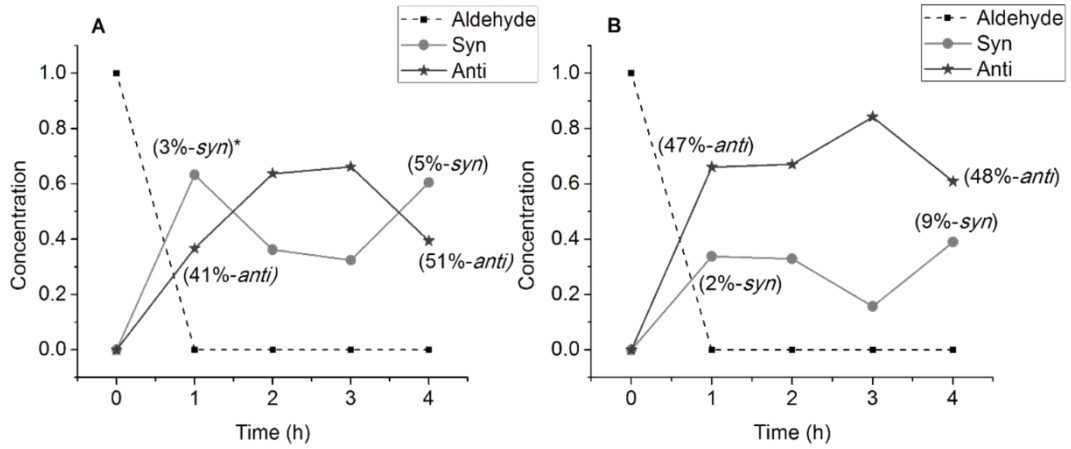


**Figure 2.8** First 4 h of reaction: A) – LL/HT$_{rus}$-A2, B) - LL/HT$_{rus}$-R1. Reaction conditions: benzaldehyde (0.5 mmol), cyclohexanone (1.5 mmol), catalyst (2.5 mol % L-Leucine with respect to ketone) in DMSO (2 ml) and $H_2O$ (25 mmol); results obtained from $^1$H-NMR spectra. *The other enantiomer was obtained.

Figure 2.9 illustrates that the reaction proceeds slower in toluene than in aqueous DMSO and total conversion is achieved after 3 h. The catalyst obtained through the anionic exchange method (Figure 2.9-A) behaves totally different when toluene is used and in the first 4 h of reaction there is no interchanging between the diastereoisomers. In the same time, the enantioselectivity towards the other *syn*-diastereoisomer remains constant, while the enantioselectivity of the *anti*-product is much lower than in the case were DMSO was used as solvent. In addition, when LL/HT$_{rus}$-R1 is used, after 2 h of reaction an inversion between the diastereoisomers is observed, while the ee% is increasing for the *syn*-diastereoisomer and slightly decreases for the *anti* (Figure 2.9-B). As mentioned in the "Nature of the organic/inorganic interaction" section, when the catalyst is prepared through the A2 method, the active basic sites (interlamellar –OHs) are interacting with the L-Leu found in both anionic and zwitterion form. In a nonpolar solvent and with no water present, the LL/HT$_{rus}$-A2 catalyst is incapable of catalysing the interchanging between the diastereoisomers. Moreover, when only the anionic form of L-Leu is immobilized, as in the case of LL/HT$_{rus}$-R1, there are more –OH available, thus promoting the interchanging as can be seen in Figure 2.9-B.

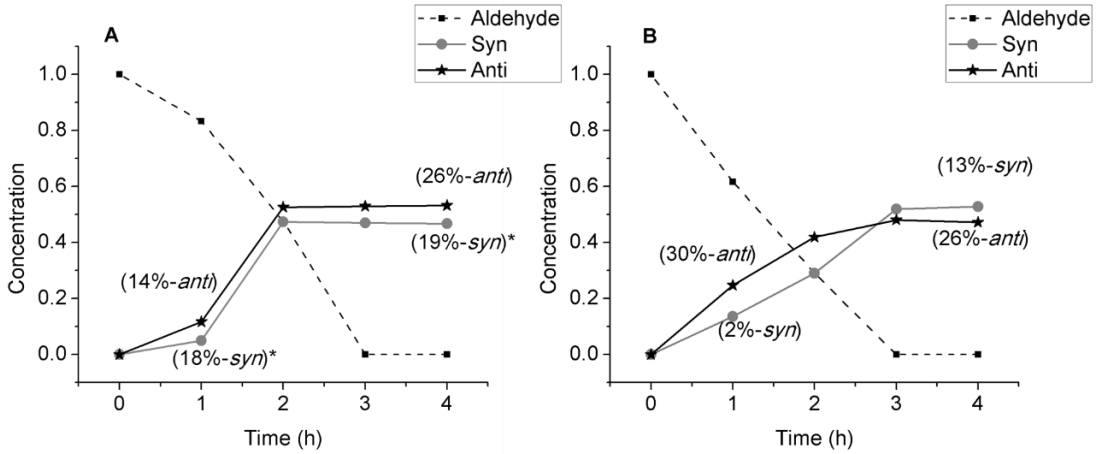


**Figure 2.9** First 4 h of reaction: A) – LL/$HT_{rus}$-A2 B) - LL/$HT_{rus}$-R1. Reaction conditions: benzaldehyde (0.5 mmol), cyclohexanone (1.5 mmol), catalyst (2.5 mol % L-Leucine with respect to ketone) in toluene (2 ml); results obtained from $^{1}$H-NMR spectra. *The other enantiomer was obtained.

Literature presents several reactions done "in water" or "in the presence of water", the last being reported to increase the reactivity and stereoselectivity [41, 42]. In this context, we have performed the 4 h kinetic study of aldol reaction in toluene and "in the presence of water", results being shown in Figure 2.10. Adding only a small amount of water in toluene completely changed the course of reaction. In both cases there was a high selectivity towards the *anti*-diastereoisomer, a very good enantioselectivity of this isomer and no enantioselectivity for the *syn* isomer (Figure 2.10 A and B). Our results show that the solute-solvent interactions are able to affect the stereochemical outcome of the aldol reaction even when a nonpolar solvent is used.

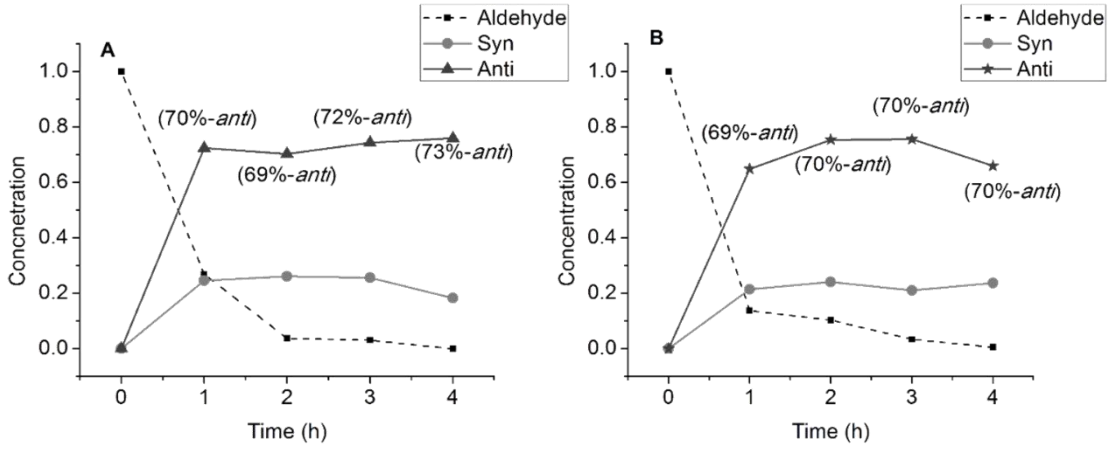


**Figure 2.10** First 4 h of reaction: A) – LL/$HT_{rus}$-A2 B) - LL/$HT_{rus}$-R1. Reaction conditions: benzaldehyde (0.5 mmol), cyclohexanone (1.5 mmol), catalyst (2.5 mol % L-Leucine with respect to ketone) in toluene (2 ml) and $H_2O$ (25 mmol); results obtained from $^{1}$H-NMR spectra.

Cordová *et al.* showed that there are three possible mechanisms by which a free AA can catalyse the aldol reaction: the carboxylic acid catalysed enamine mechanism, the amino catalysed enamine mechanism and the enaminium catalysed mechanism, where the amino acid is found in the zwitterion form [43]. These mechanisms cannot be applied when the amino acid is immobilized between the layers of hydrotalcites, due to the presence of the secondary material which is also active in aldol reaction. So far, our results show that when the reaction carried out in polar solvent (DMSO) the conversion and enantioselectivity are low, but when nonpolar solvents are used with a very small quantity of water, the catalytic activity is improved. This might be explained as follows: in the nonpolar medium, the substrate has to penetrate into the layers of the HT and, as Vijaikumar *et al.* [2] showed, the polar nature of the interlayer will help the catalysis as well as the chiral induction of the AA to occur. Scheme 2.3 presents a possible mechanism of the aldol reaction catalysed by the LL/HT catalysts. Firstly, the amino group of L-Leu activates the ketone by a nucleophilic attack at the carbonyl carbon, generating an enaminium intermediate. The *syn* diastereoselectivity is influenced by the highly basic character of the hydrotalcite. The –OH groups of the HT interact with the aldehyde, polarizing it and facilitating the nucleophilic attack of the enamine, which, in presence of water will give the corresponding *syn*-adduct. Amedjkouh showed that bases can be used as co-catalysts in the adol reaction to enforce *syn*-selectivity retaining a high level of enantioselectivity, and unbounded amino acids usually favour the formation of *anti*-aldol product [44]. Next, the *syn*-diastereoisomer can undergo isomerization, as presented in Scheme 2.3.

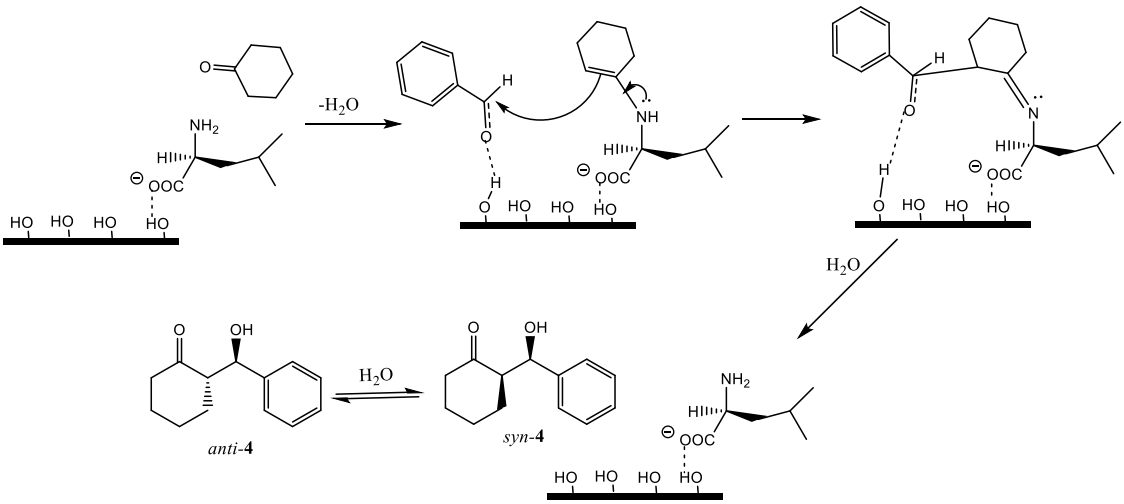


**Scheme 2.3** Proposed enamine-type mechanism for the aldol reaction catalysed by LL/$HT_{rus}$ (both R1 and A2) catalysts.

The HT interlayer space provides the perfect environment for the L-leucine, increasing its activity by promoting enantioselectivity through an oriental attack. The activity of this

bifunctional catalyst is enhanced by the polar medium found in HT galleries and by the presence of water. As Gong *et al.* showed, the double hydrogen bonding activation of carbonyl functionality influence the transition state, exhibiting high stereoselectivity towards the *syn*-aldol product if the reaction is not quenched in the first 4h [45].

The behaviour of these new bio-hybrid catalysts is extremely complicated and certainly require further investigation for a complete comprehension on how the solvent, time of reaction and the way the catalyst is prepared affect the activity and enantioselectivity.

## 2.4 Conclusions

The controllable basicity, the "memory effect" and the ion exchange property make HTs excellent materials to immobilize amino acids and study their organic/inorganic interactions. In this context, we have obtained four new materials based on L-leucine and Mg-Al HT by means of two procedures: reconstruction method and anionic exchange method.

In the anionic exchange method, the immobilization involves mainly the anionic form of L-Leu and an increase in the synthesis time and temperature permits the swelling of the HT material, allowing the immobilization to occur inside the HT layers. An excess of L-Leu in the reaction media will favour the immobilization on the edges of the HT structure. The use of ultrasound treatment during reconstruction method not only increased the basic sites of the HT, but also favoured the immobilization of L-Leu inside its layers. The absence of this treatment will favour the AA intercalation by means of H-bonding between its structure and the inorganic anions found in the interlayer space.

Regardless of the intercalation method used, we have shown that the immobilization cannot occur through the interaction between the $Al^{3+}$ atoms from the HTs structure and the anionic L-Leu. Moreover, according to the XRD results, the immobilization could occur in a vertical or oblique orientation with respect to the HT layers (Scheme 2.1). When the AA was immobilized in the zwitterionic form, the orientation depended on the chemical environment in the interlayer space from the HT.

These new materials were more active in the asymmetric aldol reaction of cyclohexanone with different aromatic aldehydes (up to 99% conversion and moderate to good enantioselectivity) than the corresponding physical mixture and the mere amino acid. When the reaction was carried out in aqueous DMSO, the catalysts lost their activity after the first run, due to the exothermic reaction that takes place during work-up (adding brine over reaction mixture) when L-Leu is removed from the HT. Just by using toluene, both conversion and selectivity were highly improved.

The kinetic studies we performed have shown that the aldol reaction between cyclohexanone and benzaldehyde carried out using these new catalysts, toluene and "in the presence of water" is completed in less than 4 h, achieving 99% yield and maintaining the enantioselectivity in the case of the *anti*- diastereoisomer.

The mechanism of reaction is very complex and involves simultaneous activity of the two parts of the catalyst: the hydrotalcite and the immobilized L-Leu. If in general the free amino acid favours the formation of the *anti*-diastereoisomer, the presence of the basic HT leads to the formation of the *syn*-diastereoisomer. Moreover, depending on the conditions of reaction, the *syn* and *anti*-diastereoisomers can undergo isomerization.

Therefore, the different synthesis protocols and different reaction conditions can be employed to obtain a specific aldol-product. Further studies will be carried out to exploit the potential advantages and properties of these LL/$HT_{rus}$ catalysts in the asymmetric aldol reaction of cycloketones. This future work will focus on understanding how the solvent, time and the way the catalyst is prepared affect the activity and enantioselectivity, making use of theoretical computations and possible transition states.

# Bibliography

[1] J.-H. Choy, S.-J. Choi, J.-M. Oh, T. Park, *Applied Clay Science*, **36**, 122–132, **2007**.

[2] S. Vijaikumar, A. Dhakshinamoorthy, K. Pitchumani, *Applied Catalysis A: General*, **340**, 25–32, **2008**.

[3] J.-H. Yang, Y.-S. Han, M. Park, T. Park, S.-J. Hwang, J.-H. Choy, *Chemistry of Materials*, **19**, 2679-2685, **2007**.

[4] M.D. Arco, E. Cebadera, S. Gutiérrez, C. Martín, M. Montero, V. Rives, J. Rocha, M.A. Sevilla, *Journal of Pharmaceutical Sciences*, **93**, 1649-1658, **2004**.

[5] B. Ballarin, A. Mignani, F. Mogavero, S. Gabbanini, M. Morigi, *Applied Clay Science*, **114**, 303-308, **2015**.

[6] R.J. Chimentão, S. Abelló, F. Medina, J. Llorca, J.E. Sueiras, Y. Cesteros, P. Salagre, *Journal of Catalysis*, **252**, 249–257, **2007**.

[7] D.-H. Park, G. Choi, J.-H. Choy, *Bio-layered double hydroxides nanohybrids for theranostics applications*, in: Photofunctional Layered Materials, 137-175, **2015**.

[8] N.T. Whilton, P.J. Vickers, S. Mann, *Journal of Materials Chemistry*, **7**, 1623–1629, **1997**.

[9] S. Aisawa, S. Takahashi, W. Ogasawara, Y. Umetsu, E. Narita, *Journal of Solid State Chemistry*, **162**, 52-62 **2001**.

[10] B.M. Choudary, B. Kavita, N.S. Chowdari, B. Sreedhar, M.L. Kantam, *Catalysis Letters*, **78**, 373-377, **2002**.

[11] Q. Yuan, M. Wei, Z. Wang, G. Wang, X. Duan, *Clays and Clay Minerals*, **52**, 40–46, **2004**.

[12] M. Wei, J. Guo, Z. Shi, Q. Yuan, M. Pu, G. Rao, X. Duan, *Journal of Materials Science*, **42**, 2684-2689, **2007**.

[13] Å. Fudala, I. Pálinkó, B. Hrivnák, I. Kiricsi, *Journal of Thermal Analysis and Calorimetry*, **56**, 317-322, **1999**.

[14] Á. Fudala, I. Pálinkó, I. Kiricsi, *Journal of Molecular Structure*, **482-483**, 33-37, **1999**.

[15] Á. Fudala, I. Pálinkó, I. Kiricsi, *Inorganic Chemistry*, **38**, 4653-4658, **1999**.

[16] S. Aisawa, H. Kudo, T. Hoshi, S. Takahashi, H. Hirahara, Y. Umetsu, E. Narita, *Journal of Solid State Chemistry*, **177**, 3987–3994, **2004**.

[17] H. Nakayama, N. Wada, M. Tsuhako, *International Journal of Pharmaceutics*, **269**, 469–478, **2004**.

[18] B. List, R.A. Lerner, C.F.B. III, *Journal of American Chemical Society*, **122**, 2395-2396, **2000**.

[19] A. Córdova, W. Zou, I. Ibrahem, E. Reyes, M. Engqvist, W.-W. Liao, *Chemical Communications*, 3586–3588, **2005**.

[20] X. Wu, Z. Jiang, H.-M. Shen, Y. Lu, *Advanced Synthesis & Catalysis*, **349**, 812 – 816, **2007**.

[21] S.S.V. Ramasastry, K. Albertshofer, N. Utsumi, F. Tanaka, C.F.B. III, *Angewandte Chemie International Edition*, **46**, 5572–5575, **2007**.

[22] Z. Jiang, Z. Liang, X. Wu, Y. Lu, *Chemical Communications*, 2801–2803, **2006**.

[23] X.-Y. Xu, Y.-Z. Wang, L.-Z. Gong, *Organic Letters*, **9**, 4247-4249, **2007**.

[24] T. Kanemitsu, A. Umehara, M. Miyazaki, K. Nagata, T. Itoh, *European Journal of Organic Chemistry*, 993–997, **2011**.

[25] F. Orsini, F. Pelizzoni, M. Forte, R. Destro, P. Gariboldi, *Tetrahedron*, **44**, 519-541, **1988**.

[26] F. Cavani, F. Trifirò, A. Vaccari, *Catalysis Today*, **11**, 173-301, **1991**.

[27] M.G. Álvarez, R.J. Chimentão, F. Figueras, F. Medina, *Applied Clay Science*, **58**, 16-24, **2012**.

[28] S. Aisawa, S. Sasaki, S. Takahashi, H. Hirahara, H. Nakayama, E. Narita, *Journal of Physics and Chemistry of Solids*, **67**, 920–925, **2006**.

[29] A.R. Garcia, R.B.d. Barros, A. Fidalgo, L.M. Ilharco, *Langmuir*, **23**, 10164-10175, **2007**.

[30] N.B. Colthup, L.H. Daly, S.E. Wiberley, *Introduction to infrared and raman spectroscopy*, 3rd ed., **1990**.

[31] M. Kakihana, T. Nagumo, M. Okamoto, H. Kakihana, *The Journal of Physical Chemistry B*, **91**, 6128-6136, **1987**.

[32] A. Béres, I. Pálinkó, J.-C. Bertrand, J.B. Nagy, I. Kiricsi, *Journal of Molecular Structure*, **410-411**, 13-16, **1997**.

[33] J. Rocha, M.d. Arco, V. Rives, M.A. Ulibarri, *Journal of Materials Chemistry*, **9**, 2499-2503, **1999**.

[34] F. Rey, V. Fornés, *Journal of the Chemical Society, Faraday Transactions*, **88**, 2233-2238, **1992**.

[35] P. Zhou, S. Luo, J.-P. Cheng, *Organic & Biomolecular Chemistry*, **9**, 1784–1790, **2011**.

[36] B. Rodríguez, A. Bruchmann, C. Bolm, *Chemistry - A European Journal*, **13**, 4710 – 4722, **2007**.

[37] L. Li, S. Gou, F. Liu, *Tetrahedron Letters*, **54**, 6358–6362, **2013**.

[38] K.T. Barrett, A.J. Metrano, P.R. Rablen, S.J. Miller, *Nature*, **509**, 71-75, **2014**.

[39] E. Dumitriu, V. Hulea, C. Chelaru, C. Catrinescu, D. Tichit, R. Durand, *Applied Catalysis A: General*, **178**, 145-157, **1999**.

[40] S. Paladhi, A. Chauhan, K. Dhara, A.K. Tiwari, J. Dash, *Green Chemistry*, **14**, 2990–2995, **2012**.

[41] Y. Hayashi, *Angewandte Chemie International Edition*, **45**, 8103 – 8104, **2006**.

[42] A.P. Brogan, T.J. Dickerson, K.D. Janda, *Angewandte Chemie International Edition*, **48**, 8100 – 8102, **2006**.

[43] A. Bassan, W. Zou, E. Reyes, F. Himo, A. Córdova, *Angewandte Chemie International Edition*, **44**, 7028 –7032, **2005**.

[44] M. Amedjkouh, *Tetrahedron: Asymmetry*, **18**, 390–395, **2007**.

[45] X.-H. Chen, J. Yu, L.-Z. Gong, *Chemical Communications*, **46**, 6437–6448, **2010**.

# 3 Highly Selective Multifunctional Nanohybrid Catalysts for the One - pot Synthesis of α, β - Epoxy-chalcones

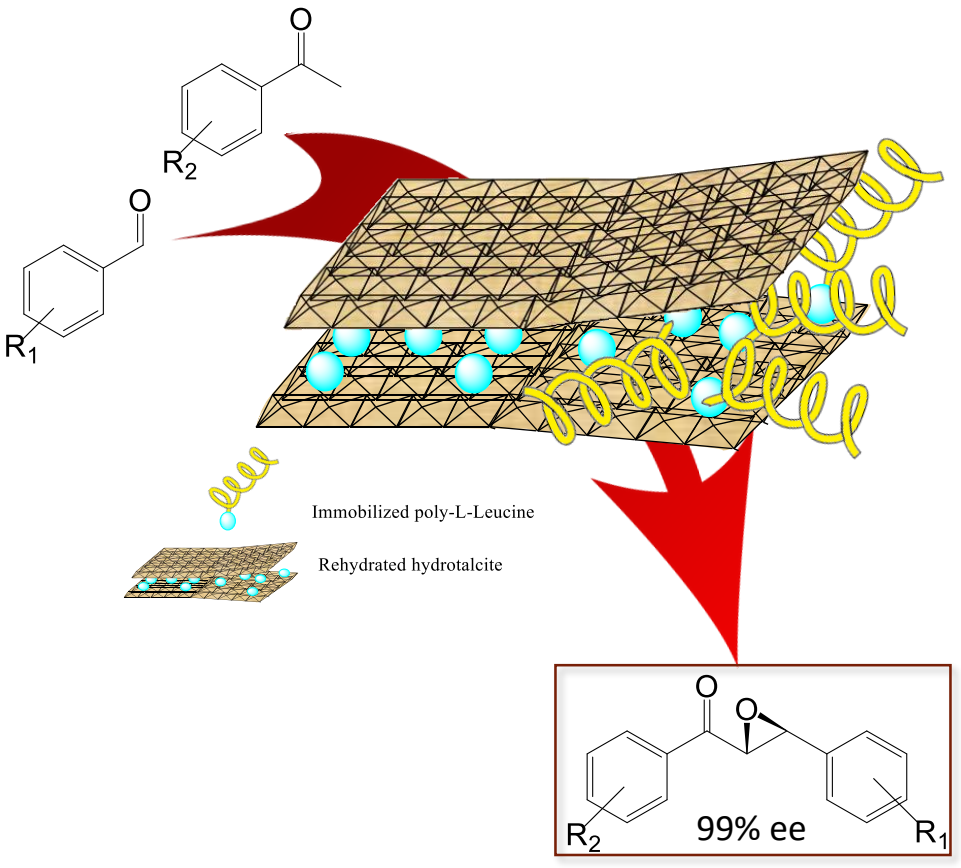


Dana-Georgiana Crivoi, Anna Segarra, Francesc Medina, *Journal of Catalysis*, **2016**, 334, 120-128

## 3.1 Introduction

Catalytic asymmetric synthesis is an important technique for the preparation of chiral epoxides in both academia and industry. These epoxides are versatile products that can easily undergo stereospecific ring-opening reactions to form multifunctional compounds. They are not only important chiral building blocks, but also key intermediates in the synthesis of more complex molecules with important bioactivity like leukotriene, erythromycin, (+)-aurilol or brevetoxin B [1-3].

The main pathway to obtain the chiral epoxides consists in the epoxidation of olefins by either metal-catalysed reactions [2] or peptide-type reactions [4-6]. Even though metal-catalysed reactions gained much attention in the last years, they are not suitable to produce bioactive molecules due to some possible drawbacks: metal leaching, toxic effects of the metal used, etc. Thus, peptide-catalysed reactions represent a possible solution to these drawbacks.

In 1983 Colonna *et al.* introduced a triphasic catalytic system based on water-organic solvent-poly-amino acids which afforded optical active epoxides [7]. The long reaction time and the problems regarding the recovery of the catalyst were overcome by Roberts *et al.* who developed a biphasic system composed of an organic base and anhydrous urea-hydrogen peroxide and poly-amino acids on silica as catalyst [8].

To increase the yield of the epoxidation reaction, Geller *et al.* modified the triphasic protocol by adding tetrabutylammonium bromide (TBAB) as co-catalyst. Using this method and in the presence of poly-L-leucine, the reaction time was considerably decreased and the enantiomeric excess was improved [9].

Recently, our group developed a new catalyst based on poly-L-leucine immobilized into hydrotalcites able to catalyse the Juliá-Colonna epoxidation of *trans*-chalcone under triphasic conditions with good conversions and enantioselectivity [10].

Industry favours catalytic processes that require less workup and where intermediates are obtained *in-situ*, avoiding unnecessary purification procedures. Various α,β-unsaturated ketones used in asymmetric epoxidation reactions require the preparation from the corresponding aldehydes and ketones, which can be troublesome according to the available procedures [11-13].

In literature there are several homogeneous systems [14-17], but only two heterogeneous systems able to carry out the Claisen-Schmidt condensation-asymmetric epoxidation reaction. Choudary *et al*. used nanomagnesium oxide (NAP-MgO), but the conversion and enantioselectivity obtained were moderate. Additionally, the catalytic system lost its activity by poisoning with the water formed during the condensation reaction [18]. Liu *et al.* carried out

the first part of the reaction in homogeneous medium and added afterwards poly-L-leucine for the asymmetric epoxidation. Though they recycled the polymer, the system is not completely heterogeneous and the process requires longer reaction time [19].

Herein, we wish to report an efficient green one-pot way to synthesise chiral epoxy-chalcones from the corresponding aldehydes and ketones using poly-L-Leucine immobilized into rehydrated hydrotalcites (Scheme 3.1).

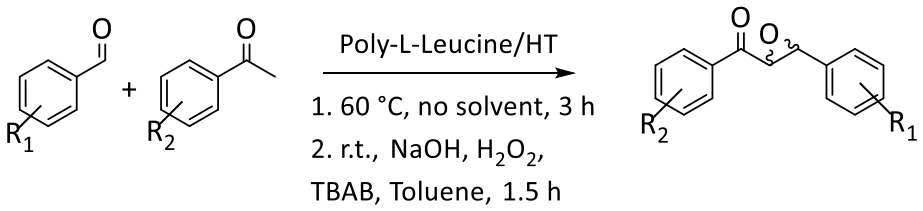


**Scheme 3.1** One-pot synthesis of chiral epoxy-chalcones catalysed by immobilized poly-L-Leucine (IPL)

## 3.2 Experimental

### 3.2.1 General

All chemicals and solvents were commercially available (Aldrich Chemical, Fluka) and used without further purification/ drying unless otherwise mentioned.

XRD measurements were made using a Siemens D5000 diffractometer (Bragg-Brentano parafocusing geometry and vertical - goniometer) fitted with a curved graphite diffracted-beam monochromator and diffracted-beam Soller slits, a 0.06° receiving slit and scintillation counter as a detector. The angular 2θ diffraction range was between 1 and 70°. The sample was dusted on to a low background Si(510) sample holder. The data were collected with an angular step of 0.05° at 3s per step and sample rotation. CuK radiation was obtained from a copper X-ray tube operated at 40 kV and 30 mA.

Thermogravimetric analyses coupled with MS and differential thermal analyses (TGA-MS/DTA) were performed on a SenSys Evo TG coupled with HiCube-Pfeiffer Vacuum system.

MALDI-TOF analyses were performed using a Voyager-DE STR MALDI mass spectrometer from Applied Biosystems equipped with a nitrogen laser using the following conditions: emission wavelength 337 nm, pulse duration 3 ns and 20 Hz repetition rate.

$^1$H-NMR spectra were recorded on a Varian NMR System 400 spectrometer in $CDCl_3$. Chemical shifts (δ) are given in ppm and J values are given in Hz.

HPLC analyses were performed on a Shimadzu RID-10A (Refractor Index Detector) using CHIRALPACK IA column and heptane/ethanol 3:1 as mobile phase. Optical rotations were measured on a Perkin-Elmer 241 MC Polarimeter using Na-lamp and $CH_2Cl_2$ as solvent.

### 3.2.2 Synthesis of Hydrotalcite Materials (HTs)

Mg-Al HTs (molar ratio 2:1) were prepared by the coprecipitation method at room temperature and pH = 10. The appropriate amounts of $Mg(NO_3)_2.6H_2O$ and $Al(NO_3)_3.9H_2O$ were dissolved in 110 ml Milli-Q water and added dropwise into a vessel containing 150 ml of Milli-Q water. The pH was kept constant using 2M NaOH solution. The suspension was stirred overnight at room temperature. The obtained solid was filtered and washed several times with water and dried under vacuum. The solids were calcined in air at 450 °C overnight to obtain the corresponding mixed oxides ($HT_{cc}$). $HT_{rus}$ was obtained by the rehydration of $HT_{cc}$ in inert atmosphere using decarbonated water and sonication for 30 minutes [10].

### 3.2.3 Synthesis of Poly-L-Leucine (PLL)

PLL was synthesised by the ring opening polymerisation method using trimethylamine as initiator, as previously reported [10]. The L-leucine-NCA (0.6 g) was dissolved in anhydrous 1,4-dioxane (11.4 ml) under Ar atmosphere and stirred at 60 °C. After 15 minutes the corresponding amount of trimethylamine (monomer/initiator ratio = 5) was added and the flask was closed with a freshly prepared $CaCl_2$ drying tube. The final mixture was left under stirring at 60 °C for 4 days. Milli-Q water was used as workup solvent and the mixture was stirred for another 2 hours. The obtained solid was filtered and dried under vacuum. The polymer was characterised by MALDI-TOF spectroscopy.

### 3.2.4 Preparation of Immobilized Poly-L-Leucine (IPL)

The poly-L-leucine synthesised using a monomer/initiator ratio of 5 at 60 °C was immobilized into Mg-Al $HT_{rus}$ (molar ratios 2:1). In a typical procedure, 100 mg PLL were added over a mixture containing 300 mg $HT_{rus}$ and 5 ml decarbonated water. The suspension was stirred for 1 h and subjected to ultrasounds for another 30 minutes. The obtained material was washed with THF and dried at 40 °C under inert atmosphere. The nanohybrid materials were characterised by MALDI-TOF and XRD spectroscopy. The amount of PLL immobilised was determined by TGA analysis.

### 3.2.5 Standard Conditions for the Claisen-Schmidt Condensation Reaction

The Claisen-Schmidt condensation reaction was performed in a 10 ml tube. The general procedure was as follows: acetophenone (0.19 mmol) and benzaldehyde (0.20 mmol) were added, along with the solvent – in some cases - over the catalyst (PLL, IPL, uncalcined HTs). The mixture was stirred for 3 h at different temperatures: 30 °C, 60 °C or 80 °C. The catalyst was

recovered by centrifugation and washed several times with the solvent. The organic layer was dried over $MgSO_4$ and the solvent was removed by evaporation under reduced pressure. The products were identified by $^1$H-NMR.

### 3.2.6 Standard Conditions for the One-pot Claisen-Schmidt Condensation / Juliá–Colonna Epoxidation Reaction

The one-pot Claisen-Schmidt condensation/Juliá-Colonna epoxidation reaction was performed in a 10 ml tube. The corresponding ketones (0.19 mmol) and aldehydes (0.20 mmol) were added over IPL (100 wt% PLL with respect to ketone) and stirred for 3 h at 60 °C. In all the experiments the molar ratio ketone/aldehyde was 0.95. The reaction mixture was cooled at room temperature and TBAB (3.7 mg), $H_2O_2$ (169.7 µl), NaOH 2M (245 µl) and 1 ml toluene were added. The reaction mixture was stirred at room temperature for another 1.5 h. The catalyst recovered by centrifugation was washed several times with toluene and water and reused without drying. The organic layer was dried over $MgSO_4$ and the solvent was removed by evaporation under reduced pressure. The products were identified by $^1$H-NMR. The ee% of the corresponding epoxide was determined by chiral HPLC. The configuration of the major enantiomer was in each case determined by comparison with the literature data.

## 3.3 Results and Discussion

### 3.3.1 Catalyst Preparation and Characterization

Mg-Al HTs (molar ratio 2:1) were prepared by the coprecipitation method at pH 10. The obtained materials were calcined at 450 °C and rehydrated with decarbonated water under sonication, to increase the basic sites found between HT layers.

We have showed that the immobilization of the PLL material into the $HT_{rus}$ is favoured by the presence of the carboxylic group [10] in the bio-guest, while the N-terminal group of the polymer is important in the catalytic activity [5]. In this context, the polymer was synthesized by the ring-opening polymerization of the L-leucine-NCA using trimethylamine as initiator, to afford the N- and C-terminals (Scheme 3.2).

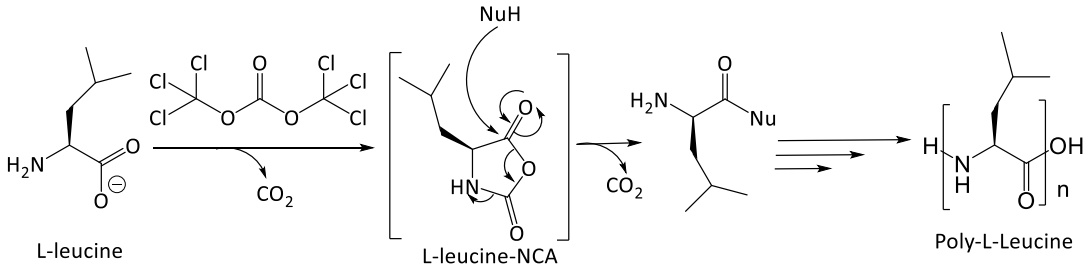


**Scheme 3.2** Synthesis of PLL by ring-opening polymerization of L-leucine-NCA

The MALDI-TOF MS spectrum of the polymer (Figure 3.1) shows a regular series of peaks, ranging from m/z 500 to 5000. The inset figure shows that the spectrum is a repetition of 3 peaks, corresponding peaks in two consecutive series being separated by 113 Da - representing the leucine residue. For example, the first peak at 1528 Da in the inset spectrum corresponds to a linear polymer containing 13 monomers adducted with potassium; the second peak at 1550 Da corresponds to a linear polymer of the same magnitude, deprotonated and adducted with sodium and potassium; the peak at 1599 Da is specific for a cyclic polymer of 13 monomers adducted with potassium and having an additional mass of two molecules of $CO_2$. The obtained polymer had a molecular weight of 2805.7 Da and a polydispersity of 1.38.

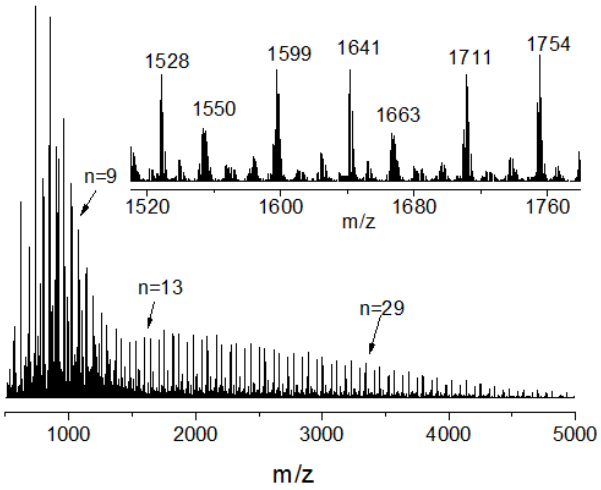


**Figure 3.1** MALDI-TOF spectrum of PLL. Insert: MALDI-TOF spectrum in the m/z range – 1500-1760

Nanohybrid materials based on PLL immobilised into rehydrated hydrotalcites were synthesised as previously mentioned [10]. The XRD patterns of all the synthesised materials presented $d_{003}$ and $d_{006}$ diffraction peaks corresponding to meixnerite structure (Figure 3.2). Rehydrated hydrotalcite ($HT_{rus}$) displayed a main peak at 11.4 $2\Theta$ corresponding to a $d_{003}$ = 7.7 Å (Figure 3.2-b). The XRD spectra of IPL materials showed a new diffraction peak at 7.5 $2\Theta$ indicating that the PLL was immobilised in the interlayer structure of the hydrotalcite (Figure 3.2-c) [20].

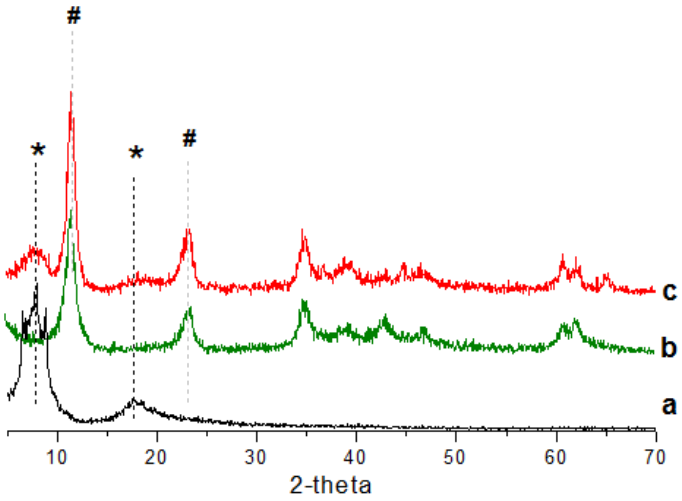


**Figure 3.2** XRD patterns of nanohybrid PLL/HTr$_{us}$ materials: (a) PLL; (b) HT$_{rus}$ and (c) IPL. * Basal peaks of *(0 0 3)* plane with immobilized PLL. # Basal peaks of *(0 0 3)* and *(0 0 6)* planes of the starting HT$_{rus}$ material

The thermal decomposition of the nanohybrid materials corresponds to the decomposition of both the immobilized polymer and the rehydrated hydrotalcite. The curve presented three characteristic weight loss: (i) between room temperature and 200 °C, with a maximum at 130 °C corresponding to the removal of surface-absorbed water, the presence of some residual THF after washing and interlayer water molecules; (ii) between 200 °C and 300 °C with a maximum at 246 °C corresponding to the loss of water absorbed in the PLL structure and (iii) from 300 °C to 785 °C with two maxima at 358 °C and 438 °C corresponding to the dihydroxylation of the HT and the decomposition of the PLL structure and the elimination of $CO_2$ remained from the HT structure (Figures C.1 and C.2 – Appendix C). The immobilization ratio computed from thermogravimetric analysis varied, depending on the amount of polymer used. The typical amount of immobilized polymer was 0.1461 mg PLL/mg HT.

### 3.3.2 Claisen-Schmidt Condensation Reaction

Claisen-Schmidt condensation is a common reaction catalysed by either an acidic or basic catalyst. Consequently, hydrotalcite materials have been intensively used in the aldol condensation of different aldehydes and ketones. Tichit *et al.* presented a kinetic study of chalcone synthesis involving calcined and rehydrated hydrotalcites. The later materials showed better activity due to the presence of the –OH groups at the edges of the HT layers [21]. The same behaviour was observed by Corma *et al.* [22] and Figueras *et al.* [23] in the synthesis of flavones and condensation of benzaldehyde with acetone, respectively.

De Jong *et al*. [24] and Medina *et al*. [25] reported the synthesis of different more active HT materials prepared by sonication and rehydration, and demonstrated that the rehydration time

strongly influenced the solid catalysts. Climent *et al.* demonstrated that the activity of rehydrated hydrotalcites in the Claisen-Schmidt condensation of acetophenone with aldehyde is dependent on the amount of water used in the rehydration process [26]. The role of the solvent in this reaction was also investigated confirming that solvents' acidity reduces the activity of the HTs by poisoning of the strong basic centres. One disadvantage of using HTs in the C-C bond-forming reactions is the acid-base character of the materials. Both the strong basic centres and the metals located on the surface are able to catalyse side-reactions such as self-condensation of ketones or condensation between the reagent and the formed chalcone [27].

Interestingly, Córdova *et al.* showed that amino acids can catalyse not only the asymmetric aldol addition reaction, but also the aldol condensation reaction. The mechanism proposed can follow two pathways, depending on the amount of catalyst used: either the aldol pathway via the enamine intermediate or the Mannich one via the iminium ion [28].

Thus, this nanohybrid catalyst presents two potential active sites in the Claisen-Schmidt condensation reaction: the rehydrated hydrotalcite and the poly-amino acid. As hydrotalcites are already benchmarks of this reaction, we tested the PLL in the aldol condensation of benzaldehyde and acetophenone at 80 °C and water as solvent. The PLL inactivity in this reaction demonstrates that the last 3-4 monomers in the polymer structure - which are not involved in the hydrogen-bonding of the α-helical form of the polymer - are unable to form the desired iminium ion which would lead to chalcone formation (as Scheme 3.3 shows).

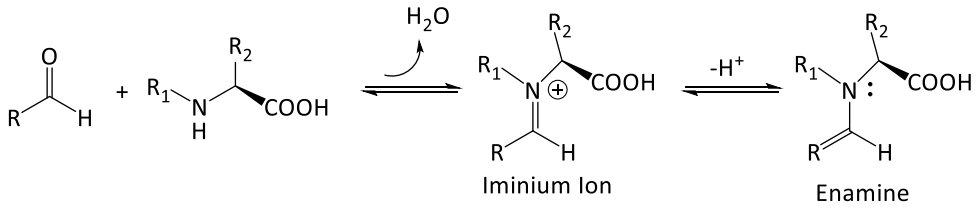


**Scheme 3.3** Iminium and enamine ion formation in Claisen-Schmidt condensation catalysed by amino acids [28]

Consequently, we investigated the activity of the new material in the Claisen-Schmidt condensation of benzaldehyde and acetophenone. Under the conditions mentioned above, the main product of reaction was *trans*-chalcone with the formation of different side products: *cis*-chalcone and 1,3,5-triphenylpentane-1,5-dione (Scheme 3.4).

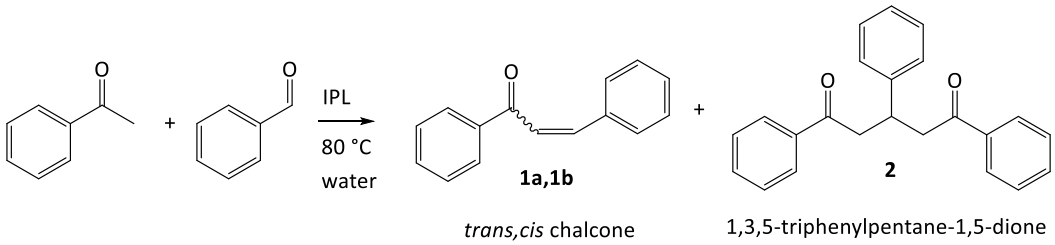


*trans,cis* chalcone 1,3,5-triphenylpentane-1,5-dione

**Scheme 3.4** Claisen-Schmidt condensation reaction between benzaldehyde and acetophenone. Reaction conditions: aldehyde and ketone in molar ratio of 0.95, 100 wt% PLL with respect to ketone, 1 ml water, 3 h, 80 °C.

Jong *et al.* previously showed that the Claisen-Schmidt condensation reaction catalysed by rehydrated HT proceeds through the extraction of a proton from the α-carbon atom of the ketone by the Brönsted basic sites of the catalysts, mainly the $OH^-$ groups found at the edges of the laminar structure of the catalyst. In our preceding work we have demonstrated that the immobilization of the poly-L-leucine proceeds via the interlayered hydroxyl groups and/or the $OH^-$ anions located at the edges of the HTs [20]. Because in the IPL system the access to some of the $OH^-$ groups is hindered by the presence of the polymer, the active basic sites involved in the catalytic process might be also located on the surface of the catalyst. This assumption was tested by using an uncalcined HT containing nitrates in the Claisen-Schmidt condensation reaction. The very low activity suggests the possible presence of active sites on the surface of the hydrotalcite.

Our results demonstrate that in the IPL material, the hydrotalcite is the only active catalyst in the Claisen-Schmidt condensation reaction.

### *3.3.2.1 Temperature Effect*

To better understand the catalytic process, we studied the effect of temperature upon the Claisen-Schmidt condensation reaction. Figure 3.3 presents the results of the IPL-catalysed reaction between acetophenone and benzaldehyde at 30 °C, 60 °C and 80 °C.

When the reaction was carried out at 80 °C the conversion was 70% while the selectivity towards *trans*-chalcone (**1a**) was only of 49%. The other side products observed were *cis*-chalcone (**1b**) and the Michael addition product (**2**) between chalcone and acetophenone. Until now, the *cis*-isomer was obtained in the Claisen-Schmidt reaction only in the presence of the acidic zeolites [29]. Hence, hydrotalcites have dual functionality represented by the presence of the Brönsted basic sites and the Lewis acidic sites ($Al^{3+}$) found on the surface of the catalysts.

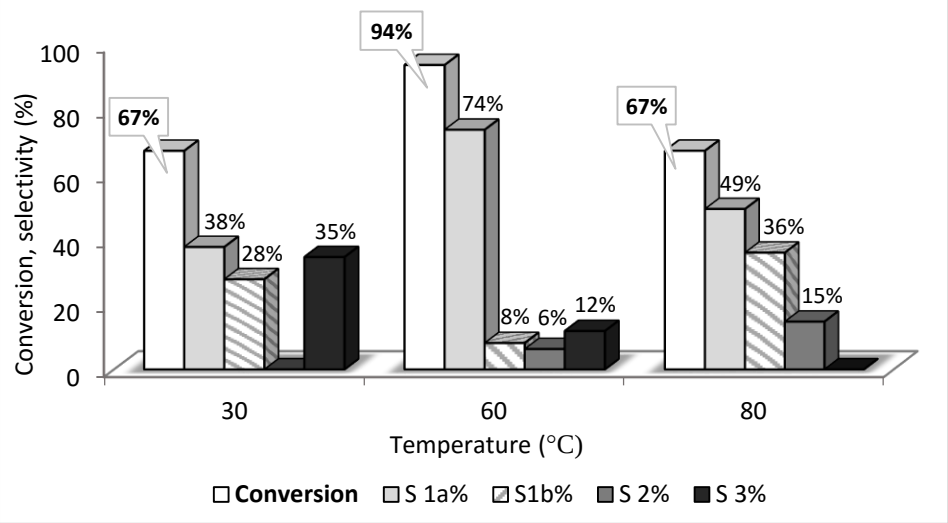


**Figure 3.3** Effect of temperature upon Claisen-Schmidt condensation. 1a – trans-chalcone; 1b – cis-chalcone; 2 - 1,3,5-triphenylpentane-1,5-dione; 3 - 3-hydroxy-1,3-diphenylpropan-1-one. Reaction conditions: 100 wt% PLL with respect to ketone, acetophenone and benzaldehyde 0.95 molar ratio, 1 ml water, 3 h. Conversion and selectivity from $^{1}$H-NMR spectra of the crude material.

On the other hand, the presence of the Michael addition product (**2**) is explained by the reactivity of the enolate formed during the Claisen-Schmidt reaction. This enolate will interact with the aldehyde to form chalcone and will further interact with the obtained chalcone to form substance (**2**).

Knowing that temperature favours the formation of side products in the Claisen-Schmidt condensation, we have carried out the reaction at 30 °C. Curiously, under these conditions, the aldol addition product is favoured (**3**) and no Michael adduct was obtained (Figure 3.4).

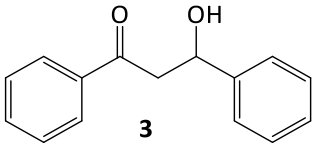


**3**

3-hydroxy-1,3-diphenylpropan-1-one

**Figure 3.4** The aldol addition product obtained in the Claisen-Schmidt condensation

Our present results demonstrate that the optimum temperature to carry out the Claisen-Schmidt condensation reaction catalysed by the IPL is 60 °C. At this temperature total conversion was obtained with very good selectivity towards the *trans*-chalcone.

### *3.3.2.2 Solvent Effect*

It is widely acknowledged the importance of solvent effects on the chemical reactivity. Thus, we performed the Claisen-Schmidt condensation reaction in different solvents (toluene,

ethanol, water) and without solvent (Figure 3.5). The low conversion observed when ethanol (a non-aqueous protic solvent) was used can be explained through its acidic character which, during 3 h of reaction, could deactivate the strong basic sites of the hydrotalcite. The only detected product was *trans* – chalcone (**1a**). In the case of non-protic solvents (ex. Toluene), the reaction proceeded with a better conversion than in the case of ethanol, with the formation of both *cis* and *trans*-chalcone.

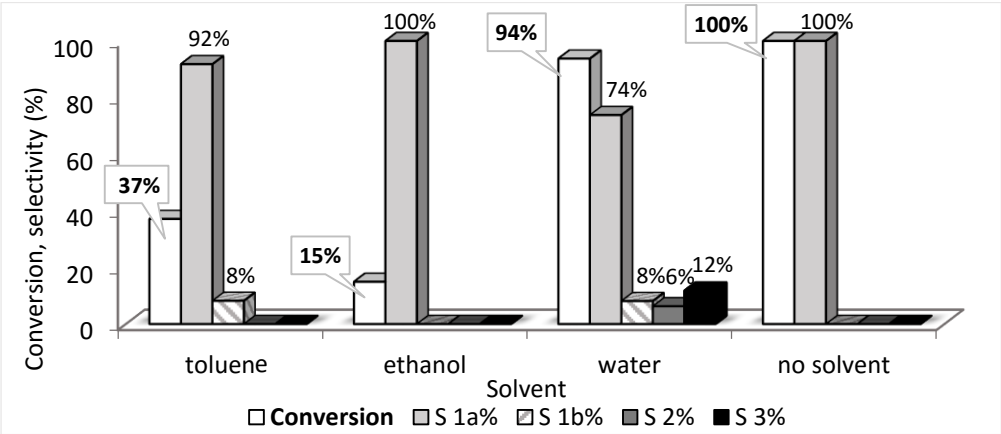


**Figure 3.5** Claisen-Schmidt condensation using different solvents: 1a – trans-chalcone; 1b – cis-chalcone; 2 - 1,3,5-triphenylpentane-1,5-dione; 3 - 3-hydroxy-1,3-diphenylpropan-1-one. Reaction conditions: 100 wt% PLL with respect to ketone, acetophenone and benzaldehyde 0.95 molar ratio, 1 ml solvent, 3 h. Conversion and selectivity from $^{1}$H-NMR spectra of the crude material.

When water was used as solvent, despite attaining a good conversion, the aldol addition product (**3**) was obtained, demonstrating that in an aqueous medium the formed chalcone can be hydrolysed.

Green chemistry implies the use of safer solvents or their elimination [30]. In this context, we have run Claisen-Schmidt condensation reaction under neat conditions. Literature reports that when this reaction was carried out without solvent, it either requires longer reaction times [31], high reaction temperatures [32] or leads to very low conversions [33]. On the contrary, this new nanohybrid catalyst favours the aldol condensation reaction in absence of solvent, affording total selectivity towards *trans*-chalcone and total conversion.

### 3.3.3 One-pot Claisen-Schmidt Condensation / Juliá–Colonna Epoxidation Reaction

The results presented above demonstrate that the Claisen-Schmidt condensation reaction between acetophenone and benzaldehyde can be carried out at a lower temperature without solvent. To test the effectiveness of this nanohybrid catalyst, we studied its activity in the one-pot Claisen-Schmidt condensation/Juliá-Colonna epoxidation reaction. The protocol for α,β-

epoxy ketone synthesis involves two steps: (i) formation of enone from the corresponding ketone and aldehyde catalysed by the HT part of the IPL and (ii) asymmetric epoxidation of enone with $H_2O_2$, catalysed by the immobilized poly-amino acid. To enhance the enantioselectivity, the length of the poly-L-leucine is of crucial importance, as Berkessel *et al*. showed [34]. Hence, we synthesised poly-L-leucine with a length between 30 and 45 monomers.

We studied the one-pot reaction with a Claisen-Schmidt condensation of benzaldehyde and acetophenone at 60 °C under neat conditions, followed by the addition of the phase-transfer co-catalyst (TBAB), $H_2O_2$, NaOH and solvent. The IPL catalyst was re-used for 4 consecutive runs, to study its stability and selectivity (Table 3.1). The material proved to be very stable and efficient in terms of selectivity and enantioselectivity (both of which remained constant in all the 4 runs).

**Table 3.1** One-pot Claisen-Schmidt condensation/Juliá-Colonna epoxidation of acetophenone and benzaldehyde

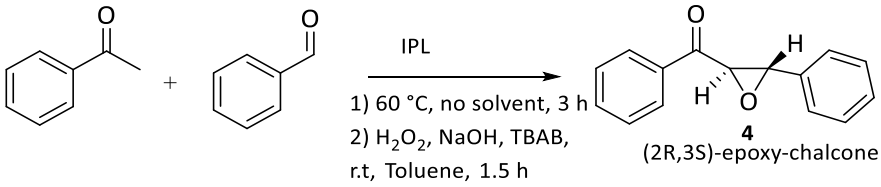


| Run[a] | Conversion (%)[b] | Selectivity (%)[b] | Yield (%) | ee (%)[c] |
|---|---|---|---|---|
| **1** | >99 | >99 | >98 | 91 |
| **2** | >99 | >99 | >98 | 89 |
| **3** | >99 | >99 | >98 | 88 |
| **4** | >99 | >99 | >98 | 87 |

[a]Reaction conditions: acetophenone and benzaldehyde in molar ratio of 0.95 were added over the catalyst (100 wt% PLL with respect to the ketone), stirred 3 h at 60 °C; 3.7 mg TBAB, 1 ml toluene, 245 µL NaOH, 169.7 µL $H_2O_2$ were added and the reaction was further stirred for 1.5 h at room temperature; [b]conversion and selectivity were computed from $^1$H-NMR spectra of the crude material; [c]ee was computed from HPLC spectra.

To identify if the hydrotalcite-part of the IPL plays a role in the second part of the reaction we have carried out four control experiments, using the same conditions as previously mentioned (results presented in Table 3.2). The first two experiments consisted in carrying out the epoxidation reaction with and without rehydrated hydrotalcite (entries 1 and 2, Table 3.2) and in both cases total conversion was obtained. Knowing that rehydrated hydrotalcites possess basic properties, we have run the epoxidation reaction without the presence of NaOH using $HT_{rus}$ and IPL (entry 3, Table 3.2). In the former case a conversion of 5% was obtain while in the latter

one no epoxide was observed. This information suggests than any basic centre found in the $HT_{rus}$ capable to deprotonate the hydrogen peroxide is deactivated when the polymer is immobilized. All these findings demonstrate that in the second part of the one-pot reaction the only active catalyst is the poly-L-Leucine.

**Table 3.2** Control experiments for the epoxidation reaction

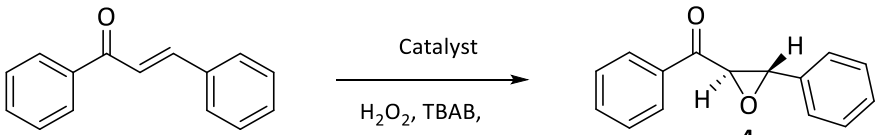


**4**
(2R,3S)-epoxy-chalcone

| Experiment[a] | Catalyst | NaOH (µL) | Conversion (%)[b] |
|---|---|---|---|
| **1** | - | 245 | >99 |
| **2** | $HT_{rus}$ (120 mg) | 245 | >99 |
| **3** | $HT_{rus}$ (120 mg) | - | 5 |
| **4** | IPL (100 wt% PL) | - | - |

[a]Reaction conditions: 10 mg chalcone, 3.7 mg TBAB, 1 ml toluene, 169.7 µL $H_2O_2$ were added and the reaction was stirred for 1.5 h at room temperature; [b]conversion was computed from $^1$H-NMR spectra of the crude material

As mentioned in the section dedicated to the Claisen-Schmidt condensation, there are several side products that might appear, depending on the basicity of the environment, excess of reactants and the solvent used. A key point in recycling the catalyst for the one-pot reaction is washing the material after each run, to eliminate: i) any unreacted NaOH, ii) any unreacted reagent and iii) traces of the obtained product, which may lead to side products in the next run.

The TGA pattern of the catalyst after 4 consecutive runs resembles to that of the catalyst before reaction and no difference in weight loss is observed, ruling out the possible leaching of the catalyst (Figure C.3 – Appendix C).

### 3.3.4 One-pot Claisen-Schmidt Condensation / Juliá–Colonna Epoxidation Reaction – Scope of Reaction

To confirm the activity of this new nanohybrid system, we studied the one-pot reaction using acetophenone/ benzaldehyde with different aldehydes / ketones bearing electron donating or electron withdrawing groups in 4 consecutive runs (Table 3.3 and Table 3.4).

**Table 3.3** One-pot Claisen-Schmidt condensation/Juliá-Colonna epoxidation of acetophenone and different benzaldehydes

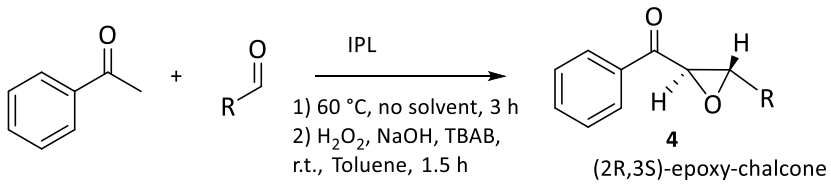


**4**
(2R,3S)-epoxy-chalcone

| Entry | R | Run[a] | Conversion[b] (%) | Selectivity[b] (%) | Yield (%) | ee[c] (%) |
|---|---|---|---|---|---|---|
| **1** | o-$NO_2$- $C_6H_4$ | 1 | 98 | 98 | 96 | 91* |
| | | 2 | 96 | 98 | 94 | 84* |
| | | 3 | 94 | 98 | 92 | 79* |
| | | 4 | 94 | 98 | 92 | 79* |
| **2** | p-$NO_2$-$C_6H_4$ | 1 | 95 | 99 | 94 | 94 |
| | | 2 | 98 | 99 | 97 | 92 |
| | | 3 | 98 | 99 | 97 | 90 |
| | | 4 | 97 | 99 | 96 | 86 |
| **3** | p-Cl-$C_6H_4$ | 1 | 97 | 95 | 92 | 94 |
| | | 2 | 97 | 94 | 91 | 95 |
| | | 3 | 98 | 92 | 90 | 96 |
| | | 4 | 97 | 93 | 90 | 91 |
| **4** | p-$CH_3$-$C_6H_4$ | 1 | 87 | 94 | 82 | 87 |
| | | 2 | 84 | 92 | 77 | 82 |
| | | 3 | 82 | 92 | 75 | 77 |
| | | 4 | 85 | 95 | 81 | 72 |

[a]Reaction conditions: acetophenone and corresponding aldehyde in molar ratio of 0.95 were added over the catalyst (100 wt% PLL with respect to the ketone), stirred 3 h at 60 °C; 3.7 mg TBAB, 1 ml toluene, 245 µL NaOH, 169.7 µL $H_2O_2$ were added and the reaction was further stirred for 1.5 h at room temperature; [b]conversion and selectivity were computed from $^1$H-NMR spectra of the crude material; [c]ee was computed from HPLC spectra; *The (2S,3R) is the major enantiomer.

Strong electronic withdrawing groups (EWG) on benzaldehyde led to the highest conversion and selectivity in all the 4 consecutive runs (entries 1 and 2, Table 3.3). The presence of the EWG make the carbonyl carbon more electron deficient, thus being more vulnerable to the nucleophilic attack in the Claisen-Schmidt part of the reaction. The steric effect of the nitro group (present in the *ortho* or *para* position) is observed in the stereochemistry of the epoxide. When the nitro group is found in *ortho* position the *(2S,3R)*-epoxy-chalcone was obtained with a very good enantioselectivity. On the other hand, when a weak EWG was in *para* position the selectivity towards the epoxide decreased slowly (variation which is in the error limit of the equipment) during the 4 runs, even though the conversion was constant (entry 3, Table 3.3).

Last but not least, the presence of a weak electron donating group (EDG) in *para* position deactivates the benzaldehyde - effect observed on both conversion and enantiomeric excess of the final epoxide (entry 4, Table 3.3).

As expected, the substituted acetophenones were far less reactive than the corresponding aldehydes. In this case, the ketones bearing weak EWD and the EDG found in *para* position favoured the Claisen-Schmidt condensation/Juliá-Colonna epoxidation reaction, generating very good conversion, selectivity and good enantiomeric excess (entries 3 and 4, Table 3.4).

**Table 3.4** One-pot Claisen-Schmidt condensation/Juliá-Colonna epoxidation of benzaldehyde with different acetophenones

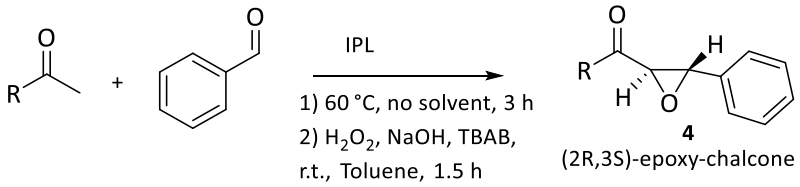


**4**
(2R,3S)-epoxy-chalcone

| Entry | R | Run[a] | Conversion[b] (%) | Selectivity[b] (%) | Yield (%) | ee[c] (%) |
|---|---|---|---|---|---|---|
| **1** | o-$NO_2$-$C_6H_4$ | 1 | 82 | 75 | 62 | 63 |
| | | 2 | 80 | 72 | 58 | 63 |
| | | 3 | 76 | 65 | 49 | 62 |
| | | 4 | 70 | 67 | 47 | 60 |
| **2** | p-$NO_2$-$C_6H_4$ | 1 | 97 | 99 | 96 | 89 |
| | | 2 | 91 | 95 | 87 | 81 |
| | | 3 | 82 | 84 | 69 | 78 |
| | | 4 | 85 | 82 | 70 | 75 |
| **3** | p-Cl-$C_6H_4$ | 1 | 99 | 97 | 96 | 91 |
| | | 2 | 99 | 97 | 96 | 89 |
| | | 3 | 99 | 98 | 97 | 81 |
| | | 4 | 99 | 98 | 97 | 71 |
| **4** | p-$CH_3$-$C_6H_4$ | 1 | 94 | 97 | 91 | 80 |
| | | 2 | 92 | 96 | 88 | 79 |
| | | 3 | 90 | 98 | 88 | 79 |
| | | 4 | 91 | 99 | 90 | 74 |

[a]Reaction conditions: acetophenone and corresponding aldehyde in molar ratio of 0.95 were added over the catalyst (100 wt% PLL with respect to the ketone), stirred 3 h at 60 °C; 3.7 mg TBAB, 1 ml toluene, 245 µL NaOH, 169.7 µL $H_2O_2$ were added and the reaction was further stirred for 1.5 h at room temperature; [b]conversion and selectivity were computed from $^1$H-NMR spectra of the crude material; [c]ee was computed from HPLC spectra.

The *ortho*-nitro acetophenone was less reactive than the *para*-nitro acetophenone (entries 1 and 2, Table 3.4). The low ee% obtained in this case is directly related to the steric effect created by the nitro group in *ortho* position during the epoxidation reaction.

### 3.3.5 Mechanism of the Claisen-Schmidt Condensation/Juliá-Colonna Epoxidation Reaction

The proposed mechanism of Claisen-Schmidt condensation/ Juliá-Colonna epoxidation reaction catalysed by the nanohybrid material proceeds at the Brönsted basic sites near the edges of the hydrotalcite part of the IPL catalyst (Figure 3.6-A) and/or the basic sites located at the surface of the $HT_{rus}$. The $OH^-$ groups remove the alpha hydrogen from the aromatic ketone, producing the corresponding enolate ion which will further attack the carbonyl carbon of the aldehyde molecule. Depending on the basicity of the catalyst and on the functional groups attached to the aromatic ring, the aldol product formed undergoes dehydration producing the *cis* and *trans* α,β-unsaturated ketone. The very reactive enolate ion can further give a Michael addition reaction with the freshly formed chalcone. All the side products can be avoided if no solvent is used in the first part of the one-pot reaction.

In the next step, chalcone interacts with the immobilized polymer to give the corresponding chiral epoxide. The last 4 terminal amino groups of the α-helical structure of the immobilized polymer create an oxyanion hole which facilitates the bonding of the hydroperoxide anion with the already formed chalcone [34]. The specific pattern in which they interact dictates the stereochemistry of the final epoxide. Even though the kinetic models present in the literature [5, 6, 35, 36] have postulated that the epoxide formation proceeds through two possible pathways (Figure 3.6-B) we have recently observed that the favoured one is pathway I, where hydroperoxide anion interacts with the polymer and only afterwards with chalcone, leading to the formation of the PLL:$HOO^-$:chalcone complex (unpublished work). These experiments were done using Quartz Crystal Microbalance with Dissipation (QCM-D), a sensitive mass sensor which measures a mass per unit area by monitoring the frequency shift of the crystal sensor. A change in frequency is induced by molecular deposition on the sensor surface. QMC-D is now well-established to study biomolecular interactions or binding events at the solid-liquid interface with detection limits at around nanograms per $cm^2$ [37] and can be used to distinguish between different mechanism by monitoring the enzymatic activity [38].

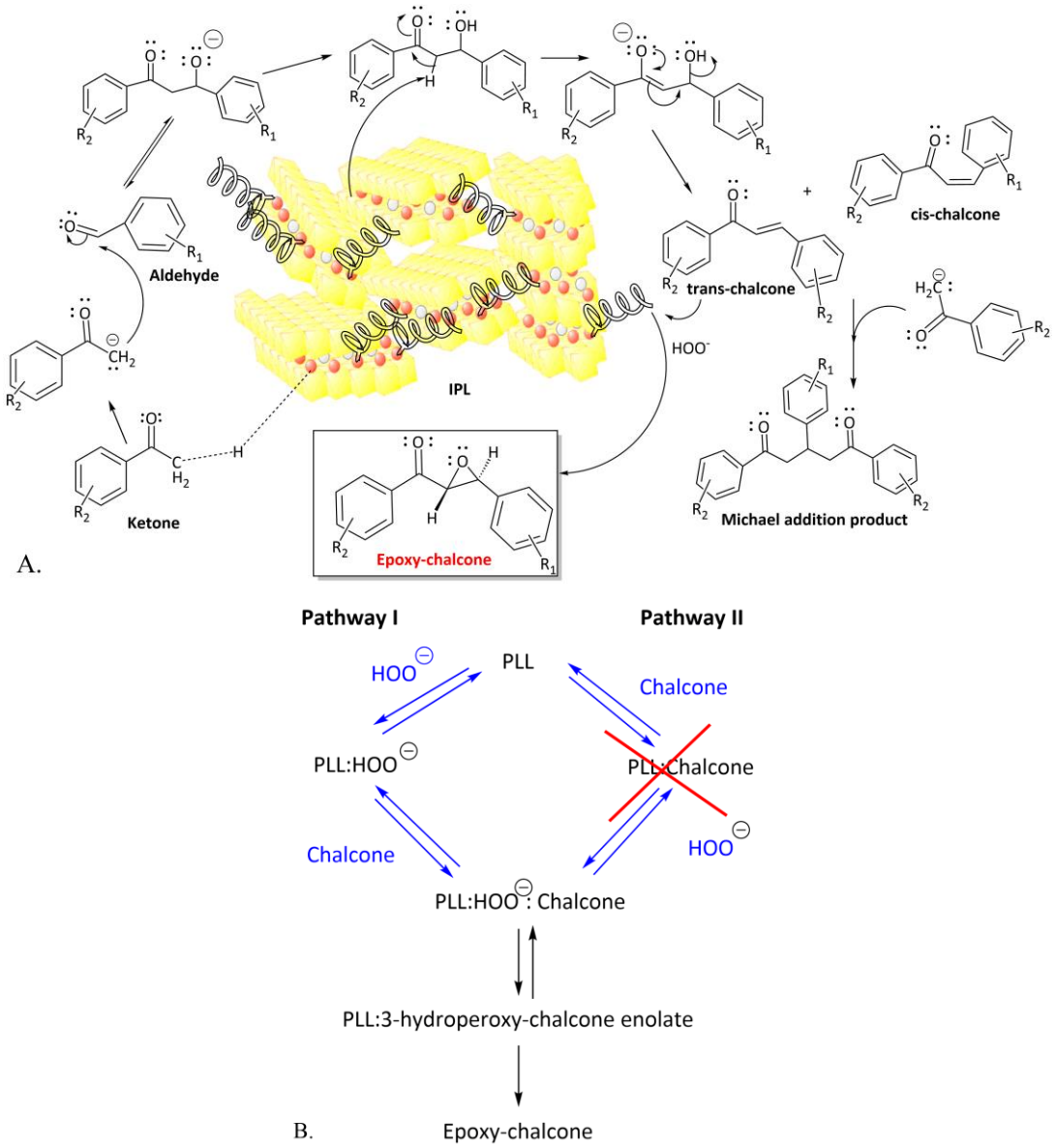


**Figure 3.6** A – General mechanism of the one-pot Claisen-Schmidt condensation/Juliá-Colonna epoxidation reaction catalysed by IPL; B – proposed kinetic pathways for the Juliá-Colonna epoxidation

## 3.4 Conclusions

Nowadays, research is focused on developing catalytic processes that require less workup and where intermediates are obtained *in-situ*, avoiding unnecessary purification procedures. We have managed to successfully develop a convenient and efficient one-pot process for production of chiral α,β-epoxy-chalcones starting from the corresponding acetophenones and benzaldehydes, catalysed by poly-L-leucine immobilized into rehydrated hydrotalcite.

The removal of the solvent in the Claisen-Schmidt condensation part not only creates a greener process, but eludes the presence of side products.

The catalyst has been continuously reused without any further pre-activation and recycled for 4 consecutive runs without losing its activity in terms of selectivity towards the epoxide, enantioselectivity and conversion. Moreover, the unique properties of this catalytic system were observed when *ortho* nitro substituted benzaldehyde was used leading to the formation of the (2S,3R)-isomer. The present work demonstrates the viability and sustainability of this nanohybrid catalytic system in the synthesis of chiral epoxides.

# Bibliography

[1] Q.-H. Xia, H.-Q. Ge, C.-P. Ye, Z.-M. Liu, K.-X. Su, *Chemical Reviews (Washington, D. C.)*, **105**, 1603-1662, **2005**.

[2] P. Besse, H. Veschambre, *Tetrahedron*, **50**, 8885-8927, **1994**.

[3] Y. Zhu, Q. Wang, R.G. Cornwall, Y. Shi, *Chemical Reviews (Washington, D. C.)*, **114**, 8199-8256, **2014**.

[4] M.J. Porter, S.M. Roberts, J. Skidmore, *Bioorganic & Medicinal Chemistry*, **7**, 2145-2156, **1999**.

[5] S. Colonna, D. Perdicchia, E.D. Mauro, *Tetrahedron: Asymmetry*, **20**, 1709-1714, **2009**.

[6] G. Carrea, S. Colonna, A.D. Meek, G. Ottolina, S.M. Roberts, *Tetrahedron: Asymmetry*, **15**, 2945-2949, **2004**.

[7] S. Colonna, H. Molinari, S. Banfi, S. Juliá, J. Masana, A. Alvarez, *Tetrahedron*, **39**, 1635-1641, **1983**.

[8] T. Geller, S.M. Roberts, *Journal of the Chemical Society, Perkin Transactions 1*, 1397-1398, **1999**.

[9] T. Geller, A. Gerlach, C.M. Krüger, H.-C. Militzer, *Journal of Molecular Catalysis A: Chemical*, **251**, 71-77, **2006**.

[10] R.-A. Miranda, J. Llorca, F. Medina, J.E. Sueiras, A.M. Segarra, *Journal of Catalysis*, **282**, 65-73, **2011**.

[11] J. Li, J. Feng, M. Li, Q. Wang, Y. Su, Z. Jia, *Solid State Sciences*, **21**, 1-5, **2013**.

[12] D. Kakati, N.C. Barua, *Tetrahedron*, **70**, 637-642, **2014**.

[13] S.-D. Yang, L.-Y. Wu, Z.-Y. Yan, Z.-L. Pan, Y.-M. Liang, *Journal of Molecular Catalysis A: Chemical*, **268**, 107-111, **2007**.

[14] Y. Wang, J. Ye, X. Liang, *Advanced Synthesis & Catalysis*, **349**, 1033-1036, **2007**.

[15] L.-Z. Dai, M. Shi, *Tetrahedron Letters*, **50**, 651-655, **2009**.

[16] J.-T. Li, Y. Yin, M.-X. Sun, *Ultrasonics Sonochemistry*, **17**, 363-366, **2010**.

[17] D. Ngo, M. Kalala, V. Hogan, R. Manchanayakage, *Tetrahedron Letters*, **55**, 4496-4500, **2014**.

[18] B.M. Choudary, M.L. Kantam, K.V.S. Ranganath, K. Mahendar, B. Sreedhar, *Journal of American Chemical Society*, **126**, 3396-3397, **2004**.

[19] W. Luo, Z. Yu, W. Qiu, F. Yang, X. Liu, J. Tang, *Tetrahedron*, **67**, 5289-5292, **2011**.

[20] R.-A. Miranda, E. Finocchio, J. Llorca, F. Medina, G. Ramis, J.E. Sueiras, A.M. Segarra, *Physical Chemistry Chemical Physics*, **15**, 15645-15659, **2013**.

[21] D. Tichit, M.H. Lhouty, A. Guida, B.H. Chiche, F. Figueras, A. Auroux, D. Bartalini, E. Garrone, *Journal of Catalysis*, **151**, 50-59, **1995**.

[22] M.J. Climent, A. Corma, S. Iborra, J. Primo, *Journal of Catalysis*, **151**, 60-66, **1995**.

[23] K.K. Rao, M. Gravelle, J.S. Valente, F. Figueras, *Journal of Catalysis*, **173**, 115-121, **1998**.

[24] J.C.A.A. Roelofs, D.J. Lensveld, A.J.v. Dillen, K.P.d. Jong, *Journal of Catalysis*, **203**, 184-191, **2001**.

[25] S. Abelló, F. Medina, D. Tichit, J. Pérez-Ramírez, J.C. Groen, J.E. Sueiras, P. Salagre, Y. Cesteros, *Chemistry - A European Journal*, **11**, 728-739, **2005**.

[26] M.J. Climent, A. Corma, S. Iborra, A. Velty, *Journal of Catalysis*, **221**, 474-482, **2004**.

[27] A. Guida, M.H. Lhouty, D. Tichit, F. Figueras, P. Geneste, *Applied Catalysis A: General*, **164**, 251-264, **1997**.

[28] B. Nozière, A. Córdova, *Journal of Physical Chemistry A*, **112**, 2827-2837, **2008**.

[29] M.J. Climent, H. Garcia, J. Primo, *Catalysis Letters*, **4**, 85-92, **1990**.

[30] P. Anastas, J. Warner, *Green chemistry: Theory and practice*, Oxford University Press, Oxford, UK, **2000**.

[31] A. Davoodnia, G. Yassaghi, *Chinese Journal of Catalysis*, **33**, 1950-1957, **2012**.

[32] S.K. Sharma, P.A. Parikh, R.V. Jasra, *Journal of Molecular Catalysis A: Chemical*, **278**, 135-144, **2007**.

[33] F. Toda, K. Tanaka, K. Hamai, *Journal of the Chemical Society, Perkin Transactions 1*, 3207-3209, **1990**.

[34] A. Berkessel, N. Gasch, K. Glaubitz, C. Koch, *Organic Letters*, **3**, 3839-3842, **2001**.

[35] D.R. Kelly, S.M. Roberts, *Chemical Communications*, 2018-2020, **2004**.

[36] S.P. Mathew, S. Gunathilagan, S.M. Roberts, D.G. Blackmond, *Organic Letters*, **7**, 4847-4850, **2005**.

[37] G.V. Dubacheva, P. Dumy, R. Auzély, P. Schaaf, F. Boulmedais, L. Jierry, L. Coche-Guerente, P. Labbé, *Soft Matter*, **6**, 3747-3750, **2010**.

[38] A. Bouchet-Spinellia, L. Coche-Guérenteb, S. Armanda, F. Lenouvela, P. Labbéb, S. Forta, *Sensors and Actuators B: Chemical*, **176**, 1038-1043, **2013**.

# 4 *In-situ* Study of Substrate-Catalyst Interactions in a Juliá - Colonna Epoxidation Using Quartz Crystal Microbalance with Dissipation

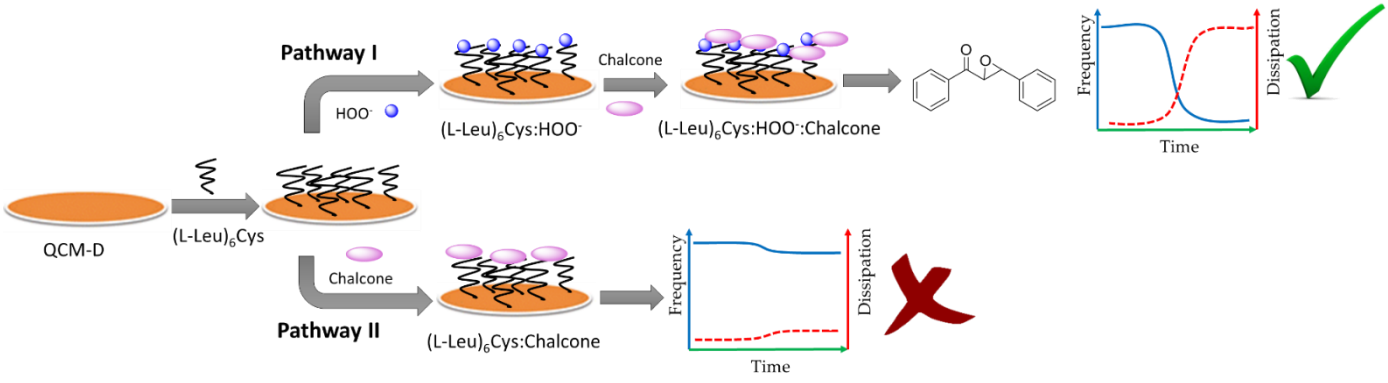


Deborah Wakeham, Dana G. Crivoi, Francesc Medina, Anna Segarra, Mark W. Rutland, *Journal of Colloid and Interface Science*, 469, **2016**, 263-268

## 4.1 Introduction

The Juliá-Colonna reaction is an efficient methodology in the poly-amino acid catalysed epoxidation of α,β-unsaturated ketones [1-4]. The obtained enantiopure epoxides are versatile intermediates for the synthesis of pharmaceuticals and biologically active compounds. Although a wide range of amino acids have been tested in the Juliá-Colonna epoxidation of chalcone (Figure 4.1-a), poly-L-leucine (PLL) has become the benchmark [5-18], and the mechanism of the PLL catalysed Juliá-Colonna epoxidation has been the focus of considerable research interest [6, 8-11, 19-23]. Although the mechanism is not yet completely understood, the current model suggests that the PLL oligomer forms an α-helical structure wherein the last four N-terminal amino groups create an oxyanion hole which interacts with the substrates [19, 20, 24-28]. This facilitates the hydroperoxide-chalcone enolate formation on the peptide, leading to the $HO^-$ elimination and probably dictating the stereochemistry of the resulting epoxide [6, 11, 20, 23]. The kinetic models [15, 21, 22] have postulated that this mechanism takes place via random steady-state formation of the hydroperoxide enolate (PLL:$HOO^-$:chalcone), which can proceed through two possible pathways (Figure 4.1-b), although studies alluded that Pathway I is kinetically preferred [15, 21, 22].

The many studies which have focused on the poly-amino acid conformation dictating substrate binding and the kinetics have availed some mechanistic aspects of the Juliá-Colonna reaction, others have helped to overcome some of the limitations of the process as: long reaction times [12, 13, 16, 29-31], catalyst recovery [7, 30, 32-35], and the scope of compatible substrates [14, 29, 34]. However, the experimental techniques used do not allow the *in-situ* study of the reaction. Thus, there is scant information on the actual intermediates formed in this catalytic process.

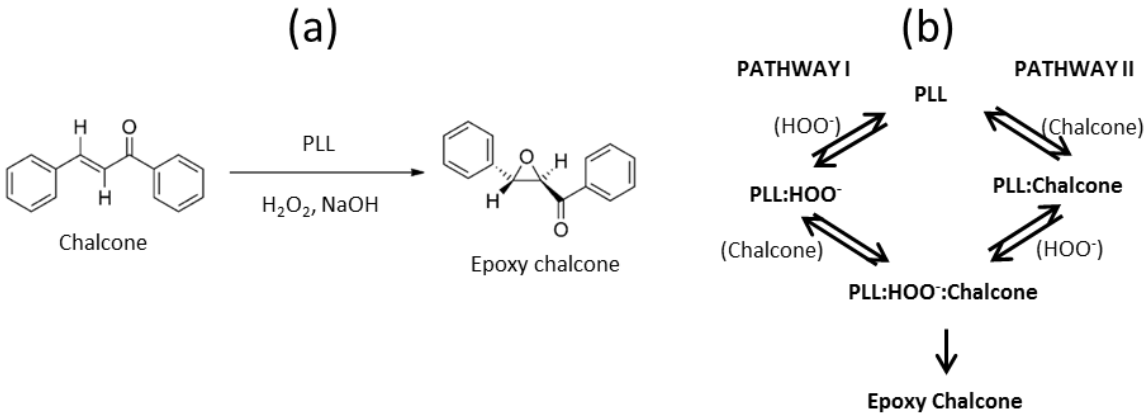


**Figure 4.1 .** Juliá-Colonna PLL catalysed asymmetric epoxidation of chalcone (a) and the proposed kinetic pathway (b).

Quartz crystal microbalance with dissipation monitoring (QCM-D) could be a potentially relevant response to the limitations we have mentioned above. QCM-D is a sensitive mass sensor which measures a mass per unit area by monitoring the frequency shift, *Δf*, of the crystal sensor. A change in frequency is induced by molecular deposition on the sensor surface. In addition, the energy dissipation factor, *ΔD*, can be measured and represents the ability of the surface adsorbed molecules to dissipate the vibrational energy of the system, which in turn gives information on the rigidity of their binding. QCM-D is widely used to study biomolecular interactions and mechanisms, enzymatic activity, and binding events at the solid-liquid interface with detection limits at around nanograms per $cm^2$ [36] .

Here we report the *in-situ* monitoring of the interaction of the substrates - chalcone and $HOO^-$ - with a PLL-type catalyst to better understand the epoxide species formation.

## 4.2 Materials and Methods

### 4.2.1 Materials

The poly-L-leucine used in this work has been modified to include a cysteine group at one end of the poly-amino acid chain, (denoted as $(L\text{-leu})_6$-Cys, Figure D.1 – Appendix D). This inclusion introduces a thiol group which is able to covalently bond to the gold surface. The $(L\text{-leu})_6$-Cys was purchased from Ansyth Service B.V (90%). *Trans*-chalcone (97%), hydrogen peroxide (PERDROGEN™ 30% $H_2O_2$ w/w), sodium hydroxide (≥98%), tetrabutylammonium bromide (TBAB, ≥98%), tetrahydrofuran (THF, anhydrous, 99.9%, 250 ppm BHT inhibitor), and toluene (anhydrous, 99.8%) were all purchased from Sigma-Aldrich. All chemicals were used as received. Milli-Q water with a resistivity of 18.2 MΩ was used for the aqueous solutions.

### 4.2.2 Solution Preparation

The $(L\text{-leu})_6$-Cys solution (100 µM) and chalcone solutions (5 mM) were prepared in a mix of 99% THF and 1% Toluene. $H_2O_2$ (10 mM) was prepared in water with NaOH and TBAB. All solutions were prepared just prior to introduction into the QCM-D.

### 4.2.3 QCM-D Measurements

A Q-Sense E4 quartz crystal microbalance with dissipation (Biolin Scientific, Sweden) was used to monitor the adsorption of a $(L\text{-leu})_6$-Cys layer and the subsequent interaction with the individual components ($HOO^-$ and chalcone) of the Juliá-Colonna epoxidation reaction. The crystal is an AT-cut quartz crystal with a gold coating supplied by Q-Sense (QSX 301, fundamental

frequency of 5 MHz). Solutions were pumped into the cell via an Ismatec IPC-N4 peristaltic pump. The pump was set to a flow rate of 90 µl.min$^{-1}$ and the pump was switched off after sufficient time to fill the cell with the solution (during the rinse stages a constant flow was maintained). The cells and pump were fitted with high resistant Kalrez o-rings, sealing gaskets, tubing and ferrules. Measurements were made at 25 °C and repeated three times.

QCM-D is a sensitive mass sensor which measures a mass per unit area by monitoring the frequency shift, *Δf*, of the crystal sensor. A change in frequency is induced by molecular deposition on the sensor surface, and this adsorbed mass can be estimated for evenly distributed, thin, rigid films using the Sauerbrey equation [37]:

$$\Delta m = -C\frac{\Delta f}{n}$$

where *Δm* is the adsorbed mass per unit area, *C* is the mass sensitivity constant for the crystal (0.177 mg.m$^{-2}$ for our crystals), and *n* is the overtone number (n = 1, 3, 5, 7, 9, and11).

In addition, the energy dissipation factor, *ΔD*, can be measured and represents the ability of the surface adsorbed molecules to dissipate the vibrational energy of the system, which in turn gives information on the rigidity of their binding (viscoelasticity) [38-40]. Dissipation is defined as:

$$D = \frac{E_{diss}}{2\pi E_{stor}}$$

where $E_{diss}$ and $E_{stor}$ are the dissipated and stored energies respectively. The data were analysed using Q-Tools software (Q-Sense) applying both the Sauerbrey and viscoelastic (Voigt) [41] models.

## 4.3 Results and Discussion

The Juliá-Colonna reaction of chalcone was monitored by QCM-D using the (L-leu)$_6$-Cys as a catalyst. The epoxidation in THF was previously tested (using $^1$H-NMR) and was shown to give high conversion to epoxide (>99%) (Figure D.2 - Appendix D).

The change in frequency and dissipation as a function of time during the (L-leu)$_6$-Cys adsorption process is shown in Figure 4.2. The first 45 minutes corresponds to the solvent present within the QCM-D cell. Upon introduction of the (L-leu)$_6$-Cys, the frequency rapidly decreased indicating (L-leu)$_6$-Cys adsorption to the sensor surface. Once the QCM-D cell was filled, the pump was stopped and the frequency slowly decreased over a long period. This slow decrease is the result of the diffusion and subsequent adsorption of the oligomers to the sensor surface. Meanwhile, the dissipation increased gradually, suggesting that the adsorbed oligomers were rearranging on the surface to allow more (L-leu)$_6$-Cys to bind to the surface. After the

system was rinsed with pure solvent, there is a small increase in the frequency and a small decrease in dissipation, attributed to the removal of any unbound or loosely adsorbed material. The overall change in frequency is -20 Hz, while the dissipation change is 10 x $10^{-6}$, demonstrating successful (L-leu)$_6$-Cys adsorption to the gold surface. The large dissipation change indicates the adsorbed (L-leu)$_6$-Cys is viscoelastic rather than rigid and therefore the layer was fit using the Voigt model (Figure D.3 – Appendix D). This gave an adsorbed mass of 18.4 ± 0.6 mg.m$^{-2}$.

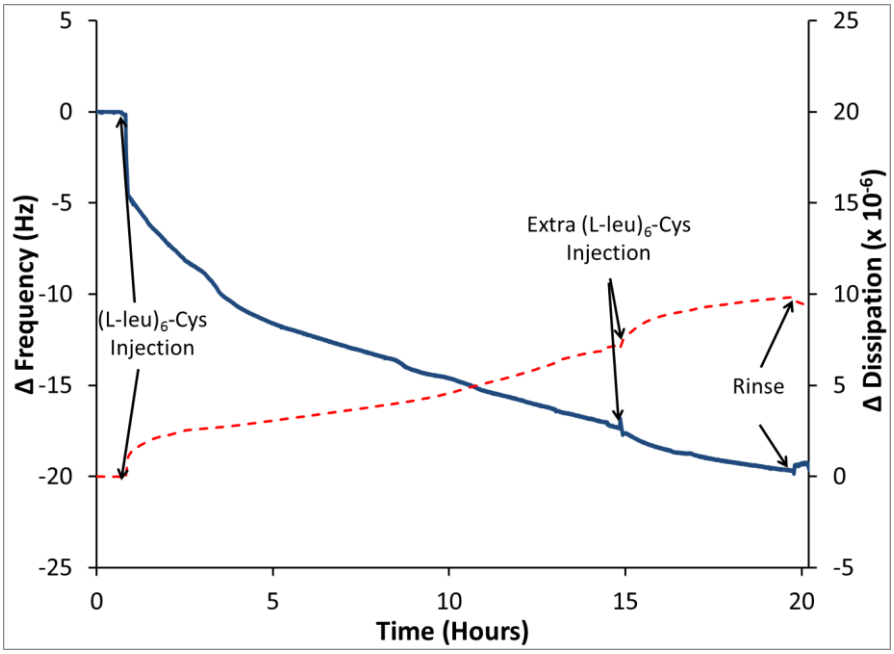


**Figure 4.2** Plot of the frequency shift (solid line) and dissipation factor (dashed line) of the gold coated QCM-D crystal sensor in response to the adsorption of (L-leu)6-Cys. (Average Δf of repeat measurements is 18.0 ± 3.5 Hz).

To gain insight into the interaction of the Juliá-Colonna reagents with the adsorbed (L-leu)$_6$-Cys layer, individual solutions of $HOO^-$ ($H_2O_2$/NaOH) and chalcone were prepared and flowed over the (L-leu)$_6$-Cys layer while the frequency and dissipation were monitored. It should be noted that the (L-leu)$_6$-Cys and chalcone were prepared in THF/toluene solutions while the $HOO^-$ was an aqueous solution. Therefore, each solvent was pumped into the cell and a stable baseline was established for both the frequency and dissipation for at least 30 minutes before the corresponding reagent was passed into the cell. This baseline was used to determine the frequency and dissipation changes induced by the samples. The different solvents resulted in a significant frequency and dissipation response. When changing from THF/toluene to water a decrease in frequency (≈ -120 Hz) and an increase in dissipation (≈ 45 x $10^{-6}$) were observed (Figure D.4 – Appendix D). This could be due to a change in the adsorbed layer or due to

variances in the solvent viscosity ($\eta$) and density ($\rho$) [42]. The theoretical frequency shift due to the solvent bulk properties can be calculated using the equation by Kanazawa and Gordon [42]:

$$\Delta f = \frac{1}{2\pi t_q \rho_q}\left(\frac{\omega \rho_{s1}\eta_{s1}}{2}\right)^{\frac{1}{2}} - \frac{1}{2\pi t_q \rho_q}\left(\frac{\omega \rho_{s2}\eta_{s2}}{2}\right)^{\frac{1}{2}}$$

where $t_q$ is the thickness of the quartz crystal, $\omega = 2\pi f_0$ ($f_0$ refers to the fundamental frequency) and the subscripts *q*, *s1* and *s2* refer to the quartz crystal, solvent 1 and solvent 2 respectively. Similarly, the dissipation change can be calculated by the relationship proposed by Rodahl and Kasemo [43]:

$$\Delta D = \frac{1}{t_q \rho_q}\left(\frac{2\rho_{s1}\eta_{s1}}{\omega}\right)^{\frac{1}{2}} - \frac{1}{t_q \rho_q}\left(\frac{2\rho_{s2}\eta_{s2}}{\omega}\right)^{\frac{1}{2}}$$

The calculated frequency change (≈ -95 Hz) was less than the observed changed suggesting an increase in sensed mass on the crystal surface. This may be due to an increased association of water with the layer. There was essentially no difference between the calculated and experimentally observed dissipation change indicating that the change in solvent does not alter the conformation of the layer. Similarly, when switching solvent from water back to THF/toluene, the frequency and dissipation shifts were the same magnitudes (but opposite in direction) to the first solvent change.

To follow Pathway I (Figure 4.1-b), the (L-leu)$_6$-Cys layer was first exposed to $HOO^-$. Figure 4.3-a shows the frequency and dissipation response upon addition of the $HOO^-$ to the cell, and after rinsing with solvent. The final change in frequency is approximately -30 Hz, indicative of $HOO^-$ interacting with the (L-leu)$_6$-Cys layer. Previous studies have shown the sequestration of $HOO^-$ by PLL [14, 17], and therefore the observed change here can be attributed to the formation of a (L-leu)$_6$-Cys:$HOO^-$ intermediate.

The dissipation value (after rinsing) is slightly negative of the starting value. While this primarily indicates there has been no significant change in the conformation or viscoelasticity of the layer (as is expected due to the small size of the $HOO^-$ group), the negative change suggests that the $HOO^-$ units have increased the density of the (L-leu)$_6$-Cys layer, either through incorporation of $HOO^-$ within the layer, or the $HOO^-$ has induced a form of cross-linking between the adsorbed (L-leu)$_6$-Cys oligomers.

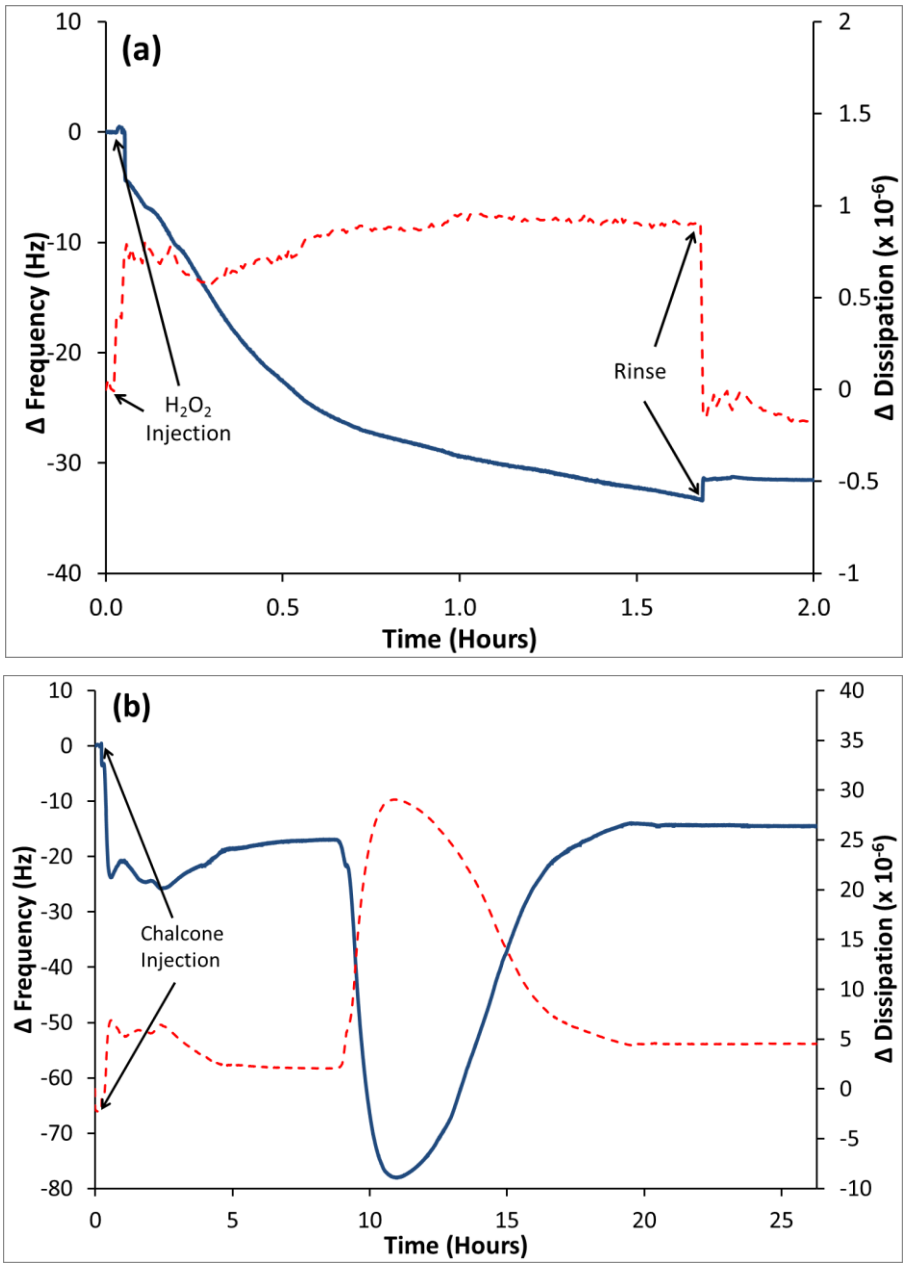


**Figure 4.3** Plot of the frequency shift (solid line) and dissipation factor (dashed line) of the gold coated QCM-D crystal sensor with an adsorbed $(L\text{-leu})_6$-Cys layer in response to a) $HOO^-$ and b) Chalcone. The $\Delta f$, $\Delta D$, and time are normalized to zero to highlight the absolute changes (the original data is available in Figure D.4 - Appendix D; average $\Delta f$ of repeat measurements a) 28 ± 2.5 Hz and b) 19.1 ± 2.8 Hz).

Upon addition of chalcone to the $HOO^-$ modified $(L\text{-leu})_6$-Cys layer, there is a rapid decrease in the frequency (Figure 4.3-b) indicating chalcone adsorption and the formation of the $(L\text{-leu})_6$-Cys:$HOO^-$:chalcone complex. The fluctuation in the frequency shift and dissipation factor in the first five hours after addition suggests surface reactions occurring. This can be attributed to a combination of events including mainly removal of excess $HOO^-$ from the PLL layer, reversible addition of chalcone to the PLL-bound hydroperoxide and also some $^-OH$ elimination before establishing the steady-state cycle. Our observation is consistent with the model suggested by

Roberts *et al*. [20] in which the hydroperoxyenolate needs to reach the appropriate conformation before the $HO^-$ elimination proceeds, which requires an induction period. However, a very large change in both $\Delta f$ and $\Delta D$ is observed after ~8.5 hours which is attributed to chalcone binding onto the PLL-bound hydroperoxide and subsequent reaction. At this point of the experiment, we could not distinguish between epoxidation reaction and reversible dissociation of chalcone. Blackmond *et al*. [22] suggest that the PLL:$HOO^-$:chalcone complex mainly goes back to free chalcone and rarely gives the enantioselective elimination of $HO^-$. Nonetheless, these are reversible processes which finally lead to the epoxide. In our measurements, $\Delta f$ and $\Delta D$ return to their starting values after 10 hours indicating no more interaction between chalcone and the catalytic species. This indicates that either the initial conformation of the PLL:$HOO^-$ has changed (and no epoxidation took place) or we have obtained a different intermediate. The high ratio between free chalcone and PLL:$HOO^-$ complex used in the experiment, together with the high affinity of the $HOO^-$ anion to the free PLL (non-significant dissociation of $HOO^-$ is expected) suggests that the chalcone epoxidation has gone to completion and the hydroperoxide ion from the PLL:$HOO^-$ was totally consumed. In addition, the experiment reveals that the free leftover chalcone does not interact with the formed PLL complex (after 10 hours) which could be (L-leu)$_6$-Cys or (L-leu)$_6$-Cys:chalcone complex. At this point, it could be possible for the chalcone binding to specific sites to inhibit the catalytic function of the PLL or, such as Blackmond suggests, the absence of the formation of PLL:chalcone complex [22]. To better understand what was occurring, several further measurements were performed.

A new (L-leu)$_6$-Cys layer was adsorbed to a gold surface and exposed to the chalcone. Introducing the chalcone first induced a change in both the frequency shift and dissipation factor (Figure 4.4-a), however the values are much less than that of the immediate $\Delta f$ and $\Delta D$ changes observed in Figure 4.3-b. The initial changes in Figure 4.3-b are attributed to the adsorption of chalcone to the $HOO^-$ modified (L-leu)$_6$-Cys layer, whereas the much lower frequency and dissipation changes in Figure 4.4-a are primarily due to the viscosity and density differences between the pure solvent and the chalcone/solvent solution. There may be some chalcone binding with the (L-leu)$_6$-Cys layer, as after rinsing there is a small variance in the starting and final $\Delta f$ value. However, the change is insignificant in comparison to the values observed in Figure 4.3-b and therefore implies the absence of a (L-leu)$_6$-Cys:chalcone intermediate. This is in concordance with previous kinetic models which indicated that PLL:$HOO^-$ is the only significant intermediate [21, 22] in the Juliá-Colonna mechanism. Although theoretical calculations suggest the existence of a PLL:chalcone intermediate in the absence of $HOO^-$ [20], the results here support the idea that in the absence of $HOO^-$ the interaction between the peptide and chalcone

is not favoured. A possible explanation is that the binding of the $HOO^-$ anion at the oxyanion hole of the peptide induces the necessary affinity between chalcone and the active site of the synzyme, thus favouring the reversible "docking" of chalcone [20]. If the interaction leads to a correct orientation of chalcone, the enantioselective epoxidation takes place. This diminishes the possibility of chalcone substrate inhibition. In addition, the results suggest Pathway I as preferred by the $(L\text{-leu})_6$-Cys, perhaps the only pathway.

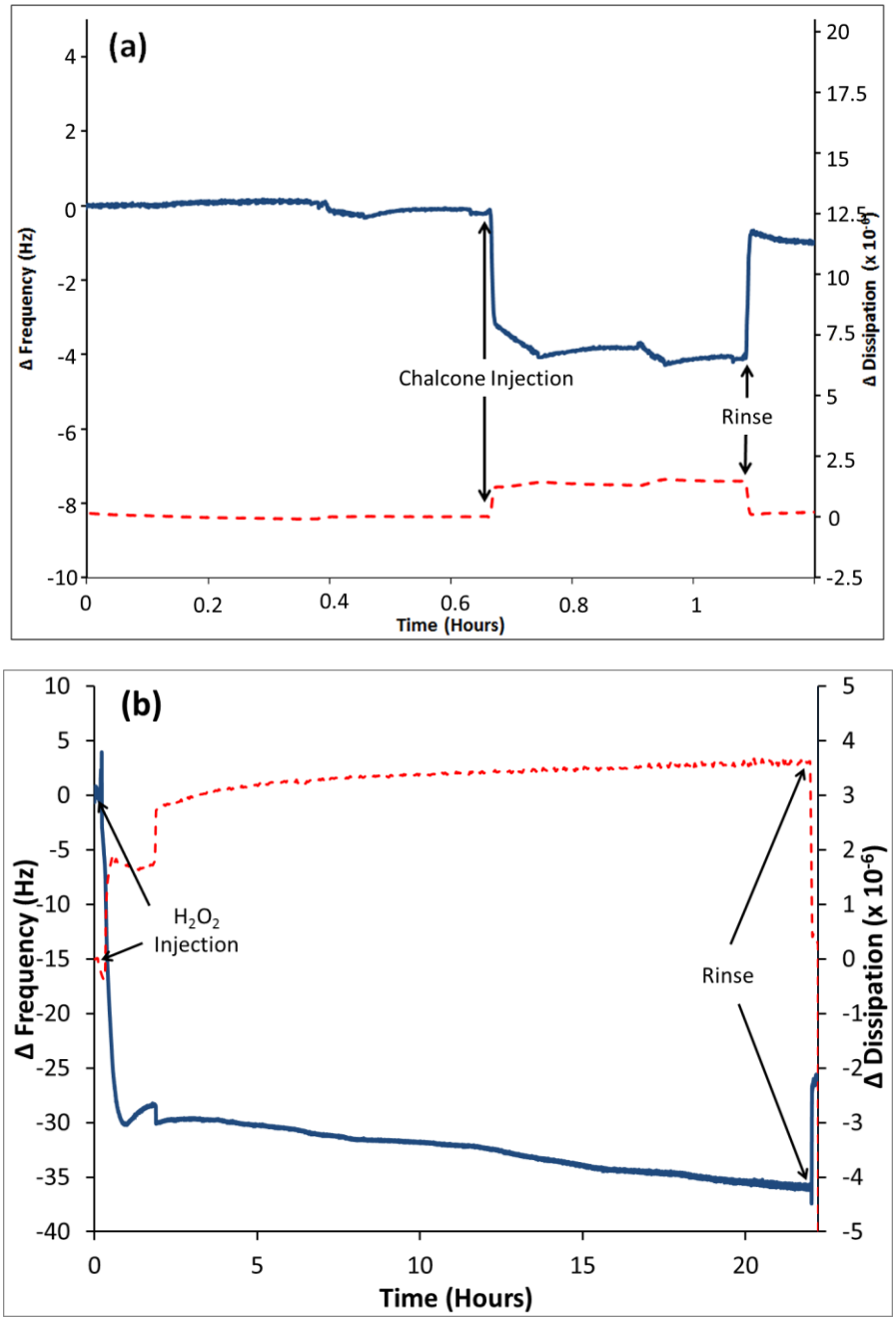


**Figure 4.4** Plot of the frequency shift (solid line) and dissipation factor (dashed line) of the gold coated QCM-D crystal sensor with an adsorbed $(L\text{-leu})_6$-Cys layer in response to a) Chalcone, and b) $HOO^-$. The $\Delta f$, $\Delta D$, and time are normalized to zero to highlight the absolute changes (the original data is available in Figure D.5 – Appendix D; average $\Delta f$ of repeat measurements a) 1.1 ± 0.1 Hz and b) 27.6 ± 2.3 Hz).

To further test this conclusion, $HOO^-$ was added to the cell and permitted to interact with the (chalcone exposed) $(L\text{-leu})_6$-Cys layer for 20 hours. Over this period there was no evidence of chalcone epoxidation (Figure 4.4-b) confirming the lack of a $(L\text{-leu})_6$-Cys:chalcone intermediate. The final $\Delta f$ and $\Delta D$ values (after solvent rinsing) are similar to that obtained in Figure 4.3-a, indicating that the $HOO^-$ has again interacted with the $(L\text{-leu})_6$-Cys layer, most likely forming the $(L\text{-leu})_6$-Cys:$HOO^-$ intermediate, as was previously observed. To establish that the adsorbed $(L\text{-leu})_6$-Cys layer conformation was in a catalytic active state and comparable to the layer formed in the previous experiment, a second chalcone solution was added to the cell (Figure D.5 – Appendix D). In this case (*i.e.* only after exposure to $HOO^-$) a large change in both $\Delta f$ and $\Delta D$ is observed (as in Figure 4.3-b) consistent with the epoxidation occurring.

## 4.4 Conclusions

The mechanism of the poly-L-leucine catalysed Juliá-Colonna chalcone epoxidation has been the focus of considerable research interest. The proposed mechanism postulates two possible pathways in which intermediate species, PLL:$HOO^-$, PLL:chalcone, and PLL:$HOO^-$:chalcone complex, are generated [15, 21, 22]. However, information on the formation of these individual species is limited. Knowledge of the separate intermediates is beneficial for the mechanistic understanding of the binding events which can either facilitate or impede the reaction.

In this work we focus on the formation of the intermediates by following the interaction of the substrates, $HOO^-$ and chalcone, with a bound modified poly-L-leucine layer, $(L\text{-leu})_6$-Cys, using quartz crystal microbalance with dissipation (QCM-D). Our work is consistent with a preferred formation of the $(L\text{-leu})_6$-Cys:$HOO^-$ complex followed by reversible chalcone interaction leading to the steady state cycle (Pathway I), while there is no interaction between $(L\text{-leu})_6$-Cys and chalcone in the absence of $HOO^-$ (Pathway II). Our findings imply the epoxidation reaction only takes place via Pathway I and, additionally, that chalcone substrate inhibition does not occur [20].

Finally, the present work demonstrates that QCM-D, which detects any interaction between the substrate and the catalyst supported on the crystal sensor, provides mechanistic insights and we envisage that following the formation of the intermediate species may provide insight into the degradation of catalytic activity. The scope of this new QCM-D application covers the study of all those reactions where the catalyst, or a modified version, has an appropriate functional group that can be attached to the QCM-D sensor (e.g. peptides, amino acids, organometallic compounds etc.

# Bibliography

[1] S. Julia, J. Masana, J.C. Vega, *Angewandte Chemie-International Edition in English*, **19**, 929-931, **1980**.

[2] S. Julia, J. Guixer, J. Masana, J. Rocas, S. Colonna, R. Annuziata, H. Molinari, *Journal of the Chemical Society-Perkin Transactions 1*, 1317-1324, **1982**.

[3] S. Colonna, H. Molinari, S. Banfi, S. Julia, J. Masana, A. Alvarez, *Tetrahedron*, **39**, 1635-1641, **1983**.

[4] S. Banfi, S. Colonna, H. Molinari, S. Julia, J. Guixer, *Tetrahedron*, **40**, 5207-5211, **1984**.

[5] P.A. Bentley, S. Bergeron, M.W. Cappi, D.E. Hibbs, M.B. Hursthouse, T.C. Nugent, R. Pulido, S.M. Roberts, L.E. Wu, *Chemical Communications*, 739-740, **1997**.

[6] P.A. Bentley, M.W. Cappi, R.W. Flood, S.M. Roberts, J.A. Smith, *Tetrahedron Letters*, **39**, 9297-9300, **1998**.

[7] T. Geller, S.M. Roberts, *Journal of the Chemical Society-Perkin Transactions 1*, 1397-1398, **1999**.

[8] R. Takagi, A. Shiraki, T. Manabe, S. Kojima, K. Ohkata, *Chemistry Letters*, 366-367, **2000**.

[9] R. Takagi, T. Manabe, A. Shiraki, A. Yoneshige, Y. Hiraga, S. Kojima, K. Ohkata, *Bulletin of the Chemical Society of Japan*, **73**, 2115-2121, **2000**.

[10] R.W. Flood, T.P. Geller, S.A. Petty, S.M. Roberts, J. Skidmore, M. Volk, *Organic Letters*, **3**, 683-686, **2001**.

[11] A. Berkessel, N. Gasch, K. Glaubitz, C. Koch, *Organic Letters*, **3**, 3839-3842, **2001**.

[12] T. Geller, A. Gerlach, C.M. Kruger, H.C. Militzer, *Tetrahedron Letters*, **45**, 5065-5067, **2004**.

[13] T. Geller, C.M. Kruger, H.C. Militzer, *Tetrahedron Letters*, **45**, 5069-5071, **2004**.

[14] J.M. Lopez-Pedrosa, M.R. Pitts, S.M. Roberts, S. Saminathan, J. Whittall, *Tetrahedron Letters*, **45**, 5073-5075, **2004**.

[15] G. Carrea, S. Colonna, A.D. Meek, G. Ottolina, S.M. Roberts, *Chemical Communications*, 1412-1413, **2004**.

[16] A. Gerlach, T. Geller, *Advanced Synthesis & Catalysis*, **346**, 1247-1249, **2004**.

[17] D.R. Kelly, E. Caroff, R.W. Flood, W. Heal, S.M. Roberts, *Chemical Communications*, 2016-2017, **2004**.

[18] R. Takagi, S. Begum, A. Siraki, A. Yoneshige, K. Koyama, K. Ohkata, *Heterocycles*, **64**, 129-141, **2004**.

[19] P.A. Bentley, R.W. Flood, S.M. Roberts, J. Skidmore, C.B. Smith, J.A. Smith, *Chemical Communications*, 1616-1617, **2001**.

[20] D.R. Kelly, E. Caroff, R.W. Flood, W. Heal, S.M. Roberts, *Chemical Communications*, 2016-2017, **2004**.

[21] G. Carrea, S. Colonna, A.D. Meek, G. Ottolina, S.M. Roberts, *Tetrahedron-Asymmetry*, **15**, 2945-2949, **2004**.

[22] S.P. Mathew, S. Gunathilagan, S.M. Roberts, D.G. Blackmond, *Organic Letters*, **7**, 4847-4850, **2005**.

[23] A. Berkessel, B. Koch, C. Toniolo, M. Rainaldi, Q.B. Broxterman, B. Kaptein, *Biopolymers*, **84**, 90-96, **2006**.

[24] D.R. Kelly, S.M. Roberts, *Biopolymers*, **84**, 74-89, **2006**.

[25] G. Carrea, S. Colonna, D.R. Kelly, A. Lazcano, G. Ottolina, S.M. Roberts, *Trends in Biotechnology*, **23**, 507-513, **2005**.

[26] S. Colonna, D. Perdicchia, E. Di Mauro, *Tetrahedron-Asymmetry*, **20**, 1709-1714, **2009**.

[27] K.M. Weiss, S.B. Tsogoeva, *Chemical Record*, **11**, 18-39, **2011**.

[28] A. Weyer, D. Diaz, A. Nierth, N.E. Schlorer, A. Berkessel, *Chemcatchem*, **4**, 337-340, **2012**.

[29] T. Geller, A. Gerlach, C.M. Kruger, H.C. Militzer, *Journal of Molecular Catalysis a-Chemical*, **251**, 71-77, **2006**.

[30] R.A. Miranda, J. Llorca, F. Medina, J.E. Sueiras, A.M. Segarra, *Journal of Catalysis*, **282**, 65-73, **2011**.

[31] S.B. Tsogoeva, J. Woltinger, C. Jost, D. Reichert, A. Kuhnle, H.P. Krimmer, K. Drauz, *Synlett*, 707-710, **2002**.

[32] H. Yi, G. Zou, Q. Li, Q. Chen, J. Tang, M.Y. He, *Tetrahedron Letters*, **46**, 5665-5668, **2005**.

[33] F. Yang, L.M. He, H. Yi, G. Zou, J. Tang, M.Y. He, *Journal of Molecular Catalysis a-Chemical*, **273**, 1-4, **2007**.

[34] W.W. Qiu, L.M. He, Q. Chen, W.R. Luo, Z.C. Yu, F. Yang, J. Tang, *Tetrahedron Letters*, **50**, 5225-5227, **2009**.

[35] R.A. Miranda, E. Finocchio, J. Llorca, F. Medina, G. Ramis, J.E. Sueiras, A.M. Segarra, *Physical Chemistry Chemical Physics*, **15**, 15645-15659, **2013**.

[36] M.A. Cooper, V.T. Singleton, *Journal of Molecular Recognition*, **20**, 154-184, **2007**.

[37] G. Sauerbrey, *Zeitschrift für Physik*, **155**, 206-222, **1959**.

[38] M. Rodahl, F. Hook, A. Krozer, P. Brzezinski, B. Kasemo, *Review of Scientific Instruments*, **66**, 3924-3930, **1995**.

[39] M. Rodahl, B. Kasemo, *Review of Scientific Instruments*, **67**, 3238-3241, **1996**.

[40] D. Johannsmann, K. Mathauer, G. Wegner, W. Knoll, *Physical Review B*, **46**, 7808-7815, **1992**.

[41] M.V. Voinova, M. Rodahl, M. Jonson, B. Kasemo, *Physica Scripta*, **59**, 391-396, **1999**.

[42] K.K. Kanazawa, J.G. Gordon, *Analytical Chemistry*, **57**, 1770-1771, **1985**.

[43] M. Rodahl, B. Kasemo, *Sensors and Actuators a-Physical*, **54**, 448-456, **1996**.

# 5 *In-situ* Epoxidation of Chalcone

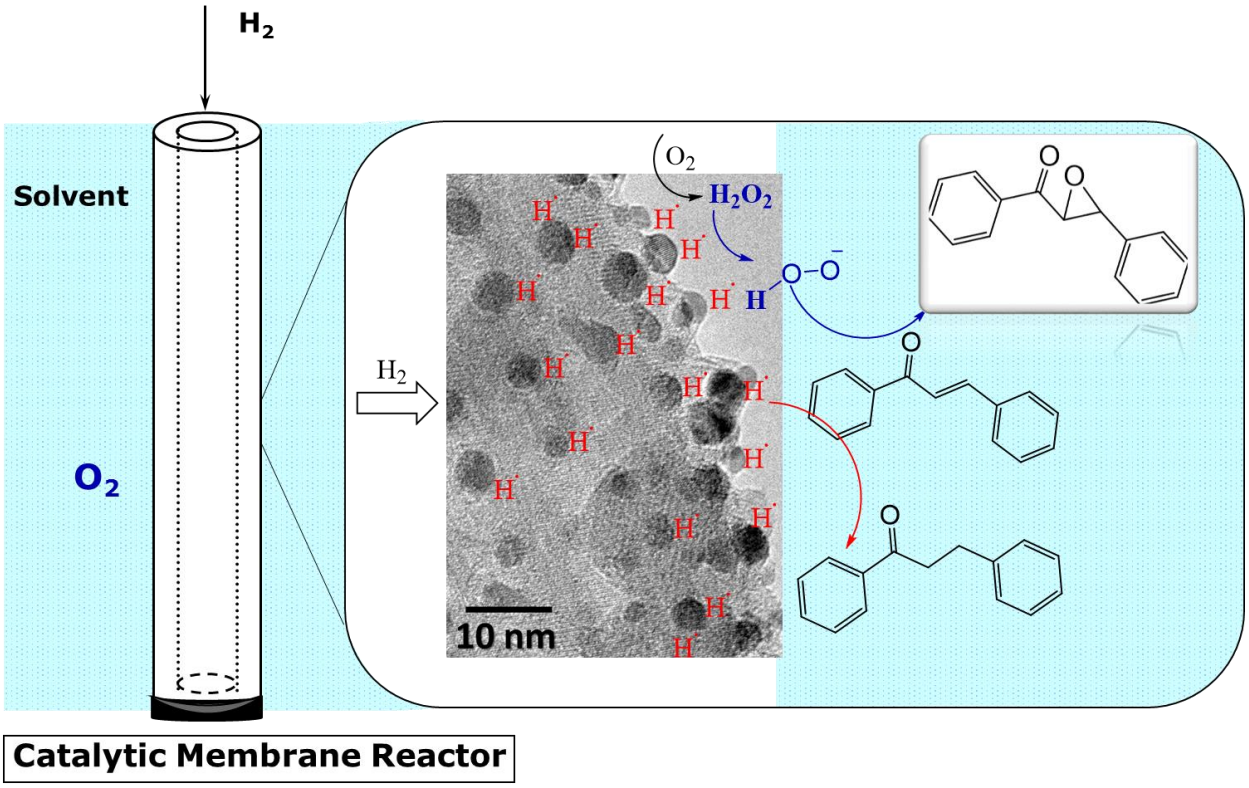

## 5.1 Introduction

Epoxidation of electron-deficient α,β-unsaturated ketones (Scheme 5.1) is of great interest not only because the products of this reaction are versatile building blocks in drug synthesis, but also because both the ketone and epoxide functional groups can be further functionalized to produce new and interesting products [1].

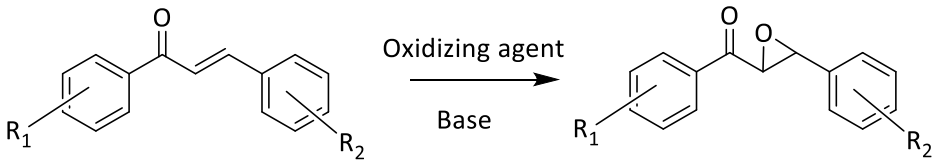


**Scheme 5.1** Epoxidation of electron-deficient α,β-unsaturated ketones

The general epoxidation reaction of the α,β-unsaturated ketones requires an oxidant and a base. From the environmental point of view, molecular oxygen is the most desirable oxidizing agent for an epoxidation reaction as it is readily available and has a low cost of production. However, $O_2$ cannot be used directly as secondary oxidation pathways might occur (e.g. autooxidation radical reactions). The use of both oxygen atoms from diatomic oxygen seems to be a promising approach; yet, utilizing only one oxygen atom will impose an asymmetry in the catalytic process. The process using bulk silver is the only system that uses molecular oxygen through the dissociative adsorption of oxygen on its surface. In rest of the cases, the oxygen molecule requires activation, which can be done either directly or indirectly. The most common example of a direct activation is the use of hydrogen peroxide and organic peroxides with bases, as they retain the O-O bond. The indirect activation is done by the use of substances like $N_2O$, hypochlorite or persulfates which contain a single oxygen atom in a highly activated state [2].

Before presenting a brief summary of the different oxidizing systems used in the epoxidation of chalcone-type substrates, it is of great importance to differentiate between the two epoxidation reactions: the Juliá-Colonna epoxidation and the Weitz-Scheffer epoxidation. While in both cases hydrogen peroxide is used as an oxidizing agent, the product of the Juliá-Colonna epoxidation is chiral due to the use of the poly-L-leucine as catalyst (more information of this reaction is given in Section 3). The fundamental way of obtaining an epoxide from a α,β-unsaturated ketone is through the Weitz-Scheffer epoxidation reaction, the process described in 1921 by the two scientists who gave its name. The mechanism (Scheme 5.2) is based on a two-step addition-elimination reaction, where the hydrogen peroxide is deprotonated in the presence of a base and added to the β-carbon of the ketone, thus forming a β-peroxyenolate intermediate (**2**) [3].

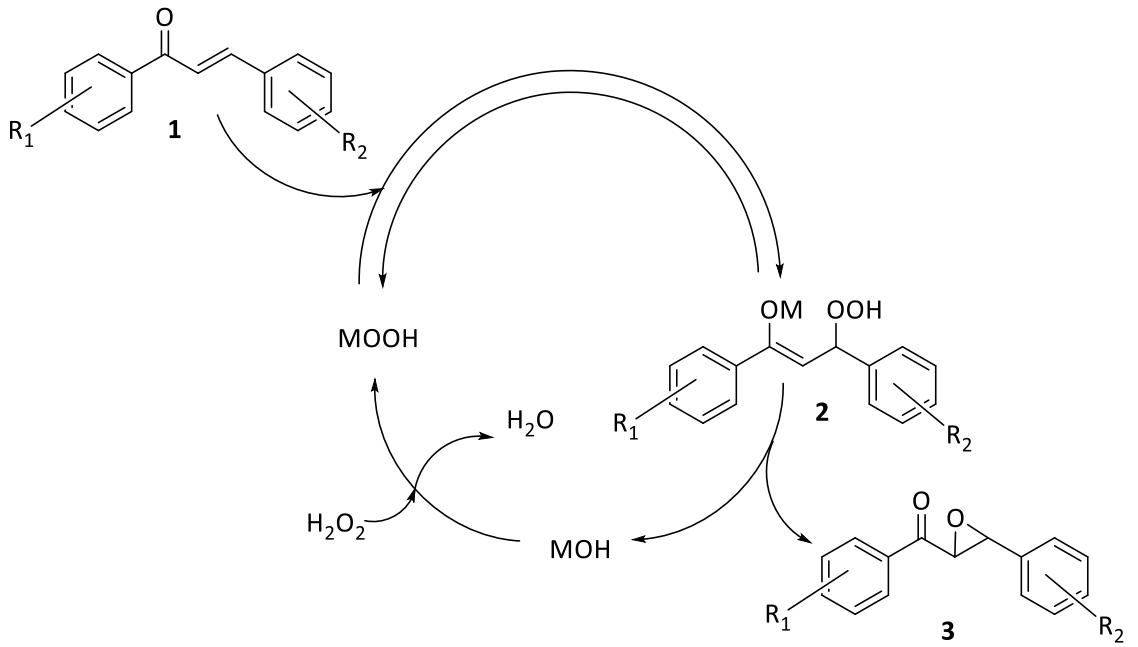


**Scheme 5.2** The Weitz-Scheffer epoxidation reaction mechanism

The use of hydrogen peroxide was only the beginning of a long series of oxidants, such as: metal peroxides [4], organic peroxides (tetra-butyl hydroxyperoxide [5], cumene hydroperoxide [6], dimethyldioxirane [7], cyclohexylidenebishydroperoxide [8], ethaneperoxoic acid [9], (+)-norcamphor-derived hydroperoxide[10] , inorganic oxidants ($NaBO_3$ [11], NaClO [12], $NaClO_2$ [13], Oxazone [14], $Na_2CO_3$ [15]) or organic oxidants (2,6-dichloropyridine N-oxide [16], chiral tertiary amine N-oxides [17], hypervalent $\lambda^3$- and $\lambda^5$-organoiodanes [18]).

Over the last decades, numerous efforts have been devoted in search of better and greener oxidizing agents for the epoxidation of chalcones, some of them involving the *in-situ* production of hydrogen peroxide. There are several ways for *in-situ* production of $H_2O_2$, however the most commonly used ones are: the anthraquinone oxidation (AO) process, oxidation of alcohols, and directly from hydrogen and oxygen.

In a typical anthraquinone oxidation process, 2-alkylanthraquinone (AQ) is hydrogenated to the corresponding anthraquinol (AHQ) (Scheme 5.3 a), which can be further hydrogenated to 5,6,7,8-tetrahydroanthrahydroquinone (Scheme 5.3 b) as a side reaction. The AHQ is oxidized to yield equimolar amounts of hydrogen peroxide and AQ, where AQ is regenerated (Scheme 5.3 c). The side product obtained during the hydrogenation reaction can also be oxidized to give hydrogen peroxide (Scheme 5.3 d). Even though the AO process produces a high yield of hydrogen peroxide, the major disadvantage comes from the side reactions which require regeneration of the solution and the separation of the organic impurities formed during production [19], which makes AO process unsuitable for the *in-situ* epoxidation of chalcone.

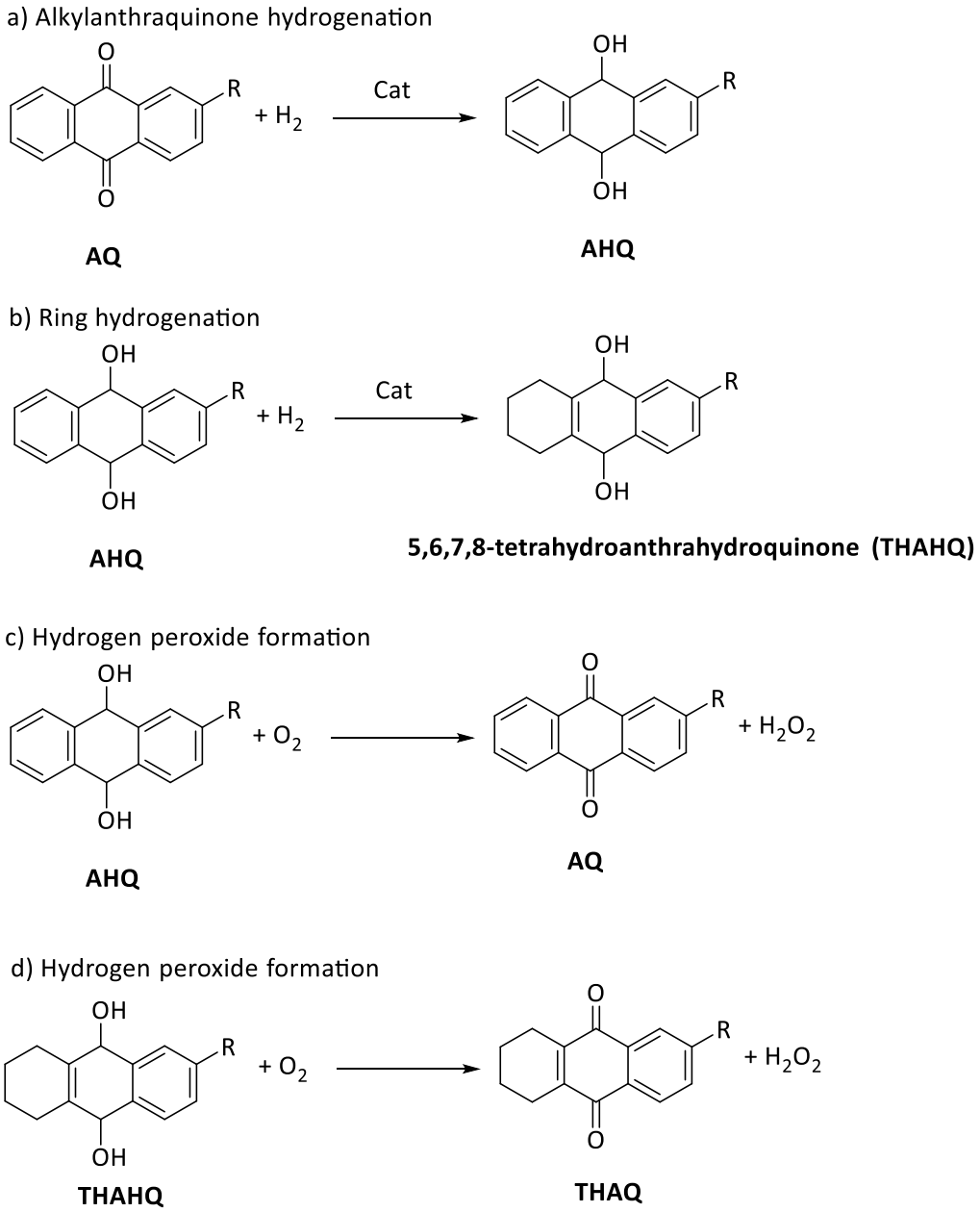


**Scheme 5.3** Anthraquinone autoxidation reaction

To the best of our knowledge, so far there is only one study which presents the epoxidation of chalcone using hydrogen peroxide obtained from the aerobic photooxidation of 2-propanol [20]. In their work, Cui *et al.* studied the efficient generation of hydrogen peroxide by oxidation of 2-propanol with organophotocatalysts in air, using visible light irradiation. The study proposed that the excited form of anthraquinone (formed during the absorption of visible light) abstracts a hydrogen radical from the 2-propanol, producing the radical species (**4**) (Scheme 5.4). This will trap molecular oxygen to form the corresponding peroxyradical (**5**) which will further transform into the hydroxyl hydroperoxide (**6**). This hydroxyl hydroperoxide will decompose into

acetone and hydrogen peroxide which, in basic medium and in the presence of a chalcone molecule will produce the epoxidation reaction [20].

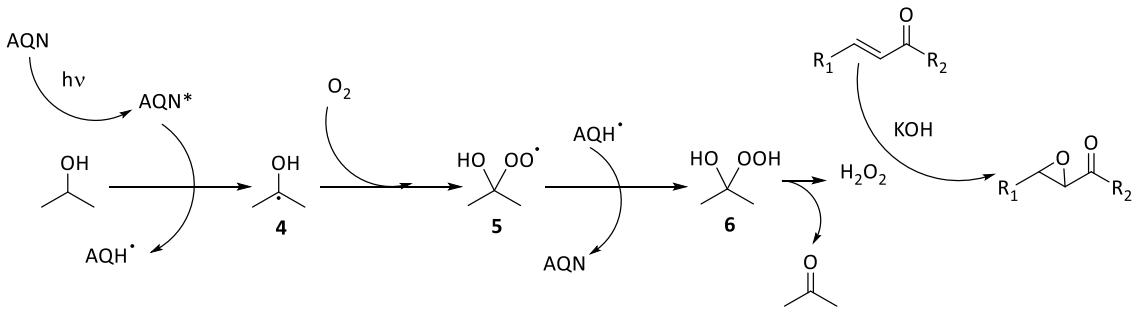


**Scheme 5.4** Possible mechanism for the chalcone epoxidation with $H_2O_2$ from 2-propanol oxidation

Despite the new insights in the *in-situ* epoxidation of chalcone, the procedure proposed by Cui *et al.* is exhaustive and requires several intermediate steps. The most suitable process for the *in-situ* epoxidation could be the direct production of $H_2O_2$ from $H_2$ and $O_2$, a 100 years old reaction. Since 1914, it is known that palladium is able to catalyse the liquid-phase oxidation of hydrogen by oxygen to give hydrogen peroxide; however, there are several side reactions that can occur: i) non-selective oxidation of $H_2$ to water, ii) decomposition of hydrogen peroxide and iii) hydrogenation of hydrogen peroxide, all of them being catalysed by Pd (Scheme 5.5). Moreover, reactions i) and iii) are thermodynamically favourable in comparison with the production of $H_2O_2$ hence, the selectivity towards the desired product is severely limited [21].

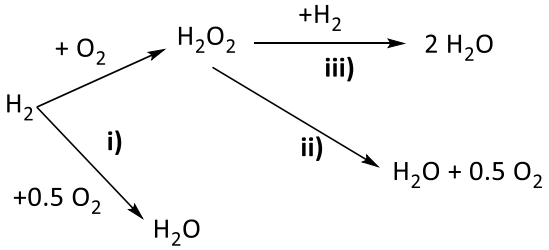


**Scheme 5.5** Reactions involved in the direct synthesis of $H_2O_2$

Besides the side reactions that cannot be minimized, the flammability and detonability limits of hydrogen in oxygen and air are another major disadvantages, which can be avoided by using diluted $H_2/O_2$ streams.

Although Pd is unanimously considered the best catalyst for the direct production of $H_2O_2$, there are several factors that should be taken into consideration when designing the catalytic process, such as: factors affecting the $H_2O_2$ decomposition and hydrogenation, reaction medium and the catalytic support.

For example, the major factors that can influence the Pd - catalysed decomposition of $H_2O_2$ are: i) presence of protons in the reaction medium; ii) hydrophobicity of the catalysts; iii)

oxidation state of Pd in the catalyst; iv) the presence of halide ions in the reaction medium, and v) presence of a secondary metal in the catalyst. On the other hand, the factors that can influence the hydrogenation of newly formed $H_2O_2$ over the Pd surface are: i) reaction medium; ii) the presence of an acid or halide ions; iii) catalyst amount, and iv) $H_2/O_2$ ratio [21].

The $H_2O_2$ production from the constituent elements takes place in a three-phase system; thus, the product selectivity enormously depends on the overall rate of mass transfer from the gaseous phase to the catalytic surface. Consequently, the mass transfer can be increased by: i) increasing the gas solubility, either by increasing the reaction pressure or by using a solvent with a higher gas solubility or/and ii) using solvents with lower viscosity and surface tensions [22]. Knowing that the solubility of $H_2$ in alcohols is 4-5 times higher than in water and the solubility of $O_2$ is 8 times higher, alcohols seem to be the perfect solvents for the epoxidation reactions.

Another important point to take into account is the catalyst support. The most suitable ones in the direct $H_2O_2$ synthesis are the ones that permit the formation of the metal-proton adducts on the Brönsted acidic sites, therefore basic oxides seem to be unsuitable.

An improvement in the three-phase contact can be achieved by using a catalytic membrane reactor (CMR), defined as a device combining a membrane-based separation and a chemical reaction in one unit. The use of CMR in the direct $H_2O_2$ synthesis requires a membrane intrinsically active for catalytic reactions e. g. metallic dense, zeolites or inert membranes with an incorporated catalytic active phase [23]. Over time, the CMRs have become the benchmark of the direct hydrogen peroxide synthesis due to their great advantages over the conventional catalysts, such as: i) the distribution of the gases avoids the explosion mixture; ii) the active phase can be easily regenerated and iii) there is a lower deactivation of the catalysts [24].

A variety of procedures were implied to improve the performance of the CMRs for the direct synthesis of hydrogen peroxide [25-33] culminating with the work of Osegueda *et al.* who used a commercial hollow fibre impregnated with palladium [34, 35]. This CMR was used for the production of $H_2O_2$ in contaminated wastewater effluents and it was observed that the hydrogen peroxide obtained in the pores of the CMR is further transformed into the hydroxyl radicals which oxidize the undesired organic compounds.

As mentioned above, the epoxidation of chalcone requires the hydroperoxide anions rather than the hydroxyl radicals, hence the presence of a base in the reaction medium is of crucial importance; thus, creating a hybrid CMR containing Pd and a basic catalyst seems to be a viable alternative.

Hydrotalcites are basic materials that proved to be efficient catalysts for the epoxidation reaction using hydrogen peroxide as oxidant. Cativiela *et al.* used hydrotalcites containing Mg:Al 2.8 for the epoxidation of different unsaturated ketones and observed that in the case of less

hindered substrates the hemiperketals were formed as secondary products [36]. Ueno *et al.* showed that the basic properties of hydrotalcite (HT) promote the formation of peroxycarboximidic acid leading to moderate to good yield of the epoxides [37]. Yamaguchi *et al.* discovered that the use of cationic surfactants having long alkyl chain increase the yield of epoxidation in a three phase system: hydrotalcite – hydrogen peroxide – organic phase. They proposed that the hydrogen peroxide reacts with the basic hydroxyl group found on the surface of the hydrotalcite to form the perhydroxyl anion (Scheme 5.6). This will attach to the β-olefinic carbon of the unsaturated ketone to give the corresponding epoxide. At the same time, the surface hydroxyl function will be regenerated on the hydrotalcite. The epoxidation of less reactive substrates is strongly promoted by the use of phase transfer co-catalysts, where the perhydroxyl anion interacts with the ammonium cation and moves towards the organic phase, as $Q^+HOO^-$, to react with the α,β-unsaturated ketone. The presence of the quaternary salt increases the contact area of the interface between the water and organic phase, ensuring the transfer of the substrate from the organic phase to the surface boundary and gathering the hydroperoxide anion from water phase to the surface boundary [38].

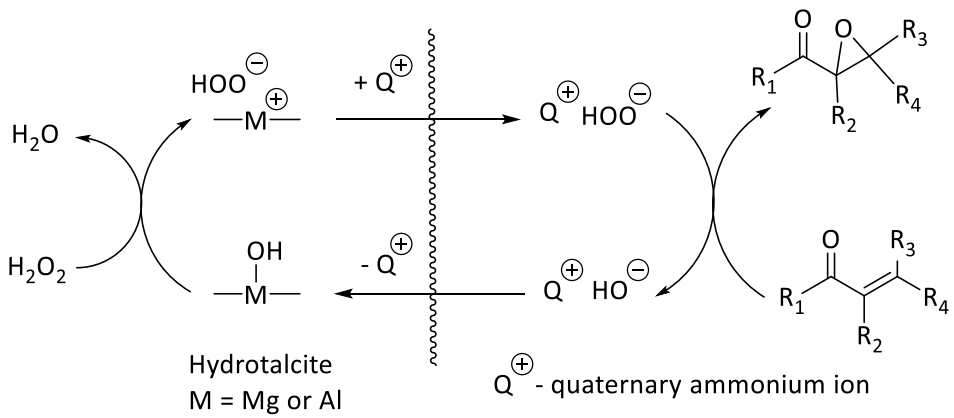


**Scheme 5.6** Mechanism of chalcone-type epoxidation using hydrogen peroxide in the presence of hydrotalcites and ammonium quaternary salts

Fraile *et al.* studied the epoxidation of alkenes derived from D-glyceraldehyde using two different heterogeneous systems: TBHP + KF/alumina and $H_2O_2$ + hydrotalcite, and concluded that the first one was more efficient and selective [39]. Honma *et al.* demonstrated that the system composed of Mg-Al hydrotalcite, hydrogen peroxide and n-dodecyltrimethylammonium bromide is efficient in the epoxidation of different substrates leading to almost complete conversion after 24 h [40].

In 2003, Pillai *et al.* managed to decrease the amount of hydrotalcite used in the epoxidation reactions of unsaturated olefins by using ultrasound treatment during reaction. The acoustic streaming from the ultrasounds enhanced the molecular motion, accelerating the reaction [41].

However, the increase of the reaction rate might be also due to the use of acetonitrile as solvent, which can easily activate the hydrogen peroxide.

Though the use of hydrotalcites as epoxidation catalysis represents a breakthrough, the protocols published so far present several disadvantages: the difficulty of recovering the catalyst and the high amount of $H_2O_2$ used. It might be possible to overcome these limitations through a greener process involving *in-situ* production of hydrogen peroxide and subsequent epoxidation of chalcone in the presence of hydrotalcite. The Brönsted basic sites found in the interlayer structure of HT are able to deprotonate $H_2O_2$ and produce the $HOO^-$ required for the epoxidation reaction [36, 42].

In this context, the aim of the present work was to develop a new catalytic system using CMR based on hydrotalcites and Pd nanoparticles for the epoxidation of trans-chalcone using *in-situ* production of hydrogen peroxide. This section presents our preliminary results.

## 5.2 Experimental

### 5.2.1 General

All chemicals and solvents were commercially available (Aldrich Chemical, Fluka) and used without further purification/ drying unless otherwise mentioned.

XRD measurements were made using a Siemens D5000 diffractometer (Bragg-Brentano parafocusing geometry and vertical - goniometer) fitted with a curved graphite diffracted-beam monochromator and diffracted-beam Soller slits, a 0.06° receiving slit and scintillation counter as a detector. The angular 2θ diffraction range was between 1 and 70°. The sample was dusted on to a low background Si (510) sample holder. The data were collected with an angular step of 0.05° at 3s per step and sample rotation. CuK radiation was obtained from a copper X-ray tube operated at 40 kV and 30 mA.

$^1$H-NMR spectra were recorded on a Varian NMR System 400 spectrometer in $CDCl_3$. Chemical shifts (δ) are given in ppm and J values are given in Hz.

### 5.2.2 Synthesis of Hydrotalcite Materials (HTs)

Mg-Al HTs (molar ratio 2:1) were prepared by the coprecipitation method at room temperature and pH = 10. The appropriate amounts of $Mg(NO_3)_2.6H_2O$ and $Al(NO_3)_3.9H_2O$ were dissolved in 110 ml Milli-Q water and added dropwise into a vessel containing 150 ml of Milli-Q water. The pH was kept constant using 2M NaOH solution. The suspension was stirred overnight

at room temperature. The obtained solid was filtered and washed several times with Milli-Q water and dried under vacuum.

Mg-Al-Fe HTs (molar ratio 3:1:1) were prepared by the coprecipitation method at room temperature and pH = 10. The appropriate amounts of $MgCl_2.6H_2O$, $AlCl_3.6H_2O$ and $FeCl_3.6H_2O$ were dissolved in 110 ml Milli-Q water and added dropwise into a vessel containing 150 ml of Milli-Q water. The pH was kept constant using 2M NaOH solution. The suspension was stirred overnight at room temperature. The obtained solid was filtered and washed several times with Milli-Q water and dried under vacuum.

Mg-Al-Pd HTs (molar ratio Mg:Al 2:1 containing 1 wt% Pd) were prepared by the coprecipitation method at room temperature and pH = 10. The appropriate amounts of $Mg(NO_3)_2.6H_2O$ and $Al(NO_3)_3.9H_2O$ were dissolved in 110 ml Milli-Q water and added dropwise into a vessel containing 150 ml of Milli-Q water. In the same time an acetone solution of $Pd(OAc)_2$ was added dropwise. The pH was kept constant using 2M NaOH solution. The suspension was stirred overnight at room temperature. The obtained solid was filtered and washed several times with Milli-Q water and dried under vacuum. The solid was calcined in air at 450 °C overnight to obtain the corresponding mixed oxides and then reduced in $H_2$ 15 Nml/min for 3 h at 350 °C.

### 5.2.3 Synthesis of Palladium Impregnated HTs

The Mg-Al and Mg-Al-Fe hydrotalcites were impregnated with different Pd loadings through the incipient wetness impregnation method to yield the corresponding catalysts.

The typical procedure for the synthesis of x wt% Pd/HT (Mg-Al or Mg-Al-Fe), where x is 1 or 0.5, was the following: to 1.2 g of HT (either Mg-Al or Mg-Al-Fe) a solution containing the appropriate amount of Pd (either from $PdCl_2$ or $Pd(OAc)_2$ precursors) was added dropwise and stirred continuously. The solvent was removed and the resulting material was calcined in air at 450 °C overnight to obtain the corresponding mixed oxides and then reduced in $H_2$ 15 Nml/min for 3 h at 350 °C.

### 5.2.4 Preparation of the Catalytic Membrane Reactor (CMR)

Commercial corundum hollow fibre with nominal pore diameter of 1400 nm was used as starting material. The CMRs were impregnated with the catalyst precursor solution using an incipient wetness technique. The impregnated membrane was calcined at 300 °C or 450 °C followed by a reduction step for 2 h at 300 °C under $H_2$ flow. The deposited active phase was computed by the mass difference between the original membrane and the modified membrane.

Two types of CMRs were prepared containing: 0.75 wt.% Pd and 0.3 wt.% Pd-1.5 wt.% $CeO_2$-1.5 wt.%$Fe_2O_3$.

### 5.2.5 Preparation of the Hybrid HT-CMR

For the preparation of the hybrid Mg-Al HT-CMR two procedures were used:

Method A: The 0.75 wt% Pd CMR closed to one end was attached to a vacuum system and introduced into a recipient containing Mg-Al HT suspended in solution (containing 2 wt% HT with respect to the CMR). The entire system was continuously stirred. When the vacuum was started the HT was retained on the surface of the CMR. This process was repeated three times, then the CMR was washed with MilliQ water several times, dried and calcined at 450 °C in air overnight. Finally, the hybrid CMR was reduced in $H_2$ 15 Nml/min for 3 h at room temperature.

Method B: The 0.75 wt% Pd CMR closed to both ends was introduced first into a solution containing $Mg(NO_3)_2.6H_2O$ and left there for 3 minutes, then introduced into a solution of $Al(NO_3)_3.9H_2O$ and left there for 3 minutes. This process was repeated three times (to assure a 2 wt% HT deposited on the CMR) and afterwards, without washing, the CMR was introduced into a 2M NaOH solution and left there for 10 minutes. After this, the CMR was washed with MilliQ water overnight, dried and calcined at 450 °C in air overnight. Finally, the hybrid CMR was reduced for 2 h at room temperature under $H_2$ flow.

### 5.2.6 Standard Conditions for the *In-situ* Epoxidation of Chalcone

#### *5.2.6.1 Using Pd/HT or Pd-based HT*

The catalyst was added in a test tube over which 10 mg of chalcone were added. 40 ml of solvent was added over and $H_2$ was introduced by means of a mass flow controller (30 Nml/min), while $O_2$ was used in excess. The entire reaction was stirred for a certain period of time, then filtered, the solvent removed by vacuum distillation and the products analysed by $^1$H-NMR. A sketch with the experimental set-up can be found in Figure E.1 - Appendix E.

#### *5.2.6.2 Using CMR and HT/CMR*

One end of the CMR was tightly closed and to the other a flow of $H_2$ was supplied by means of a mass flow controller (30 Nml/min). The CMR was immersed in a reaction vessel which contained 40 ml solvent, 10 mg chalcone and in some cases, rehydrated hydrotalcite. The reaction was performed at room temperature and normal pressure and after 6h, the solvent was removed by vacuum distillation and the products were analysed by $^1$H-NMR. A sketch with the experimental set-up can be found in Figure E.2 - Appendix E.

# 5.3 Results and Discussion

## 5.3.1 Catalyst Preparation and Characterization

### *5.3.1.1 HTs and M-HTs*

Different types of HTs were prepared by the coprecipitation method at pH 10 and the obtained materials were calcined at 450 °C in air. The XRD patterns of all the synthesized materials presented $d_{003}$ and $d_{006}$ diffraction peaks corresponding to hydrotalcite-like structure (as can be seen in the Appendix E – Figure E.3). The presence of Pd was detected through the colour change observed after the reduction process and no other additional analysis were done to study the size of the nanoparticles, their dispersion or their location, as this was not the subject of the present work.

### *5.3.1.2 HT-CMR*

The two initial CMRs used in this study (0.75 wt% Pd and 0.3 wt.% Pd-1.5 wt.% $CeO_2$-1.5 wt.% $Fe_2O_3$) were already in depth characterized by Osegueda *et al*. [34, 35], but to prove that the Pd is homogeneous distributed overall the entire membrane reactor, we have attached the μ-XRD diffractograms in the Appendix E.

Our first try in creating a hybrid HT-CMR was based on immersing the 0.75 wt% Pd-CMR into a suspension of HT, defined as Method A. Upon applying the vacuum, the HT was unevenly distributed over the external surface of the CMR and after the drying and calcination processes, the entire HT was completely lost. This suggests that the HT was not able to penetrate the pores of the membrane. The XRD diffractograms of the CMR did not show the presence of the HT neither in the interior nor the exterior of the reactor.

The second method used (Method B) proved to be more efficient. When the 0.75 wt% Pd-CMR previously immersed in the Mg and Al salt solutions, was immersed in the 2M NaOH solution the HT crystals started to grow in the pores of the reactor, phenomenon observed with the naked eye. After an in-depth washing, drying, calcination and reduction processes, the HT crystals still remained in the CMR pores as observed from the XRD diffractograms (Figure E.5 - Appendix E).

## 5.3.2 Catalytic Results

### *5.3.2.1 Using M-HT Materials*

It is commonly accepted that the direct catalytic combination of hydrogen with oxygen will preferentially form water and not hydrogen peroxide. Moreover, catalysts active in the

hydrogen peroxide production will also be active in its depletion hence, our first aim was to study the apparent production of hydrogen peroxide using Pd-impregnated hydrotalcites.

In order to compare the results quantitatively, we defined the average specific production rate of hydrogen peroxide as the moles of $H_2O_2$ cumulated over a specified interval of time, $\Delta t$, scaled to the amount of catalyst [43]:

$$P_{H_2O_2} = \frac{\Delta N_{H_2O_2}}{\Delta t * m_{catalyst}}$$

As expected, the solubility of gases in the studied solvents plays an important role in the production of $H_2O_2$ (Figure 5.1). The best results were obtained when methanol and tetrahydrofuran were used in the case of the 1 wt% Pd/HT Mg-Al and methanol when the 0.5 wt% Pd/HT Mg-Al was used.

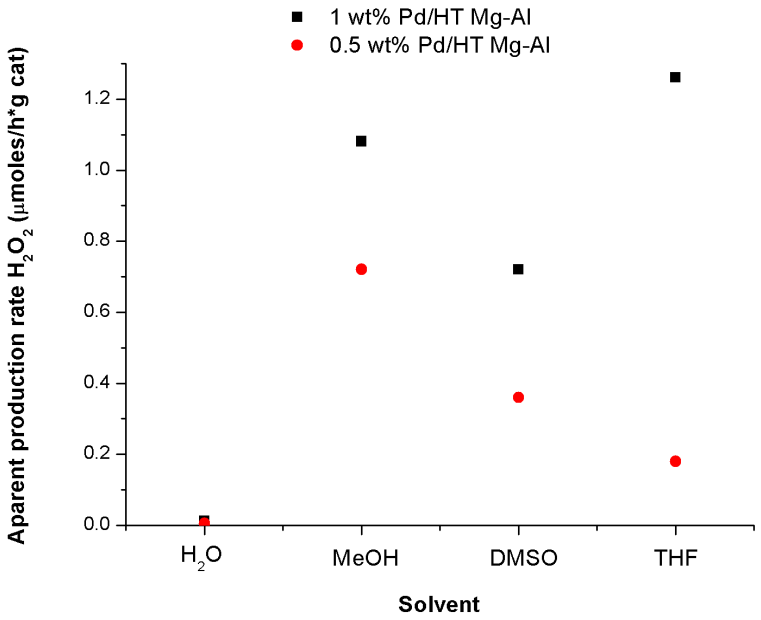


**Figure 5.1** Comparison between the 1 wt% and 0.5 wt% Pd/HT Mg-Al catalysts. Typical procedure: 136 mg catalyst were added in a tubular glass reactor over which 40 ml solvent were added; under continuous stirring 30 ml/min $H_2$ and $O_2$ in excess were bubbled in the mixture; after 6 h samples were taken and analysed either by colorimetry or by using hydrogen peroxide test strips.

To verify that hydrotalcites are capable to produce the hydroperoxide anion for the epoxidation reaction, we have done a control experiment using calcined HT, hydrogen peroxide and chalcone. Under the studied conditions, the conversion towards the epoxide was found to be only 5 %. With this knowledge, we studied the *in-situ* epoxidation reaction of chalcone using first THF as solvent. As expected, THF was completely oxidized to γ-butyrolactone, 2-hydroxytetrahydrofuran and 4-hydroxybutyraldehyde (even after 1 h of reaction) and the identification of any epoxide present in the reaction mixture was impossible.

Further, the reactivity of the 1 wt% Pd/HT Mg-Al in the epoxidation reaction was studied using MeOH as solvent. After 6 h, chalcone was completely transformed into the hydrogenated product (Figure 5.2), even though hydrogen peroxide was still formed. As Pd is also a very good catalyst in the hydrogenation reaction, we have performed the same experiment using less Pd (0.5 wt%), however, after 6 h, chalcone was completely converted to its hydrogenated product.

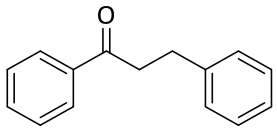


**Figure 5.2** The hydrogenation product of chalcone

These results demonstrate that under the studied conditions, Mg-Al HT is not basic enough to produce the hydroperoxide anion so, we have focused on the use of a Mg-Al-Fe hydrotalcite. Iron oxides have been widely used in the decomposition of hydrogen peroxide hence, a material containing iron (III) oxide will probably favour the epoxidation reaction. The as prepared Mg-Al-Fe HT was impregnated through incipient wetness impregnation with 1 wt% and 0.5 wt% Pd, respectively, then calcined and reduced in $H_2$. Compared to the materials based on Mg-Al HT, the production of hydrogen peroxide was reduced considerably, suggesting that the presence of iron decomposes the formed $H_2O_2$. In spite of these, the materials were totally selective towards the hydrogenation of chalcone. The XRD diffractogram of the 1 wt% Pd/HT and 1 wt% Pd/Mg-Al-Fe HT materials after reaction present a loss of crystallinity, which might explain why the HT part was not able to catalyse the epoxidation reaction (Figures E.6 and E.7 – Appendix E).

To gain some insights on the role of the catalysts and the processes that are taking place, two control experiments were done: one involved the use of hydrotalcite (either Mg-Al or Mg-Al-Fe), chalcone and hydrogen in methanol while the second one using a Mg-Pd-Al hydrotalcite (previously calcined and reduced in hydrogen) with chalcone, hydrogen, oxygen and methanol. In the first case no hydrogenation occurred, demonstrating that Pd is the active “ingredient” in the hydrogenation reaction, a fact proven by the second control experiment. The Mg-Pd-Al hydrotalcite was active in producing hydrogen peroxide (up to ~ 30 mg/L) although, no epoxidation occurred. It was found that, after the reaction, the catalyst completely lost its crystallinity. Moreover, the presence of strong visible peaks corresponding to Pd atoms reveals that the two exothermic reactions (reduction reaction in $H_2$ and hydrogen peroxide synthesis) might destroy the structures of the mixed oxides and possible the rehydrated HT (Figure E.8 – Appendix E). This might explain why these materials were not selective for the epoxidation reaction of chalcone. This behaviour can also be described through the cluster sintering of the Pd nanoparticles.

### 5.3.2.2 Using CMR and HT-CMR

To minimize the direct exposure of chalcone to the hydrogen, we used two CMRs which have been already used in the production of $H_2O_2$ by Osegueda *et al.* [34], mainly the 0.75 wt% Pd and 0.3 wt.% Pd-1.5 wt.% $CeO_2$-1.5 wt.% $Fe_2O_3$. The two CMRs proved to be active in the hydrogen peroxide production in aqueous solutions, so initially we have studied them in the epoxidation reaction of chalcone using MeOH in aqueous solution. In both cases the CMR was closed to one end and to the other hydrogen was supplied. The reactors were introduced in the corresponding solution (containing chalcone and aqueous MeOH) where oxygen was continuously bubbling and the entire solution was stirred for 6 h. In neither of the cases epoxidation occurred, but compared to the powder catalyst the conversion towards the hydrogenation product was lower.

These results demonstrate once more the necessity of a basic activator capable of transforming the peroxide into the desired anion and not into the radical. Thus, the above mentioned experiment was repeated using the 0.75 wt% Pd-CMR, but adding in the reaction medium 160 mg of rehydrated Mg-Al HT. Surprisingly, after 6 h of reaction the epoxide was obtained along with the hydrogenated product, even though chalcone conversion was small (Scheme 5.7).

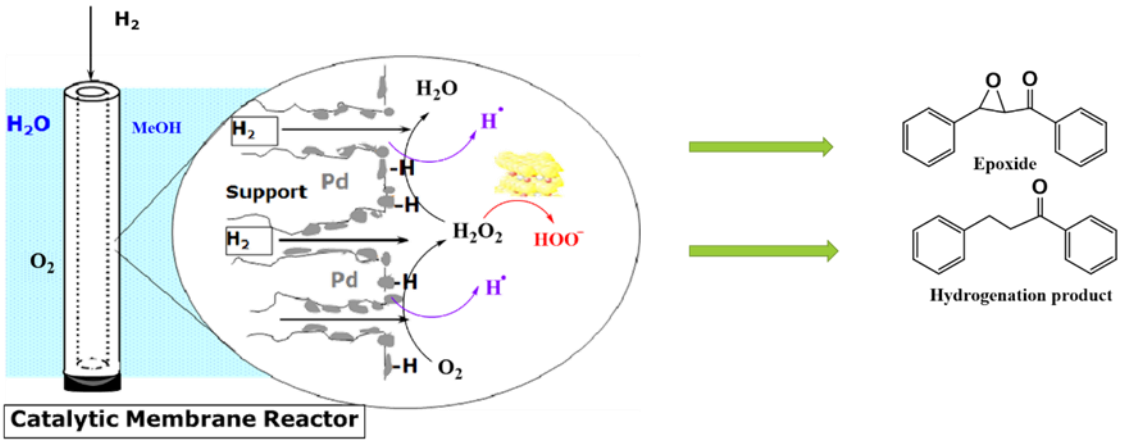


**Scheme 5.7** Schematic of the *in-situ* epoxidation of chalcone using 0.75 wt% Pd-CMR with Mg-Al HT dispersed in solution.

Despite the low selectivity towards the epoxide, this new finding led us to the idea of introducing HT directly into the CMR. By using Method A (see Section 5.2.5), the layer of HT was dispersed only at the surface of the CMR and, during the calcination treatment in air, it was almost completely lost. The presence of the HT was not detected by XRD analysis. To ensure the presence of the HT in the membrane, the material must be formed in the pores of the CMR, fact achieved by employing Method B.

The hybrid CMR prepared by Method B was used in the *in-situ* chalcone epoxidation using a series of solvents both protic and aprotic, as can be shown from Table 5.1. The hydrogenated product was obtained in all of the cases, but the epoxide was obtained only when methanol was used as solvent (entries 1 and 2, Table 5.1). These results suggest once again that the $H_2$ and $O_2$ solubility in the solvent used is crucial. Moreover, if both the formed hydrogen peroxide and chalcone are soluble in the solvent, the contact between the formed hydroperoxide anion and the substrate will increase, leading to the epoxidation reaction. Besides gas solubility, the ability of the solvent to create hydrogen bonds with the formed peroxide and the amphiprotic neutral character seem to affect the epoxidation reaction.

**Table 5.1** Screening of solvents for the *in-situ* epoxidation of chalcone using the hybrid HT-CMR

| Entry[a] | Solvent | 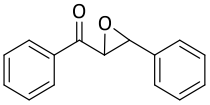 Selectivity (%)[b] | 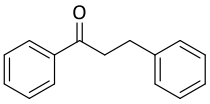 Selectivity (%)[b] |
|---|---|---|---|
| **1** | $H_2O$ / MeOH | 6 | 65 |
| **2** | MeOH | 9 | 45 |
| **3** | EtOH | 0 | 22 |
| **4** | 2-Propanol | 0 | 60 |
| **5** | DMSO | 0 | 100 |
| **6** | ACN | 0 | 55 |
| **7** | Heptane | 0 | 61 |

[a]Typical procedure: HT-CMR closed to one end and passing 30 Nml/min $H_2$ to the other end was introduced in 40 ml solvent containing 10 mg chalcone; oxygen was directly bubbled in the mixture. After 6h the solvent was evaporated; [b]Determined from $^1$H-NMR spectra

As gas solubility is temperature dependent, we have studied the *in-situ* epoxidation of chalcone using the new HT-CMR at 0 °C. As expected, in these conditions, the solubility of oxygen in methanol increased considerably leading to a higher production of hydrogen peroxide and a decrease in the hydrogenation process (entry 2, Table 5.2). One can deduce that the limiting factor in the epoxidation reaction is the production of hydrogen peroxide which also hinders the undesired reaction.

**Table 5.2** Influence of temperature on the in-situ epoxidation of chalcone

| Entry[a] | Temperature | Solvent | 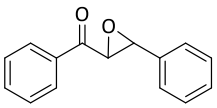 Selectivity (%)[b] | 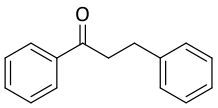 Selectivity (%)[b] |
|---|---|---|---|---|
| **1** | r. t. | MeOH | 9 | 45 |
| **2** | 0 °C | MeOH | 19 | 30 |
| **3**[c] | r. t | MeOH | 22 | 23 |

[a]Typical procedure: HT-CMR closed to one end and passing 30 Nml/min $H_2$ to the other end was introduced in 40 ml methanol containing 10 mg chalcone; oxygen was directly bubbled in the mixture. After 6h the solvent was evaporated; [b]Determined from $^1$H-NMR spectra; [c] Extra $H_2O_2$ was added

To demonstrate this, we performed a new control experiment at room temperature but adding external $H_2O_2$ after 6 h of reaction (entry 3, Table 5.2). After another 2 h of reaction an increase in the selectivity towards the epoxide was observed but none towards the hydrogenated product, as compared to the reaction done in normal conditions (entry 1, Table 5.2).

### 5.3.3 Mechanism of Reaction Using HT-CMR

As mentioned in the previous sections, the hydrogen flow is subjected through one end of the CMR while the other is maintained closed, creating a pressure difference which forces the hydrogen molecules to exit through the CMR pores. The pores containing Pd particles will activate the hydrogen, which, in the presence of an oxygen molecule will form hydrogen peroxide. Depending on the environment, the newly formed $H_2O_2$ can either decompose to water or transform into hydroxyl radicals.

In the case of the HT-CMR, the pores contained both HT and Pd, thus the formation of the hydrogen peroxide will subsequent be transformed into the hydroperoxide anion as can be seen in Scheme 5.8 – A. The hydroperoxide anion and a chalcone molecule(**7a**) assemble in a complex to form the corresponding peroxide enolate intermediate (**8**). This intermediate is not stable and it will close to give the epoxide (**9**).

On the other hand, the presence of activated hydrogen on the surface of Pd favours the hydrogenation reaction. The mechanism of this reaction is not exactly known, but probably chalcone also binds to the surface/ pores of the CMR, besides the hydrogen molecules already bonded, as seen in Scheme 5.8 – B. Palladium activates the π bond system of chalcone double

bond (**7b**) and the molecule is not removed from the surface until the transfer of a hydrogen atom is not completed (**10**).

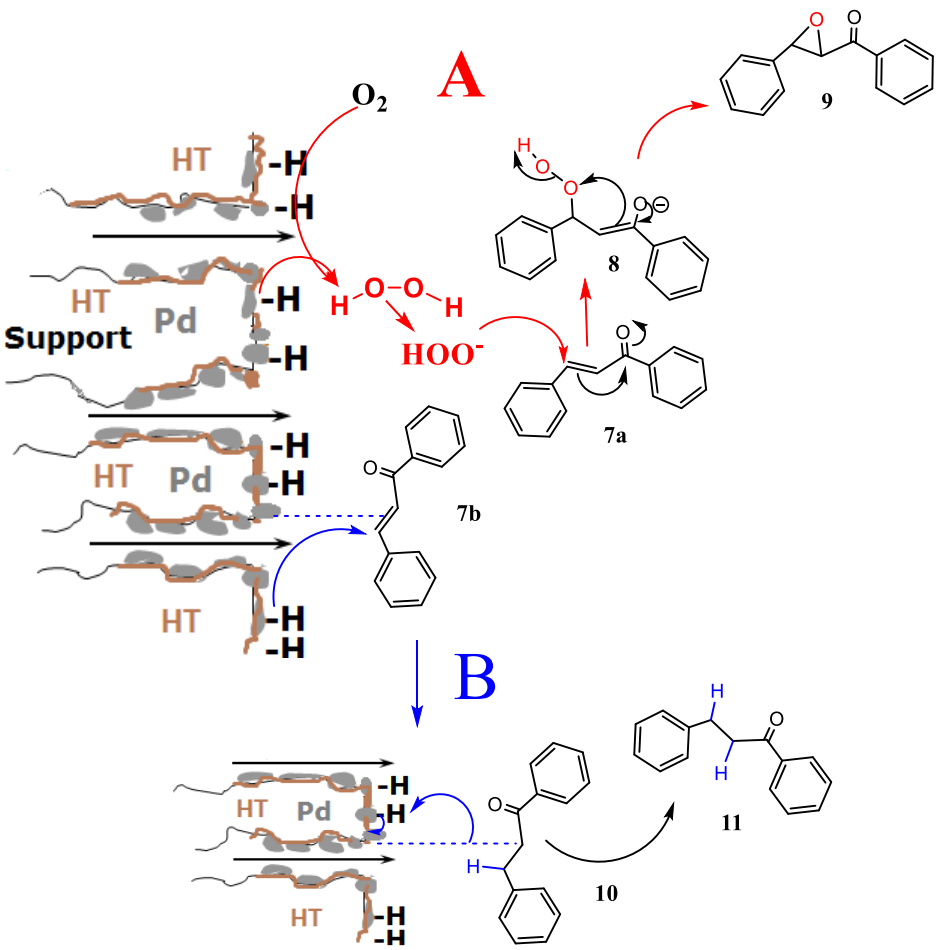


**Scheme 5.8** Proposed mechanism for the *in-situ* epoxidation of chalcone and hydrogenation of chalcone using HT-CMR: A – epoxidation reaction and B – hydrogenation reaction

## 5.4 Conclusions

Green chemistry represents "the design of chemical products and processes that reduces or eliminates the generation of hazardous substances" (according to EPA definition), which can be applied on the entire life cycle of a product: the design, manufacture, use and disposal.

Tremendous research has been done in the intent of producing hydrogen peroxide directly form hydrogen and oxygen, but the reaction still cannot be used at an industrial level due to several drawbacks, one of them being the high probability of explosion.

One method of avoiding this limitation is the use of catalytic membrane reactors (CMRs) which minimizes the direct contact between the two gases. These CMRs, impregnated with Pd, have already proven their activity in the hydrogen peroxide synthesis, opening new area of usage and implementation.

## 5 In-situ Epoxidation of Chalcone

Besides the hydrogen peroxide synthesis, the production of epoxides has a similar importance as they are intermediates in the production of other complex molecules used in medicine, perfumery, etc.

In this context we have managed to combine the two processes into a single one by *in-situ* epoxidation of chalcone using a new catalytic system based on CMR, Pd nanoparticles and hydrotalcites (HTs). We have demonstrated that hydrotalcites are of crucial importance in the epoxidation reaction, being able to activate the *in-situ* formed $H_2O_2$ into the necessary hydroperoxide anion.

All the reactions were performed using a single CMR, which did not require any pre-treatment and was used multiple times without deactivation. Moreover, the new hybrid CMR can catalyse two reactions simultaneously: hydrogenation and epoxidation reaction of the α,β-unsaturated ketones.

Although the selectivity towards the epoxide was not very high, the entire systematic process is the first one of its kind and our preliminary outcomes show that hydrotalcites incorporated in CMRs are promising materials which would open new routes for developing and designing new type of hybrid reactors that can be used in different processes.

# Bibliography

[1] C. Lauret, *Tetrahedron: Asymmetry*, **12**, 2359–2383, **2001**.

[2] S.T. Oyama, *Rates, Kinetics, and Mechanisms of Epoxidation: Homogeneous, Heterogeneous, and Biological Routes*, in: S.T. Oyama (Ed.) Mechanisms in Homogeneous and Heterogeneous Epoxidation Catalysis, 3-99, **2008**.

[3] O. Lifchits, M. Mahlau, C.M. Reisinger, A. Lee, C. Farès, I. Polyak, G. Gopakumar, W. Thiel, B. List, *Journal of American Chemical Society*, 6677-6693, **2013**.

[4] Y. Tanaka, K. Nishimura, K. Tomioka, *Tetrahedron*, **59**, 4549-4556, **2003**.

[5] N.C. Yang, R.A. Finnegan, *Journal of American Chemical Society*, **80**, 5845-5848, **1958**.

[6] M. Bougauchi, S. Watanabe, T. Arai, H. Sasai, M. Shibasaki, *Journal of American Chemical Society*, **119**, 2329-2330, **1997**.

[7] W. Adam, L. Hadjiarapoglou, B. Nestler, *Tetrahedron Letters*, **31**, 331-334, **1990**.

[8] K. Jakka, J. Liu, C.-G. Zhao, *Tetrahedron Letters*, **48**, 1395-1398, **2007**.

[9] X. Lu, Y. Liu, B. Sun, B. Cindric, L. Deng, *Journal of American Chemical Society*, **130**, 8134-8135, **2008**.

[10] A. Lattanzi, M. Cocilova, P. Iannece, A. Scettri, *Tetrahedron: Asymmetry*, **15**, 3751-3755, **2004**.

[11] T.S. Straub, *Tetrahedron Letters*, **36**, 663-664, **1995**.

[12] S. Marmor, *Journal of Organic Chemistry*, **28**, 250–251, **1963**.

[13] X.-L. Geng, Z. Wang, X.-Q. Li, C. Zhang, *Journal of Organic Chemistry*, **70**, 9610-9613, **2005**.

[14] A. Armstrong, G. Ahmed, B. Dominguez-Fernandez, B.R. Hayter, J.S. Wailes, *Journal of Organic Chemistry*, **67**, 8610-8617, **2002**.

[15] J.V. Allen, K.-H. Drauz, R.W. Flood, S.M. Roberts, J. Skidmore, *Tetrahedron Letters*, **40**, 5417-5420, **1999**.

[16] J.-L. Zhang, C.-M. Che, *Organic Letters*, **4**, 1911-1914, **2002**.

[17] K. Oh, J. Ryu, *Tetrahedron Letters*, **49**, 1935-1938, **2008**.

[18] M. Ochiai, A. Nakanishi, T. Suefuji, *Organic Letters*, **2**, 2923-2926, **2000**.

[19] J.M. Campos-Martin, G. Blanco-Brieva, J.L.G. Fierro, *Angewandte Chemie International Edition*, **45**, 6962 – 6984, **2006**.

[20] L. Cui, S. Furuhashi, Y. Tachikawa, N. Tada, T. Miura, A. Itoh, *Tetrahedron Letters*, **54**, 162-165, **2013**.

[21] C. Samanta, *Applied Catalysis A: General*, **350**, 133-149, **2008**.

[22] V.V. Krishnan, A.G. Dokoutchaev, M.E. Thompson, *Journal of Catalysis*, **196**, 366-374, **2000**.

[23] J.G.S. Marcano, T.T. Tsotsis, *Catalytic Membranes and Membrane Reactors*, Wiley-VCH, **2002**.

[24] S. Miachon, J.-A. Dalmon, *Topics in Catalysis*, **29**, 59-65, **2004**.

[25] S. Melada, F. Pinna, G. Strukul, S. Perathoner, G. Centi, *Journal of Catalysis*, **235**, 241-248, **2005**.

[26] S. Abate, G. Centi, S. Melada, S. Perathoner, F. Pinna, G. Strukul, *Catalysis Today*, **104**, 323-328, **2005**.

[27] M. Vospernik, A. Pintar, J. Levec, *Chemical Engineering and Processing*, **45**, 404–414, **2006**.

[28] A. Pashkova, K. Svajda, R. Dittmeyer, *Chemical Engineering Journal*, **139**, 165-171, **2008**.

[29] L. Shi, A. Goldbach, G. Zeng, H. Xu, *Catalysis Today*, **156**, 118-123, **2010**.

[30] A. Pashkova, R. Dittmeyer, N. Kaltenborn, H. Richter, *Chemical Engineering Journal*, **165**, 924-933, **2010**.

[31] M. Alame, A. Abusaloua, M. Pera-Titus, N. Guilhaume, K. Fiaty, A. Giroir-Fendler, *Catalysis Today*, **157**, 327-333, **2010**.

[32] L. Shi, A. Goldbach, G. Zeng, H. Xu, *Journal of Membrane Science*, **348**, 160-166, **2010**.

[33] T. Inoue, Y. Tanaka, D.A.P. Tanaka, T.M. Suzuki, K. Sato, M. Nishioka, S. Hamakawa, F. Mizukami, *Chemical Engineering Science*, **65**, 436-440, **2010**.

[34] O. Osegueda, A. Dafinov, J. Llorca, F. Medina, J. Suerias, *Catalysis Today*, **193**, 128– 136, **2012**.

[35] O. Osegueda, A. Dafinov, J. Llorca, F. Medina, J. Sueiras, *Chemical Engineering Journal*, **262**, 344–355, **2015**.

[36] C. Cativiela, F. Figueras, J.M. Fraile, J.I. Garcia, J.A. Mayoral, *Tetrahedron Letters*, **36**, 4125-4128, **1995**.

[37] S. Ueno, K. Yamaguchi, K. Yoshida, K. Ebitani, K. Kaneda, *Chemical Communications*, 295-296, **1998**.

[38] K. Yamaguchi, K. Mori, T. Mizugaki, K. Ebitani, K. Kaneda, *Journal of Organic Chemistry*, **65**, 6897-6903, **2000**.

[39] J.M. Fraile, J.I. García, D. Marco, J.A. Mayoral, *Applied Catalysis A: General*, **207**, 239–246, **2001**.

[40] T. Honma, M. Nakajo, T. Mizugaki, K. Ebitani, K. Kaneda, *Tetrahedron Letters*, **43**, 6229–6232, **2002**.

[41] U.R. Pillai, E. Sahle-Demessie, R.S. Varma, *Synthetic Communications*, **33**, 2017-2027, **2003**.

[42] M.a.J. Climent, A. Corma, S. Iborra, A. Velty, *Journal of Molecular Catalysis A: Chemical*, **182-183**, 327–342, **2002**.

[43] U. Rossi, S. Zancanella, L. Artiglia, G. Granozzi, P. Canu, *Chemical Engineering Journal*, **207-208**, 845-850, **2012**.

## 5 In-situ Epoxidation of Chalcone

# 6 Summary and Outlook

## 6.1 Summary

Intercalating biological species or nature-inspired ones with inorganic solids created a series of materials with different chemical and physical properties, different structures and textures, generally known as bio-nanohybrid materials. Some of the Nature's secrets have been already revealed and were used in the synthesis of materials with biological or catalytic applications, but there are still many to be discovered.

In this context, the present thesis aimed to study and understand the catalytic role of new nanohybrid materials based on amino acids or poly-amino acids and hydrotalcites in three reactions with potential applications in drug discovery, perfumery, flavouring, etc.: aldol addition reaction, the Claisen-Schmidt condensation and the Juliá-Colonna epoxidation.

Industry favours catalytic processes that require less workup and where intermediates are obtained *in-situ*, avoiding unnecessary purification procedures. Given these requirements, other objectives of this thesis were to investigate the one-pot Claisen-Schmidt condensation / Juliá – Colonna epoxidation reaction and to create a catalyst for the production of hydrogen peroxide and subsequent epoxidation of chalcone.

Undoubtedly, investigating the catalytic activity cannot be complete without studying the mechanism of reactions. Last but not the least, the thesis shielded light upon a controversial mechanism of the Juliá – Colonna epoxidation reaction, employing for the first time the use of a quartz crystal microbalance with dissipation (QCM-D) in mechanistic studies.

All the nanohybrid materials used in this thesis were based on hydrotalcite materials (HTs) due to their excellent properties: easy to prepare, non-toxic, memory-effect and swelling capacity. The HTs consist of positively charged layers; thus, amphoteric or anionic molecules can be easily immobilized in the interlayer space of the materials either by coprecipitation, anionic exchange or reconstruction method.

The first objective of the thesis was to study how different nanohybrid materials based on L-leucine (L-Leu) and HT behave in the aldol addition reaction of cyclohexanone with different aromatic aldehydes. The immobilization process of the L-Leu into the corresponding HT was done either by anionic exchange method or by reconstruction method, focusing on how the ultrasound treatment (in the case of reconstruction method) or the temperature (in the case of anionic exchange method) affects it. We have discovered that the use of ultrasound treatment breaks the HT layers creating more basic sites, which, in the presence of water and L-Leu favour the immobilization process. During this process, L-Leu is immobilized in the anionic form inside the $HT_{rus}$ (rehydrated hydrotalcite) layer. In the absence of this treatment, L-leu was immobilized in both anionic and zwitterionic form, producing a catalyst with a higher crystallinity. If in the

first case the immobilization was done by compensating the $OH^-$ groups found in the HT interlayer space, in the second case the immobilization occurs through H-bonding between the $-NH_3^+$ group of the L-Leu with water and/or $OH^-$ groups in the HT layers.

Using temperature during the anionic exchange method produced a swelling of the HT and the immobilization occurred at first by anionic exchange until all accessible centres were compensated, then occurred by interactions between the zwitterionic L-Leu with water or $OH^-$ anions located in the interlayer space. The absence of temperature did not permit the immobilization of the L-Leu inside the HT, but only at the edges of the material.

These interesting structural features of these materials reflected on their catalytic activity in the aldol addition reaction. At a first glance, we have observed that the HT catalysed the isomerization of the aldol product and the degree of interchanging between the *syn* and the *anti*-isomers depended on the nature of the catalyst. For example, in the case of the catalyst prepared by anionic exchange using temperature, the *syn* -diastereoisomer was preferred while the material prepared through reconstruction method gave mainly the *anti* diastereoisomer.

The catalytic activity is not only affected by the nature of the nanohybrid material, but also by the solvent used in the reaction. While the system composed of DMSO and $H_2O$ led to low to moderate enantioselectivity towards the *anti*-diastereoisomer, the toluene and $H_2O$ system produced the *anti*-isomer with up to 73 % ee.

Another interesting nanohybrid studied in this thesis was composed of the poly-L-leucine (PLL) and HT, prepared by an anionic exchange protocol. The starting material was the rehydrated HT which, due to the presence of the $OH^-$ groups inside its layers, favoured the immobilization of PLL through its C-end. The immobilized poly-L-leucine (IPL) was tested first in the Claisen-Schmidt condensation reaction, as it could contain two potential active sites: the rehydrated hydrotalcite and the polymer. Our results demonstrated that in the condensation reaction only the HT part of the nanohybrid is active.

Claisen-Schmidt condensation reaction might produce, besides the *trans* α,β-unsaturated ketones, other side products like the *cis* isomer, the Michael addition product between the α,β-unsaturated ketones and ketone and the aldol addition product. All of these undesired products were avoided by using IPL, a lower temperature of reaction and neat conditions.

The α,β-unsaturated ketones obtained can be further transformed into the corresponding asymmetric epoxides through the Juliá-Colonna epoxidation reaction. Therefore, our next objective was to study the activity of the IPL catalyst in the one-pot Claisen-Schmidt condensation / Juliá-Colonna epoxidation reaction. This material was continuously used without any pre-activation and recycled for 4 consecutive runs, without losing its activity, over a wide range of substrates.

## 6 Summary and Outlook

While the mechanism of the Claisen-Schmidt condensation reaction is somehow known, the mechanism of the Juliá-Colonna epoxidation reaction is still unknown. To understand the role of the polymer and how each reagent participates in this reaction, we have used the QCM-D technique for the *in-situ* monitoring. Literature presents two possible mechanistic pathways to produce the epoxide, and we have discovered that only one of the two is active: the one in which the active part of the polymer interacts first with the hydroperoxide anion and afterwards with chalcone. This study conducted towards a two-folded discovery: the Juliá-Colonna mechanism and the use of QCM-D in mechanistic investigations.

Nowadays, researchers are trying to produce greener and more sustainable processes to minimize as much as possible the use of hazardous substances which might pollute our world. The last objective of this thesis was to try to oxidize chalcone using *in-situ* formed hydrogen peroxide. For this, several materials based on HT (the basic catalysts which will activate the $H_2O_2$ for the epoxidation reaction) and Pd (the catalyst active in the hydrogen peroxide production) were tested. Nonetheless, none of them produced the desired reaction. The goal was achieved by using a hybrid catalytic membrane reactor (CMR) containing both HT and Pd in its pores. Moreover, this hybrid reactor can catalyse three reactions in the same time: production of hydrogen peroxide, epoxidation reaction and hydrogenation reactions.

In conclusion, bio-nanohybrid materials with a high variety of properties were obtained by immobilizing L-leucine and poly-L-leucine in the interlayer space of layered double hydroxides. These catalysts are eco-friendly, are easy to produce and no pre-activation is required. Substances with potential application in pharmaceutical or fine chemical industries were obtained using these nanohybrids as catalysts in the aldol addition reaction and the one-pot Claisen-Schmidt condensation / Juliá-Colonna epoxidation reaction. Cooperation between surface science and catalysis revealed the real Juliá-Colonna mechanism by using QCM-D sensor. Last but not the least, hybrid catalytic membrane reactors can be employed in transforming complex reactions into simpler ones.

## 6.2 Outlook

Compared to the rest of the elements, Carbon, found in the 2nd period, group IVA, is a unique element not only because it can form different types of bonds with itself, but also with other elements. Carbon can form single, double and triple bonds with itself in an infinite variety of chains, rings and even 3D network.

Interestingly, graphene, which is made of C hybridized $sp^2$ in the form of planar hexagonal rings, was first studied only as a theoretical material in 1947, by P. R. Wallace [1], because in that period it was considered that the 2D crystals were thermodynamically unstable and could not exist. This idea was further transformed into a theorem, in 1973, known as Mermin-Wagner theorem which states that in one and two dimensional materials, long-range fluctuations can be created with little energy costs, since they increase the entropy and are, thus, favoured [2].

The first production of a graphene-like material was done for the first time in 1859 by Benjamin Brodie, but, at that time, the material was not recognized as being one of these types [3]. The term "graphene" was introduced by Ulrich Hoffmann and Hanns-Peter Boehm who, in 1962, using transmission electron microscopy observed for the first time this material [4]. But the real "boom" related to graphene was barely in 2004, when Novoselov and Geim described the isolation of a single atomic layer of graphite [5].

Before proceeding, it is very important to underline the difference between graphite and graphene. Graphite is a layered material, where each layer consists of a hexagonal lattice of C atoms joined through covalent bonds. The layers are connected one with another through weak van der Waals bonds (Figure 6.1).

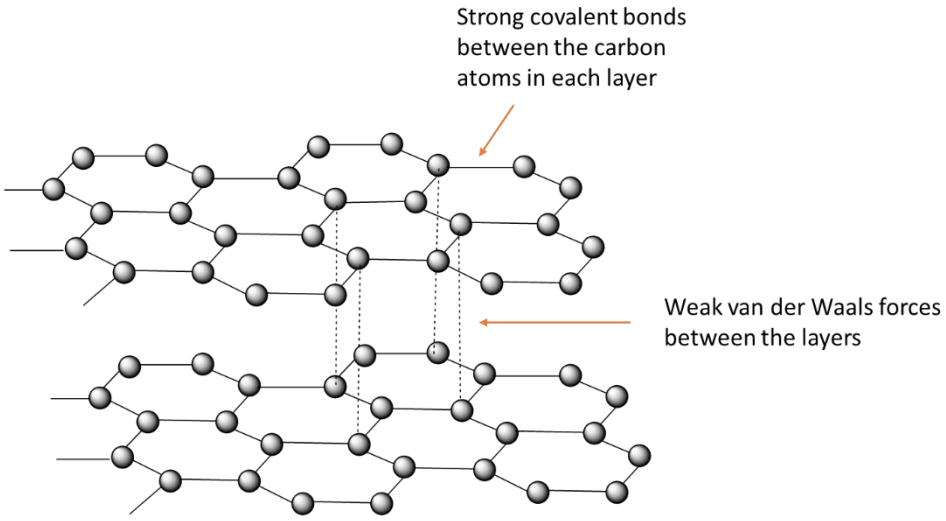


**Figure 6.1** Structure of graphite

The single atomic layer of graphite is named graphene and the unit cell of this material consists of two C atoms, due to its hexagonal structure. The carbon atoms in the hexagonal

lattice of graphene are found at a distance of $a$ = 1.42 Å, all connected through σ bonds (Figure 6.2); the π-bond is oriented outside the plane, on the z-direction [6].

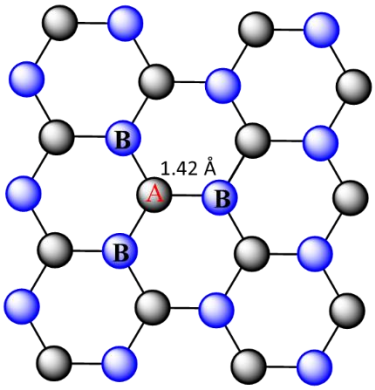


**Figure 6.2** Triangular sublattice of graphene. Each atom in one sublattice (A) has 3 nearest neighbours sublattice (B) and vice-versa

A hot topic for material science represents the design of hybrid material with multifunctional properties through the combination of various building blocks. The present thesis has already proven that combination of different materials with completely different properties can produce catalysts with unexpected properties. In this context, we have focused on new materials based on graphene and layered double hydroxides (LDHs), as both components have complementary properties and both have layered structures.

While LDHs have been used as catalysts for more than 100 years, graphene is known to be chemically inactive, but it has been regarded as an outstanding support material due to its giant carrier mobility and large special surface area. It is believed that the immobilization of LDHs on the surface of graphene or its family (as reduced graphene oxide - rGO) would produce material with special properties: i) the large surface area of graphene will expose the LDH active sites, leading to a superior catalytic performance and ii) a high electrical conductivity graphene will enhance the carrier mobility and will improve the electron-hole separation efficiency of LDH, producing good photocatalysts [7].

To test the catalytic performance of graphene (rGO)-hydrotalcite based materials, we have chosen 3 reactions which require base catalysts: the Claisen-Schmidt condensation reaction, epoxidation reaction and the *in-situ* production of hydrogen peroxide.

## 6.2.1 Claisen-Schmidt Condensation Reaction

For the Claisen-Schmidt condensation reaction between acetophenone and benzaldehyde we have decided to test a series of graphene-hydrotalcite materials obtained by direct coprecipitation.

### *6.2.1.1 Catalyst Characterization*

Graphene oxide (GO), which is commonly used as an easily water-dispersible precursor to graphene (G) or reduced graphene oxide (rGO), was prepared through a modified Hummers method [8] (the detailed procedure can be found in Appendix F). The PXRD pattern of rGO (Figure 6.3) indicates that after the hydrothermal treatment of GO, the distance between layers in the graphitic material decreases due to the loss of the oxidative debris produced during oxidation process and the rGO pattern presents a broad peak between 2θ = 20 – 30° indexed as (*002*) plane of rGO. The broadening of this peak can be attributed to the disordered restacking of exfoliated rGO sheets.

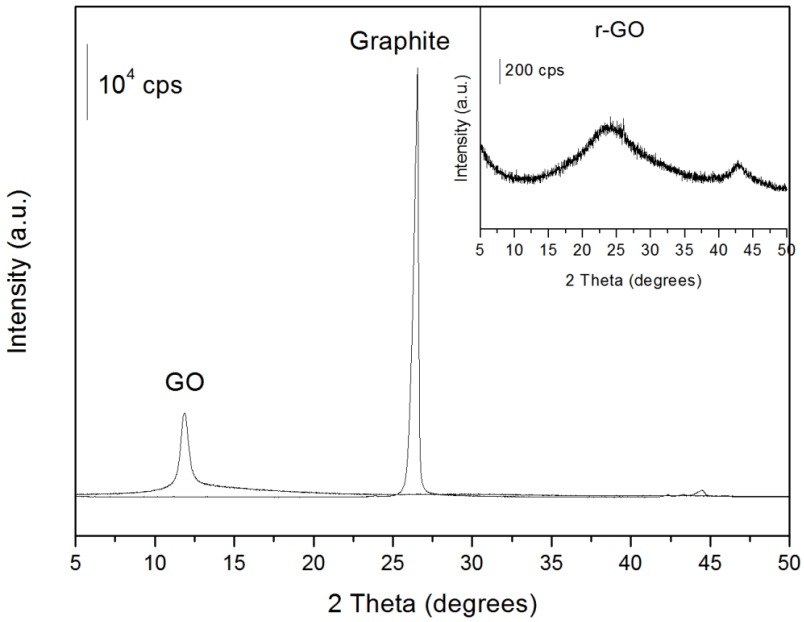


**Figure 6.3** XRD patterns of graphite, GO and reduced GO

A series of hybrid materials were prepared by the direct coprecipitation of the Mg and Al nitrate salts in a GA suspension. The ratio of the HT precursor was chosen in such a way to obtain a material with Mg-Al ratio 3:1. GO concentration was kept constant and the amount of metal salts was varied to obtain graphene-hydrotalcite material with 0.5:1, 1:1, 2:1, 5:1, 10:1 and 20:1 HT: rGO weight ratios.

The PXRD diffractograms of these materials present the typically reflections corresponding to the hydrotalcite-like materials (Figure 6.4). The absence of the basal reflection at 2θ = 11.8 Å specific to rGO suggests that the HT platelets prevent the restacking of the graphene sheets. This means that the two components are intimately in contact and highly dispersed. The breadth of the HT peaks in hybrids increases with the increase in rGO, proposing the apparent loss of crystallinity, which is in accordance with Garcia-Gallastegui *et al.*[9].

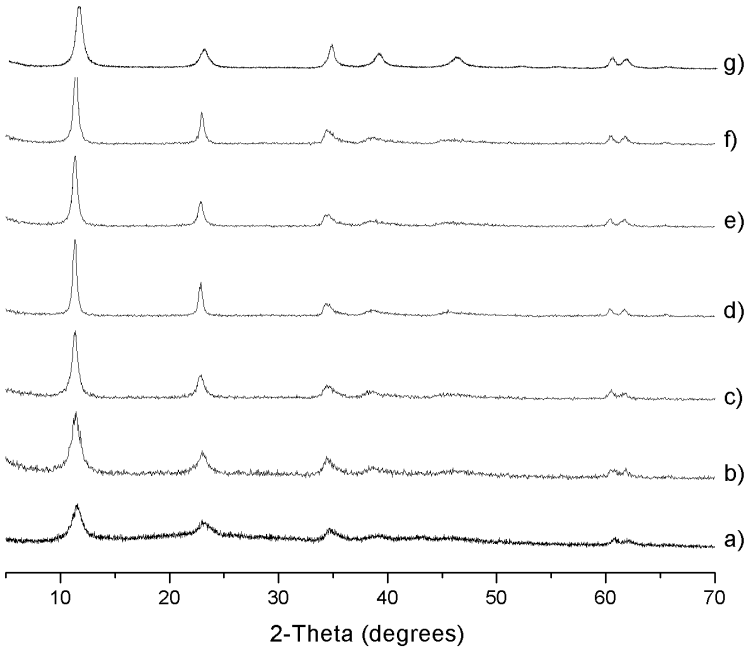


**Figure 6.4** Structure evolution of the as-prepared HT/rGO hybrid nanocomposites: a) HT/rGO-0.5; b) HT/rGO-1; c) HT/rGO-2; d) HT/rGO-5; e) HT/rGO-10; f) HT/rGO-20; g) HT.

Textural and structural data of the hybrid materials can be found in Table 6.1. There is a notable difference in specific surface area of the hybrid materials containing the lowest HT content (entry 1, Table 6.1) and the rest of the materials in the series (entries 2-6, Table 6.1). However, no remarkable differences were observed for the samples with HT:rGO ranging from 1:1 to 1:20, where the surface area varied between 133 and 148 $m^2/g$. In these cases, the presence of the rGO in the hybrids results in a higher surface area for the uncalcined materials, compared to the bulk HT. These results suggest the formation of a rather homogeneous structure in the hybrids with HT:rGO ≥ 1 , where the HT platelets may be highly dispersed on the rGO surface. On the contrary, the $N_2$ physisorption features of the hybrid HT/rGO-0.5 suggest the formation of a poorly porous material with a structure consisting of highly packed HT and rGO sheets (Figure F.1, Appendix F). These findings are in good agreement with the SEM and

TEM images of the representative samples: HT/rGO-0.5 and HT/rGO-10 (Figures F.3 and F.4, Appendix F).

Upon calcination, the surface area of the entire series of hybrids but the HT/rGO-0.5 increased by a factor of 2, in agreement with the structural transformations observed for the Mg-Al HT.

**Table 6.1** HT loading, textural and structural data of the synthesized HT/rGO hybrids

| Entry | Sample | HT:rGO | HT content wt.% | | Breadth (deg.) | $S_{BET}$ ($m^2/g$)[b] |
|---|---|---|---|---|---|---|
| | | nominal | nominal | Actual[a] | | |
| **1** | HT/rGO-0.5 | 0.5 | 33 | 37 | 1.210 | 25 |
| **2** | HT/rGO-1 | 1 | 50 | 49 | 1.148 | 148 (206) |
| **3** | HT/rGO-2 | 2 | 67 | 65 | 0.846 | 194 (222) |
| **4** | HT/rGO-5 | 5 | 83 | 81 | 0.531 | 135 (276) |
| **5** | HT/rGO-10 | 10 | 91 | 91 | 0.693 | 143 (239) |
| **6** | HT/rGO-20 | 20 | 95 | 95 | 0.572 | 133 (293) |
| **7** | $HT_{3:1}$ | -- | 100 | 100 | 0.346 | 140 (280) |

[a]Computed from TG analysis (20 ml/min air, temperature range between 80-830 °C, temperature rate 1 °C; [b]The surface area of calcined materials is presented in brackets

Pore volume of the hybrid materials increases with increasing the quantity of HT for both calcined and uncalcined samples (Figure 6.5). While the increase in surface area for the uncalcined hybrids might be related to intrinsic porosity generated by the HT incorporation and the lower stacking degree of the two components (rGO and HT) in the hybrid, the increase observed in the calcined samples is due to the pore generation produced by gas release during thermal treatment caused by the HT decomposition. The hybrid material containing 0.5 HT was not subjected to this analysis as the change in pore volume is expected to be insignificant.

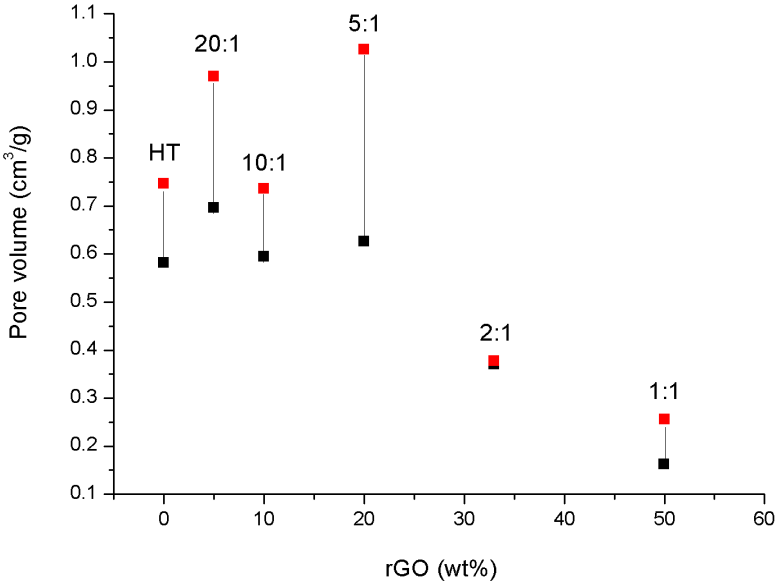


**Figure 6.5** Pore volume distribution for the as-synthesized (black dots) and calcined hybrids (red dots)

### *6.2.1.2 Catalytic Activity*

As mentioned in Section 3 of this thesis, there are four possible products of the Claisen-Schmidt condensation reaction: *trans*-chalcone (**1**), *cis*-chalcone (**2**), the Michael addition product (**3**) and the aldol addition product (**4**), as can be seen from Scheme 6.1.

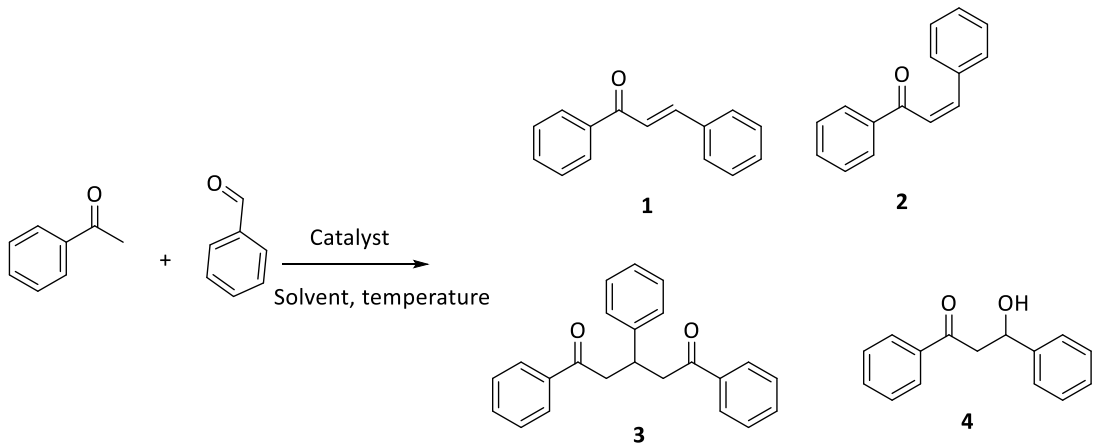


**Scheme 6.1** The Claisen-Schmidt condensation reaction

The general base catalysed mechanism of Claisen-Schmidt condensation reaction starts with the ionization of the acidic α-hydrogen of the ketone molecule by a base; the formed species undergoes a keto-enol tautomerism. The rate determining step of the entire reaction is the nucleophilic addition of the enolate to the carbonyl carbon of benzaldehydes, yielding the intermediate β-hydroxyl ketone, followed by dehydration to give chalcone (Scheme 6.2).

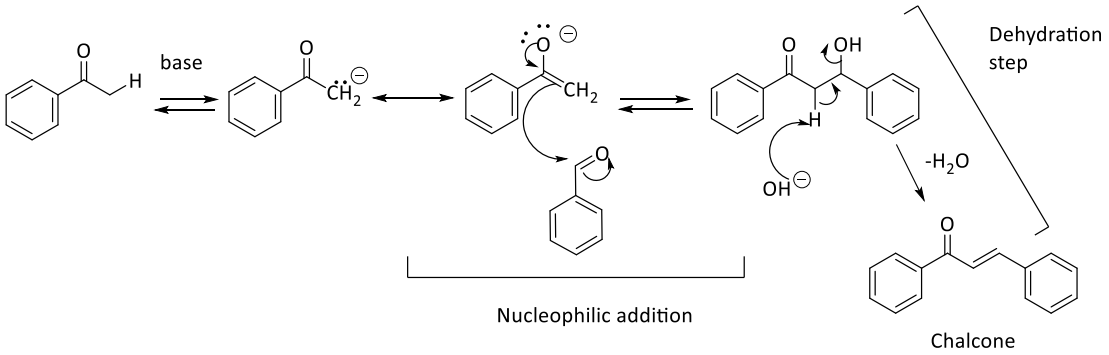


**Scheme 6.2** Accepted mechanism of the Claisen-Schmidt condensation

The solvent in which a chemical reaction takes place is rarely a non-inert medium and the complex interactions between solvent, solute molecules and possible intermediates can result in a gross modification of the reaction pathway. Based on this, we decided to study different solvents in the Claisen-Schmidt condensation reaction catalysed by these hybrid materials: a polar solvent, a polar aprotic one, a nonpolar solvent and neat conditions. The physical constants of each solvent used in this section can be found in Table F.1 – Appendix F.

In Section 3.3.2.1 it was demonstrated that the condensation reaction carried out in the presence of the IPL catalytic system gives the best results at 60 °C. As the presence of graphene will improve HT's catalytic performance, we decided to study the reaction at a lower temperature, at 40 °C.

It is already known that graphene and its family are chemically unreactive, so we started with the assumption that neither rGO nor the hybrid material containing only 0.5 HT would be active in the condensation reaction – supposition which proved to be true in all of the cases where a solvent was used. Intriguing, under neat conditions, no reaction took place, but the rGO material completely absorbed the reagents.

To better understand the catalytic activity of these new materials, we decided to evaluate their activity by comparing the entire series of catalysts with HTs containing molar ratios Mg:Al 2:1 and 3:1. The results demonstrate that not only the type of catalyst used plays a crucial role in the reaction mechanism, but also the solvent used, as can be seen from Figures 6.6, 6.7, 6.8 and 6.9.

The conversion was total in all the cases where the hybrid materials were used as catalysts. But the best results in terms of selectivity towards *trans*-chalcone (**1**) and the presence of few side products (only *cis*-chalcone and the Michael addition product) were obtained when acetonitrile (ACN) was used as solvent (Figure 6.6). This can be explained as follows: ACN is a polar aprotic solvent; thus, it cannot form hydrogen bonds with the intermediate anions formed

during the reaction (mainly the enolate anion); because of this, the anions will not get solvated and will remain "naked" in the medium and, consequently, will further react.

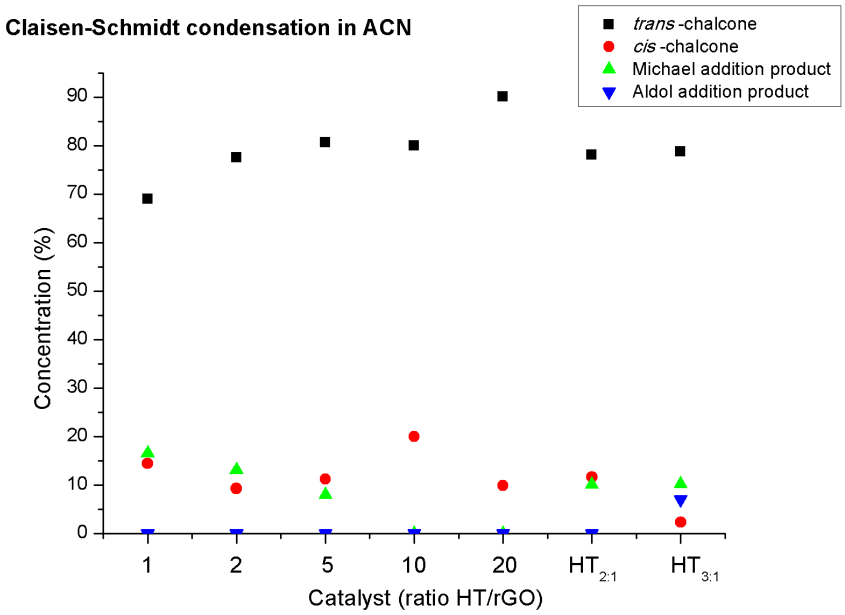


**Figure 6.6** Claisen-Schmidt condensation in ACN. Reaction conditions: 55 mg calcined catalyst, acetophenone and benzaldehyde 0.95 molar ratio, 1 ml solvent, 3 h, 40 °C. Conversion and selectivity from $^{1}$H-NMR spectra of the crude material.

From the whole series of hybrids, the highest selectivity towards *trans*-chalcone (**1**) was obtained in the case of HT/rGO-20, the hybrid with the highest HT content as well as the highest BET area and pore volume (after thermal activation). Since the catalytic activity is attributed to the HT phase (as discussed above), the difference in reactivity between the 20:1 HT/rGO material and the HT 3:1 (Figure 6.6) proves that the HT component of the hybrid presents structural differences compared to the bulk hydrotalcite, such as small crystallite size and good dispersion through the rGO surface. These characteristics are strongly mirrored in its improved catalytic activity.

In acetonitrile, the selectivity of the hybrid materials for the *trans*-chalcone (**1**) increases as the amount of HT increases. Another interesting trend can be observed in the case of the Michael addition product (**3**), which decreases in the first three cases (catalysts containing 1:1, 2:1 and 5:1 HT/rGO) and is not observed in the last two (10:1 and 20:1 HT/rGO). This catalytic behaviour can be explained by the different number and strength of basic sites present in the hybrids. A plausible explanation for this remarkable catalytic behaviour lies in the different basic sites that may be present in these hybrids. When the content of HT is low, the number and strength of these sites is expected to be lower than the hybrids with a higher HT content. This

might lead to a lower anion stabilization in the former case, which allows a faster Claisen-Schmidt condensation and a subsequent reaction of the condensation product with the anion still present in the medium. The hybrids 20:1 and 10:1 contain a higher amount of HT, thus the number and strength of basic sites is expected to be superior, inhibiting the formation of the Michael addition product (**3**).

When methanol (MeOH) was used as solvent, the results totally changed and at a first glance, no trend can be defined (Figure 6.7). Primarily, we have to underline that methanol is a polar solvent and the most acidic one from the solvents used in this study (see Table F.1 – Appendix F), thus it can act as a source of protons and a weak nucleophile. As the solvent can form hydrogen bonds, any anion formed in the reaction will be solvated, consequently it might be partially "inhibited".

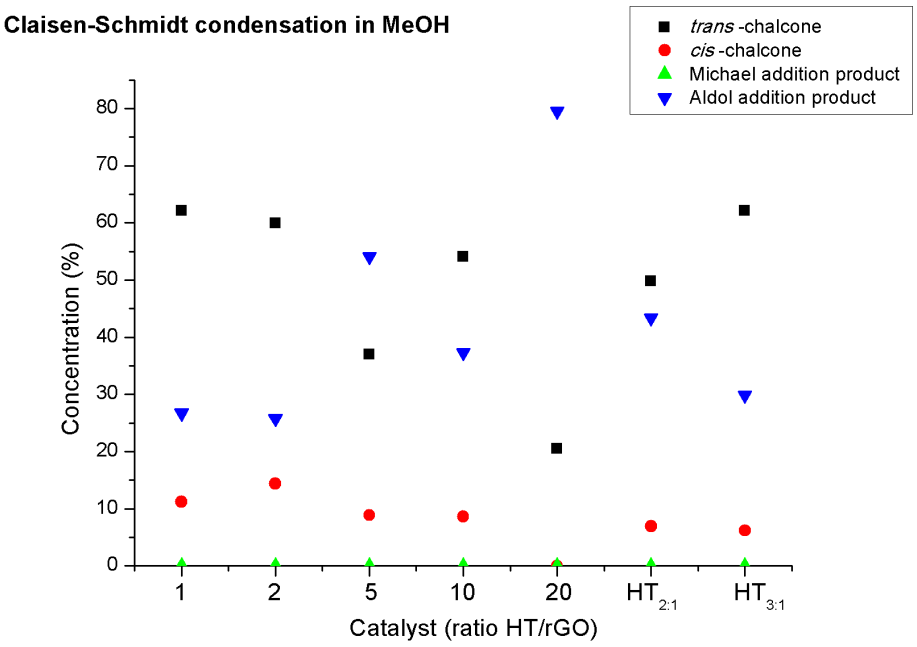


**Figure 6.7** Claisen-Schmidt condensation in MeOH. Reaction conditions: 55 mg calcined catalyst, acetophenone and benzaldehyde 0.95 molar ratio, 1 ml solvent, 3 h, 40 °C. Conversion and selectivity from $^{1}$H-NMR spectra of the crude material.

Compared to the reactions done in ACN where one of the side products was the Michael addition product (**3**), in the present case this product is not observed in any of the experiments done; instead the aldol addition product (**4**) is formed.

It seems that the dehydration step of the Claisen-Schmidt condensation is not completely favoured in the presence of methanol. This reaction proceeds by an E1cB mechanism (Scheme 6.3), in two steps: step 1 – where the base abstracts a proton from the α-C, resulting in a carbanion which in step 2 forms a π-bond and pushes the leaving group, producing chalcone.

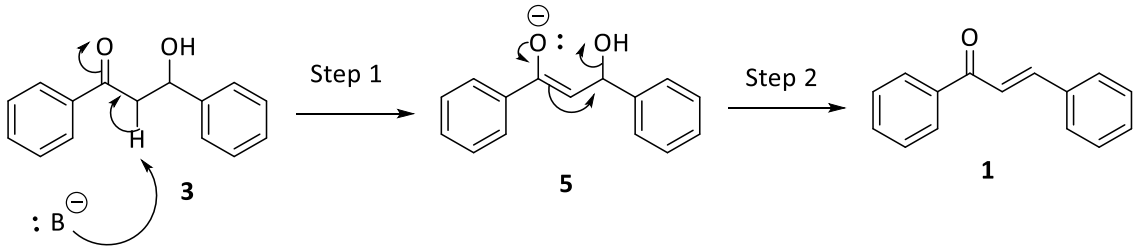


**Scheme 6.3** The E1cB mechanism involved in the chalcone formation

This E1cB mechanism is strongly favoured by the presence of a strong base, which in our case would be the HT part of the hybrid, but the use of a slightly acidic solvent might poison the basic centres. This phenomenon is especially seen in the case of HT/rGO-20, which is very selective to the aldol product; this highlights our previous hypothesis where we suggested that the hybrids with a higher HT content (10:1 and 20:1) are the most basic ones in the whole series. Moreover, as mentioned above, the anion (**5**) is solvated in MeOH and its reactivity towards the elimination step might be hindered.

If in the case when ACN was used as solvent, the best results were obtained when the 20:1 HT/rGO hybrid was employed, in MeOH the activity of the catalysts in terms of chalcone selectivity follows an interesting trend: the best activity was observed in the case of 1:1 material, decreasing slowly for 2:1, then dramatically dropping for the 5:1 to 20:1. This tendency might be explained as follows: the activated 1:1 and 2:1 materials present the lowest pore volumes and surface areas and, probably, the lower amount and weaker strength of basic centres, so, any possible deactivation with a weak acid such as methanol will be produced in a much lesser extent than in the samples with a higher number and stronger basic sites. In the former case, the basic active sites are available and strong enough to still favour the elimination process, even though some aldol product is still present. As the quantity of HT increases, the pore volume and basicity (in terms of number of basic sites and their strength) increases thus, the active centres can be easily deactivated by MeOH, which is a quite small molecule. Again, the 10:1 hybrid behaves in a totally different manner, which might be a consequence of how the material is constructed.

If in ACN, the 20:1 was the most active one, in methanol it favoured the aldol addition product, which strengthens our explanations. The difference between the catalytic activity of unsupported HT and the hybrids demonstrates once again that the HT in the new material has a new and different conformation than the bulk one.

The next study was done using toluene, a nonpolar solvent. In all the cases, no aldol product was obtained, as expected, but besides the *trans*-chalcone (**1**), a high amount of *cis* -chalcone (**2**) and Michael addition product (**3**) were observed (Figure 6.8). After a first glimpse to the

results, we can deduct that there is a similarity in products distribution between the reactions catalysed by HTs and the hybrids 1:1 and 2:1 HT/rGO, which might suggest that in toluene these hybrids behave similar to the corresponding HT, with a slightly higher activity towards the Michael addition product – phenomenon explained above, in the ACN section.

The hybrids 5:1, 10:1 and 20:1 presented another trend: if in the case of 5:1 material the selectivity towards the *cis*-chalcone (**2**) was the highest from this family of hybrids, the concentration of this product decreased with increasing the amount of hydrotalcite in the sample. In the same time, the selectivity towards the *trans*-chalcone (**1**) and the Michael addition product (**3**) increases with increasing the amount of HT.

We have to point out that our hybrids present a different polarity due to the variable HT concentration (which represents the hydrophilic part) and the carbonaceous compound (reduced graphene oxides). As toluene has similar polarity with the rGO (without taking into account any possible defects in the material), it will interact with the material through London dispersion forces, facilitating an easier penetration of the reagents molecules in the pores of the hybrids (especially in the case of hybrids 5:1, 10:1 and 20:1), hence, promoting a greater but not selective catalytic activity.

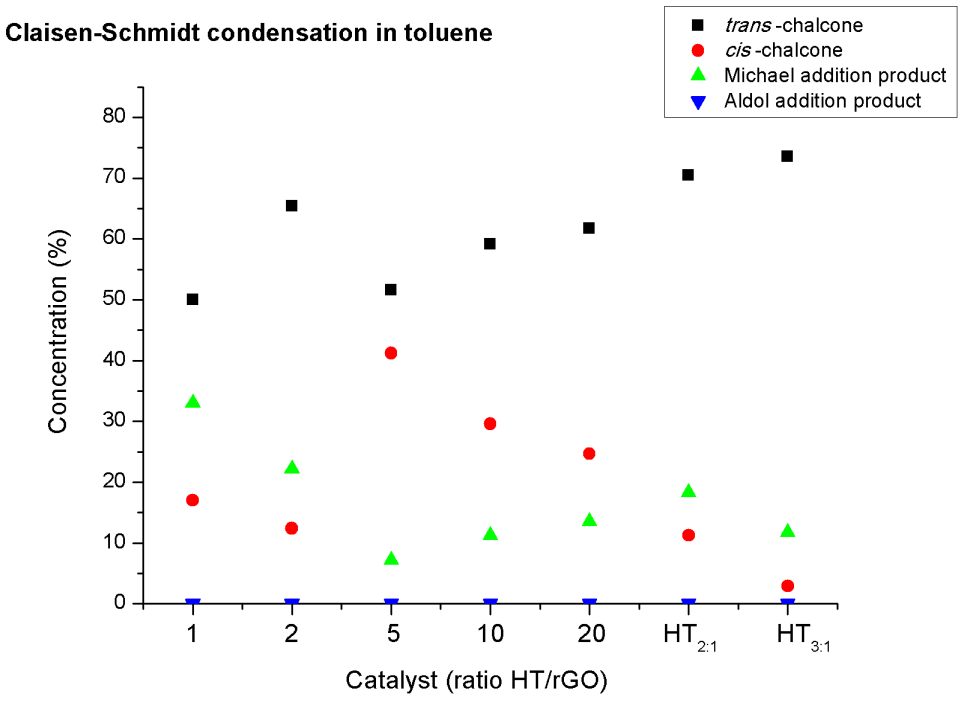


**Figure 6.8** Claisen-Schmidt condensation in toluene. Reaction conditions: 55 mg calcined catalyst, acetophenone and benzaldehyde 0.95 molar ratio, 1 ml solvent, 3 h, 40 °C. Conversion and selectivity from $^{1}$H-NMR spectra of the crude material.

## 6 Summary and Outlook

Until now, we have concentrated our attention on the role of solvent and subsequent catalyst activity in the Claisen-Schmidt condensation. To see and to understand how these hybrids really interact with the reagents, we conducted a new series of experiments in neat conditions.

The results, presented in Figure 6.9, display a similar trend as the ones where ACN was used as solvent, in the sense that the hybrids with HT:rGO ratio 1:1, 2:1 and 5:1 have a different trend than the 10:1 and 20:1.

Under neat conditions, the hybrid 1:1 HT/rGO gave as main product *trans*-chalcone (**1**) and as side products small amounts of *cis*-chalcone (**2**), the Michael addition product (**3**) and the aldol addition product (**4**). The presence of the latter one might be explained due to the low amount of HT found in the hybrid which (i) does not create a very basic medium to afford the dehydration step and/or (ii) which cannot promote a rapid absorption of the water generated during the dehydration process, thus shifting the equilibrium of this reaction towards the left. The first assumption has been highlighted in each catalytic test performed with the different solvents, where we have demonstrated the low basicity of this catalyst. Further, when the amount of HT in the hybrid increases (as in the case of 2:1, 5:1, 10:1 and 20:1 hybrids) the aldol addition product is no longer obtained, bringing a new evidence for the explanations mentioned above. The latter assumption could also be verified by a simple rehydration test, where the samples, previously activated, are immersed in deionized and decarbonated water or a water saturated flow of Ar is passed over them. It is well known that the HTs can recover their original layered structure after calcination and rehydration. This is a property widely used in this type of materials to obtain, for example, solids with Brönsted basicity. This is a rather fast reaction, occurring within one hour or even less. Our findings confirm that the rehydration of samples containing a high amount of rGO hardly occurs in 24h and that the reconstruction of the HT phase conversely depends on the rGO content in the hybrid. These simple experiments further confirmed our findings.

An increase in the HT content in the hybrid not only restraints the aldol product, but also decreases the selectivity towards the *cis*-chalcone, demonstrating that the presence of this side product in all the other experiments might be influenced by the presence of the solvent.

Notably, under neat conditions, the selectivity towards the Michael addition product increased with increasing the HT content, reaching a maximum for the 10:1 HT/rGO hybrid – which, again, behaves totally different than the rest of the hybrids in the series. This finding is in line with the results obtained throughout all the catalytic tests and points out to a higher basicity of those hybrids with a high HT:rGO ratio (i.e. 10:1 and 20:1).

The presence of the Michael addition product over all the prepared hybrids could be explained through the high reactivity of the enolate ion found in the reaction mixture; under

neat conditions, all the molecules are closer, thus, the newly formed chalcone (either in the *cis* or *trans* form) is more exposed to the enolate ion – which might also explain the disappearance of the *cis*-chalcone- producing the side product.

The best results in terms of selectivity towards the *trans*-chalcone were obtained when the 5:1 HT/rGO hybrid was used.

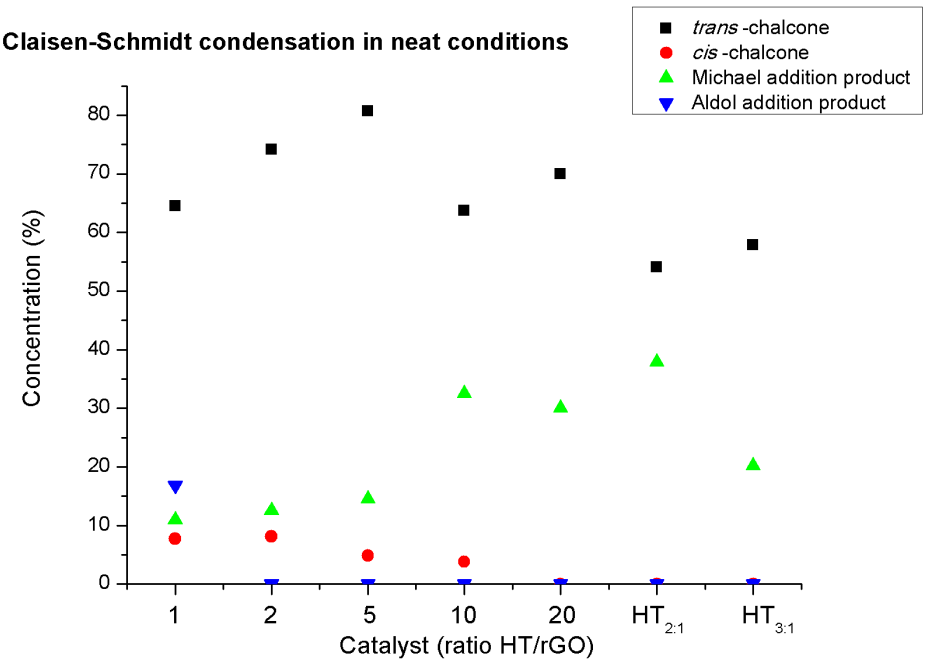


**Figure 6.9** Claisen-Schmidt condensation in neat conditions. Reaction conditions: 55 mg calcined catalyst, acetophenone and benzaldehyde 0.95 molar ratio, 3 h, 40 °C. Conversion and selectivity from $^{1}$H-NMR spectra of the crude material.

It is important to point out that in all our experiments, the hybrid materials proved to have better catalytic activities than the mere hydrotalcite, validating the idea that the presence of rGO will strengthen HT's properties.

To further test our conclusions, two new series of experiments were conducted in order to determine if the temperature will affect the catalytic activity and if the reaction is completed in less than 3 h.

To study the temperature effect on the reaction, two hybrids were chosen: the 1:1 and 5:1 HT/rGO materials (Figure 6.10). It is expected that an increase in temperature will favour the Claisen-Schmidt condensation, but this was not the case. Both materials were far less active at 60 °C, indicating that these catalysts could be used in transforming important industrial reactions which require high temperatures into more profitable and economic ones.

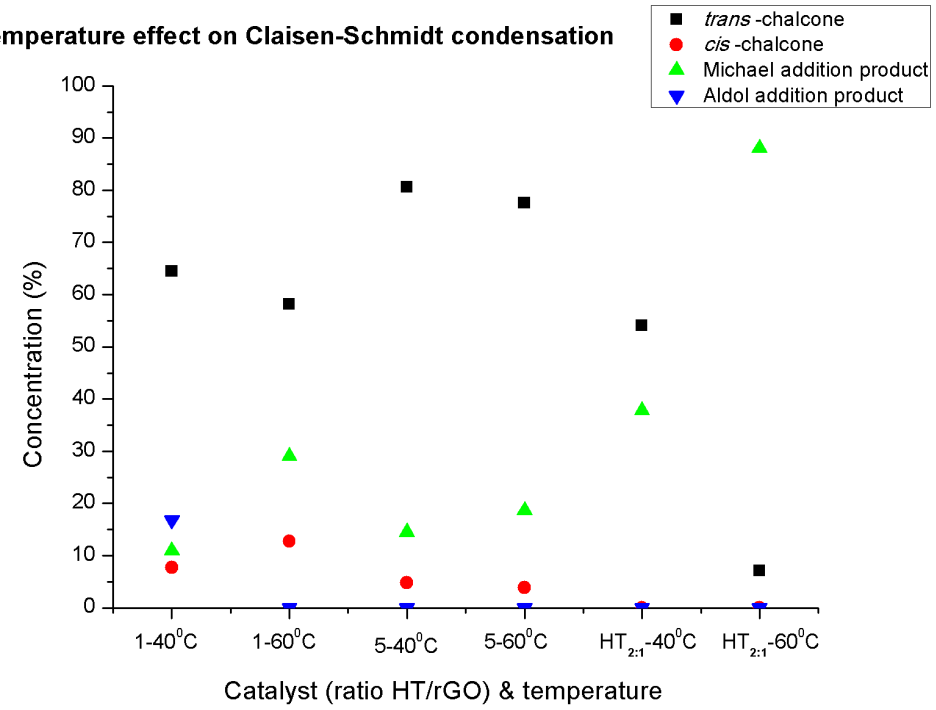


**Figure 6.10** Claisen-Schmidt condensation in neat conditions. Reaction conditions: 55 mg calcined catalyst, acetophenone and benzaldehyde 0.95 molar ratio, 3 h, 40 °C. Conversion and selectivity from $^{1}$H-NMR spectra of the crude material.

We have observed that the Claisen-Schmidt condensation reaction carried out in neat conditions and in the presence of the 5:1 HT/rGO hybrid reaches total conversion after only 90 minutes of reaction, while the bulk HT requires at least 2 h.

Moreover, we have demonstrated that these materials present great basic properties which are highly tuneable and adaptable to specific reaction products if the conditions are properly chosen. Further efforts to explore the basicity and catalytic activity are currently underway. The catalytic activity and selectivity of these nanohybrids may pave the way for improved and better applications. In this context, other catalytic applications of these hybrids are presented in the following sections.

### 6.2.2 Epoxidation Reaction

The aim of using the graphene-hydrotalcite based materials in all of the present reactions was to try to find better conditions and greener processes. Regarding the epoxidation reaction, the objective was to find a catalyst with a high basicity, able to activate the hydrogen peroxide without the need of a basic solution (Scheme 6.4).

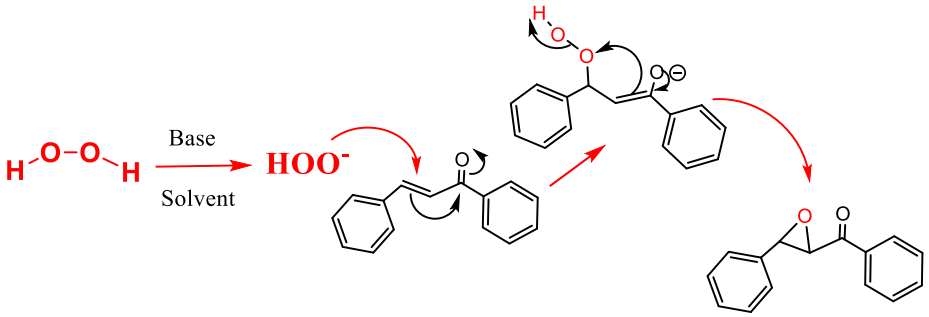


**Scheme 6.4** The epoxidation of chalcone with hydrogen peroxide

### *6.2.2.1 Catalyst Characterization*

The synthesis procedures for the constituent materials and the hybrid can be found in Appendix F.

The hybrid containing HT: rGO in the ration 20:1 was found to have a very high basicity, adsorbing 606 µmol/g $CO_2$ (the analysis protocol can be found in Appendix F).

Additional to the XRD diffractogram and the pore size distribution (which can be found in Section 6.2.1.1), the TEM image (Figure 6.11) showed the thin rGO nanosheets with a flake-like morphology (low contrast zone) and the small HT attached to these sheets.

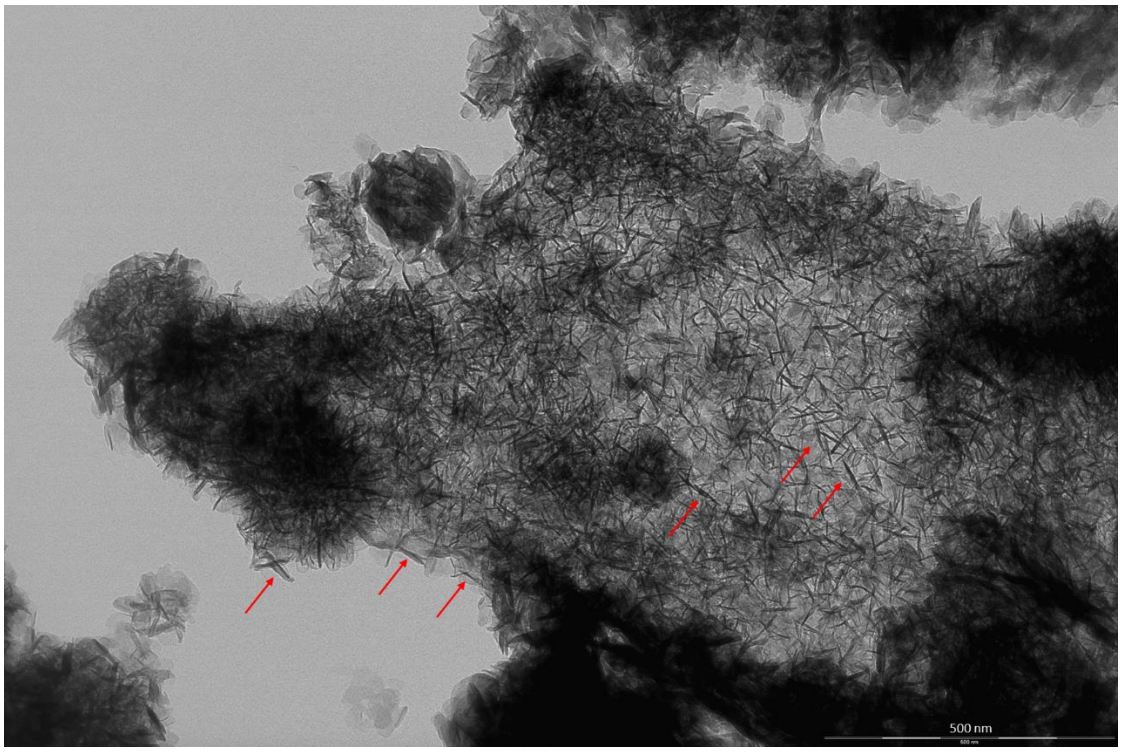


**Figure 6.11** TEM image of the 20:1 HT/rGO material. The HT platelets are indicated with red arrows.

### 6.2.2.2 *Catalytic Activity*

To avoid the use of a phase-transfer co-catalysts and the extra use of a base, one should consider the following: (i) a solvent in which both chalcone and the hydroperoxide anion are soluble and (ii) a very basic catalysts able to activate the hydrogen peroxide.

The best solvent for this reaction was found to be MeOH, thus the first series of experiments consisted in finding the optimal molar ratio $H_2O_2$ / chalcone. The information present in the literature (see Section 3) suggests that heterogeneously catalysed epoxidation reactions take places with a high conversion only when the oxidation agent is used in excess. In addition, the reaction is speeded up by the addition of a co-catalyst, which facilitates the close contact between the hydroperoxide anion and the chalcone-type reagent (see Section 3).

The basicity of the 20:1 hybrid material proved to be strong enough to activate the hydrogen peroxide even when equimolecular amounts of reagents were used (Figure 6.12).

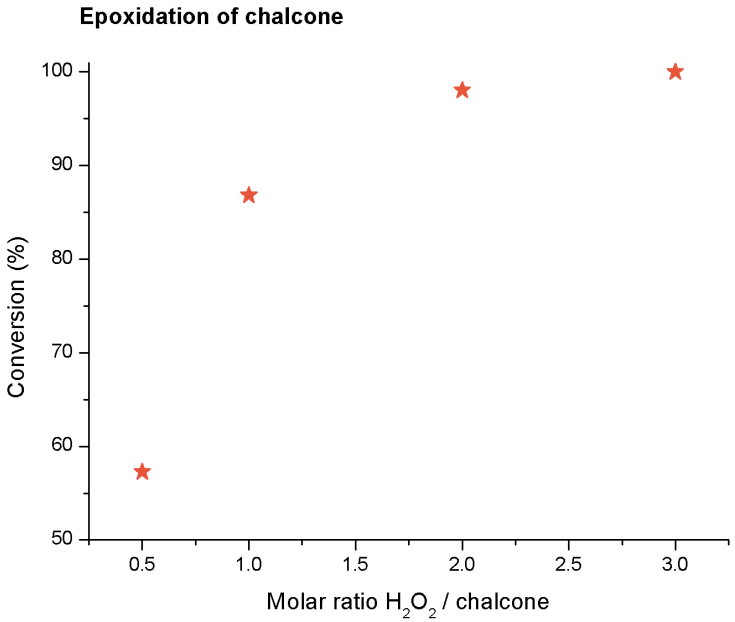


**Figure 6.12** Chalcone epoxidation using different molar ratios $H_2O_2$ / chalcone. Reaction conditions: 55 mg calcined catalyst, 24 mg chalcone, 2 h, room temperature. Conversion from $^1$H-NMR spectra of the crude material.

The obtained results are very inspiring and highlight the excellent catalytic properties of the synthesized HT/rGO hybrids, which showed superior catalytic activity than other heterogeneous catalysts found in the literature so far (for more information see Section 3). These encourage us to keep exploring on the performance of these materials in more advanced applications such as cascade-type reactions.

### 6.2.3 *In-situ* Epoxidation of Chalcone

Our preliminary findings uncovered in Section 6.2.2 suggest that a material similar to the 20:1 HT/rGO hybrid could be a perfect candidate for the *in-situ* epoxidation of chalcone, due to its high basicity. To test this hypothesis, a series of catalysts were prepared (the whole protocols can be found in Appendix F): HT containing Pd, the hybrid material 20:1 Mg-Al-Pd HT/r GO and Pd impregnated on a 20:1 HT/rGO hybrid. The reaction set-up was similar to the one in Section 5 and all the reactions were carried out at room temperature and atmospheric pressure. All the materials tested in this section were calcined at 450 °C in inert atmosphere overnight and reduced in 30 Nml/min $H_2$ for 3 h. The typical procedure consisted in adding 55 mg of active catalyst to a solution of 10 mg chalcone in 40 ml methanol and continuous bubbling hydrogen and oxygen while stirring the mixture.

The first step consisted in preparing the Mg-Al-Pd HT and verifying its catalytic activity in the two reactions: producing $H_2O_2$ from $H_2$ and $O_2$ and subsequent epoxidation of chalcone. The XRD diffractogram of the material before calcination (Figure 6.13 a) presents the $d_{003}$ and $d_{006}$ diffraction peaks corresponding to hydrotalcite-like structure, thus the HT was obtained. Although this material was active in the hydrogen peroxide production from hydrogen and oxygen at very mild conditions (for more information regarding hydrogen peroxide synthesis and subsequent use in an epoxidation reaction see Section 5), it was not able to catalyse the epoxidation reaction, but the hydrogenation of chalcone. This might be due to an insufficient basicity of the HT to activate the $H_2O_2$ molecule, maybe due to the presence of Pd atoms which can block or poison the basic centres found in the HT. As mentioned in Section 5, the hydrogen peroxide production is always followed by its decomposition into water. Upon calcination, the HT materials are transformed into corresponding mixed oxides and the presence of water will induce the rehydration of these oxides and their transformation into the corresponding hydrotalcite structure. The XRD diffractogram of the material after reaction (Figure 6.13 b) demonstrates that the catalyst completely lost its crystallinity. Moreover, the presence of strong visible peaks corresponding to Pd atoms reveals that the two exothermic reactions (reduction reaction in $H_2$ and hydrogen peroxide synthesis) might destroy the structures of the mixed oxides and possible the structure of the rehydrated HT. This behaviour can also be explained through the cluster sintering of the Pd nanoparticles.

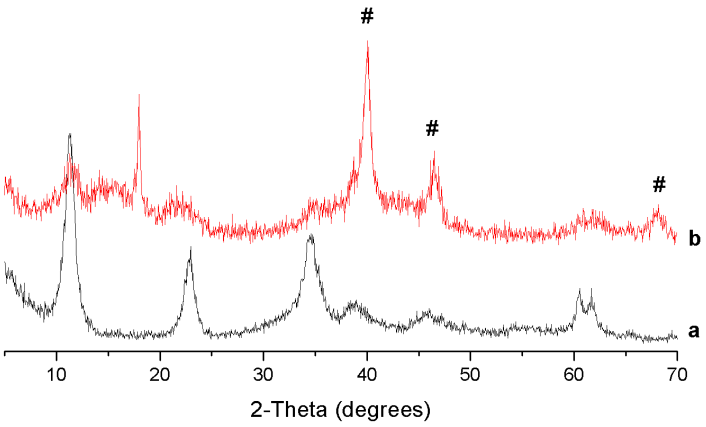


**Figure 6.13** XRD diffractograms of the Mg-Al-Pd HT a – before reaction (as prepared) and b-after reaction; # - represents the peaks characteristic for Pd

Next, a hybrid material based on the above HT and rGO was prepared through self-assembly and activated as mentioned above. Once again the material was active in hydrogen peroxide production, but not in the epoxidation reaction, confirming that Pd blocks or poisons the possible basic sites of the material. When studying the XRD pattern of this hybrid after reaction, we have observed the same pattern as in the previous case – the material lost its structure and the presence of Pd atoms is more revealed (Figure 6.14).

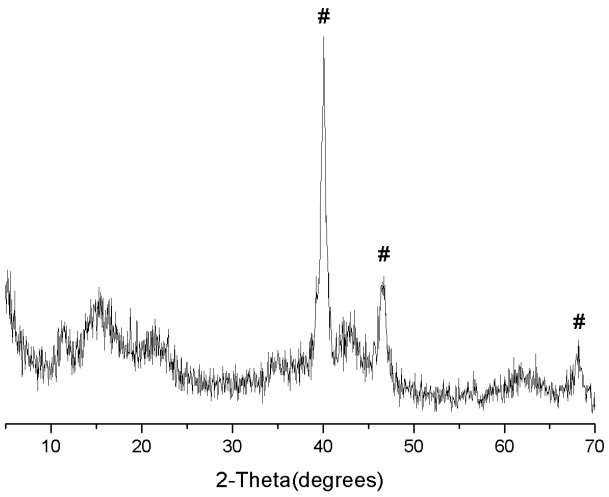


**Figure 6.14** XRD diffractogram of the 20:1 Mg-Al-Pd HT/rGO after reaction; # - represents the peaks characteristics for Pd;

To test this hypothesis, a new experiment was conducted using the 20:1 HT/rGO material (used in Section 6.2.1) impregnated with a solution containing Pd nanoparticles. The hybrid was then dried, calcined in inert atmosphere and reduced in $H_2$, to activate the Pd particles. Compared to the other tests, this material was active in both reactions (production of $H_2O_2$ and epoxidation of chalcone) and, most important of all, no hydrogenation product was observed.

At this point, it is important to mention that, in all reactions, the conversion of chalcone was very low and the scope of these experiments was to demonstrate the possible usage of these catalysts.

In conclusion, hybrid materials based on graphene and HT seem to be promising materials due to their high surface area, high pore volume and high basicity. Currently, research is done to investigate their utility in the hydrogen peroxide synthesis from $H_2$ and $O_2$ and in the *in-situ* epoxidation of chalcone.

# Bibliography

[1] P.R. Wallace, *Physical Review Letters*, **71**, 622- 634, **1947**.

[2] N.D. Mermin, H. Wagner, *Physical Review Letters*, **17**, 1133-1307, **1966**.

[3] B.C. Brodie, *Philosophical Transactions of the Royal Society of London, Series A*, **149**, 249-259, **1859**.

[4] H.P. Boehm, A. Clauss, G.O. Fischer, U. Hofmann, *Zeitschrift fur Anorganische und Allgemeine Chemie*, **316**, 119-127, **1962**.

[5] K.S. Novoselov, A.K. Geim, S.V. Morozov, D. Jiang, Y. Zhang, S.V. Dubonos, I.V. Grigorieva, A.A. Firsov, *Science*, **306**, 666-669, **2004**.

[6] D.R. Cooper, B. D'Anjou, N. Ghattamaneni, B. Harack, M. Hilke, A. Horth, N. Majlis, M. Massicotte, L. Vandsburger, E. Whiteway, V. Yu, *ISRN Condensed Matter Physics*, **2012**, 1-56, **2012**.

[7] Y. Cao, G. Li, X. Li, *Chemical Engineering Journal*, **292**, 207–223, **2016**.

[8] W.S.H. Jr., R.E. Offeman, *Journal of American Chemical Society*, **1958**, 1339-1339, **1958**.

[9] A. Garcia-Gallastegui, D. Iruretagoyena, V. Gouvea, M. Mokhtar, A.M. Asiri, S.N. Basahel, S.A. Al-Thabaiti, A.O. Alyoubi, D. Chadwick, M.S.P. Shaffer, *Chemistry of Materials*, **24**, 4531–4539, **2012**.

# 7 Appendices

# Appendix A - Supplementary Information Section 1

**Table A.1** Amino acids reference chart – from Sigma-Aldrich

| Side Chain | Structure /Name | Molecular weight (g/mole) | $pK_a$ | $pK_b$ | $pK_x$ | $p_I$ |
|---|---|---|---|---|---|---|
| Hydrophobic Aliphatic | 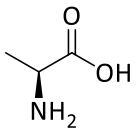 Alanine (Ala) | 89.10 | 2.34 | 9.69 | - | 6.00 |
| | 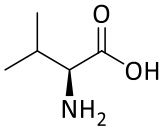 Valine (Val) | 117.15 | 2.32 | 9.62 | - | 5.96 |
| | 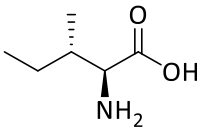 Isoleucine (Ile) | 131.18 | 2.36 | 9.60 | - | 6.02 |
| | 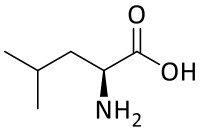 Leucine (Leu) | 131.18 | 2.36 | 9.60 | - | 5.98 |
| Hydrophobic Aromatic | 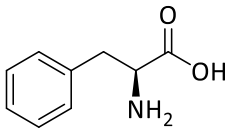 Phenylalanine (Phe) | 165.19 | 1.83 | 9.13 | - | 5.48 |
| | 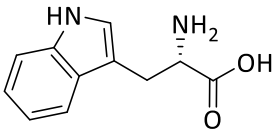 Tryptophan (Trp) | 204.23 | 2.83 | 9.39 | - | 5.89 |
| | 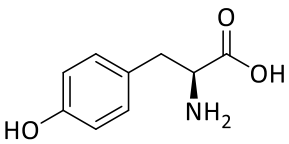 Tyrosine (Tyr) | 181.19 | 2.20 | 9.11 | 10.07 | 5.66 |
| Polar Neutral | 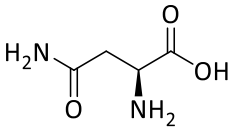 Asparagine (Asn) | 132.12 | 2.02 | 8.80 | - | 5.41 |

| Side Chain | Structure /Name | Molecular weight (g/mole) | $pK_a$ | $pK_b$ | $pK_x$ | $p_I$ |
|---|---|---|---|---|---|---|
| Polar Neutral | 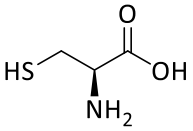 Cysteine (Cys) | 121.16 | 1.96 | 10.28 | 8.18 | 5.07 |
| | 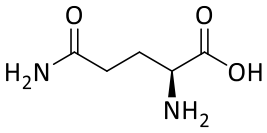 Glutamine (Gln) | 146.15 | 2.17 | 9.13 | - | 5.65 |
| | 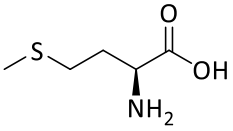 Methionine (Met) | 149.21 | 2.28 | 9.21 | - | 5.74 |
| | 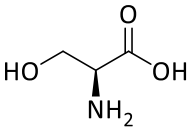 Serine (Ser) | 105.09 | 2.21 | 9.15 | - | 5.68 |
| | 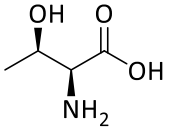 Threonine (Thr) | 119.12 | 2.09 | 9.10 | - | 5.60 |
| Electrically Charged - Acidic | 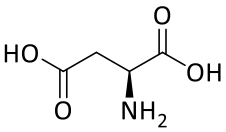 Aspartic acid (Asp) | 131.11 | 1.88 | 9.60 | 3.65 | 2.77 |
| | 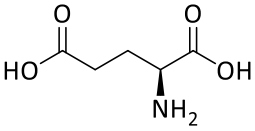 Glutamic acid (Glu) | 147.13 | 2.19 | 9.67 | 4.25 | 3.22 |
| Electrically Charged - Basic | 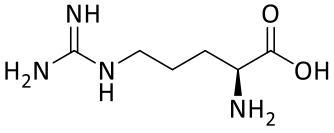 Arginine (Arg) | 174.20 | 2.17 | 9.04 | 12.48 | 10.76 |
| | 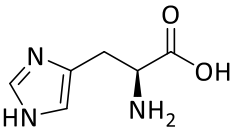 Histidine (His) | 155.16 | 1.82 | 9.17 | 6.00 | 7.59 |

## 7 Appendices

| Side Chain | Structure /Name | Molecular weight (g/mole) | $pK_a$ | $pK_b$ | $pK_x$ | $p_I$ |
|---|---|---|---|---|---|---|
| | 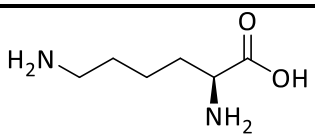 Lysine (Lys) | 146.19 | 2.18 | 8.96 | 10.53 | 9.74 |
| **Unique** | 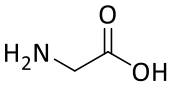 Glycine (Gly) | 75.07 | 2.37 | 9.60 | - | 5.97 |
| | 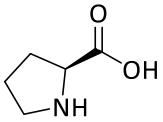 Proline (Pro) | 115.13 | 1.99 | 10.60 | - | 6.30 |

# Appendix B - Supplementary Information Section 2

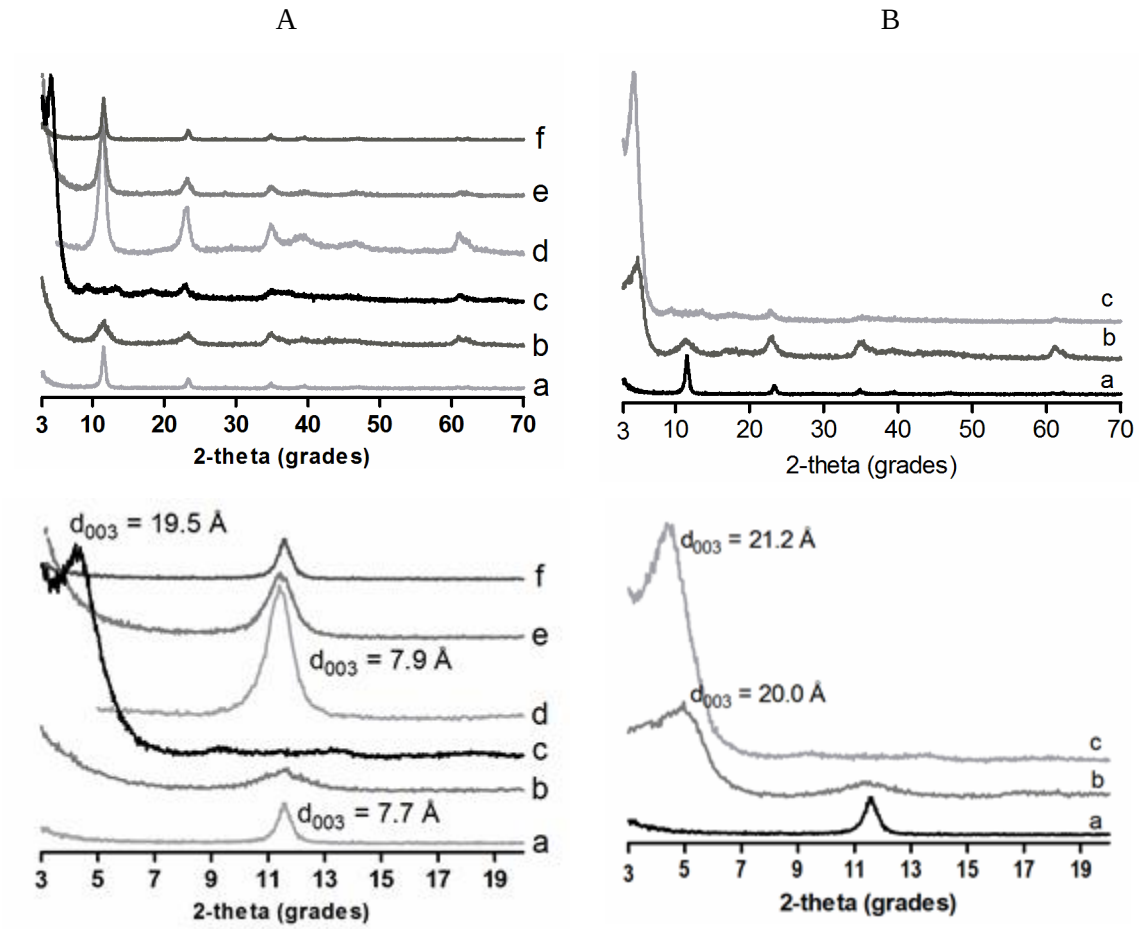


**Figure B.1** A) XRD patterns of a) $HT_{rus}$, b) LL/$HT_{rus}$-A1, c) LL/$HT_{rus}$-A2, d) $HT_{Clus}$, e) LL/$HT_{Clus}$-A1 and f) LL/$HT_{Clus}$-A2. B) XRD patterns of a) $HT_{rus}$, b) LL/$HT_{rus}$-R1 and c) LL/$HT_r$-R2. Inset: XRD pattern. Top: XRD pattern in the *2*θ range: 3-70°, bottom in the *2*θ range: 3-20°.

## 7 Appendices

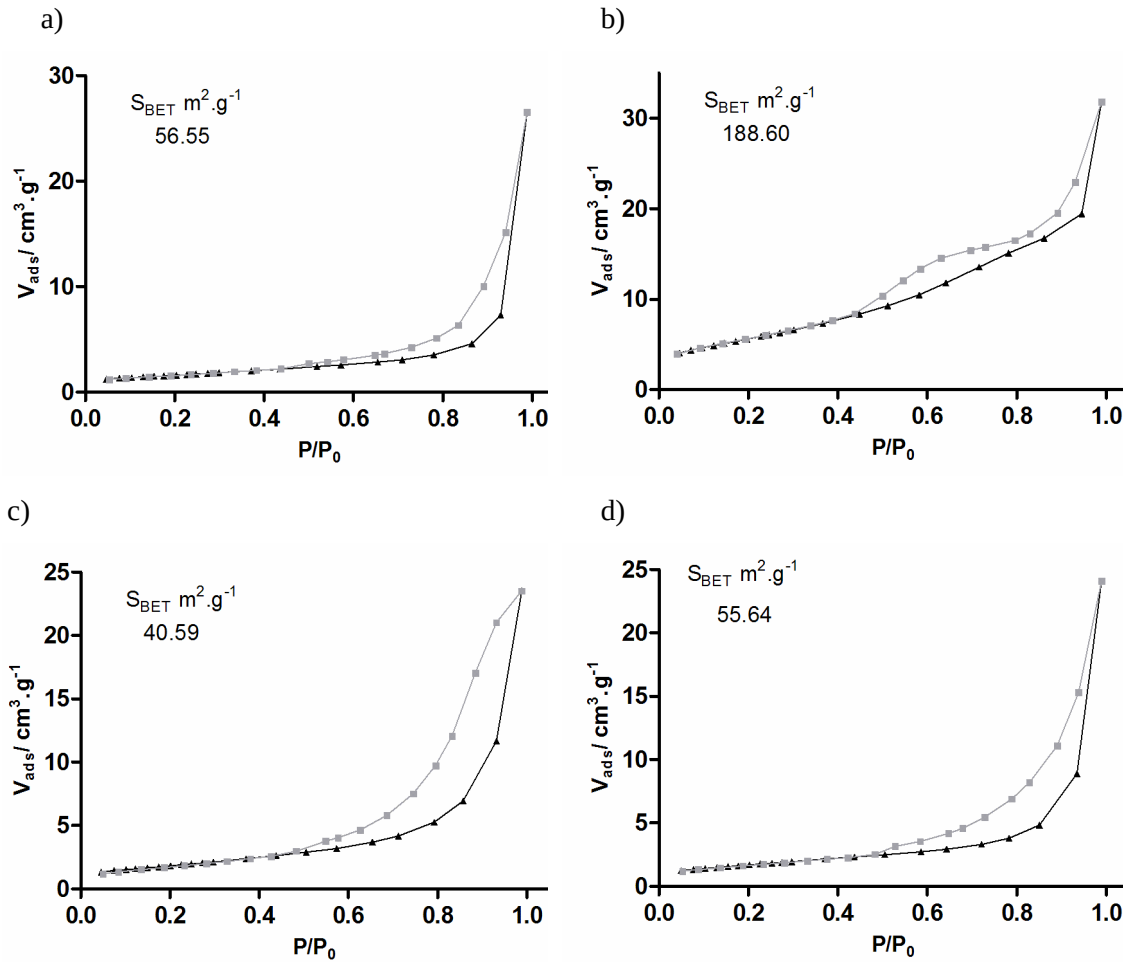


**Figure B.2** $N_2$ adsorption (▲)-desorption (■) isotherms and BET surface area of a) HT as prepared, b) $HT_{cc}$, c) $HT_{rus}$ and d) $HT_{Clus}$.

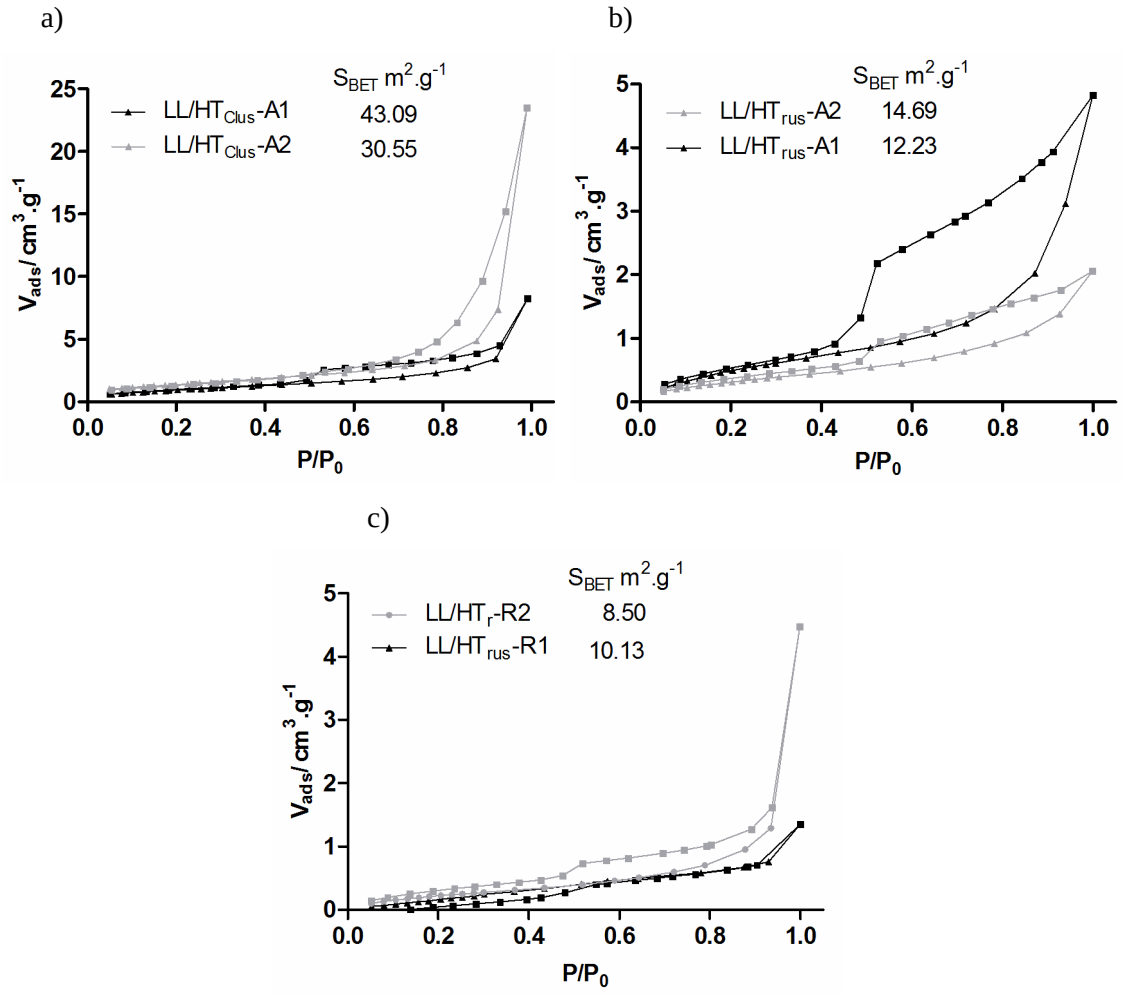


**Figure B.3** $N_2$ adsorption (▲)-desorption (■) isotherms and BET surface area of a) LL/ HT$_{Clus}$-A1 and LL/HT$_{Clus}$-A2, b) LL/HT$_{rus}$-A1 and LL/HT$_{rus}$-A2, c) LL/HT$_{rus}$-R1 and LL/HT$_r$-R2.

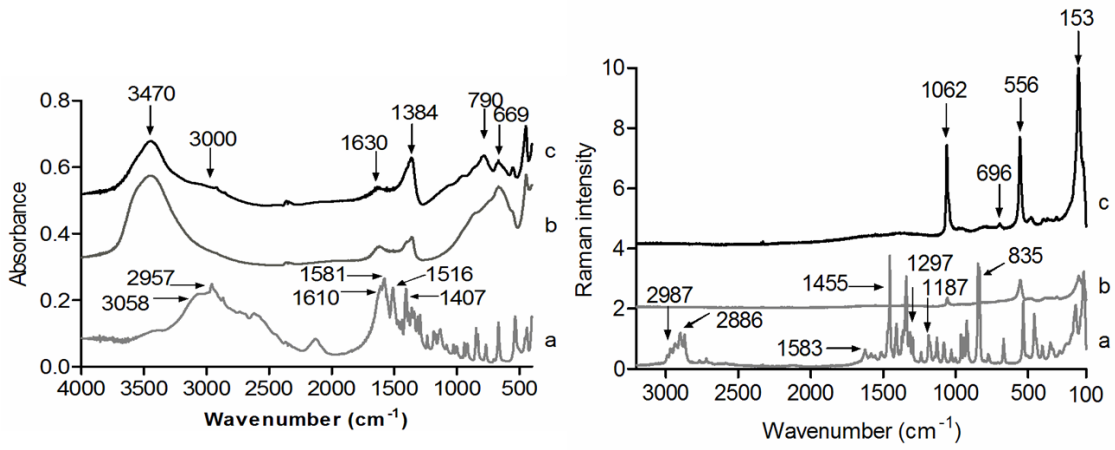


**Figure B.4** Skeletal FT-IR (left) and Raman (right) spectra of a) L-Leu, b) HT$_{Clus}$ and c) HT$_{rus}$.

## 7 Appendices

The FT-IR spectrum of L-Leu in KBr showed the typical zwitterionic nature of L-Leu. Bands due to $NH_3^+$ stretching and deformation vibrations are detected at 3058, 2130, 1610 and 1516 $cm^{-1}$. Asymmetric, $\nu_{a(COO-)}$, and symmetric, $\nu_{s(COO-)}$, stretching bands of the $COO^-$ group are detected at 1581 and 1407 $cm^{-1}$. One broad band at 3378 $cm^{-1}$, superimposed to the broad absorption due to physisorbed water on the KBr matrix, has been assigned to H-bond interactions between different molecules of L-Leu, while the bands at 2957 and 2871 $cm^{-1}$ correspond to the $-CH_3$ stretching vibrations [1]. In the Raman spectrum, three bands around 2886, 1227 and 835 $cm^{-1}$ are due to C-H and C-C stretching modes. The bands corresponding to $COO^-$ group are detected at 1454, 1297, 1129, 835, 776 and 553 $cm^{-1}$, while bands due to the $NH_3^+$ group are detected at 2987, 1625, 1583 and 1187 $cm^{-1}$ [1, 2].

Skeletal FT-IR spectra of HT-like supports show a strong and complex band between 3600 and 3000 $cm^{-1}$ which can be attributable to several vibrational modes: the twisting vibration of physisorbed water, the stretching mode of the bridging carbonate anions ($CO_3^{2-}$-$H_2O$), and the characteristic stretching modes of M-OH species [3]. A quite complex band at 1384 $cm^{-1}$, showing a shoulder at higher frequency, is assigned to vibrational modes of carbonate species, partially overlapped with signal due to residual nitrate species. In the low frequency region, bands at 880 and 669 $cm^{-1}$ are characteristic for the $\nu_4$ mode (in-plane bending) and the $\nu_2$ mode (out-plane deformation) of $CO_3^{2-}$ ions. Bands at 790 and 554 $cm^{-1}$ with the corresponding deformations at 925 and 1050 $cm^{-1}$ are due to $OH^-$ groups influenced by $Al^{3+}$. Bands at 635, 600 and 590 $cm^{-1}$ are assigned to vibrational modes of Al-OH groups influenced by nearby $Mg^{2+}$ ions. The broad band at 1630 $cm^{-1}$ is due to the HOH bending vibration of physisorbed water. The high relative intensity in bands at 3000 and 1384 $cm^{-1}$ characterizing carbonate species in $HT_{rus}$ shows the high reactivity of the basic centres, which can interact easily with atmospheric $CO_2$ during their manipulation [4, 5]. In the Raman spectra, the interlayered carbonate ions are detected as a very strong and sharp band at 1061 $cm^{-1}$ due to the $\nu_1$ mode and a very weak band at 694 $cm^{-1}$ due to the $\nu_4$ mode of $CO_3^{2-}$ ions. The band at 556 $cm^{-1}$ is due to hydroxyl groups mainly associated with $Al^{3+}$ ions, but also influenced by one $Mg^{2+}$ in its coordination environment [3]. Finally, although the band at 153 $cm^{-1}$ cannot be formally assigned, it is probably related to framework vibrations [6].

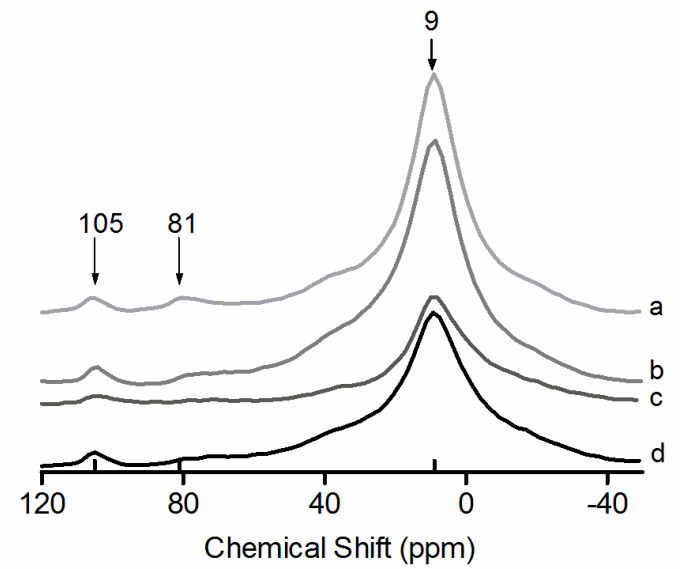


**Figure B.5** $^{27}$Al-MAS NMR of a) $HT_{rus}$, b) LL/$HT_{rus}$-A2, c) LL/$HT_{rus}$-R1 and d) LL/$HT_{r}$-R2.

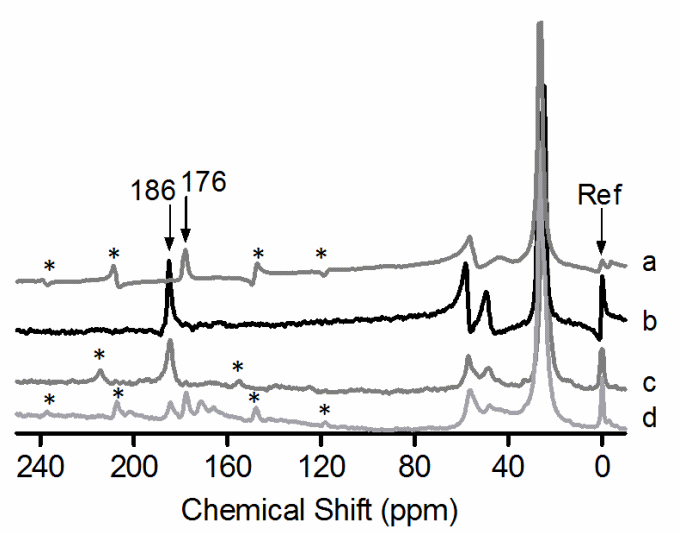


**Figure B.6** $^{13}$C-MAS NMR of a) L-Leu, b) LL/$HT_{rus}$-A2, c) LL/$HT_{rus}$-R1 and d) LL/$HT_{r}$-R2. Ref=TMS (Tetramethylsilane).

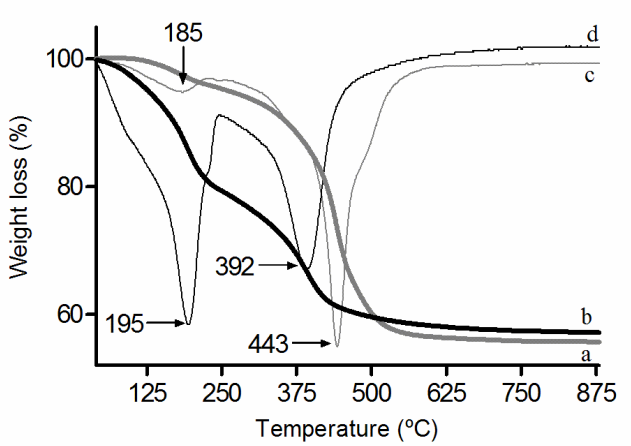


**Figure B.7** TG (a and b) and DTA (c and d) thermal analysis of HT as prepared (black line) and $HT_{rus}$ (grey line).

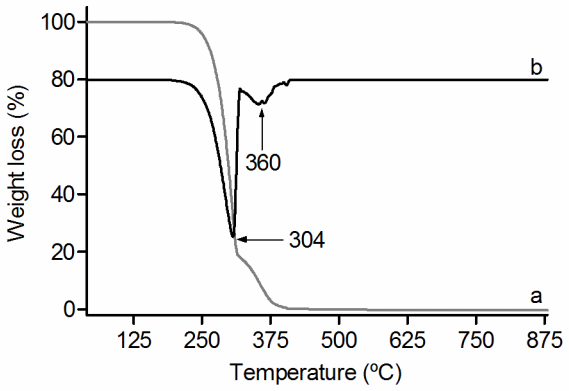


**Figure B.8** TG (a) and DTA (b) thermal analysis of L-Leu

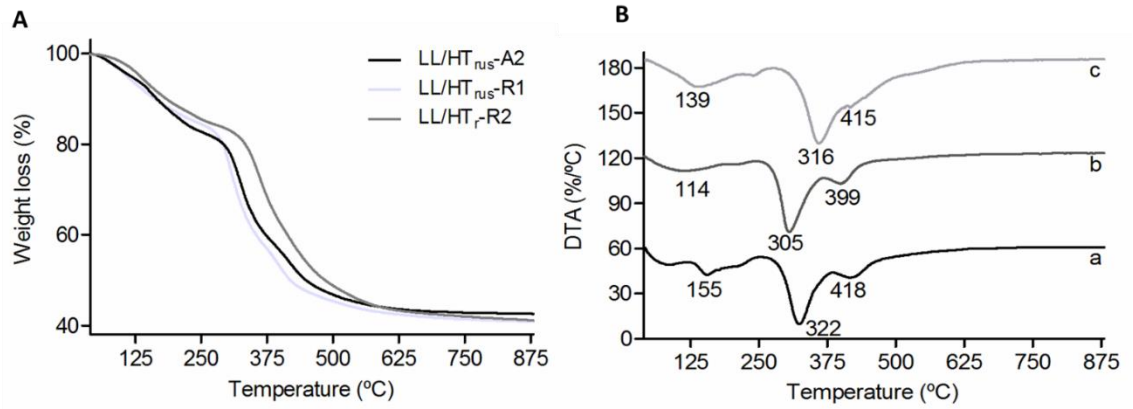


**Figure B.9** A) TG analyses of LL/$HT_{rus}$-A2, LL/$HT_{rus}$-R1 and LL/$HT_r$-R2, B) DTA analysis of a) LL/$HT_{rus}$-A2, b) LL/$HT_{rus}$-R1 and c) LL/$HT_r$-R2

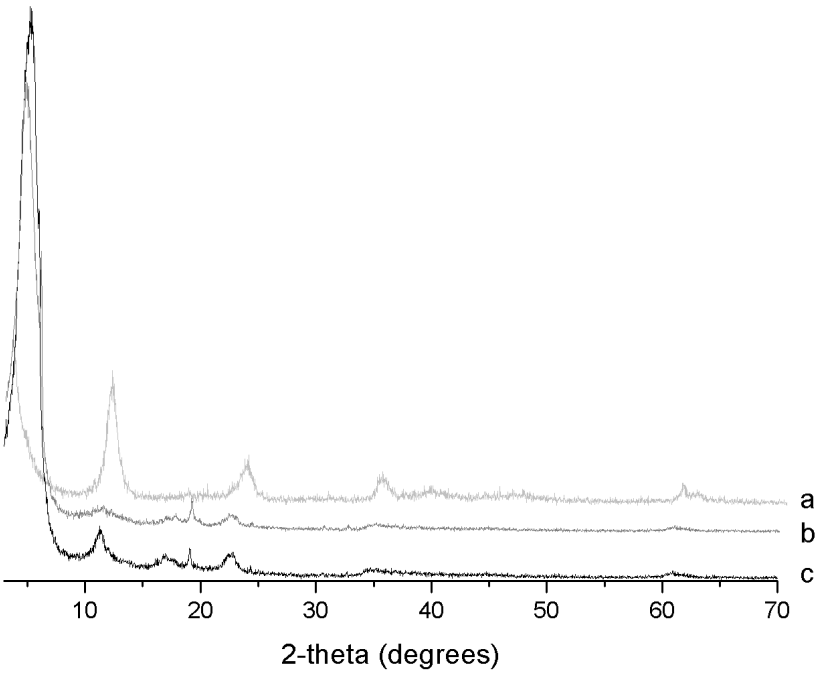


**Figure B.10** XRD patterns of a) physical mixture $HT_{cc}$ + L-Leu before reaction, b) physical mixture $HT_{cc}$ + L-Leu after reaction, c) LL/$HT_{rus}$-A2

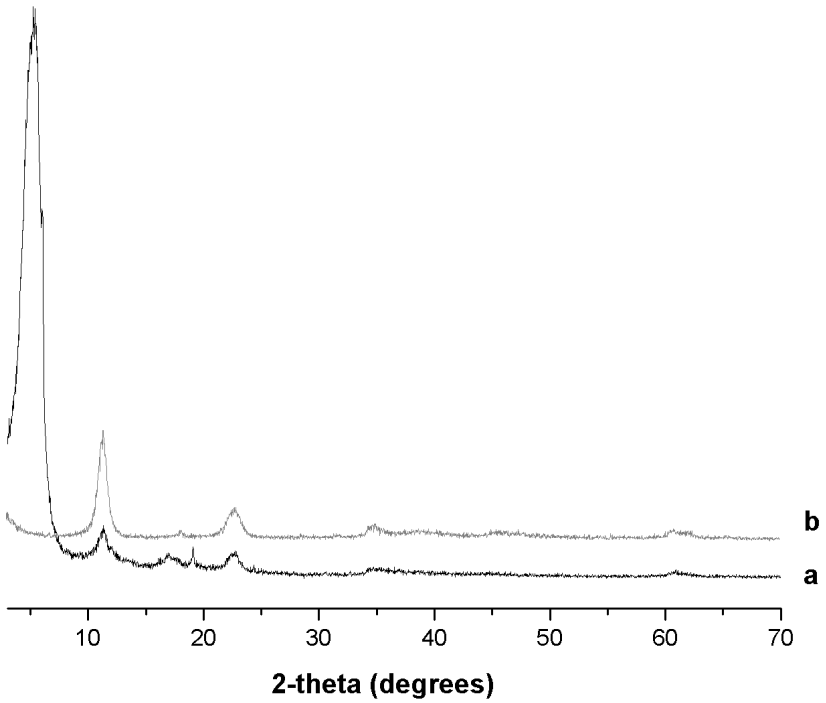


**Figure B.11** XRD patterns of a) LL/$HT_{rus}$-$A_2$ before reaction, b) LL/$HT_{rus}$-$A_2$ after reaction

## 7 Appendices

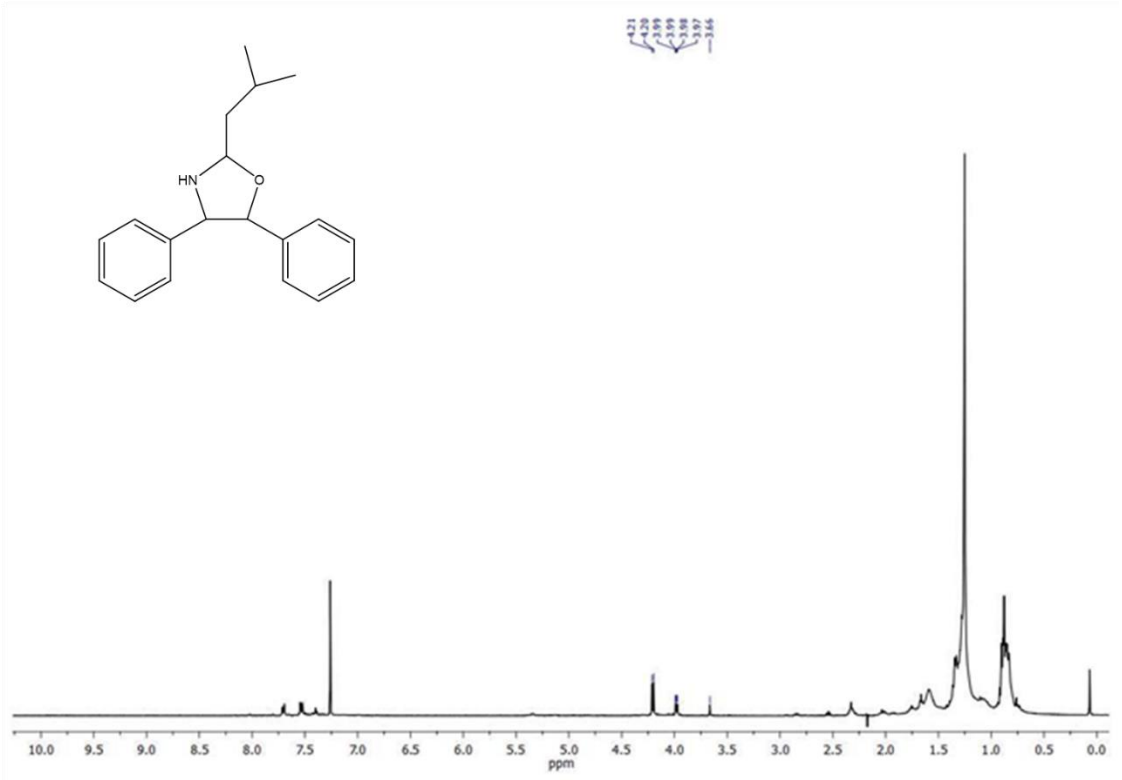


**Figure B.12** The 1,3-oxazolidine product formed between L-leucine and benzaldehyde in the second run for L-Leu/$HT_{rus}$-A2 and L-Leu/$HT_{rus}$-R1

**Spectroscopic data for aldol products:**

1. *anti*-2-(hydroxy(4-nitrophenyl)methyl)cyclohexan-1-one

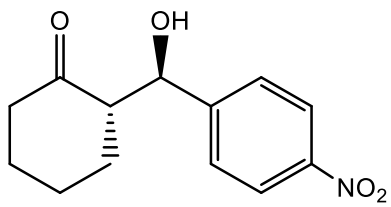


$^1$H-NMR (400 MHz, $CDCl_3$): δ 1.36-2.51 (m, 8H), 2.57-2.64 (m, 1H), 4.11 (d, *J* = 2.8 Hz, 1H), 4.90 (d, *J* = 8.0 Hz, 1H), 7.51 (d, *J* = 8.8 Hz, 2H), 8.21 (d, *J* = 8.4 Hz, 2H). $^{13}$C NMR (400 MHz, $CDCl_3$): δ 24.7, 27.6, 30.7, 57.2, 74.0, 123.6, 127.9, 148.3, 214.8 [7, 8]

HPLC analysis CHIRALPACK IA column, hexane/ethanol (75:25), 1.0 ml/min, $t_R$ = 12.7 min, 14.0 min

2. *syn*-2-(hydroxy(4-nitrophenyl)methyl)cyclohexan-1-one

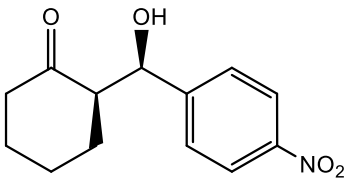


$^1$H-NMR (400 MHz, $CDCl_3$): δ 1.26-2.50 (m, 8H), 2.61-2.66 (m, 1H), 3.20 (d, *J* = 3.2 Hz, 1H), 5.49 (s, 1H), 7.49 (d, *J*= 8.8 Hz, 2H), 8.21 (d, *J* = 8.8 Hz, 2H). $^{13}$C NMR (400 MHz, $CDCl_3$): δ 24.8, 25.9, 27.9, 42.6, 56.8, 70.1, 123.5, 126.6, 147.0, 149.0, 214.1.[7, 8]

HPLC analysis CHIRALPACK IA column, hexane/ethanol (75:25), 1.0 ml/min, $t_R$ = 10.2 min, 10.6 min

3. *anti*-2-(hydroxy-(2-nitrophenyl)methyl)cyclohexan-1-one

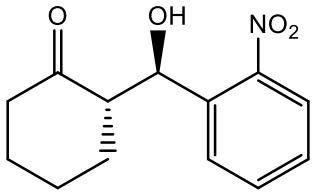


$^{1}$H-NMR (400 MHz, $CDCl_3$): δ 1.57-2.60 (m, 8H), 2.73-2.80 (m, 1H), 5.45 (d, *J* = 7.2Hz, 1H), 7.43 (dt, *J* = 1.6, 8.4 Hz, 1H), 7.64 (t, 8.0 Hz, 1H), 7.77 (d, *J* = 7.6 Hz, 1H), 7.85 (dd, *J* = 0.8, 9.2 Hz, 1H). $^{13}$C NMR (400 MHz, $CDCl_3$): δ 25.0, 27.8, 31.1, 57.3, 69.8, 124.1, 128.4, 129.0, 133.1, 136.6, 148., 215.1 [7, 8]

HPLC analysis CHIRALPACK IA column, hexane/ethanol (75:25), 1.0 ml/min, $t_R$ = 10.6 min, 12.5 min

4. *syn*-2-(hydroxy(2-nitrophenyl)methyl)cyclohexan-1-one

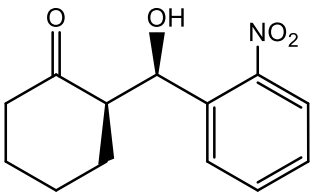


$^{1}$H-NMR (400 MHz, $CDCl_3$): δ 1.51-2.57 (m, 8H), 2.85-2.90 (m, 1H), 5.96 (d, *J* = 2.0 Hz, 1H), 7.43 (dt, *J* = 1.2, 8.4 Hz, 1H), 7.65 (dt, *J* = 1.2, 8.4 Hz, 1H), 7.84 (d, *J* = 8.4 Hz, 1H), 8.00 (dd, *J* = 1.2 Hz, 8.0 Hz, 1H). $^{13}$C NMR (400 MHz, $CDCl_3$): δ 24.8, 26.5, 28.0, 42.6, 54.8, 66.7, 124.7, 127.9, 129.6, 133.2, 214.3 [7, 8]

HPLC analysis CHIRALPACK IA column, hexane/ethanol (75:25), 1.0 ml/min, $t_R$ = 7.00 min, 12.3 min

5. *anti*-2-((4-chlorophenyl)(hydroxy)methyl)cyclohexan-1-one

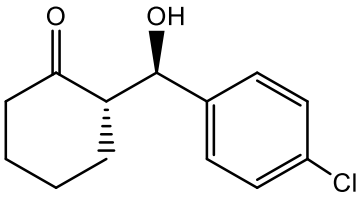


$^{1}$H-NMR (400 MHz, $CDCl_3$): δ 1.26-2.49 (m, 8H), 2.54-2.56 (m, 1H), 4.76 (d, *J* = 8.8 Hz, 1H), 7.25 (d, *J* = 8.8 Hz, 2H), 7.32 (d, *J* = 8.8 Hz, 2H). $^{13}$C NMR (400 MHz, $CDCl_3$): δ 24.6, 27.7, 30.5, 57.3, 74.2, 128.4, 128.5, 133.5, 139.4, 186.5, 215.5[7, 8]

HPLC analysis CHIRALPACK IA column, hexane/ethanol (75:25), 1.0 ml/min, $t_R$ = 13.1 min, 14.9 min

6. *syn*-2-((4-chlorophenyl)(hydroxy)methyl)cyclohexan-1-one

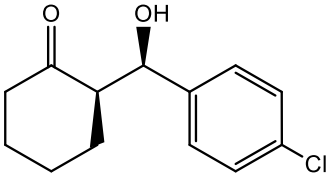


$^{1}$H-NMR (400 MHz, $CDCl_3$): δ 1.26-2.48 (m, 8H), 2.53-2.58 (m, 1H), 5.35 (d, *J* = 2.4 Hz, 1H), 7.24 (d, *J* = 8.4 Hz, 2H), 7.31 (d, *J* = 8.4 Hz, 2H). $^{13}$C NMR (400 MHz, $CDCl_3$): δ 24.6, 25.8, 27.7, 42.7, 56.7, 70.1, 127.5,128.4, 132.5, 139.7, 214.5 [7, 8]

HPLC analysis CHIRALPACK IA column, hexane/ethanol (75:25), 1.0 ml/min, $t_R$ = 7.00 min, 12.6 min

## 7 Appendices

7. *anti*-2-(hydroxy(phenyl)methyl)cyclohexan-1-one

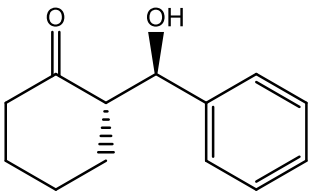


$^{1}$H-NMR (400 MHz, $CDCl_3$): δ 1.25-2.50 (m, 8H), 2.58-2.65 (m, 1H), 4.79 (d, *J* = 8.8Hz, 1H), 7.26-7.36 (m, 5H). $^{13}$C NMR (400 MHz, $CDCl_3$): δ 24.9, 28.0. 31.1, 47.9, 57.6, 75.0, 127.2, 128.1, 128.6, 141.1, 215.9 [7, 8]

HPLC analysis CHIRALPACK IA column, hexane/ethanol (75:25), 1.0 ml/min, $t_R$ = 8.75min, 19.44min

8. *syn*-2-(hydroxy(phenyl)methyl)cyclohexan-1-one

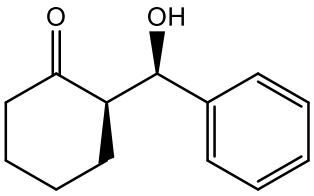


$^{1}$H-NMR (400 MHz, $CDCl_3$): δ 1.49-2.47 (m, 8H), 2.57-2.63 (m, 1H), 5.39 (d, *J* = 2.4 Hz, 1H), 7.22-7.36 (m, 5H). $^{13}$C NMR (400 MHz, $CDCl_3$): δ 25.1, 26.2, 28.2, 47.9,57.4, 70.8,126.0, 127.2, 128.4, 141.6, 215.2 [7, 8]

HPLC analysis CHIRALPACK IA column, hexane/ethanol (75:25), 1.0 ml/min, $t_R$ = 6.42 min, 10.9 min

**$^{1}$H and $^{13}$C-NMR spectra of aldol products:**

*syn*-2-(hydroxy(4-nitrophenyl)methyl)cyclohexan-1-one

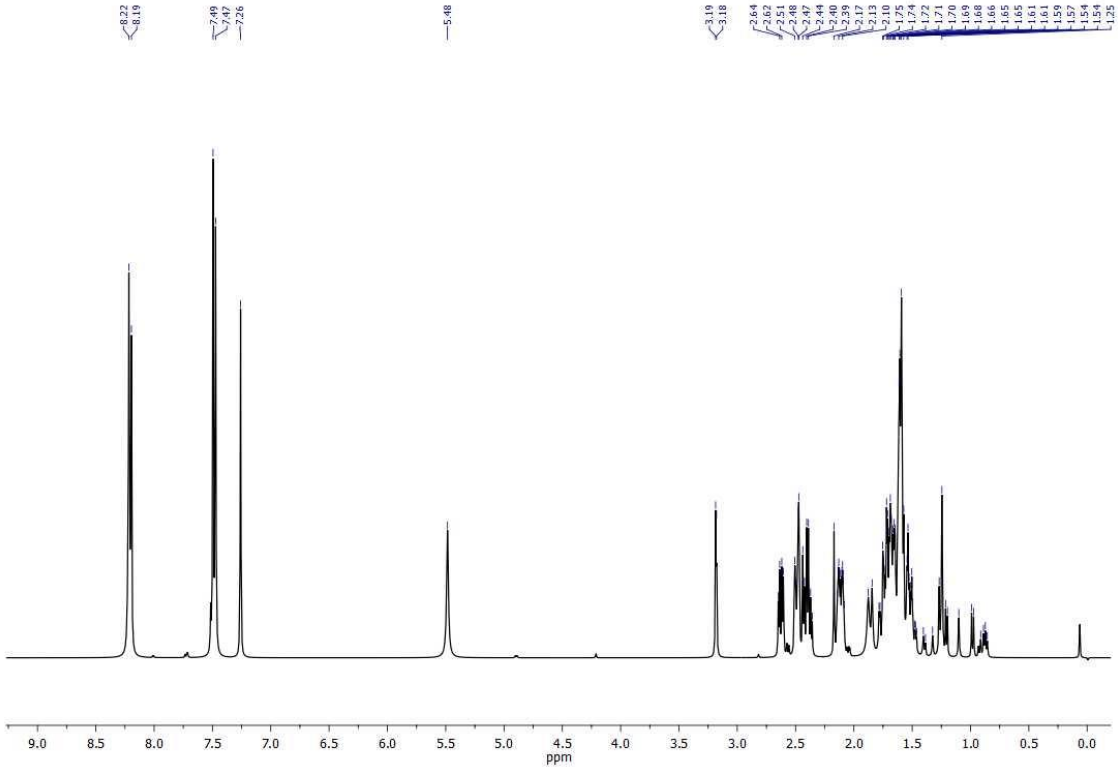


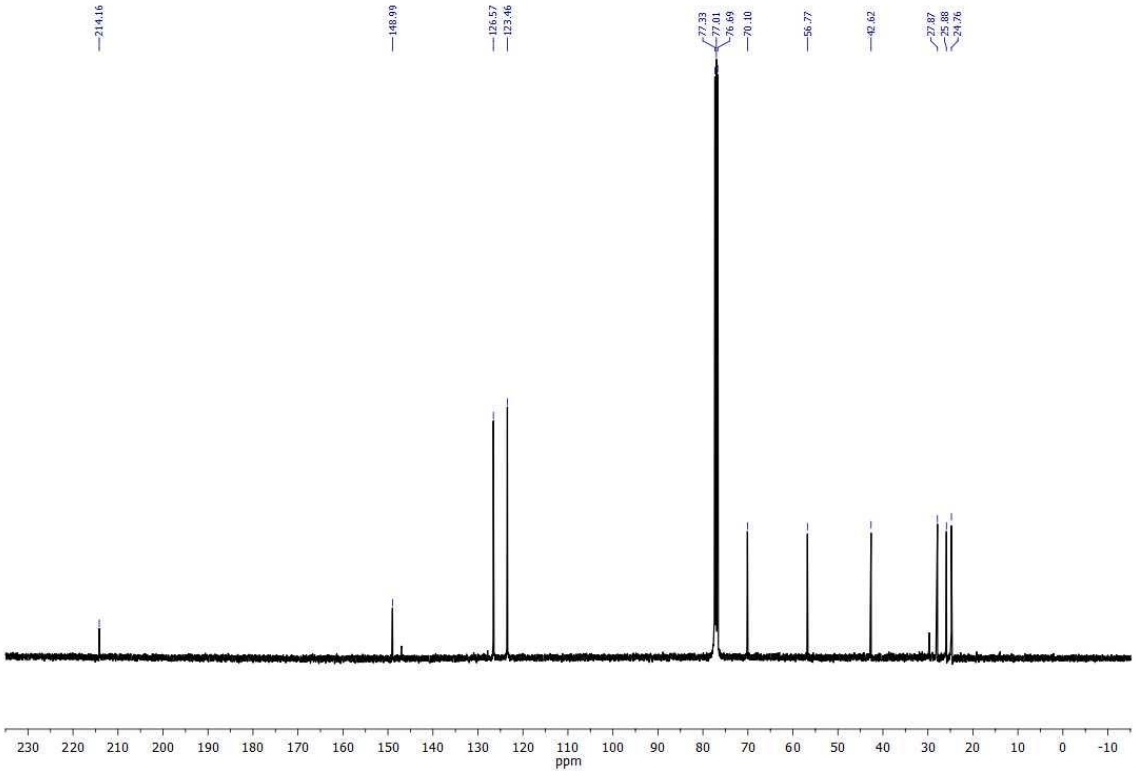

## 7 Appendices

*anti*-2-(hydroxy(4-nitrophenyl)methyl)cyclohexan-1-one

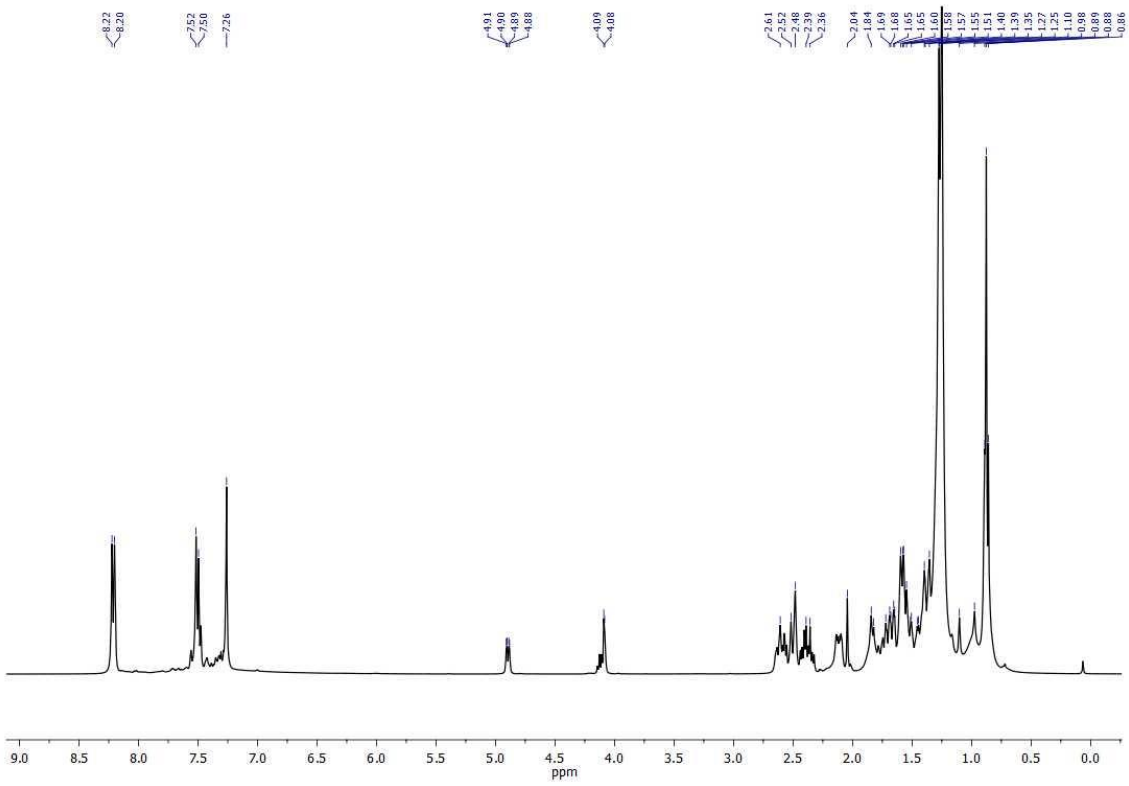


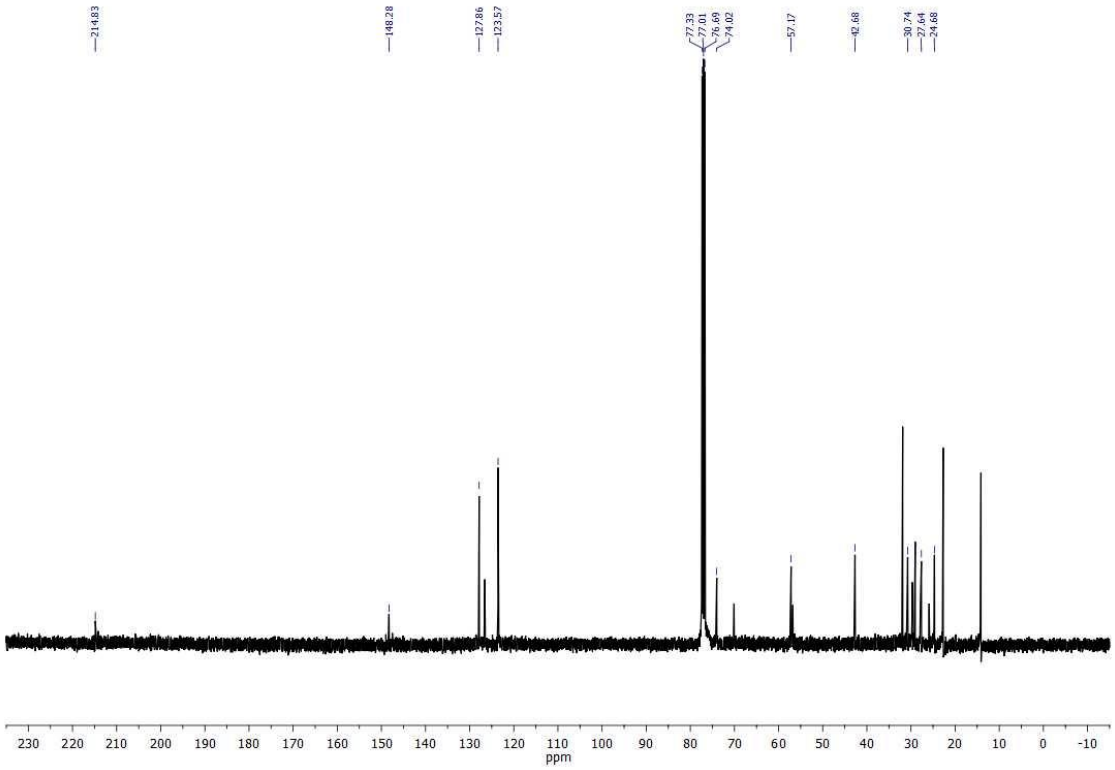

*anti*-2-(hydroxy-(2-nitrophenyl)methyl)cyclohexan-1-one

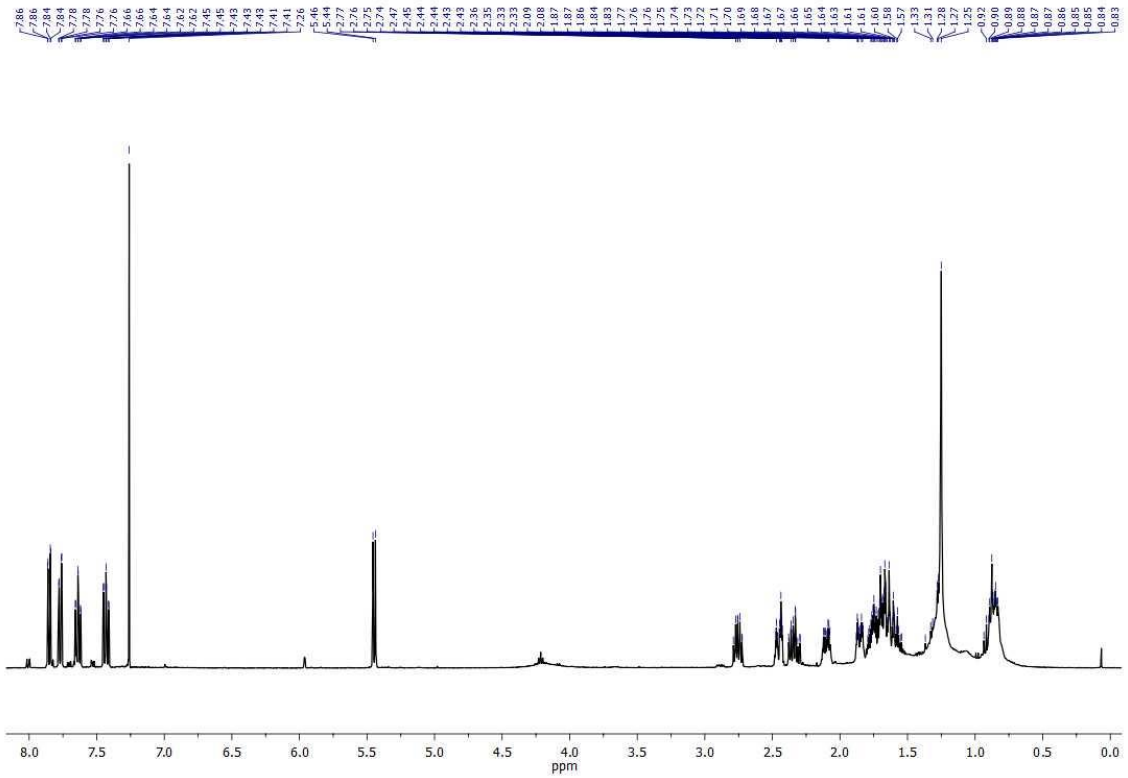


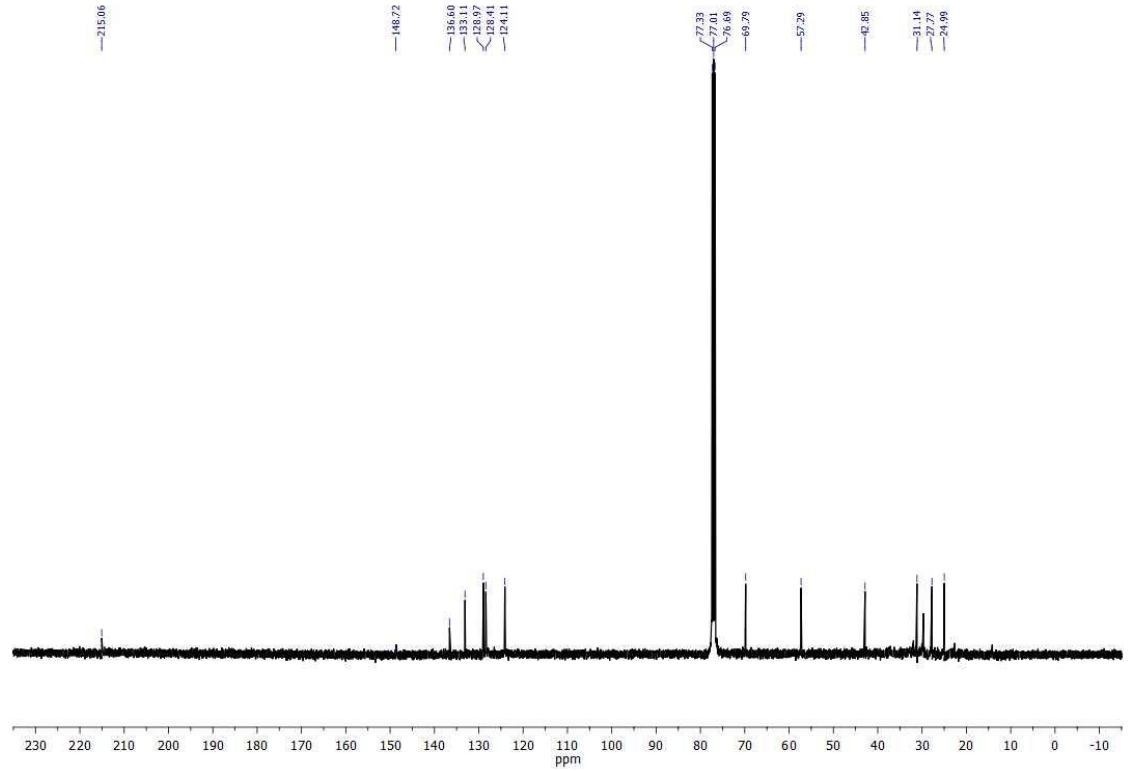

## 7 Appendices

*syn*-2-(hydroxy-(2-nitrophenyl)methyl)cyclohexan-1-one

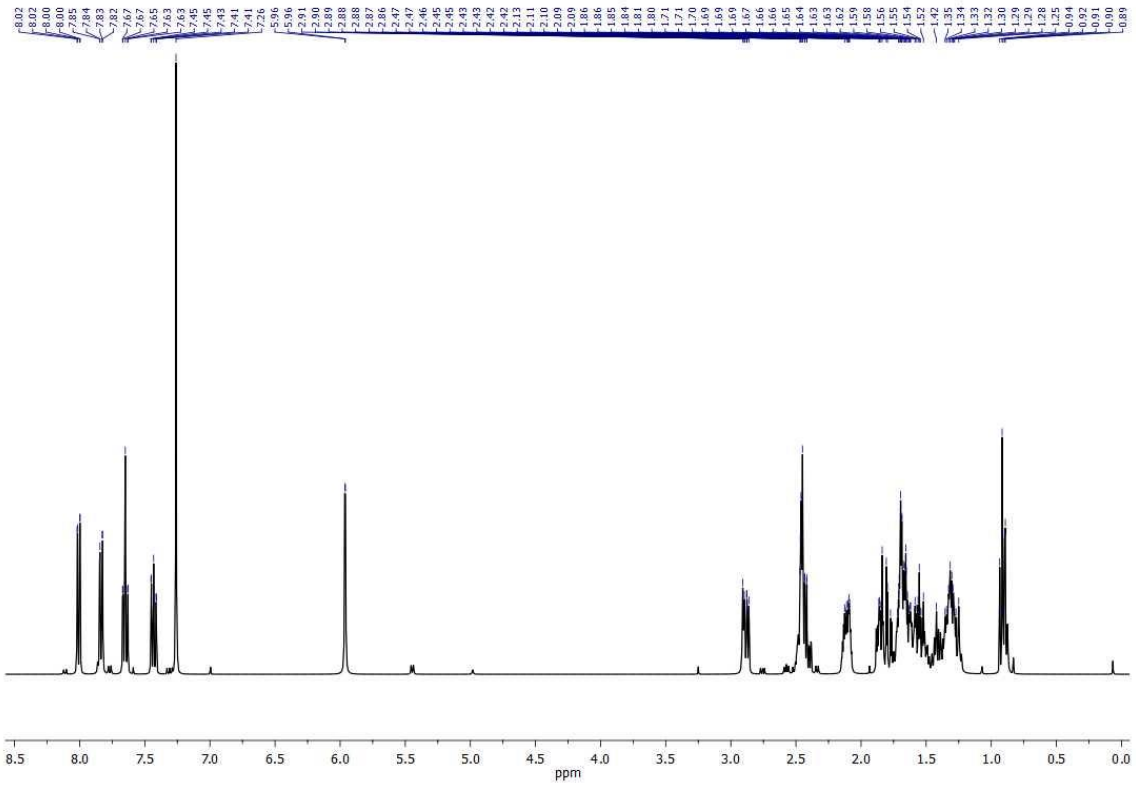


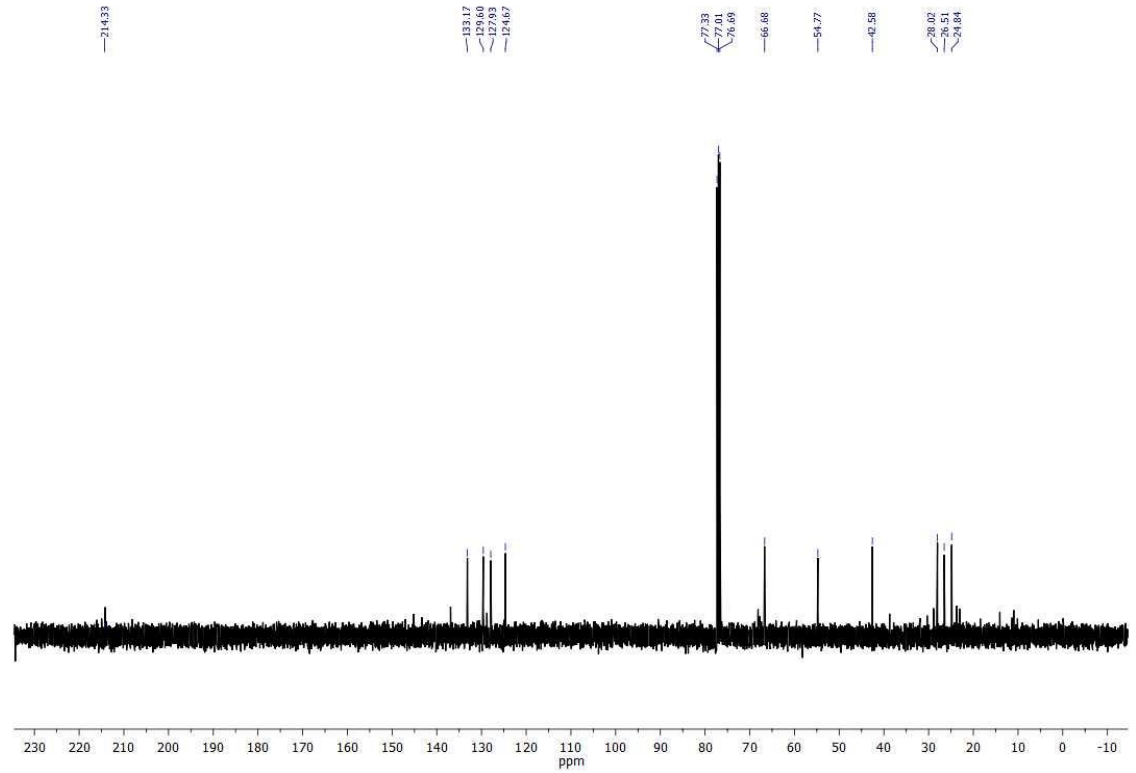

*anti*-2-((4-chlorophenyl)(hydroxy)methyl)cyclohexan-1-one

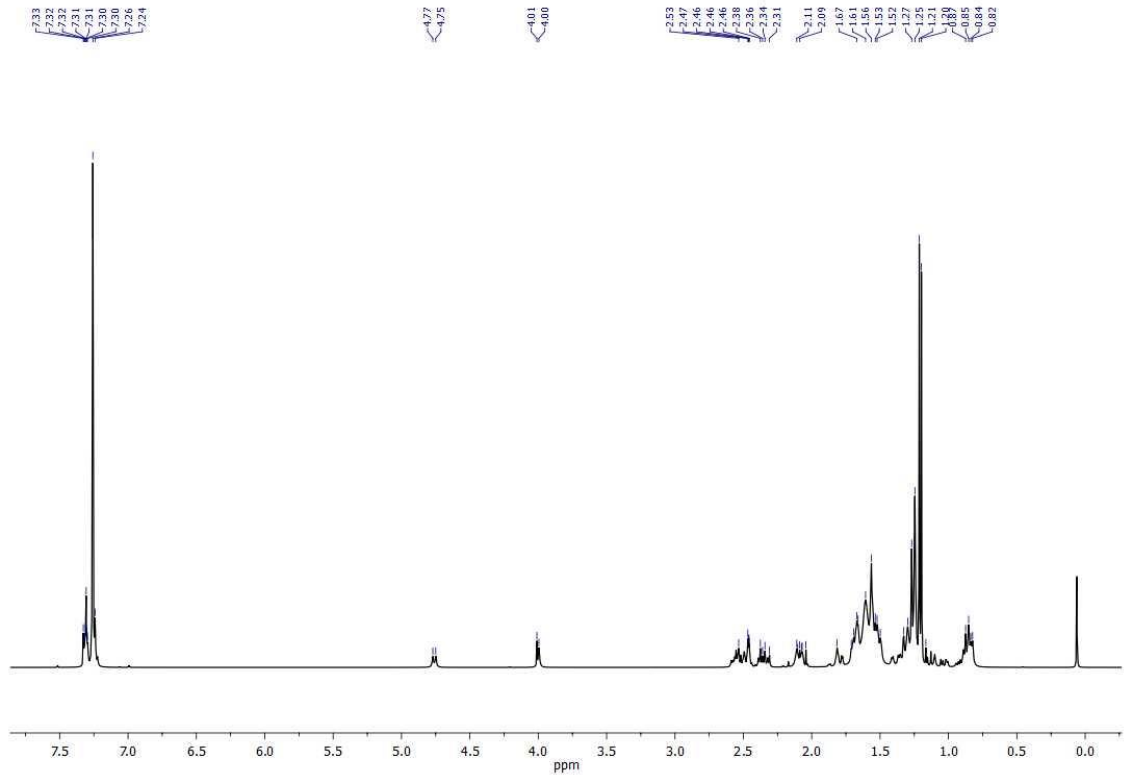


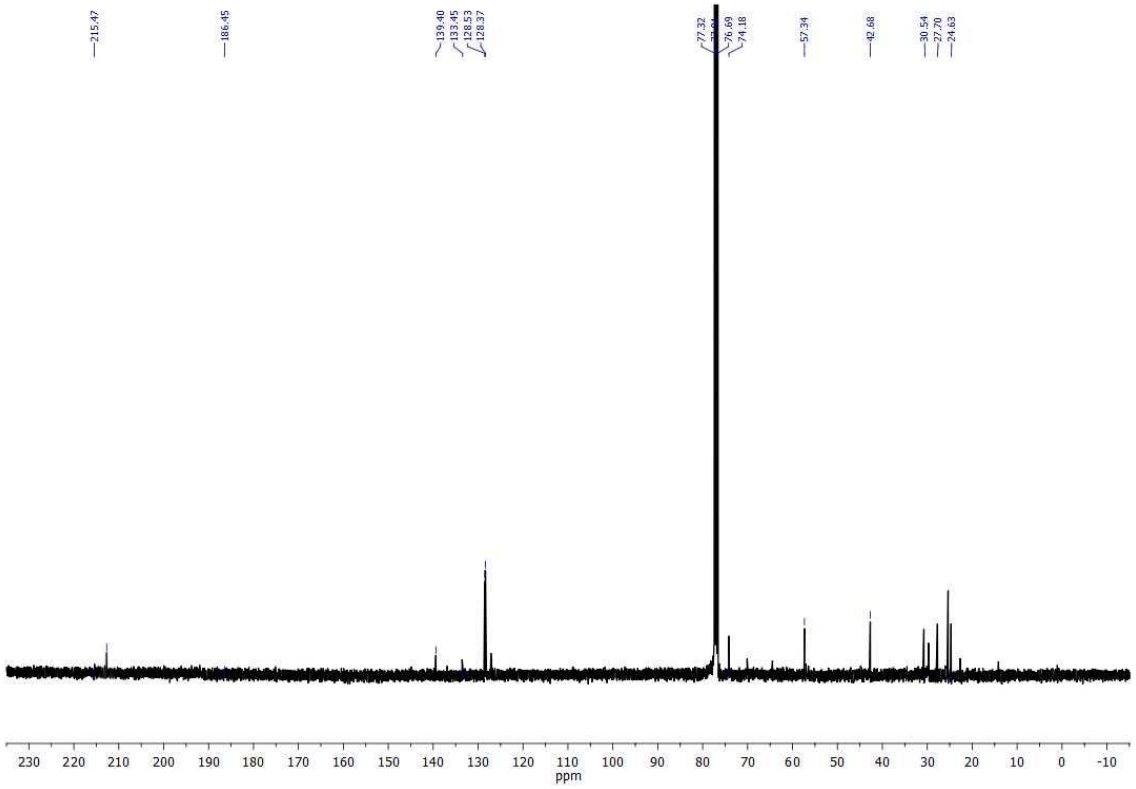

## 7 Appendices

*syn*-2-((4-chlorophenyl)(hydroxy)methyl)cyclohexan-1-one

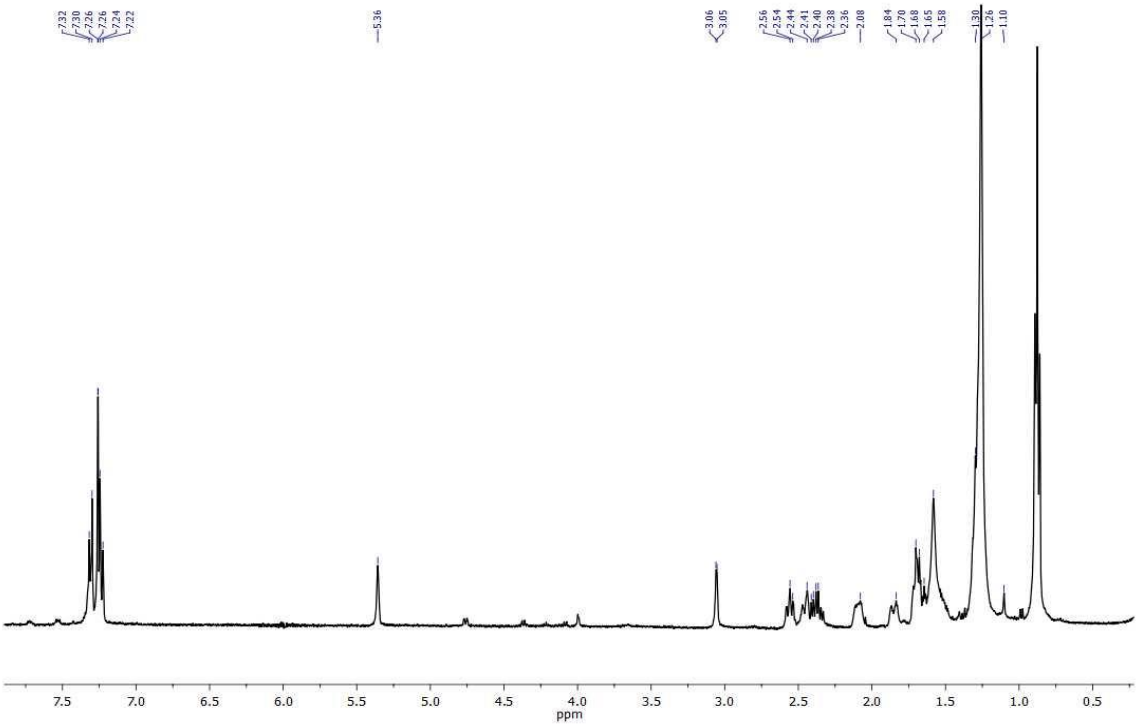


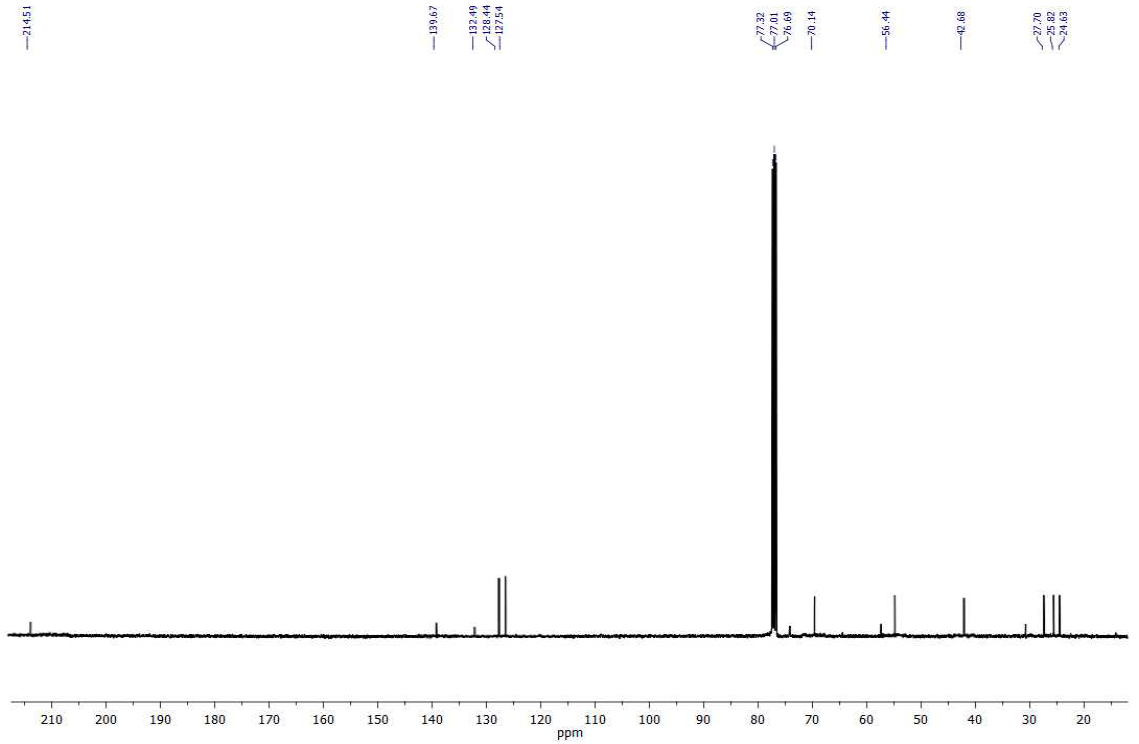

*anti*-2-(hydroxy(phenyl)methyl)cyclohexan-1-one

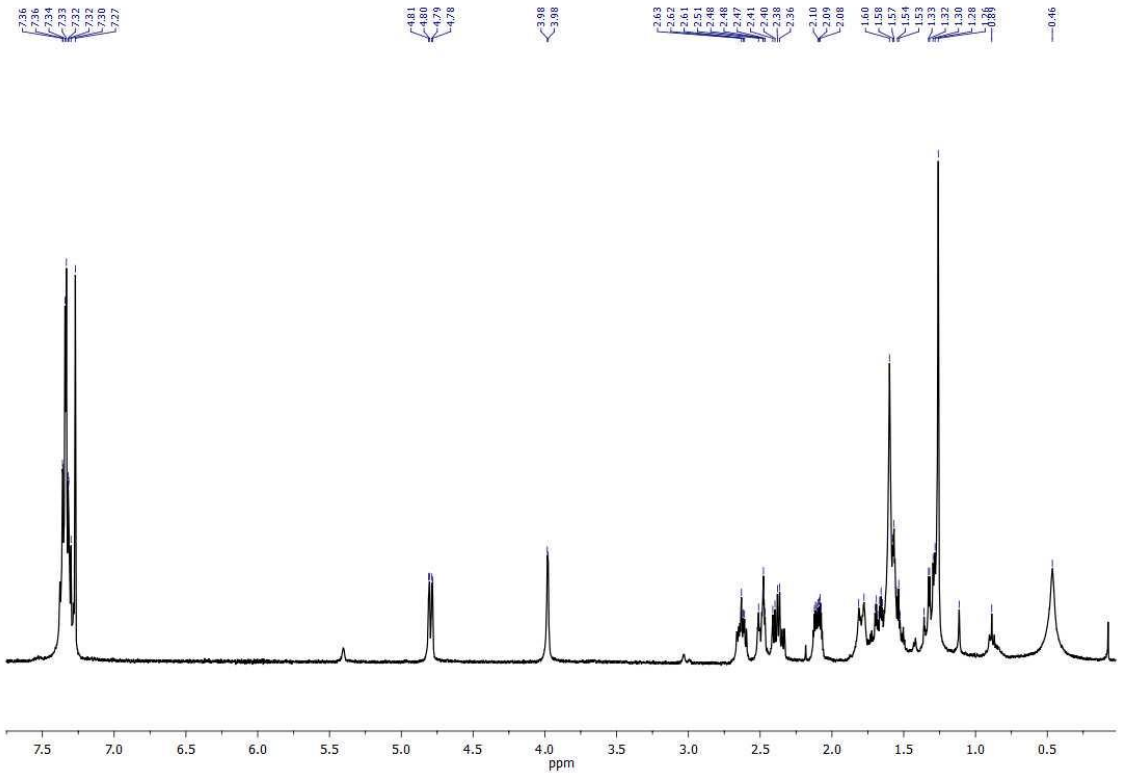


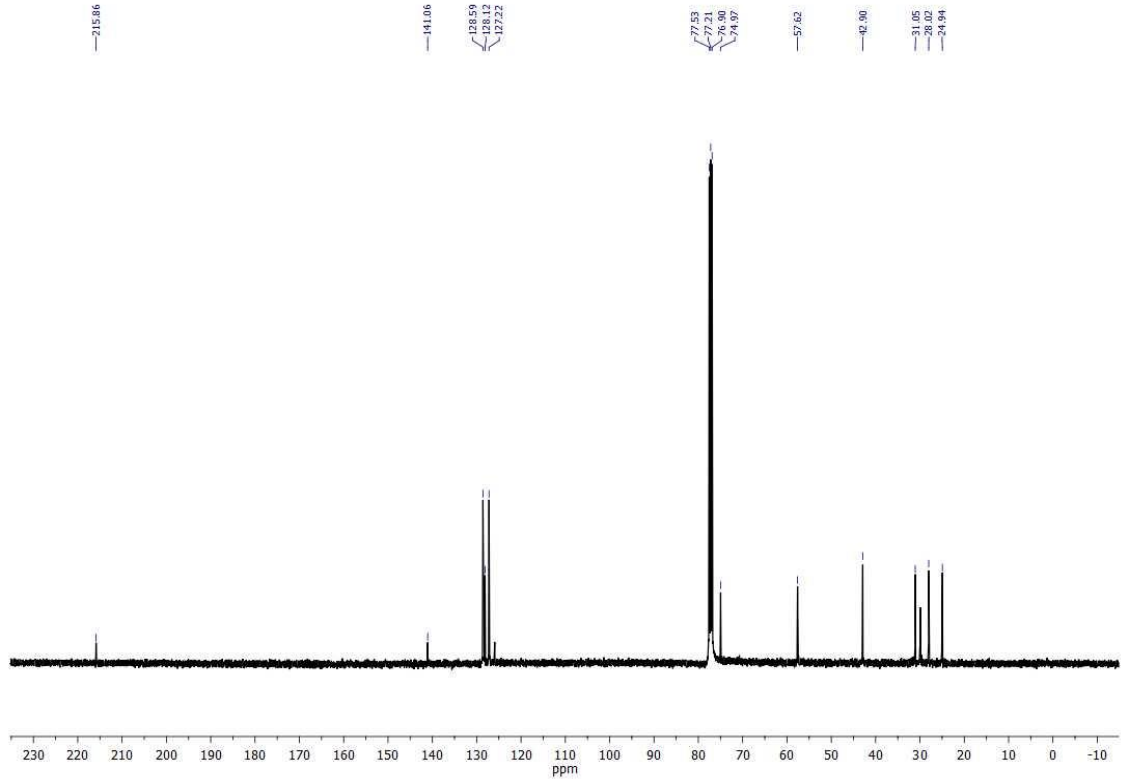

## 7 Appendices

*syn*-2-(hydroxy(phenyl)methyl)cyclohexan-1-one

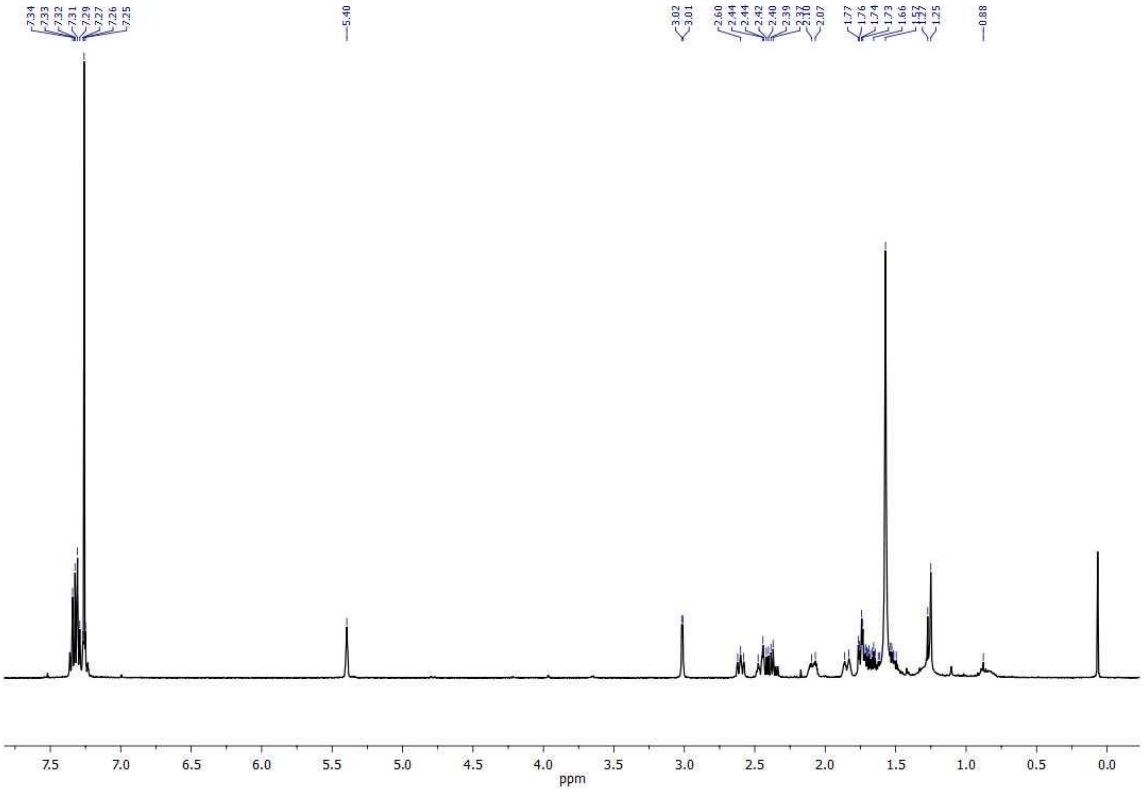


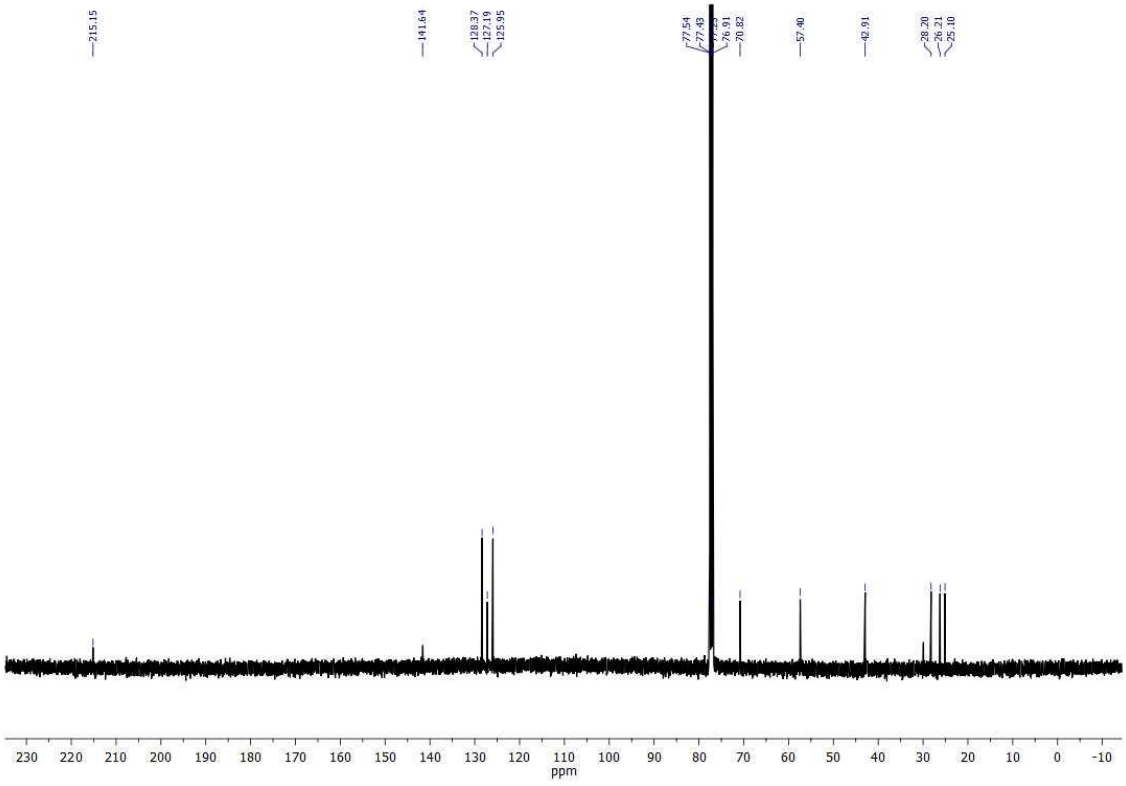

**Chromatograms of aldol products:**

*syn*-2-(hydroxy(4-nitrophenyl)methyl)cyclohexan-1-one

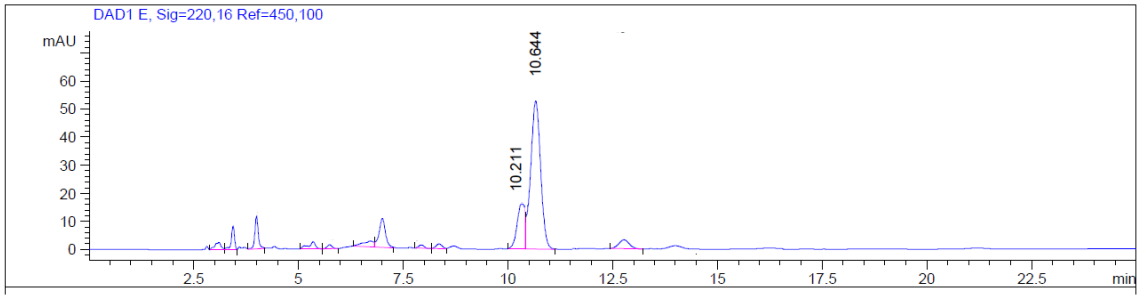


*anti*-2-(hydroxy(4-nitrophenyl)methyl)cyclohexan-1-one

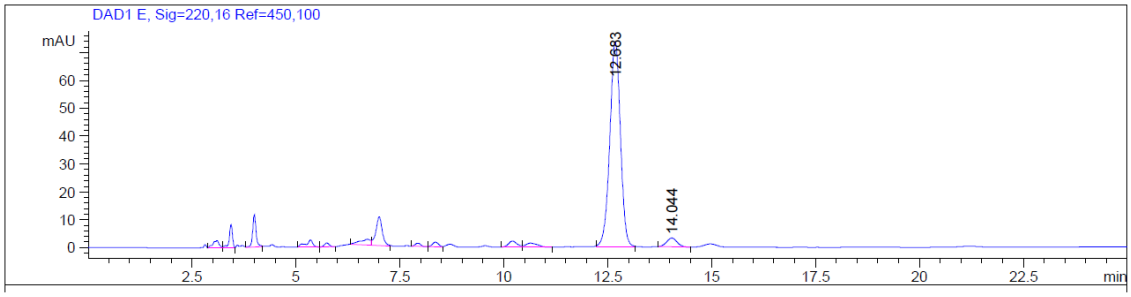


*syn*-2-(hydroxy-(2-nitrophenyl)methyl)cyclohexan-1-one

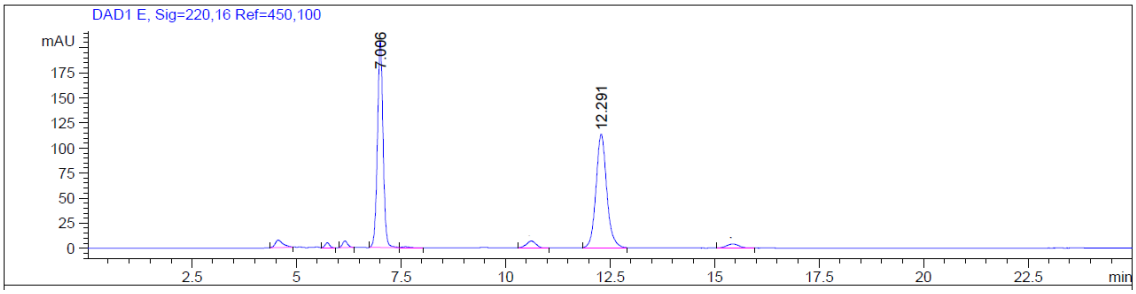


*anti*-2-(hydroxy-(2-nitrophenyl)methyl)cyclohexan-1-one

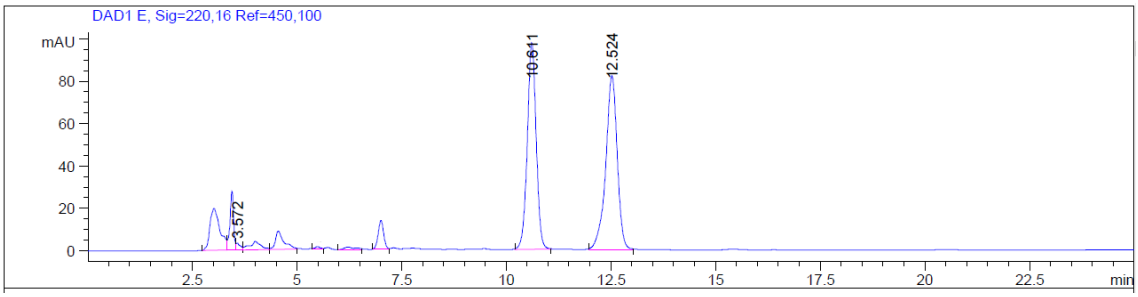

## 7 Appendices

*syn-2*-((4-chlorophenyl)(hydroxy)methyl)cyclohexan-1-one

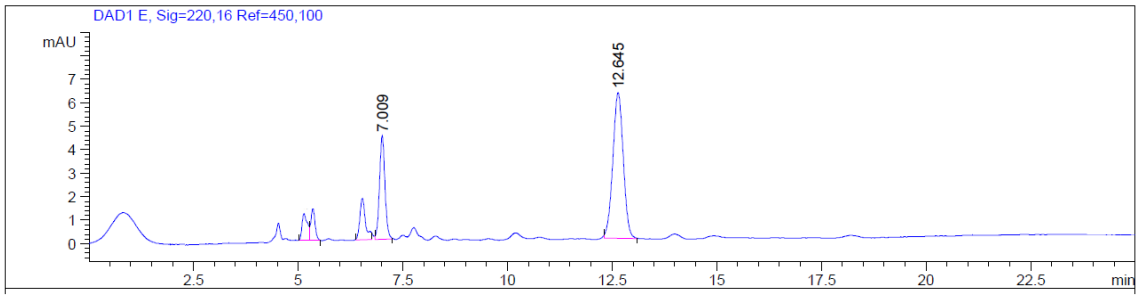


*anti-2*-((4-chlorophenyl)(hydroxy)methyl)cyclohexan-1-one

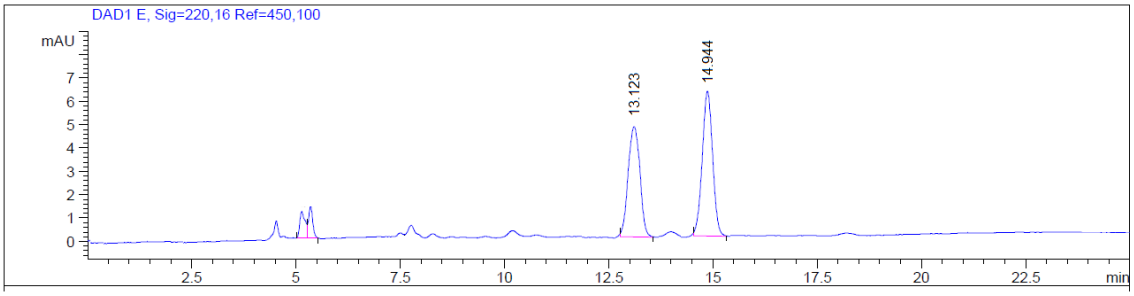


*syn*-2-(hydroxy(phenyl)methyl)cyclohexan-1-one

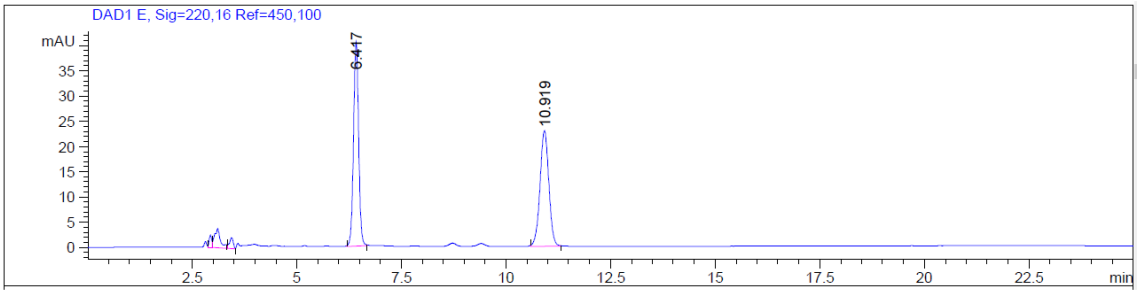


*anti*-2-(hydroxy(phenyl)methyl)cyclohexan-1-one

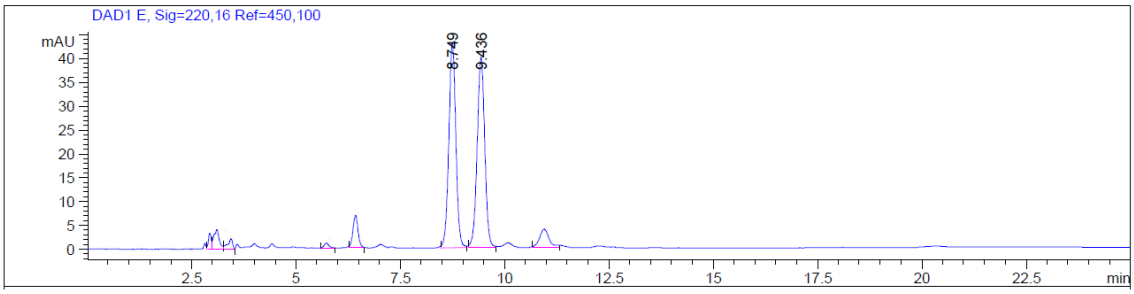

# Appendix C - Supplementary Information Section 3

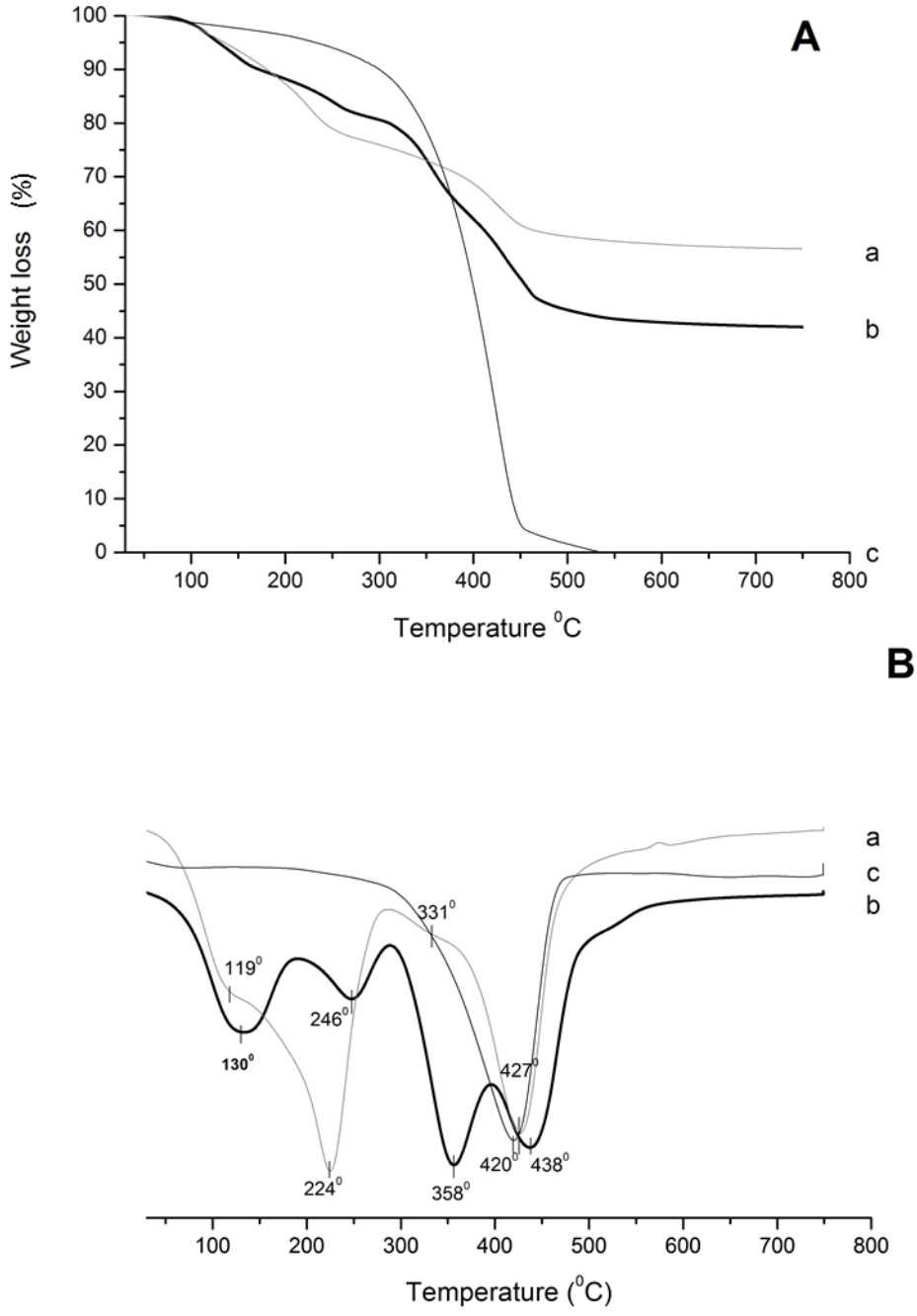


**Figure C.1** Thermogravimetric analysis: A – TGA patterns of a – $HT_{rus}$; b – IPL; c – PLL; B – DTA - patterns of a – $HT_{rus}$; b – IPL; c – PLL

## 7 Appendices

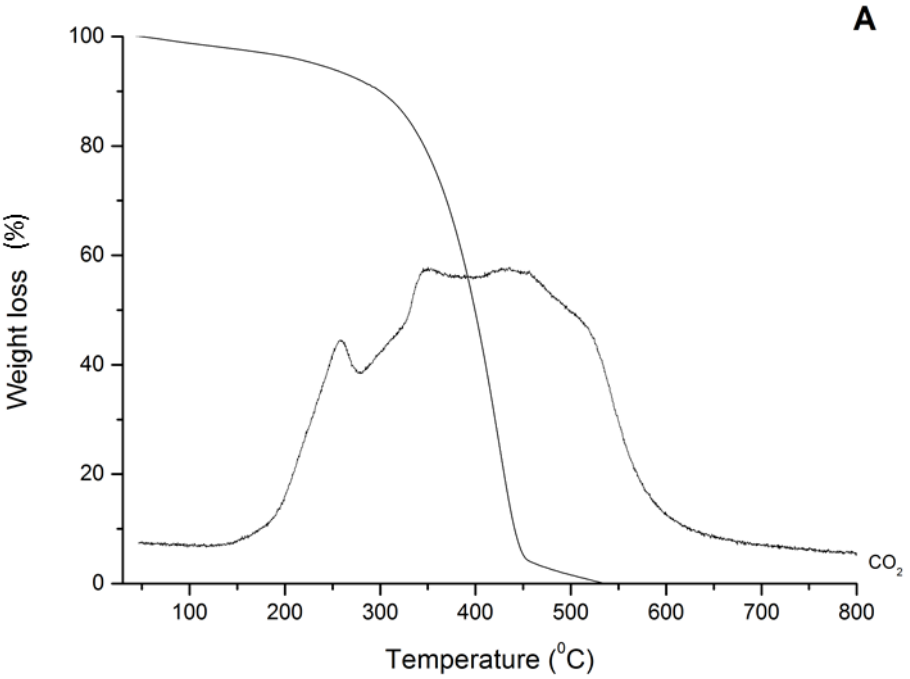


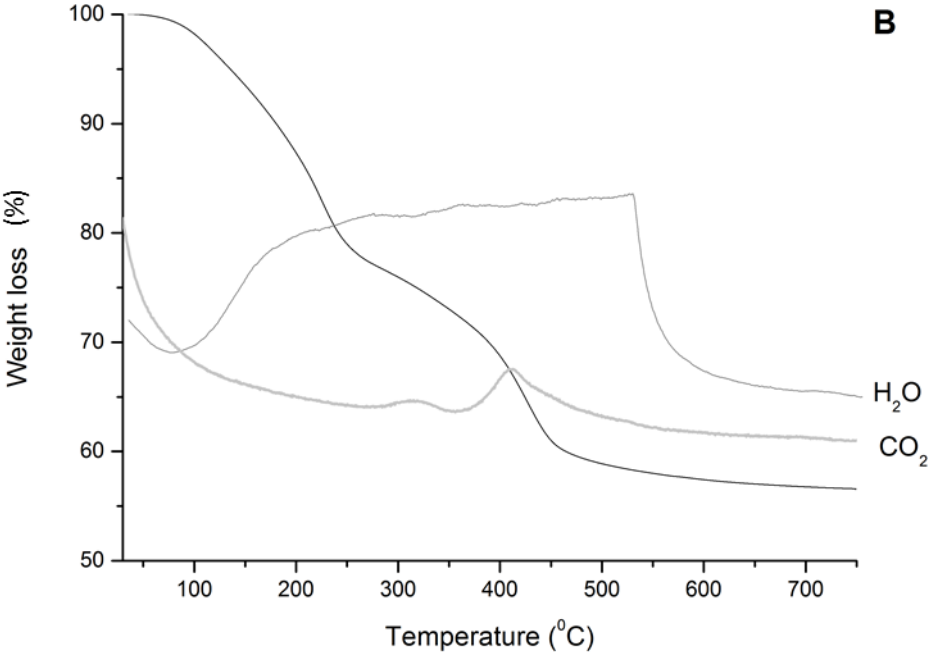

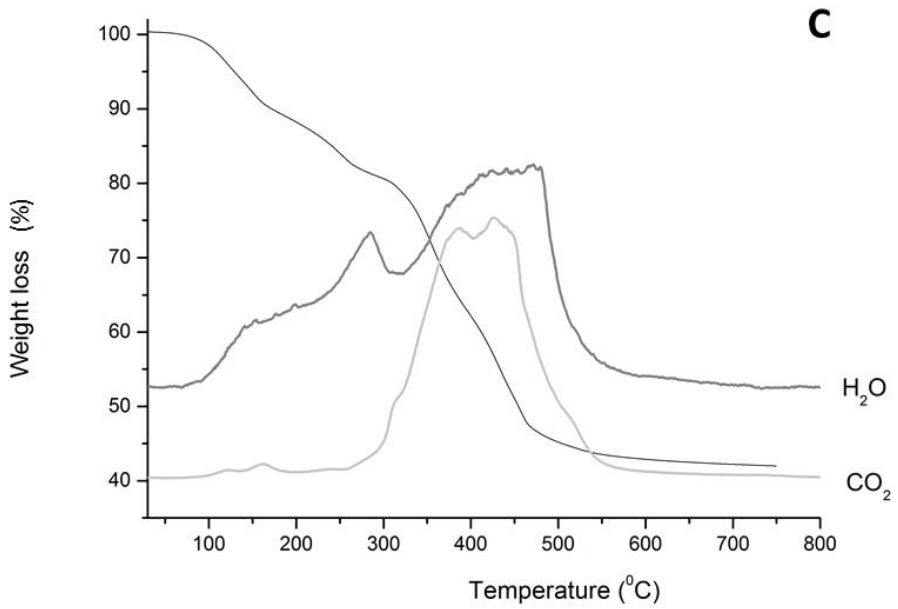


**Figure C.2** TGA-MS patterns of A – PLL; B – $HT_{rus}$ and C-IPL

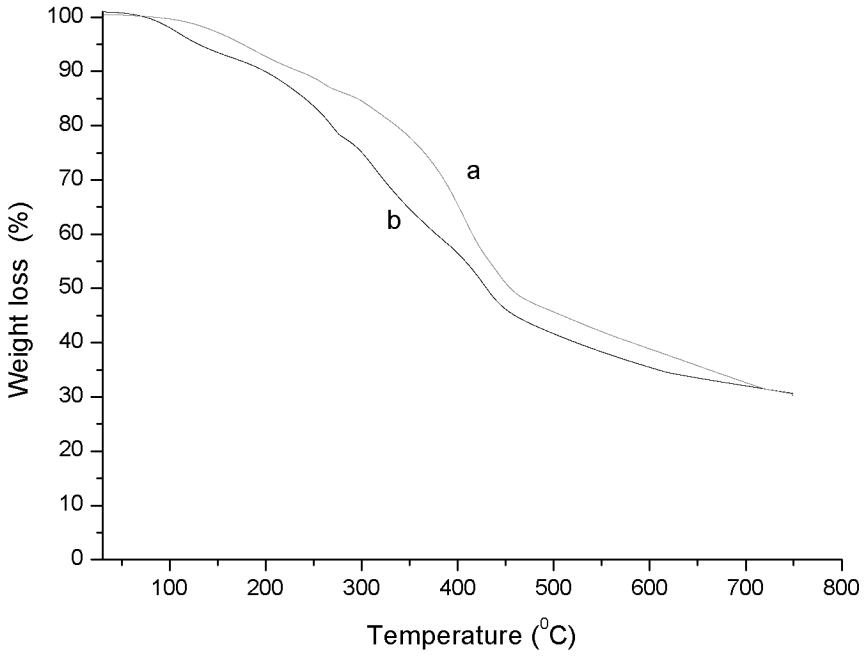


**Figure C.3** TGA-patterns of a - IPL before reaction and b – IPL after 4 consecutive runs. Reaction conditions: acetophenone and benzaldehyde with a molar ratio of 0.95 were added over the catalyst (100 wt% PLL with respect to the ketone), stirred 3 h at 60 °C; 3.7 mg TBAB, 1 ml toluene, 245 µL NaOH, 169.7 µL $H_2O_2$ were added and the reaction was further stirred for 1.5 h at room temperature.

## 7 Appendices

**Spectroscopic data for products:**

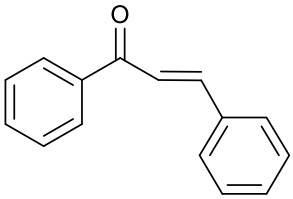

(E)-chalcone

$^1$H-NMR (400 MHz, $CDCl_3$): δ 7.42-7.44 (m, 3H), 7.50-7.67 (m, 6H), 7.82 (d, J = 15.7 Hz, 1H), 8.02-8.04 (m, 2H) ppm [9].

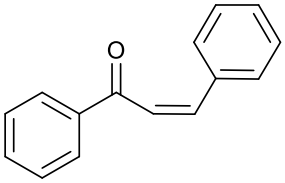

(Z)-chalcone

$^1$H-NMR (400 MHz, $CDCl_3$): δ 7.98-7.94 (m, 2H), 7.55-7.48 (m, 1H), 7.44-7.37 (m, 4H), 7.26-7.19 (m, 3H), 7.02 (d, J = 12.9 Hz, 1H), 6.62(d, J = 12.9Hz, 1H) ppm [10].

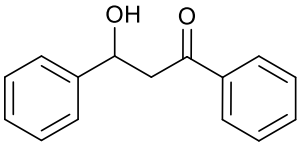

3-hydroxy-1,3-diphenylpropan-1-one

$^1$H-NMR (400 MHz, $CDCl_3$): δ 3.38-3.91 (m, 2H), 3.59 (d, J = 2.8 Hz, 2H), 5.36 (m, 1H) , 7.29-7.61 (m, 8H), 7.95-7.97 (m, 2H) ppm [11].

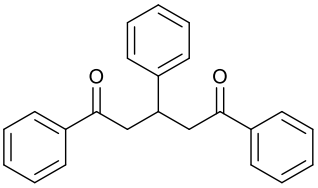

1,3,5-triphenylpentane-1,5-dione

$^1$H-NMR (400 MHz, $CDCl_3$): δ 7.88 (d, 4H), 7.48 (t, 2H,), 7.42–7.33 (m, 4H), 7.27–7.17 (m, 4H), 7.16–7.07 (m, 1H), 4.00 (quin, J = 7.0 Hz, 1H), 3.43 (dd, J = 16.7, 7.0 Hz, 2H), 3.29 (dd, J = 16.7, 7.0 Hz, 2H) ppm [11].

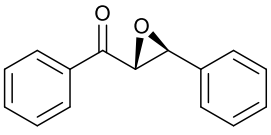

trans-(2R,3S)-Epoxy-1, 3-diphenylpropan-1-one

$^1$H-NMR (400 MHz, $CDCl_3$): δ 4.07 (d, 1 H, J = 2.0 Hz), 4.27 (d, J = 2.0 Hz, 1H), 7.25- 8.10 (m, 10H) ppm [12]. HPLC (CHIRALPACK 1A, heptane: ethanol 3:1), $t_R$ = 7.4 (major), 9.1 (minor). $[\alpha]_D^{20}$ = -115° [c = 0.13, $CH_2Cl_2$] for the product with 91 ee% (lit. $[\alpha]_D^{20}$= -196° [c = 1.0, $CH_2Cl_2$] 94 ee%[13])

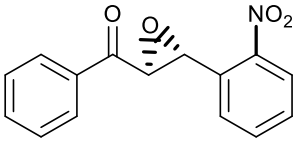

trans-(2S,3R)-Epoxy-3-(2-nitrophenyl)-1-phenylpropan-1-one

$^1$H-NMR (400 MHz, $CDCl_3$): δ 4.22 (d, J = 2.0 Hz, 1H), 4.65 (d, J = 2.0 Hz, 1H), 7.50–8.23 (m, 9H) ppm [13]. HPLC (CHIRALPACK 1A, heptane: ethanol 3:1), $t_R$ = 9.1 (minor), 14.5 (major). $[\alpha]_D^{20}$ = +120 ° [c = 0.2, $CH_2Cl_2$] for the product with 91 ee% (lit. for the other enantiomer $[\alpha]_D^{22}$= -285° [c = 1.0, $CH_2Cl_2$] 80 ee% [13])

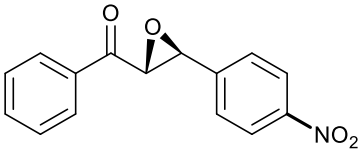

trans-(2R,3S)-Epoxy-3-(4-nitrophenyl)-1-phenylpropan-1-one

$^1$H-NMR (400 MHz, $CDCl_3$): δ 4.30 (d, 1H, J = 1.5 Hz), 4.21 (d, J = 1.5 Hz, 1H), 7.30-8.30 (m, 9H) ppm [14]. HPLC (CHIRALPACK 1A, heptane: ethanol 3:1), $t_R$ = 16.7 (major), 20.5 (minor). $[\alpha]_D^{20}$ = -161° [c = 0.10, $CH_2Cl_2$] for the product with 94 ee% (lit. $[\alpha]_D^{25}$ = -245° [c = 1.0, $CH_2Cl_2$] 98 ee% [14])

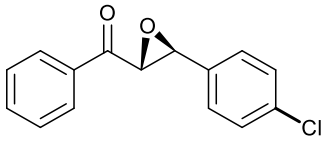

trans-(2R,3S)-Epoxy-3-(4-chlorophenyl)-1-phenylpropan-1-one

$^1$H-NMR (400 MHz, $CDCl_3$): δ 4.21 (d, J = 1.8Hz, 1H), 4.03 (d, J = 1.8Hz, 1H), 7.20-8.20(m, 9H) ppm [14]. HPLC (CHIRALPACK 1A, heptane: ethanol 3:1), $t_R$ = 8.5 (major), 10.1 (minor). $[\alpha]_D^{20}$ = -175° [c = 0.10, $CH_2Cl_2$] for the product with 94 ee% (lit. $[\alpha]_D^{31}$ = -204° [c = 0.16, $CH_2Cl_2$] 95 ee% [15])

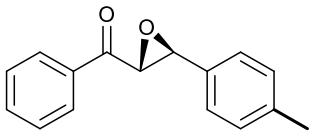

trans-(2R,3S)-Epoxy-3-(4-methylphenyl)-1-phenylpropan-1-one

$^1$H-NMR (400 MHz, $CDCl_3$): δ 2.3 (s, 3 H), 4.27 (d, J = 1.6 Hz, 1H), 4.07 (d, J = 1.6 Hz, 1H), 7.25-8.10 (m, 9H) ppm [14]. HPLC (CHIRALPACK 1A, heptane: ethanol 3:1), $t_R$ = 7.2 (major), 8.7 (minor). $[\alpha]_D^{20}$ = -82° [c = 0.19, $CH_2Cl_2$] for the product with 87 ee% (lit. $[\alpha]_D^{22}$ = -183.9° [c = 1, $CH_2Cl_2$] 86 ee% [13] )

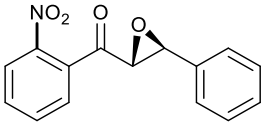

trans-(2R,3S)-Epoxy-1-(2-nitrophenyl)-3-phenylpropan-1-one

$^1$H-NMR (400 MHz, $CDCl_3$): δ 3.72 (d, J = 1.7 Hz, 1H), 3.87 (d, J = 1.8 Hz, 1H), 7.22–7.35 (m, 5H), 7.53–8.18 (m, 4H) ppm [13]. HPLC (CHIRALPACK 1A, heptane: ethanol 3:1), $t_R$ = 9.1 (major), 16.1 (minor). $[\alpha]_D^{20}$ = -126° [c = 0.19, $CH_2Cl_2$] for the product with 66 ee% (lit. $[\alpha]_D^{22}$ = -285° [c = 1, $CH_2Cl_2$] 80 ee% [13] )

## 7 Appendices

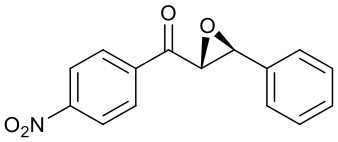

trans-(2R,3S)-Epoxy-1-(4-nitrophenyl)-3-phenylpropan-1-one

$^1$H-NMR (400 MHz, $CDCl_3$): δ d 4.21 (d, J = 1.7 Hz, 1H), 4.25 (d, J = 1.8 Hz, 1H), 7.35–7.44 (m, 5H), 8.19–8.34 (m, 4H) ppm [13]. HPLC (CHIRALPACK 1A, heptane: ethanol 3:1), $t_R$ = 12.9 (major), 25.9 (minor). $[\alpha]_D^{20}$ = -70° [c = 0.24, $CH_2Cl_2$] for the product with 89 ee% (lit. $[\alpha]_D^{22}$ = -122.6° [c = 1, $CH_2Cl_2$] 96 ee% [13] )

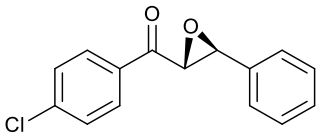

trans-(2R,3S)-Epoxy-1-(4-chlorophenyl)-3-phenylpropan-1-one

$^1$H-NMR (400 MHz, $CDCl_3$): δ 4.21 (d, J = 1.7 Hz, 1H), 4.03 (d, J = 1.7 Hz, 1H), 7.25-8.10 (m, 9H) ppm [14]. HPLC (CHIRALPACK 1A, heptane: ethanol 3:1), $t_R$ = 8.3 (major), 18.7 (minor). $[\alpha]_D^{20}$ = -111° [c = 0.27, $CH_2Cl_2$] for the product with 91 ee% (lit. $[\alpha]_D^{20}$ = -198.3° [c = 1, $CH_2Cl_2$] 96 ee% [16] )

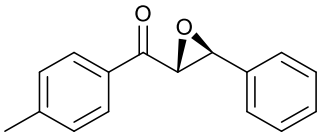

trans-(2R,3S)-Epoxy-1-(4-methylphenyl)-3-phenylpropan-1-one

$^1$H-NMR (400 MHz, $CDCl_3$): δ 2.3 (s, 3H), 4.07 (d, J = 1.6 Hz, 1H), 4.27 (d, J = 1.6 Hz, 1H), 7.30-8.10 (m, 9H) ppm [14]. HPLC (CHIRALPACK 1A, heptane: ethanol 3:1), $t_R$ = 7.8 (major), 9.6 (minor). $[\alpha]_D^{20}$ = -103° [c = 0.18, $CH_2Cl_2$] for the product with 80 ee% (lit. $[\alpha]_D^{20}$ = -169.7° [c = 1, $CH_2Cl_2$] 81 ee% [17] )

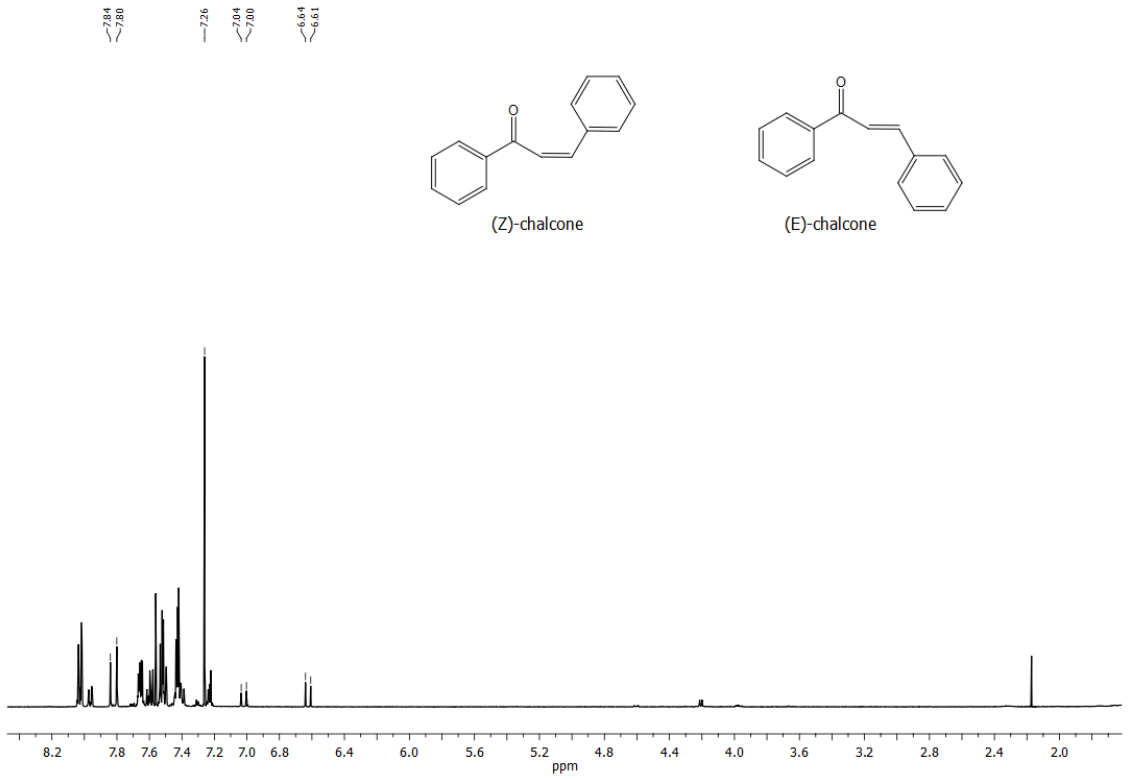
7.84
7.80
7.26
7.04
7.00
6.64
6.61
(Z)-chalcone
(E)-chalcone
8.2 7.8 7.6 7.4 7.2 7.0 6.8 6.4 6.0 5.6 5.2 4.8 4.4 4.0 3.6 3.2 2.8 2.4 2.0
ppm

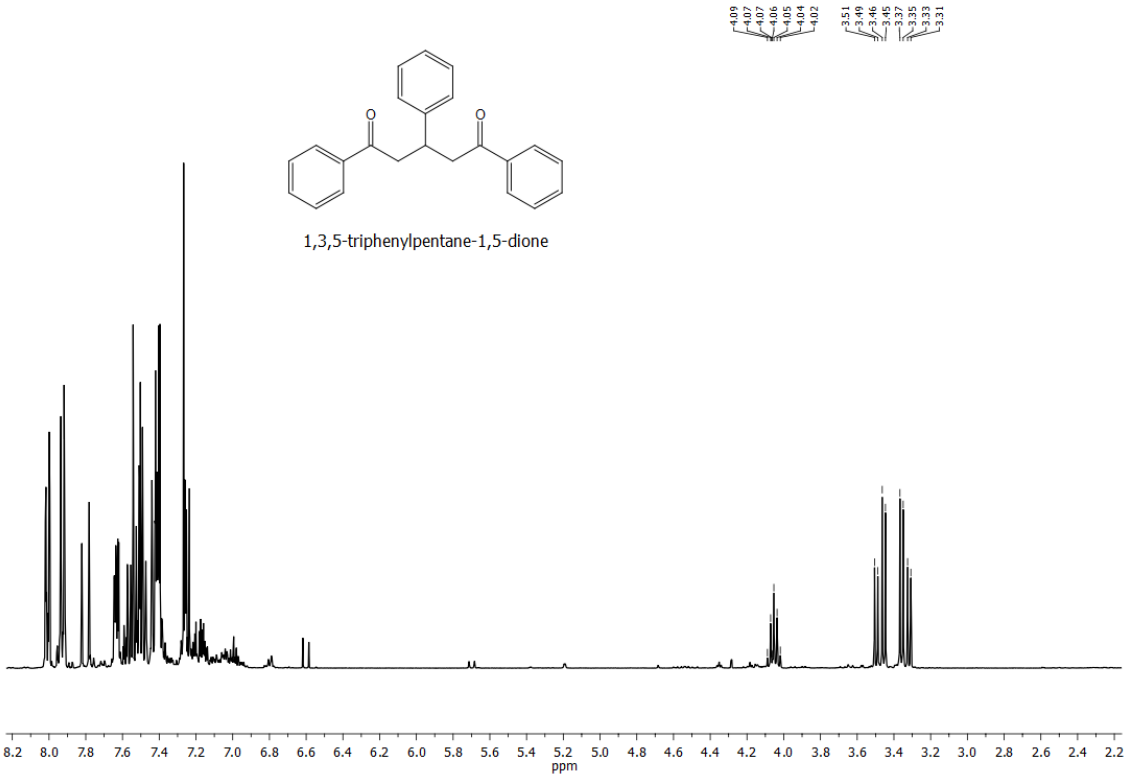
4.09
4.07
4.07
4.06
4.05
4.04
4.02
3.51
3.49
3.46
3.45
3.37
3.35
3.33
3.31
1,3,5-triphenylpentane-1,5-dione
8.2 8.0 7.8 7.6 7.4 7.2 7.0 6.8 6.6 6.4 6.2 6.0 5.8 5.6 5.4 5.2 5.0 4.8 4.6 4.4 4.2 4.0 3.8 3.6 3.4 3.2 3.0 2.8 2.6 2.4 2.2
ppm

## 7 Appendices

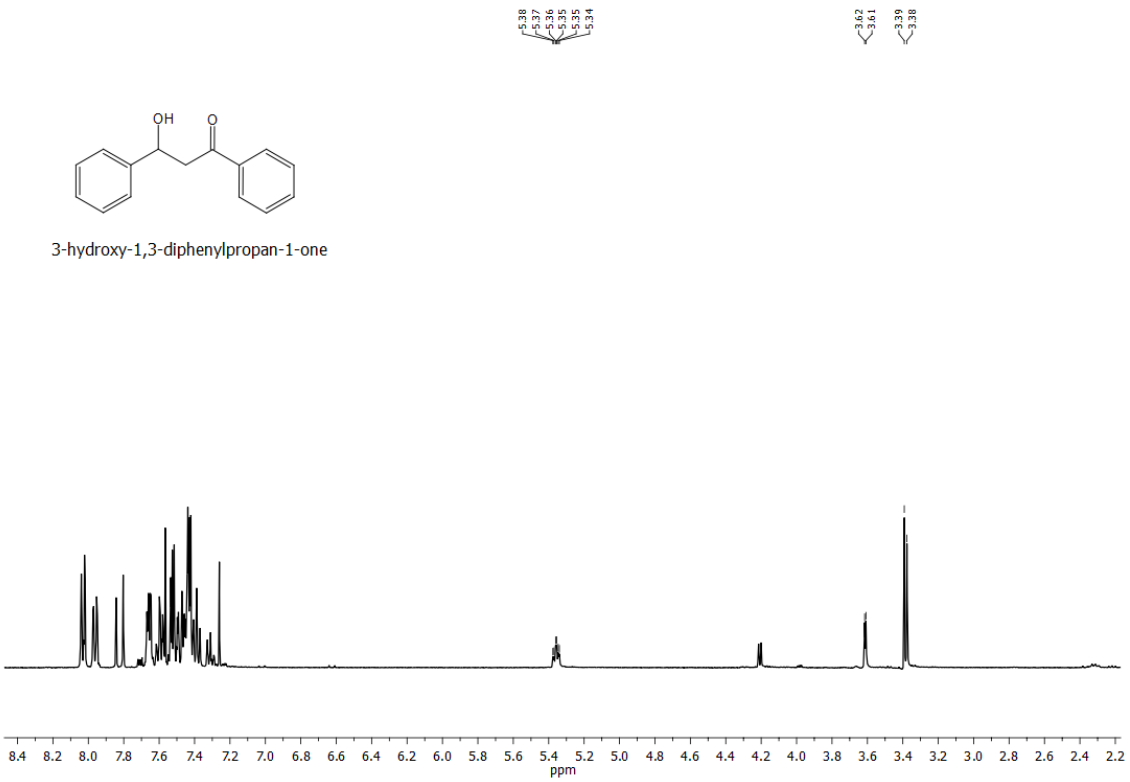


3-hydroxy-1,3-diphenylpropan-1-one

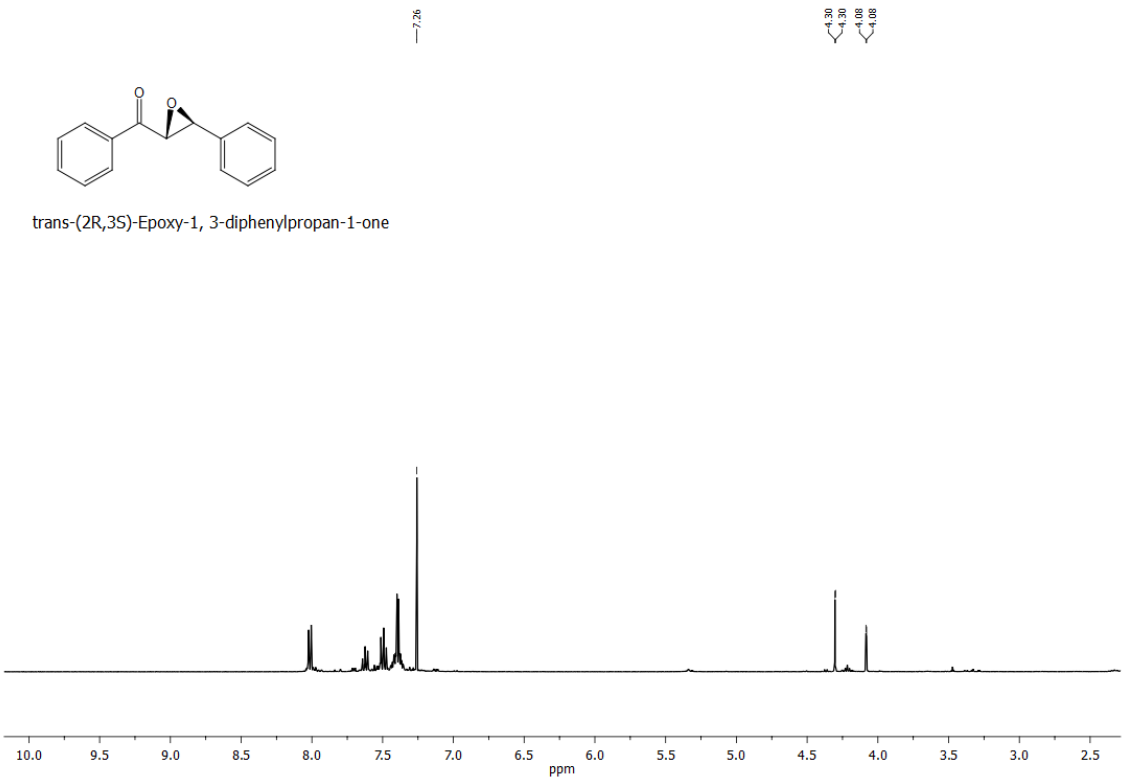


trans-(2R,3S)-Epoxy-1, 3-diphenylpropan-1-one

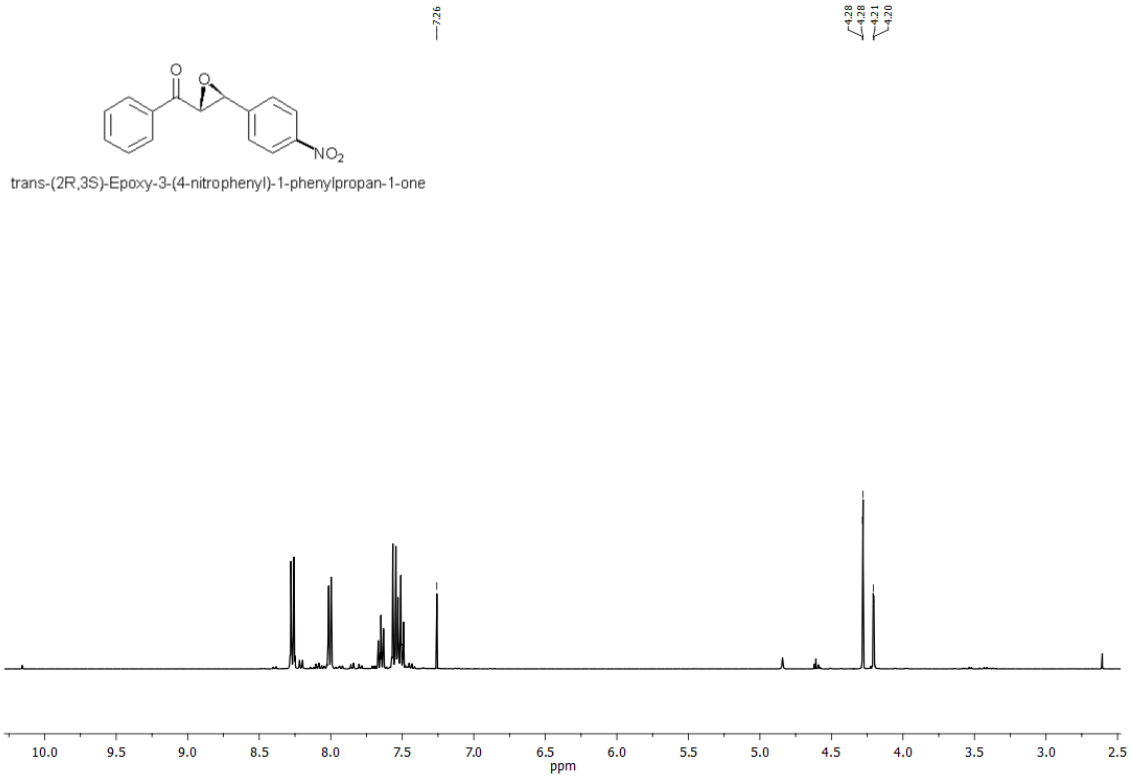


trans-(2R,3S)-Epoxy-3-(4-nitrophenyl)-1-phenylpropan-1-one

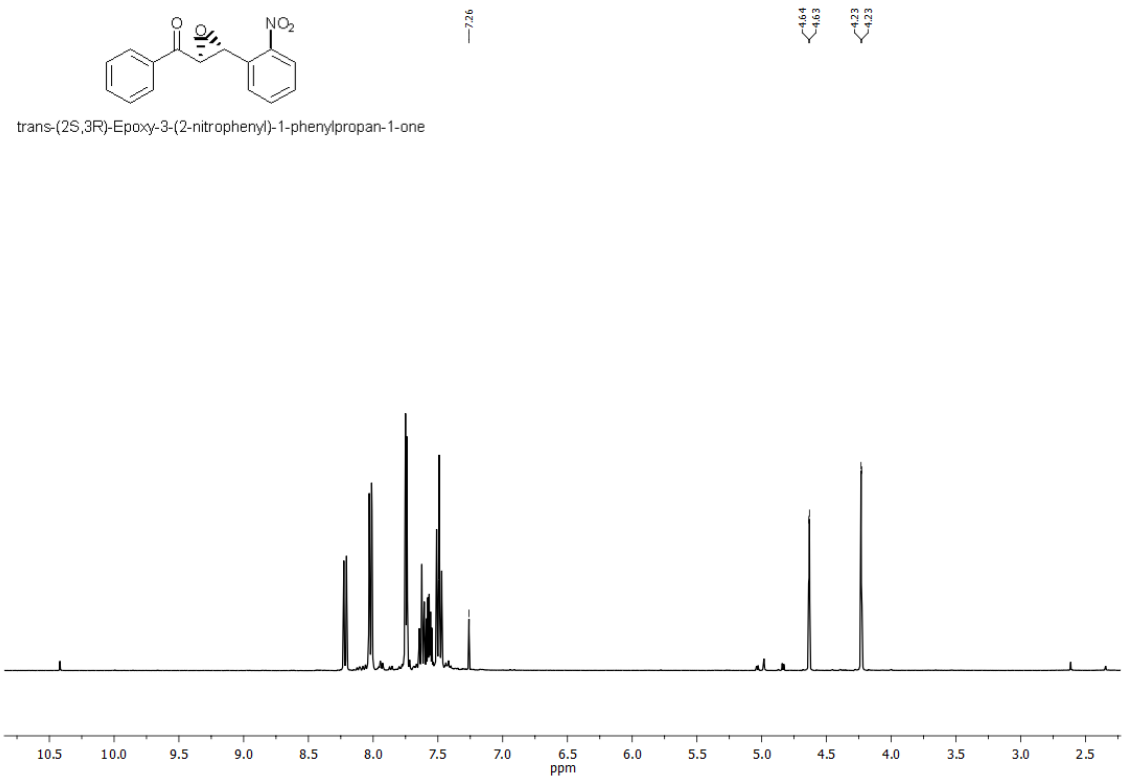


trans-(2S,3R)-Epoxy-3-(2-nitrophenyl)-1-phenylpropan-1-one

## 7 Appendices

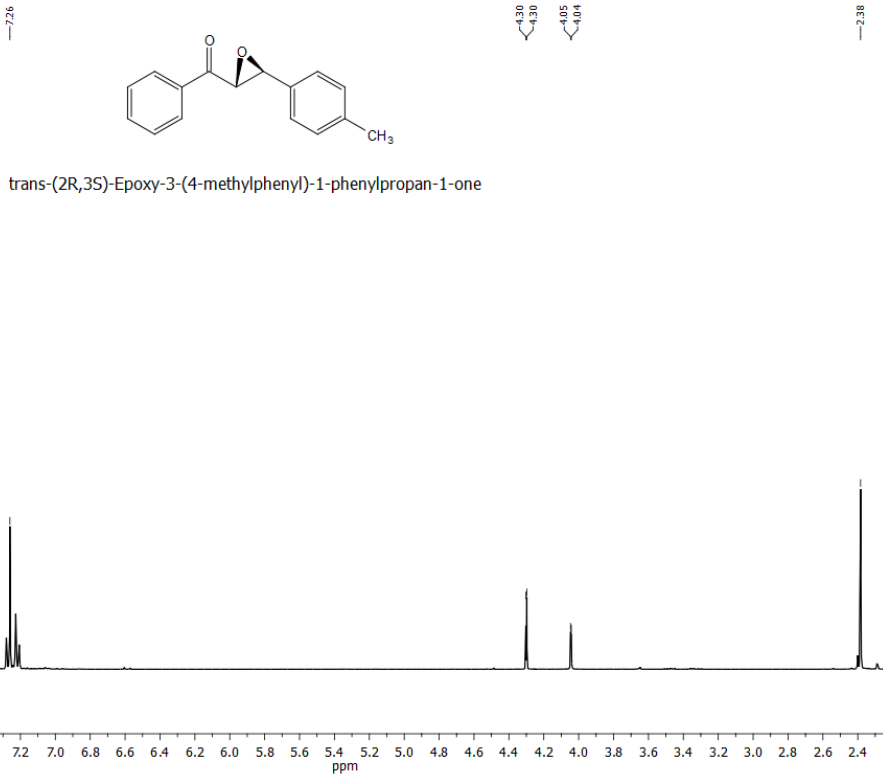


trans-(2R,3S)-Epoxy-3-(4-methylphenyl)-1-phenylpropan-1-one

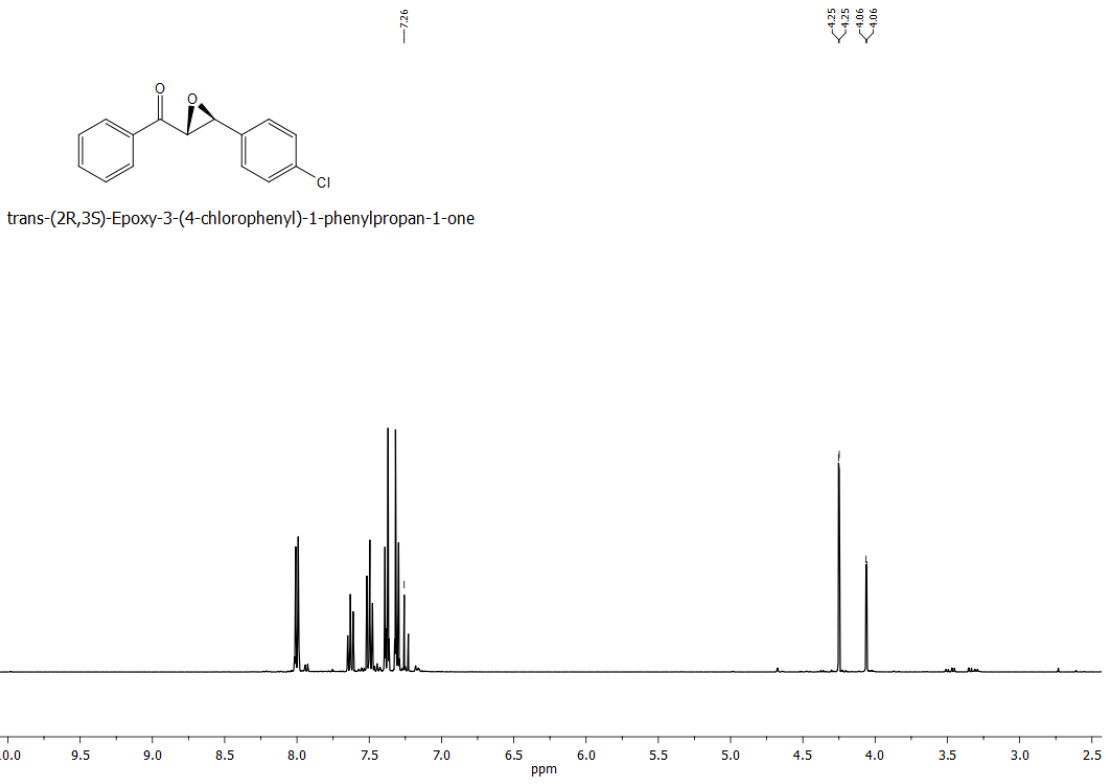


trans-(2R,3S)-Epoxy-3-(4-chlorophenyl)-1-phenylpropan-1-one

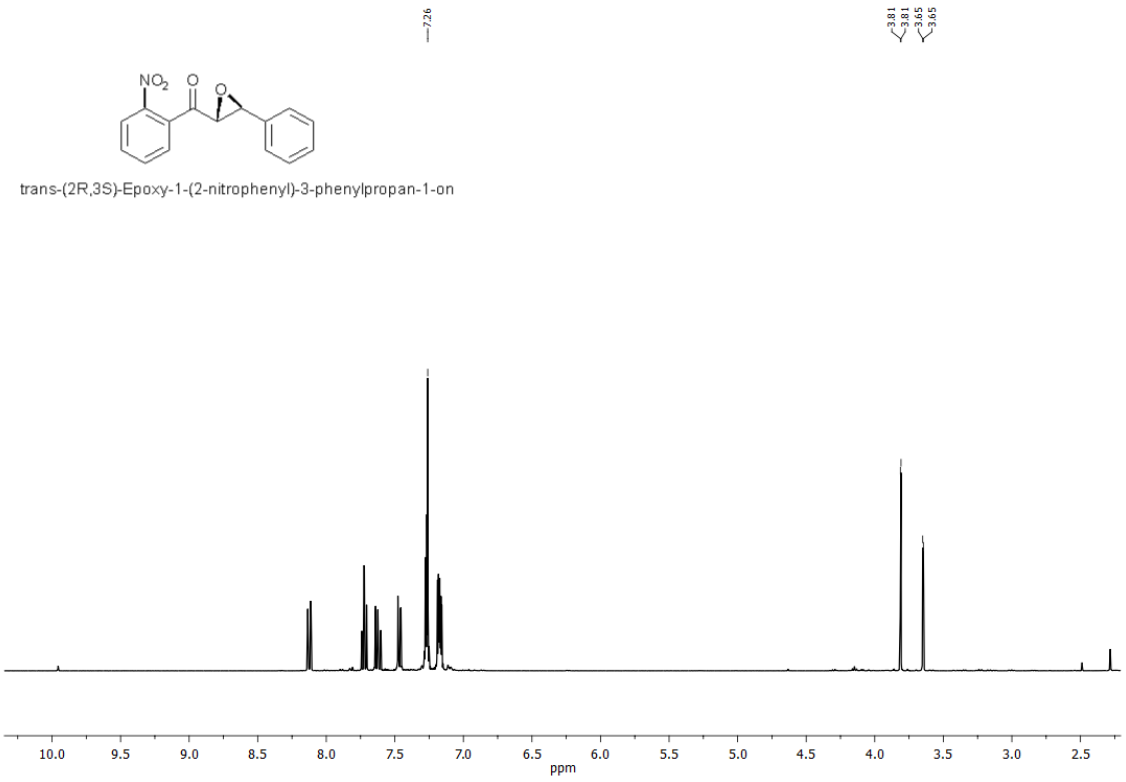
7.26
3.81
3.81
3.65
3.65
NO2
O
O
trans-(2R,3S)-Epoxy-1-(2-nitrophenyl)-3-phenylpropan-1-on
10.0
9.5
9.0
8.5
8.0
7.5
7.0
6.5
6.0
5.5
5.0
4.5
4.0
3.5
3.0
2.5
ppm

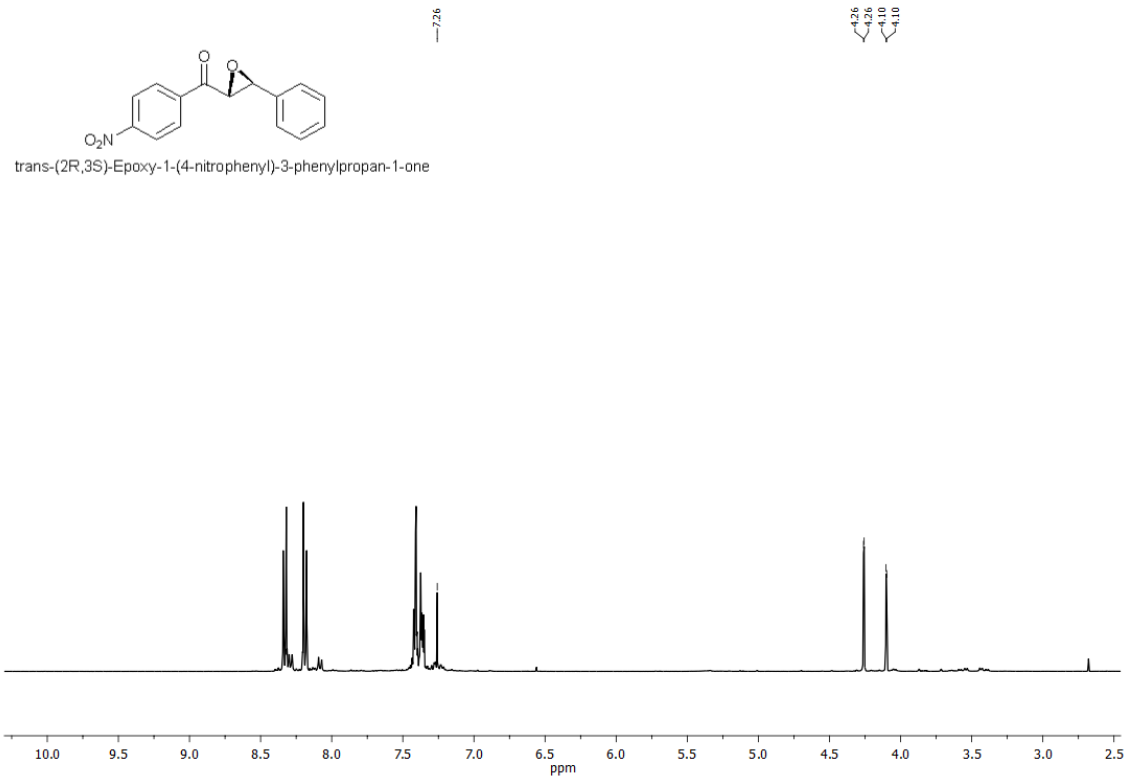
7.26
4.26
4.26
4.10
4.10
O
O
O2N
trans-(2R,3S)-Epoxy-1-(4-nitrophenyl)-3-phenylpropan-1-one
10.0
9.5
9.0
8.5
8.0
7.5
7.0
6.5
6.0
5.5
5.0
4.5
4.0
3.5
3.0
2.5
ppm

## 7 Appendices

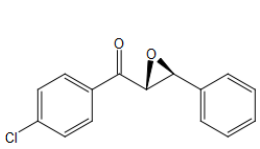






trans-(2R,3S)-Epoxy-1-(4-chlorophenyl)-3-phenylpropan-1-one

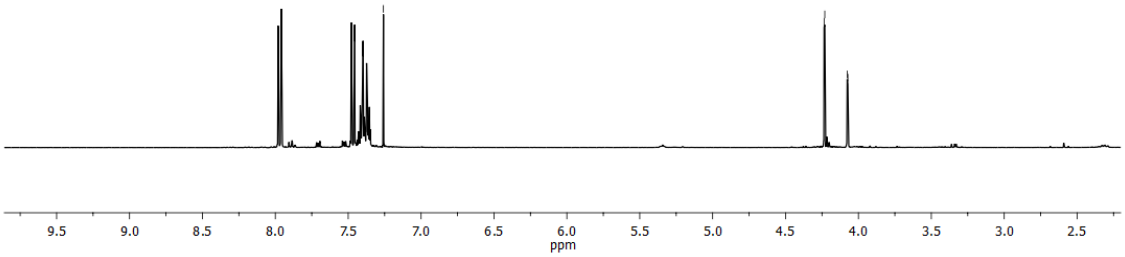


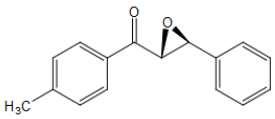






trans-(2R,3S)-Epoxy-1-(4-methylphenyl)-3-phenylpropan-1-one

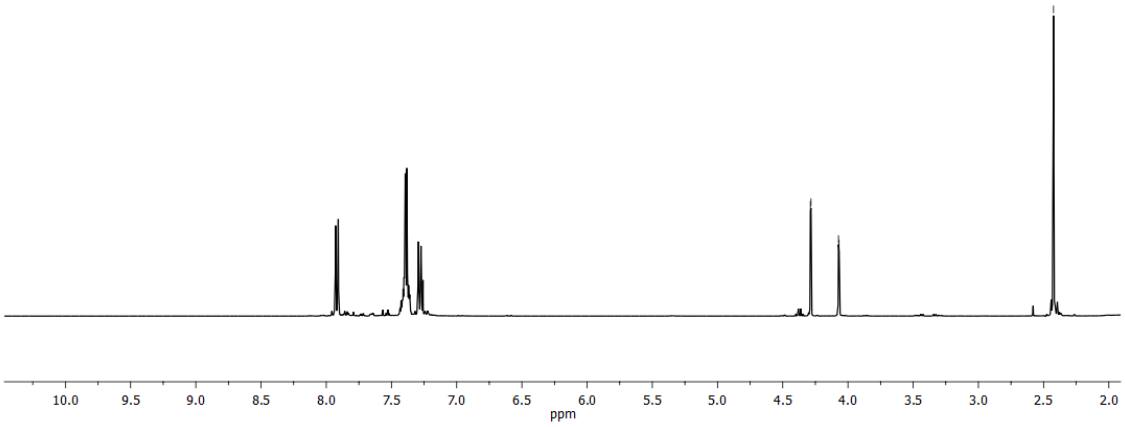

# Appendix D - Supplementary Information Section 4

### Julia–Colonna epoxidation reaction, $^1$H-NMR

8.76 mg (1.09 x $10^{-5}$ moles) of (L-leu)$_6$-Cys were added in a 10 ml closed tube. Over the catalyst a solution containing 20 mg (9.57 x $10^{-5}$ moles) of trans-chalcone in 1 ml THF was added along with TBAB (3.7 mg), $H_2O_2$ (127 µl) and NaOH 2M (143 µl). The reaction was stirred for 24 h. The liquid mixture was separated by centrifugation and the conversion was computed from $^1$H-NMR in $CDCl_3$ (Figure D.2).

### Supporting figures

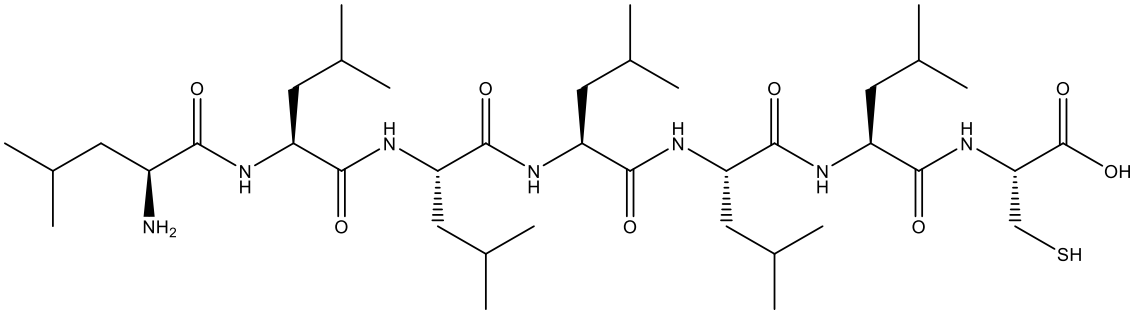


**Figure D.1** Structure of the modified poly-L-leucine (hexa leucine) to include a cysteine group, (L-leu)$_6$-Cys, to facilitate adsorption to a gold surface.

## 7 Appendices

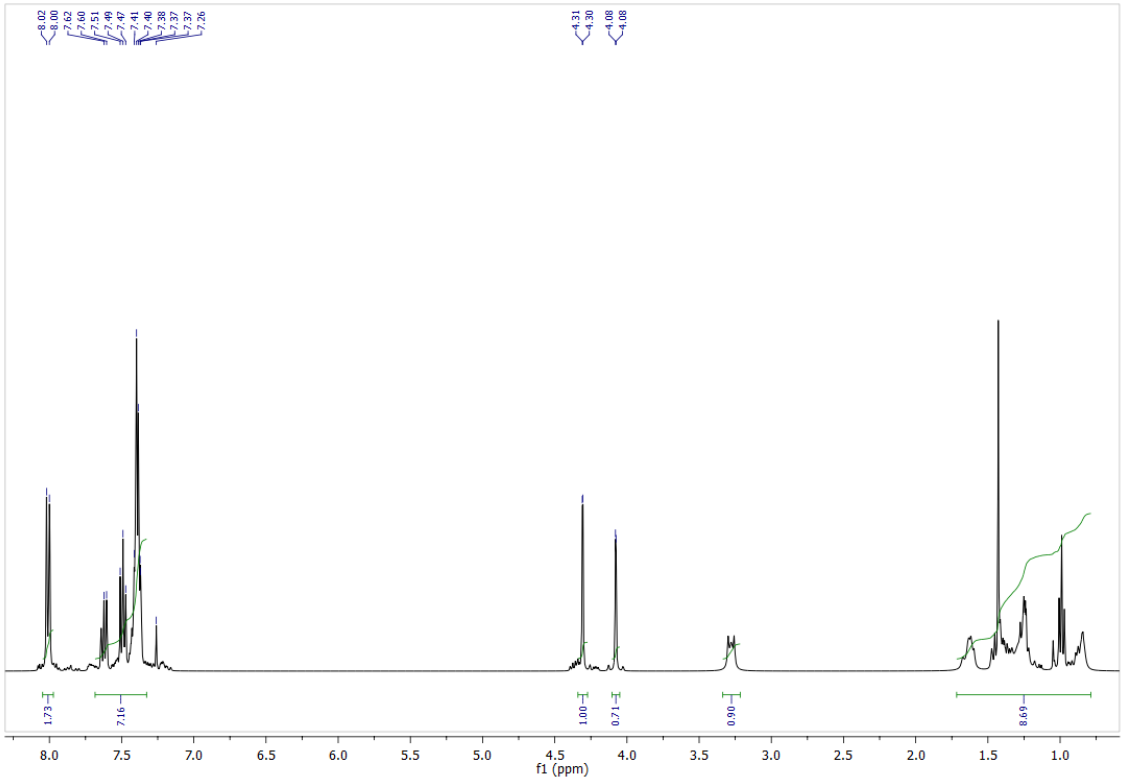


**Figure D.2** $^{1}$H-NMR spectrum of chalcone epoxidation in presence of the short oligomer. 1,3-Diphenyl-2,3-epoxy-1-propanone $^{1}$H-NMR (400 MHz, CDCl3) δ 4.08 (d, J = 1.85Hz, 1H), 4.30 (d, J = 1.85Hz, 1H), 7.37-7.62 (m, 8H), 8.00-8.03 (m, 2H); (Larraufie, M.; Pellet, R.;Fensterbank, L.; Goddard, J.P.; Lacote, E.; Malacria, M.; Olliver, C.; Angewandte Chemie, 2011,50, 4463-4466) In the range 0.5-3.25 ppm are the signals specific for tetran-butylammoniumbromine (TBAB).

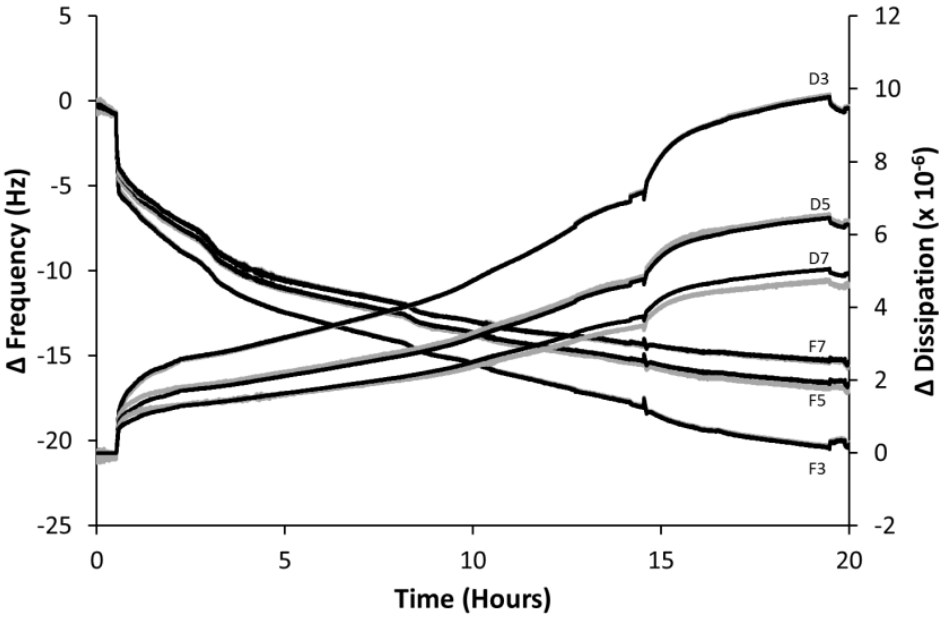


**Figure D.3** Plot of the frequency shift and dissipation factor (light grey lines) of the gold coated QCM-D crystal sensor in response to the adsorption of $(L\text{-leu})_6$-Cys, and the Voigt modelling fits (black lines). Data for the 3rd, 5th and 7th overtones are shown.

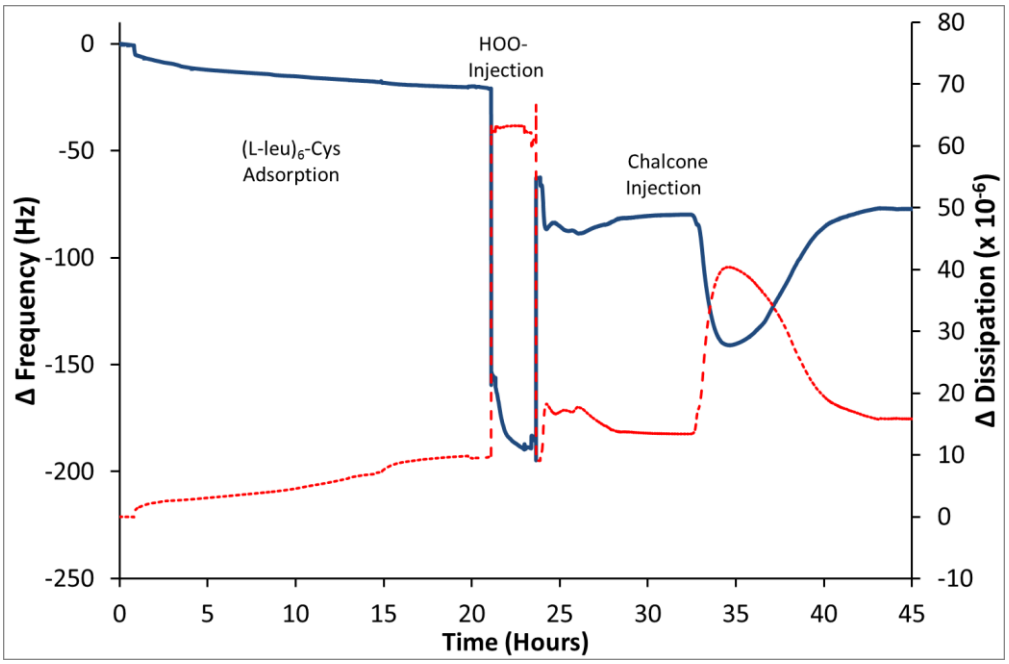


**Figure D.4** Plot of the frequency shift (solid line) and dissipation factor (dashed line) of the gold coated QCM-D crystal sensor in response to the adsorption of $(L\text{-leu})_6$-Cys, and the subsequent exposure to $HOO^-$ and chalcone, as per kinetic pathway I. Only the data for the 3rd overtone has been shown for clarity.

## 7 Appendices

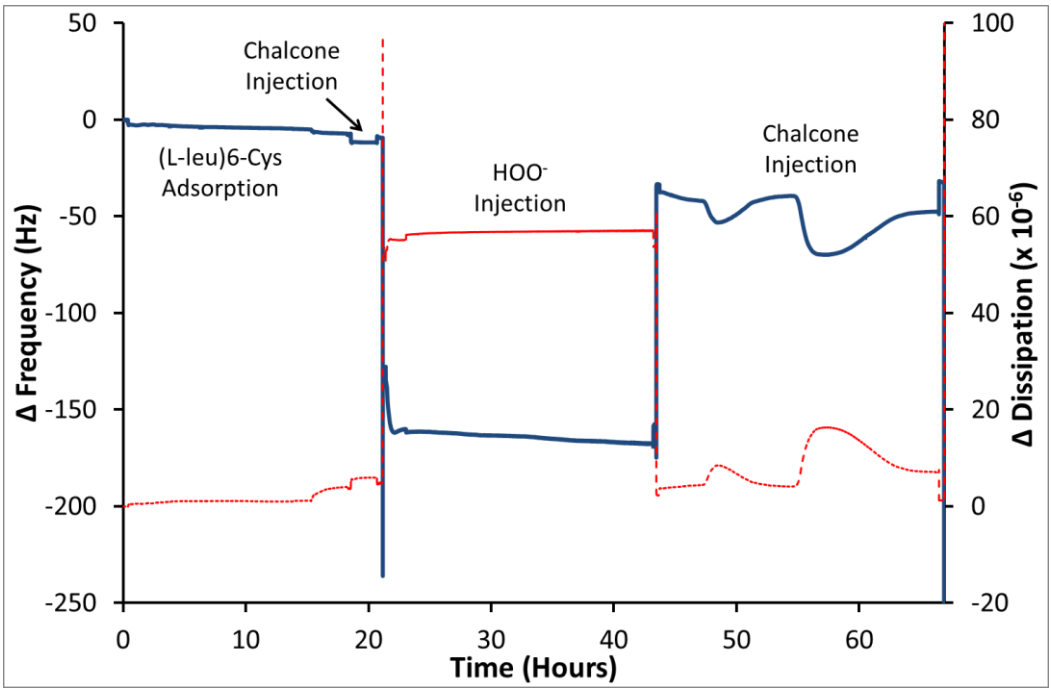


**Figure D.5** Plot of the frequency shift (solid line) and dissipation factor (dashed line) of the gold coated QCM-D crystal sensor in response to the adsorption of $(L\text{-leu})_6$-Cys, and the subsequent exposure to chalcone and $HOO^-$, as per kinetic pathway II. Only the data for the 3rd overtone has been shown for clarity.

# Appendix E - Supplementary Information Section 5

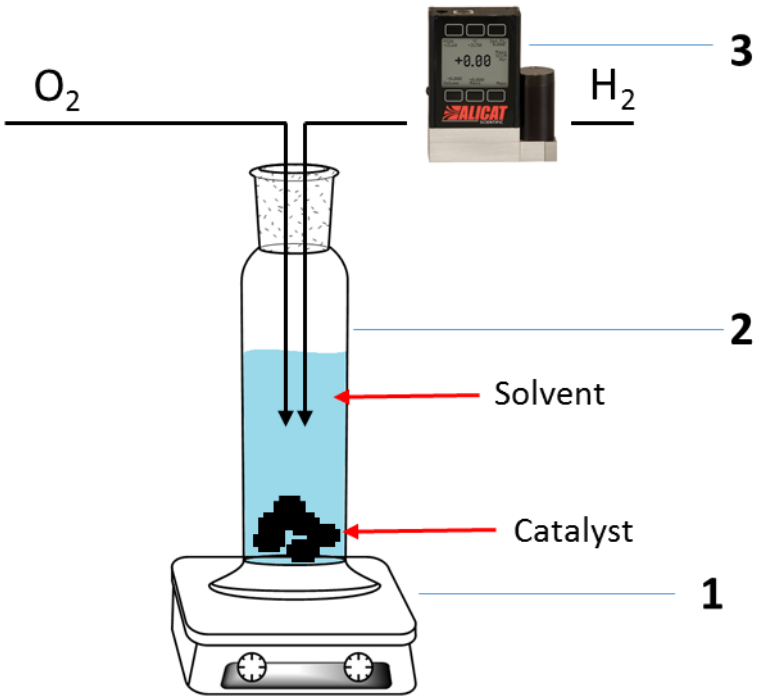


**Figure E.1** Set-up for the *in-situ* epoxidation of chalcone using Pd/HTs and HTs catalysts: 1 – stirring plate, 2 – reaction vessel, 3 – mass flow controller

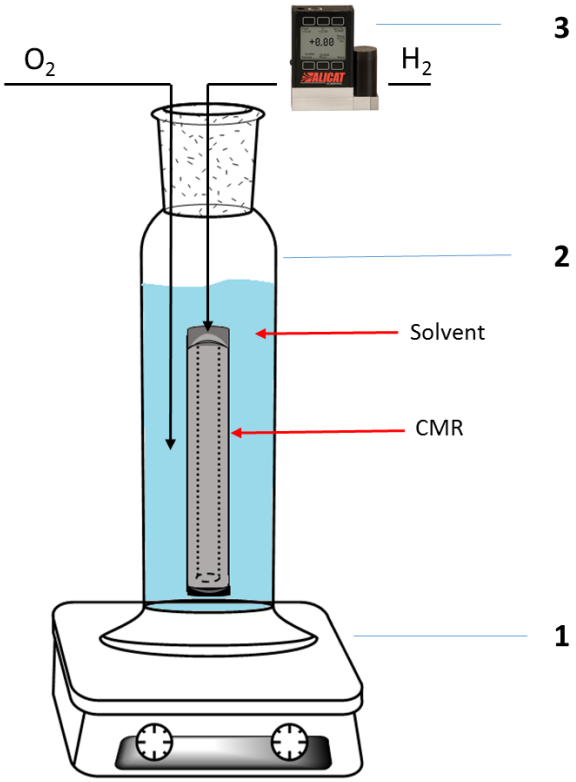


**Figure E.2** Set-up for the *in-situ* epoxidation of chalcone using CMR and HT/CMR: 1 – stirring plate, 2 – reaction vessel, 3 – mass flow controller

## 7 Appendices

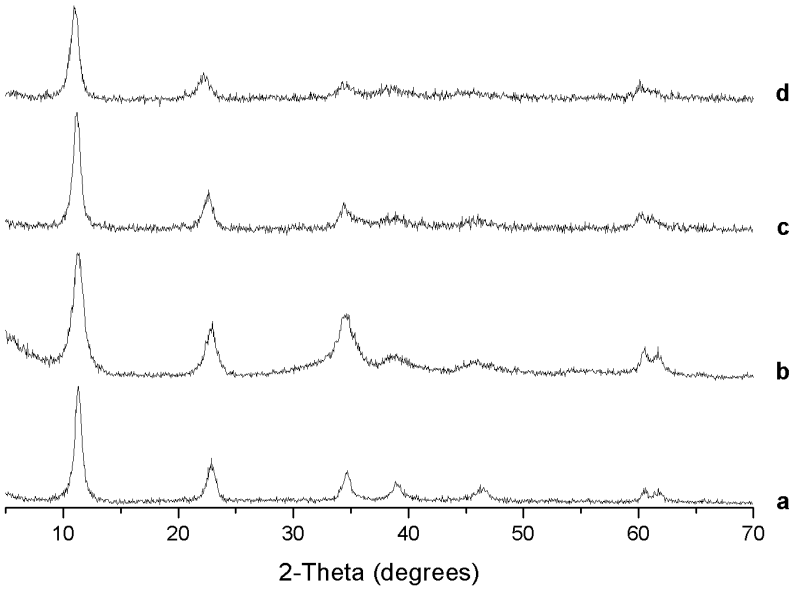


**Figure E.3** The XRD patterns for: a) 1 wt% Pd/Mg-Al HT; b) Mg-Al-Pd HT; c)1 wt% Pd/Mg-Al-Fe HT; d) Mg-Al-Fe HT

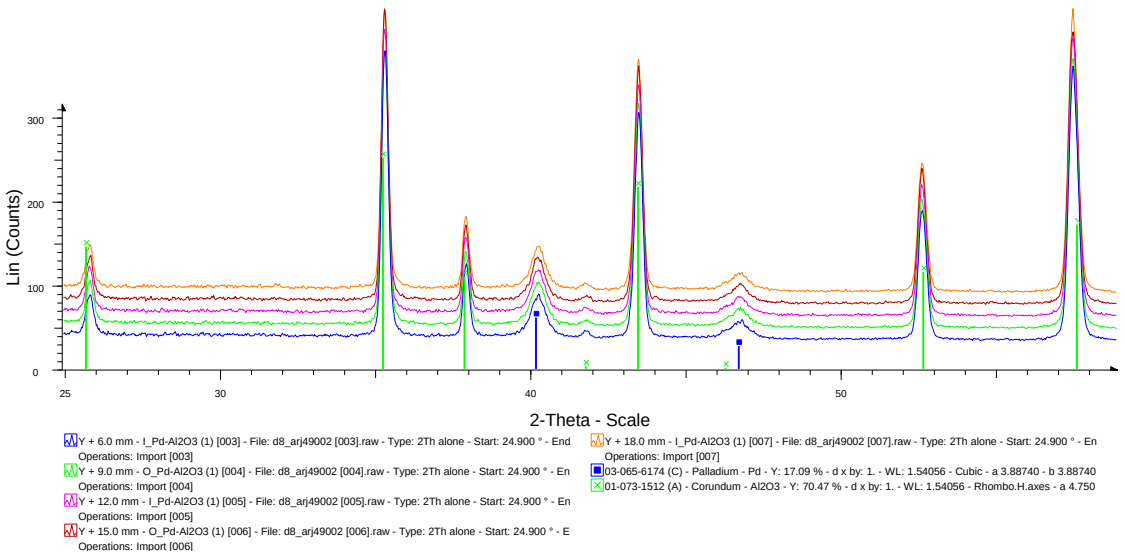


**Figure E.4** μ-XRD diffractograms of CMR performed at 5 different points, showing the homogeneous Pd distribution overall the entire membrane reactor: with I_Pd is denoted the Pd nanoparticles found in the inner part of the CMR and with O_Pd the Pd nanoparticles found in the outer part of the CMR.

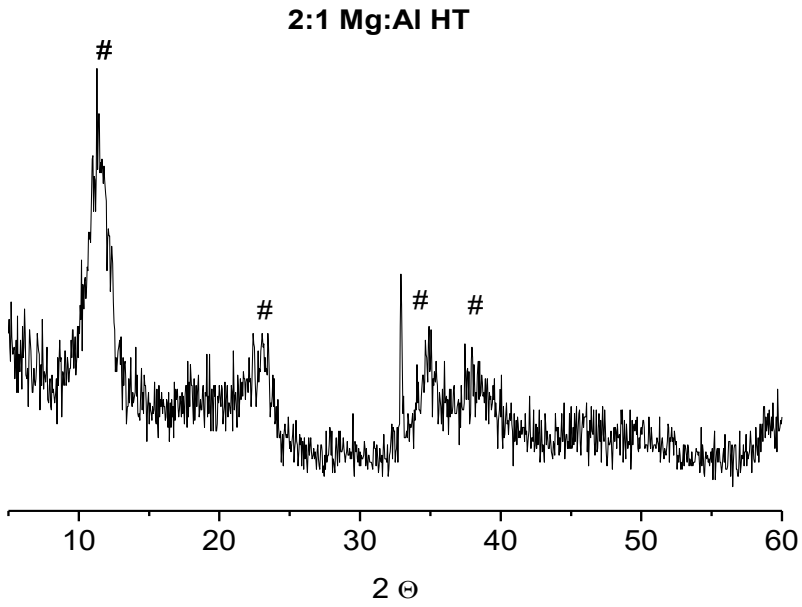


**Figure E.5** XRD diffractogram from a sample of the HT/CMR, which proves the HT was formed in the CMR.

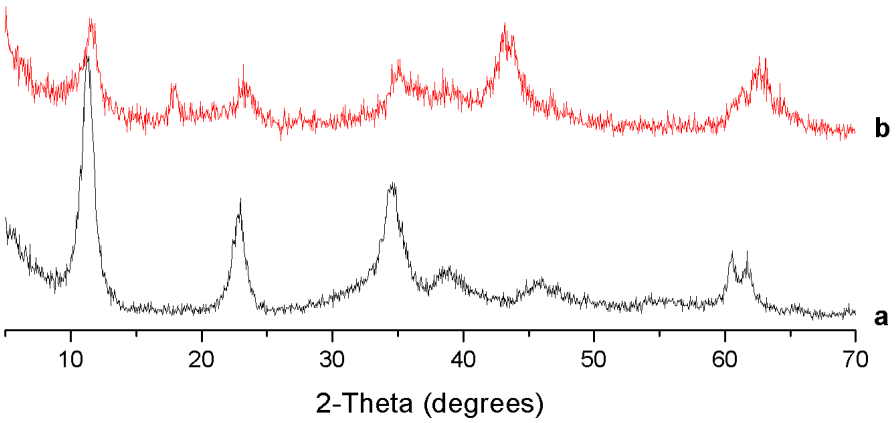


**Figure E.6** XRD diffractograms of the 1 wt% Pd/HT material a - before reaction (as prepared) and b - after reaction

## 7 Appendices

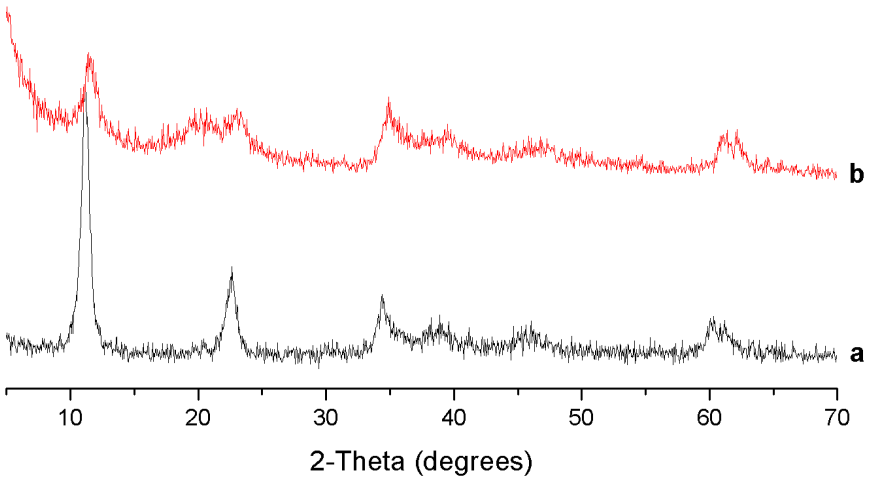


**Figure E.7** XRD diffractograms of the 1 wt% Pd/Mg-Al-Fe HT material a - before reaction (as prepared) and b - after reaction

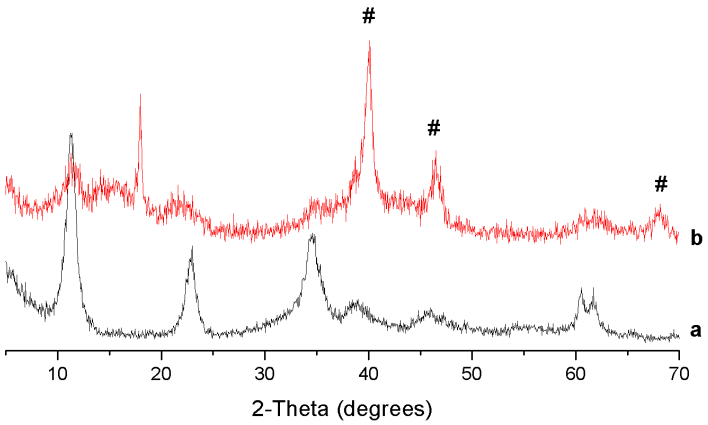


**Figure E.8** XRD diffractograms of the Mg-Al-Pd HT a – before reaction (as prepared) and b-after reaction; # - represents the peaks characteristics for Pd;

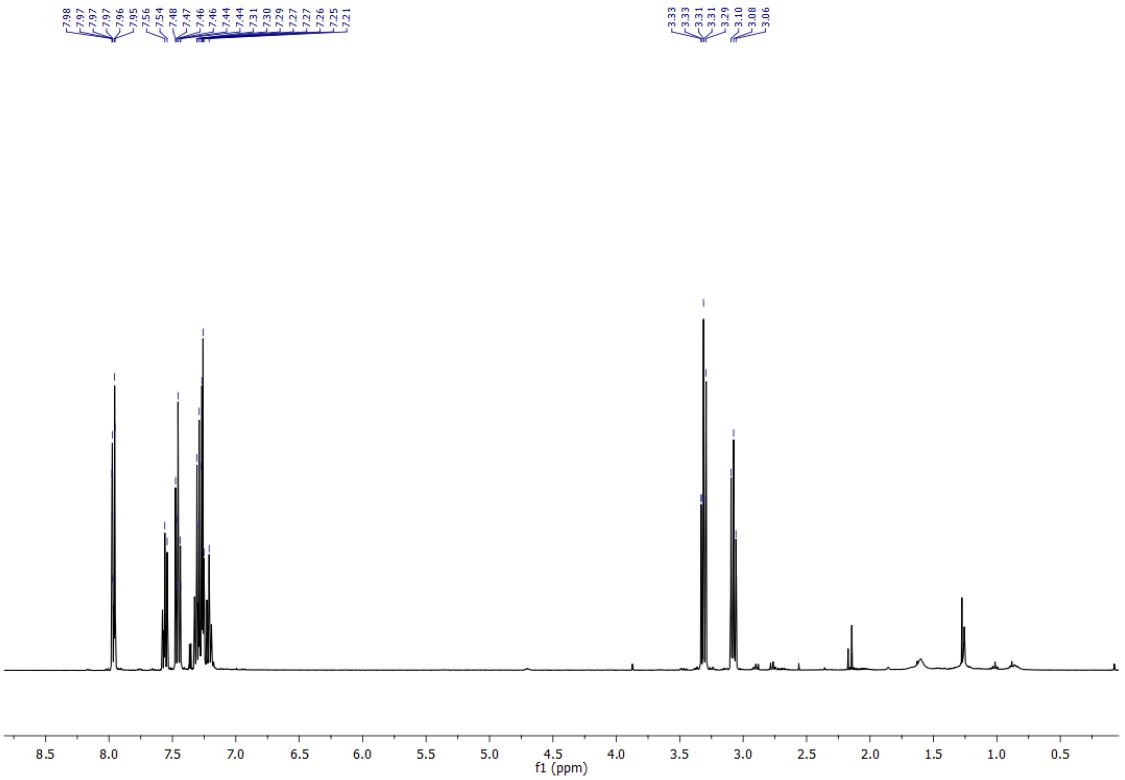


**Figure E.9** $^{1}$H-NMR spectrum of the hydrogenated product of chalcone.

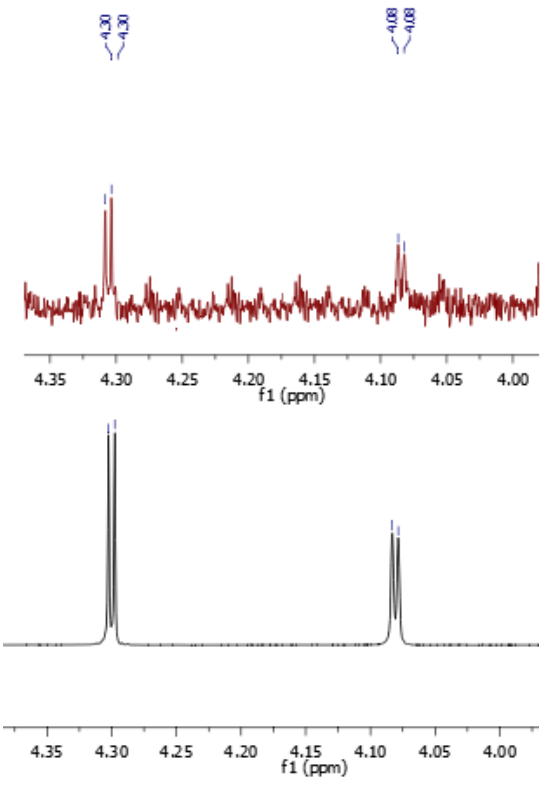


**Figure E.10.** $^{1}$H-NMR of the black – epoxy-chalcone from Aldrich and red- epoxy-chalcone obtained *in-situ*

# Appendix F - Supplementary Information Outlook

**Synthesis of Graphene Oxide:**

Graphene oxide (GO) was synthesized using a modified Hummers method [18]. Typically, 10 g of natural graphite and 5 g of $NaNO_3$ were added to 230 mL of $H_2SO_4$. The temperature of the mixture was kept at 5 °C and then 30 g of $KMnO_4$ was slowly added into the suspension. After 30 min, the temperature was increased to 35 °C and the mixture was kept for another 30 min after which 460 mL of Milli-Q water was added. Then, the temperature was increased to 90 °C and the reaction was maintained at this temperature for 1 h. The resulted suspension was then diluted with another 700 mL of $H_2O$ and treated with 30 mL of a 30 wt% $H_2O_2$ solution. The mixture was then cooled down to room temperature and repeatedly centrifuged and washed, first with a 5 wt% HCl solution and then with $H_2O$ until the pH reached ≈ 5. The resulted solid was dried at 40 °C. The GO dispersion in water (2.5 mg/mL) was prepared by submitting the suspension to mechanical stirring for 1 h and subsequent ultrasonic treatment for 1 h to further exfoliate the GO. Stable brown colloidal suspension of GO layers was obtained after this treatment.

**Synthesis of Mg-Al HT:**

Bare Mg-Al HT (Mg/Al =3) was synthesized by coprecipitation as described elsewhere [19]. Typically, 120 mmol of $Mg(NO_3)_2{\cdot}6H_2O$ and 40 mmol of $Al(NO_3)_3{\cdot}9H_2O$ were dissolved in 300 mL of distilled water and added dropwise into a glass vessel which initially contained 200 mL of deionized water. The pH was controlled by adding a 2 M NaOH + 0.5 M $Na_2CO_3$ aqueous solution and was kept at 10. Both solutions were mixed under vigorous stirring and the white suspension was stirred overnight at 90 °C. The precipitated solid was filtered and washed several times with water (≈ 3 L) until neutral pH and dried at 80 °C during 24 h.

**Synthesis of HT/rGO hybrids by direct coprecipitation:**

The corresponding amounts of salts ($Mg(NO_3)_2{\cdot}6H_2O$ and $Al(NO_3)_3{\cdot}9H_2O$) were added to 100 mL of GO dispersion in water (5 mg/mL) to obtain HT/rGO hybrid materials with a GO:HT mass ratio ranging from 1:1 to 1:20. Subsequently, a 2M NaOH + 0.5 M $Na_2CO_3$ aqueous solution was added to the mixture to fix the pH at 10 under continuous stirring. The resulting dark-brown suspension was hydrothermally treated at 90 °C and atmospheric pressure for 12h. The basic media followed by the hydrothermal treatment resulted in the GO reduction whilst forming the

HT and the solution turned from brown to black. The suspension was centrifuged and thoroughly washed with $H_2O$. The samples were dried by either freeze drying or in static air at 80 °C.

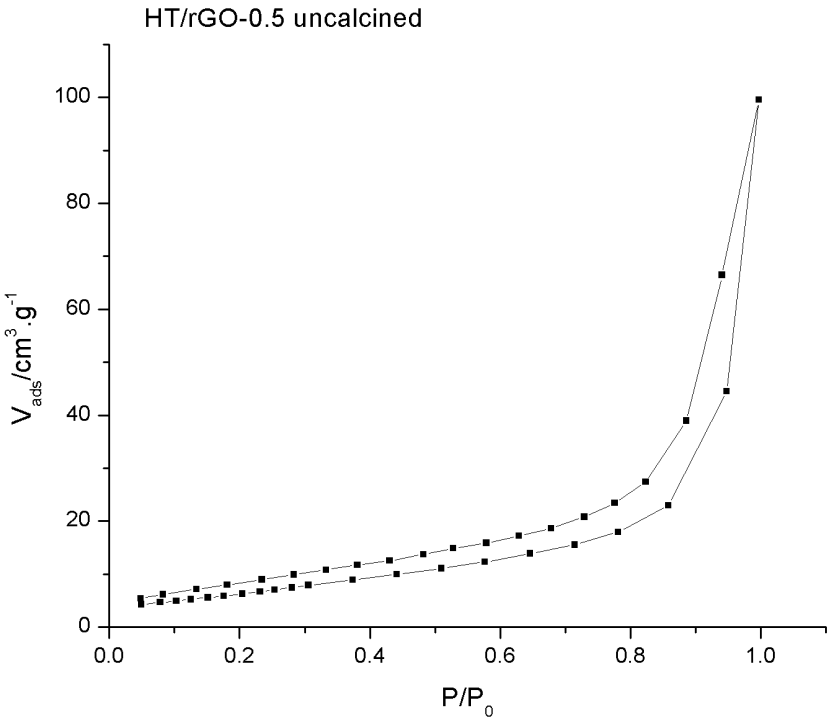


**Figure F.1** $N_2$ isotherm for the HT/rGO-0.5 hybrid

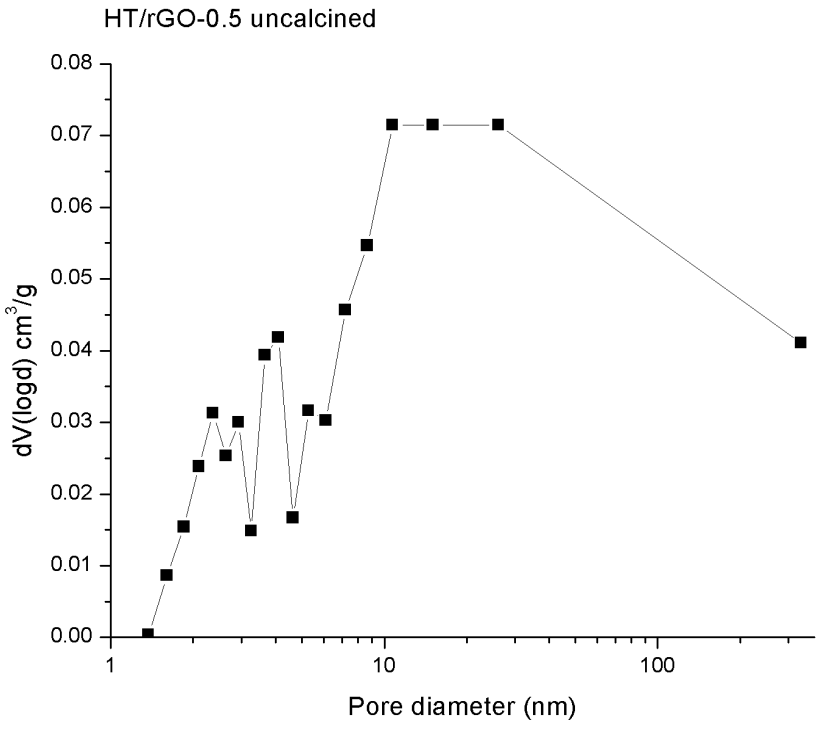

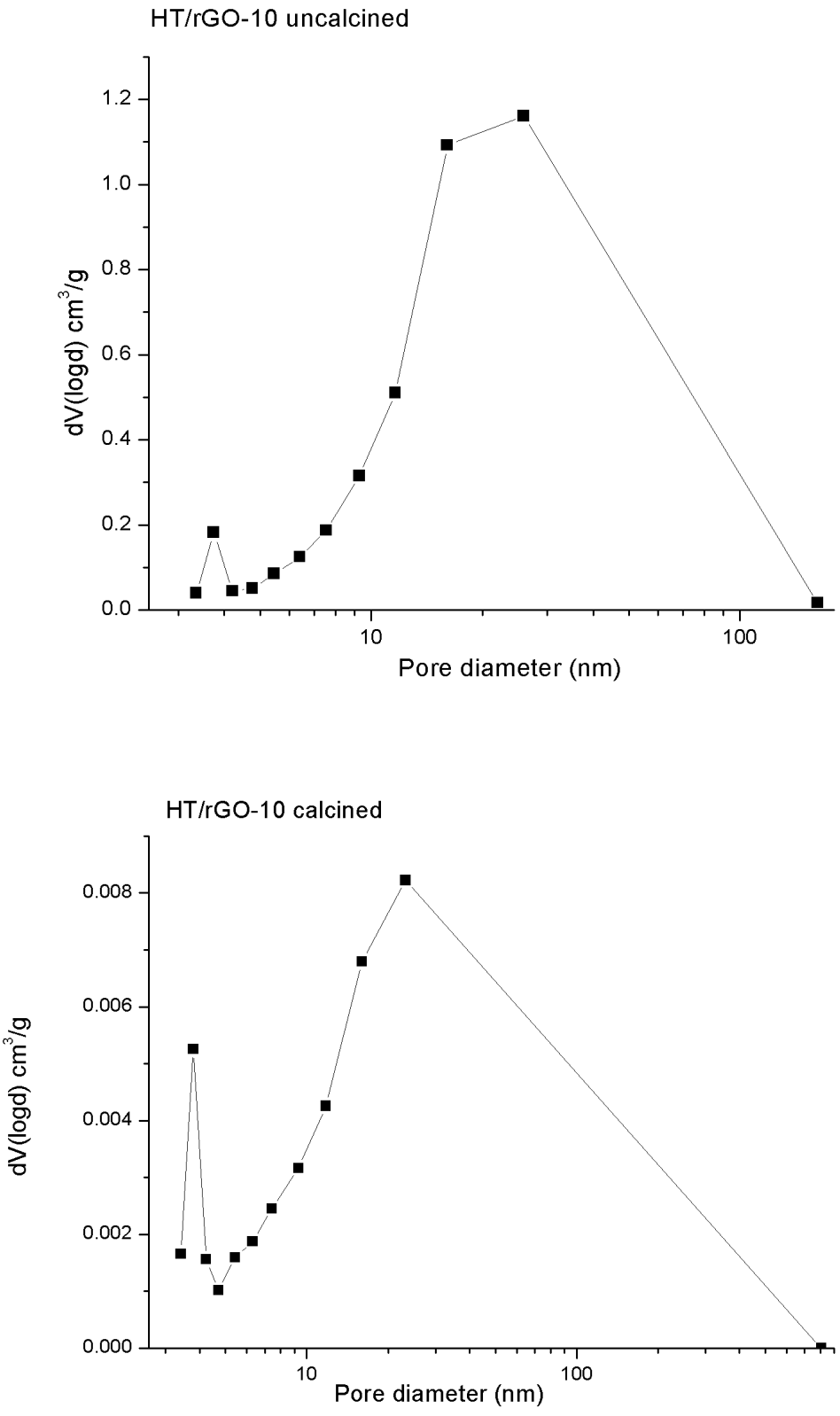


**Figure F.2** Pore diameter distribution for the HT/rGO-0.5 uncalcined and HT/rGO-10 calcined and uncalcined

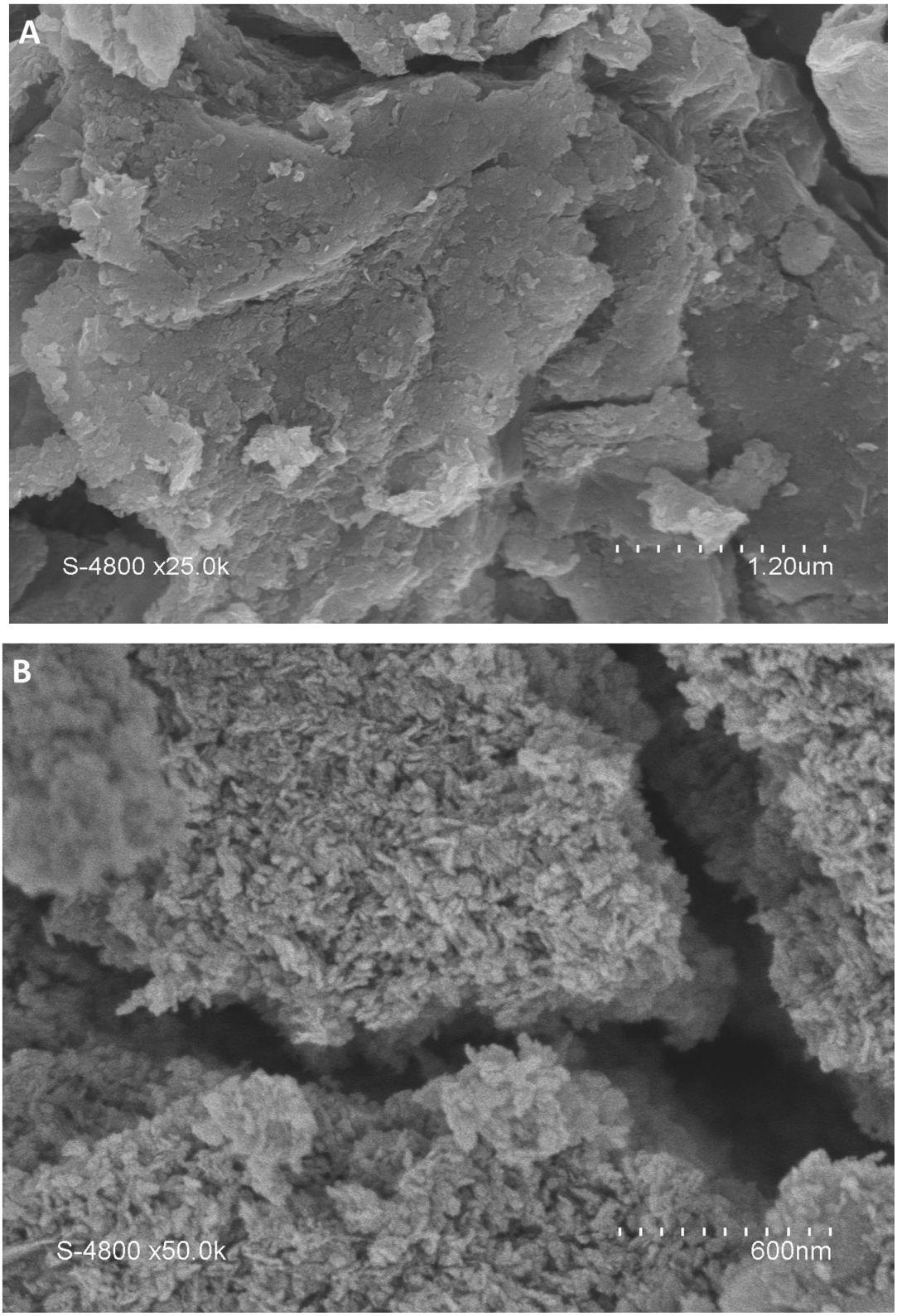


**Figure F.3** SEM images for A) HT/rGO-0.5 and B) HT/rGO-10

## 7 Appendices

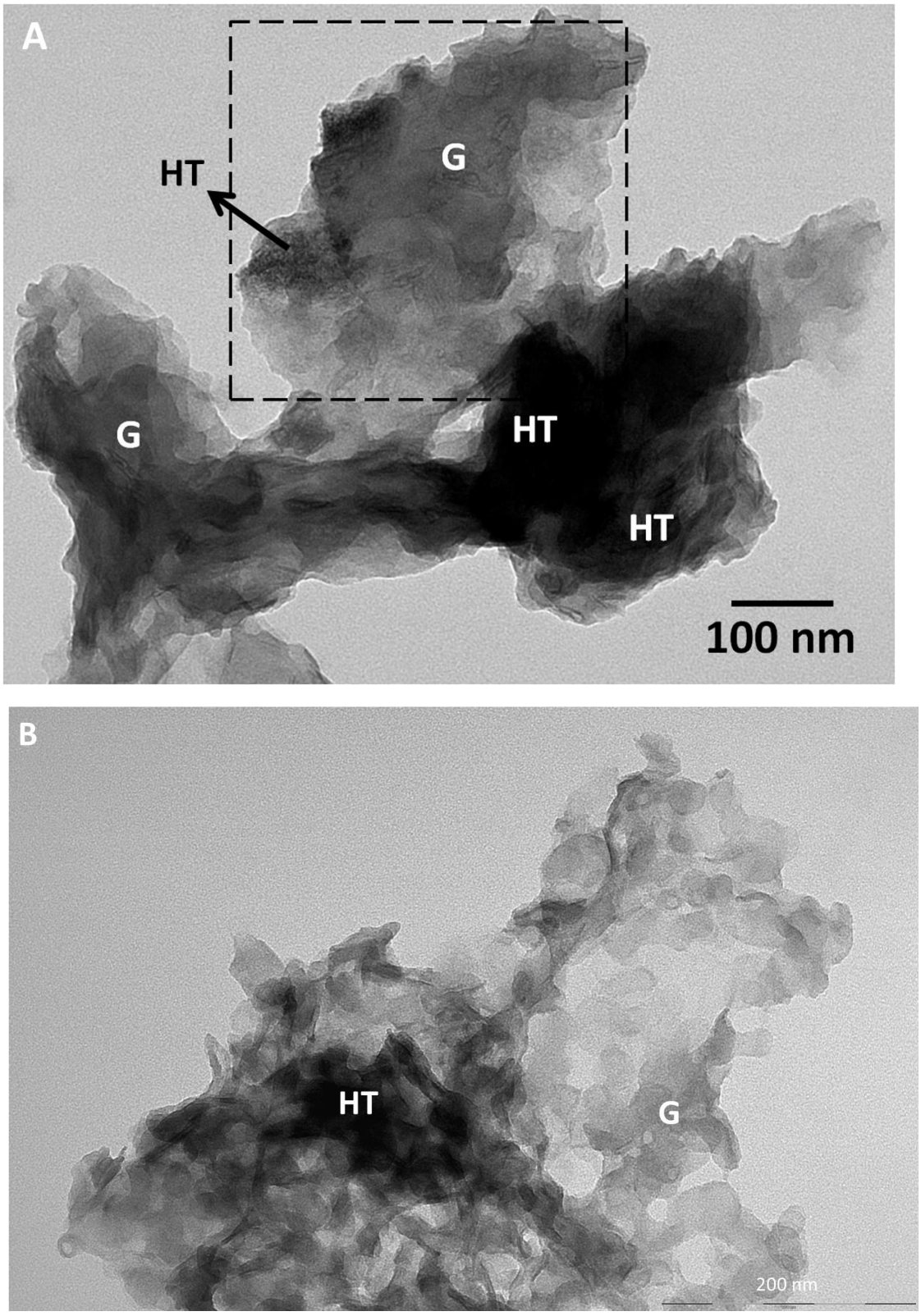


**Figure F.4** TEM images for A) HT/rGO-0.5 and B) HT/rGO-10

**Typical procedure for the Claisen-Schmidt condensation reaction:**

The Claisen-Schmidt condensation was performed in a 10 ml tube. The general procedure was as follows: acetophenone (0.19 mmol) and benzaldehyde (0.20 mmol) were added, along with the solvent – in some cases - over 55 mg of calcined hybrid. The mixture was stirred for 3 h at different temperatures: 40 °C and 60 °C. The catalyst was recovered by filtration and washed several times with the solvent. The solvent was removed by evaporation under reduced pressure. The products were identified by $^{1}$H-NMR.

**Table F.1** Physical constants of the solvents studied in the Claisen-Schmidt condensation reaction

| Solvent | Type | Dielectric constant | Dipole moment | pKa |
|---|---|---|---|---|
| **MeOH** | Polar protic | 33 | 1.7 | 15.5 |
| **ACN** | Polar aprotic | 37.5 | 3.92 | 25 |
| **Toluene** | Nonpolar | 2.38 | 0.63 | 41 |

**Analysis protocol for $CO_2$ chemisorption:**

The basicity measurements (volumetric $CO_2$ adsorption) were performed with a Micromeritics ASAP 2010 C apparatus in the range 0 – 100 mmHg at 300 K. Samples were calcined in situ at 723 K in vacuum for 5 h. After calcination and evacuation of the sample, $CO_2$ was dosed with small increments. The total number of accessible basic sites was determined by taking the amount of $CO_2$ chemisorbed at zero pressure ($cm^3$/g STP) obtained by extrapolation of the linear part of the uptake isotherm.

**Synthesis of Mg-Al-Pd HT/rGO hybrid by self-assembly:**

The Mg-Al-Pd HT was prepared by coprecipitation of the corresponding nitrate slats following the protocol reported by Morato *et al*. [20].

A known amount of the previously synthesized Mg-Al-Pd (Pd/Mg/Al =0.01/0.75/0.24) was dispersed in water (1 h mechanical stirring followed by 1 h of ultrasound treatment) and added to the GO dispersion (5 mg per mL of $H_2O$) so that hybrid materials with a GO:HT mass ratio of 1:20 were obtained. The suspension was submitted to ultrasounds for 60 min and then hydrothermally treated at 180 °C under autogenous pressure for 12 h. The hybrid materials were separated from the aqueous media and dried in static air at 80 °C.

## 7 Appendices

**Synthesis protocol for the Pd impregnated HT/rGO hybrid:**

Pd nanoparticles were prepared following the protocol published by Teranishi *et al.* [21]. The solution containing the nanoparticles was impregnated on the HT/rGO, then the material was dried and calcined in inert atmosphere.

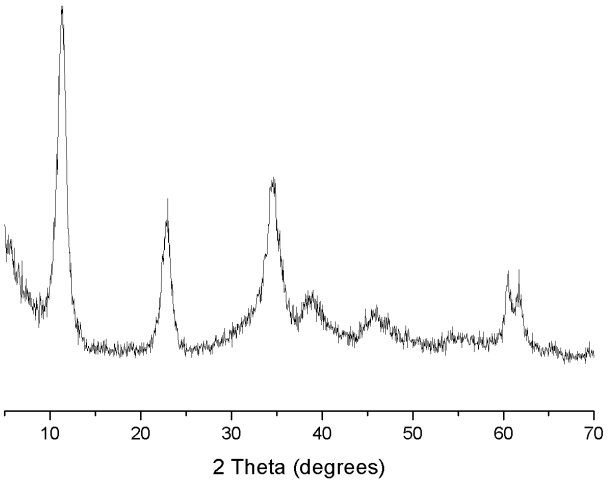


**Figure F.5** The XRD pattern of the Mg-Al-Pd HT

# Bibliography

[1] B.J.M. Rajkumar, V. Ramakrishnan, *Journal of Raman Spectroscopy*, **31**, 1107–1112, **2000**.

[2] P.F.F. Filho, P.T.C. Freire, K.C.V. Lima, J.M. Filho, F.E.A. Melo, *Condensed Matter Materials Science*, **2007**.

[3] J.T. Kloprogge, R.L. Frost, *Journal of Solid State Chemistry*, **146**, 506-515, **1999**.

[4] R.J. Chimentão, S. Abelló, F. Medina, J. Llorca, J.E. Sueiras, Y. Cesteros, P. Salagre, *Journal of Catalysis*, **252**, 249–257, **2007**.

[5] S. Miyata, *Clays and Clay Minerals*, **31**, 305-311, **1983**.

[6] J. Pérez-Ramirez, G. Mul, J.A. Moulijn, *Vibrational Spectroscopy*, **27**, 75-88, **2001**.

[7] T. Kanemitsu, A. Umehara, M. Miyazaki, K. Nagata, T. Itoh, *European Journal of Organic Chemistry*, 993–997, **2011**.

[8] P. Zhou, S. Luo, J.-P. Cheng, *Organic & Biomolecular Chemistry*, **9**, 1784–1790, **2011**.

[9] U. Farid, F. Malmedy, R. Claveau, L. Albers, T. Wirth, *Angewandte Chemie International Edition*, **52**, 7018-7022, **2013**.

[10] H.E. Zimmerman, A. Pushechnikov, *European Journal of Organic Chemistry*, 3491-3497, **2006**.

[11] T. Punirun, D. Soorukram, C. Kuhakarn, V. Reutrakul, M. Pohmakotr, *European Journal of Organic Chemistry*, 4162-4169, **2014**.

[12] Y. Wang, J. Ye, X. Liang, *Advanced Synthesis & Catalysis*, **349**, 1033-1036, **2007**.

[13] A. Makó, Z. Rapi, G. Keglevich, Á. Szöllosy, L. Drahos, L. Hegedus, P. Bakó, *Tetrahedron: Asymmetry*, **21**, 919- 925, **2010**.

[14] B.M. Choudary, M.L. Kantam, K.V.S. Ranganath, K. Mahendar, B. Sreedhar, *Journal of American Chemical Society*, **126**, 3396-3397, **2004**.

[15] T. Huang, L. Lin, X. Hu, J. Zheng, X. Liu, X. Feng, *Chemical Communications*, **51**, 11374--11377, **2015**.

[16] W. Luo, Z. Yu, W. Qiu, F. Yang, X. Liu, J. Tang, *Tetrahedron*, **67**, 5289-5292, **2011**.

[17] T. Bakó, P. Bakó, G. Keglevich, P. Bombicz, M. Kubinyi, K. Pál, S. Bodor, A. Makó, L. Töke, *Tetrahedron: Asymmetry*, **15**, 1589-1595, **2004**.

[18] W.S.H. Jr., R.E. Offeman, *Journal of American Chemical Society*, **1958**, 1339-1339, **1958**.

[19] M.G. Álvarez, R.J. Chimentão, F. Figueras, F. Medina, *Applied Clay Science*, **58**, 16-24, **2012**.

[20] A. Morato, C. Alonso, F. Medina, Y. Cesteros, P. Salagre, J.E. Sueiras, D. Tichit, B. Coq, *Applied Catalysis B: Environmental*, **1**, 167–179, **2001**.

[21] T. Teranishi, M. Miyake, *Chemistry of Materials*, **10**, **1998**.

# 7 Appendices

# SHORTHAND AND GLOSSARY

***Δf***: the frequency shift monitored by QCM-D

***ΔD***: the energy dissipation factor

***Δm***: the adsorbed mass per unit area

***C***: the mass sensitivity constant for the QCM-D crystal

***n***: the overtone number

$E_{diss}$: the dissipated energy

$E_{stor}$: the stored energy

***η***: viscosity

***ρ***: density

***δ***: chemical shift

$t_R$: retention time

$t_q$: the thickness of the quartz crystal

***ω, q, s1* and *s2***: parameters of the QCM-D crystal

**Δt**: a specific interval of time

$\Delta N_{H2O2}$: moles of $H_2O_2$

$m_{catalyst}$: mass of the catalyst

$P_{H2O2}$: the average specific production rate of hydrogen peroxide

**Å**: Angstrom

**% ee**: enantioselectivity

**AA:** amino acid

**AAs:** amino acids

**ACN**: acetonitrile

**BET:** Brunauer-Emmett-Teller theory employed for the measurement of the specific surface are of a material ($m^2/g$)

**CMR:** catalytic membrane reactor

**DAD:** diode array detector

**DMSO:** dimethyl sulfoxide

**DTA:** differential thermal analysis

**E1cB mechanism**: elimination unimolecular conjugate base mechanism

**EA:** elemental analysis

**EDG:** electron donating group

**EPA:** Environmental Protection Agency

**EtOH:** ethanol

**EWG:** electron withdrawing group

**FTIR:** Fourier transform infrared spectroscopy

**GO:** graphene oxide

**HRTEM:** high-resolution transmission electron microscopy

**HT:** hydrotalcite

**HTs:** hydrotalcites

**$HT_{cc}$:** calcined hydrotalcite

**$HT_{Cl}$:** hydrotalcite containing $Cl^-$

**$HT_{Clus}$:** hydrotalcite containing $Cl^-$ synthesized using ultrasounds

**$HT_{NO3}$:** hydrotalcite containing $NO_3^-$

**$HT_r$:** rehydrated hydrotalcite

**$HT_{rus}$:** rehydrated hydrotalcite under ultrasounds

**HPLC:** high pressure liquid chromatography

**ICP:** inductively coupled plasma analysis

**IPL:** immobilized poly-L-leucine

**LDH:** layered double hydroxide

**LDHs:** layered double hydroxides

**LL:** L-leucine

**LL/$HT_x$-Ay**: L-leucine immobilized into HT, where x represents the type of HT and y the anionic exchange method used

**LL/$HT_x$-Ry**: L-leucine immobilized into HT, where x represents the type of HT and y the reconstruction method used

**L-Leu:** L-leucine

**MALDI-TOF**: matrix-assisted laser desorption/ionization time-of-flight

**MAS-NMR:** magic angle spinning-nuclear magnetic resonance

**MeOH:** methanol

**MFC:** mass flow controller, device used to deliver an adjustable and precise gas flow rate as feed of a reactor component

**Milli-Q $H_2O$:** trademark created by Millipore Corporation to describe “ultrapure” water in terms of resistivity (typically 18.2 MΩ.cm at 25 °C)

**MS:** mass spectrometry or spectrometer

**NMR:** nuclear magnetic resonance

**Pd-CMR**: catalytic membrane reactor containing Pd

**PLL:** poly-L-leucine

**PXRD**: X-ray powder diffraction

**QCM-D:** quartz crystal microbalance with dissipation

**RAMAN:** Raman spectroscopy

**rGO:** reduced graphene oxide

**RID:** refractive index detector

**TBAB:** tetra-n-buthylammonium bromide

**THF:** tetrahydrofuran

**TGA:** thermal analysis

**TMS:** tetramethylsilane

**XRD:** X-ray diffraction

**μXRD:** micro X-ray diffraction analysis

## SHORTHAND AND GLOSSARY

# LIST OF PUBLICATIONS AND CONFERENCES

## PUBLICATIONS

"Highly selective multifunctional nanohybrid catalysts for the one-pot synthesis of α,β-epoxy-chalcones"

Dana-Georgiana Crivoi, Anna Segarra, Francesc Medina, *Journal of Catalysis*, **2016**, 334, 120-128.

"*In-situ* study of substrate – catalyst interactions in a Juliá–Colonna epoxidation using quartz crystal microbalance with dissipation"

Deborah Wakeham, Dana-Georgiana Crivoi, Francesc Medina, Anna Segarra, Mark W. Rutland, *Journal of Colloid and Interface Science,* **2016**, 263-268.

"New tuneable catalytic membrane reactor for various reactions in aqueous media"

Veronica Pinos, Dana-Georgiana Crivoi, Francesc Medina, Jesus E. Sueirs, Anton Dafinov, *ChemistrySelect*, **2016**, 1, 124-126.

"Bio-nanohybrid catalysts based on L-leucine immobilized in hydrotalcite and their activity in aldol reaction"

Dana-Georgiana Crivoi, Ronald-Alexander Miranda, Elisabetta Finocchio, Jordi Llorca, Gianguido Ramis, Jesús E. Sueiras, Anna Segarra, Francisco Medina, *Applied Catalysis A: General*, **2016**, 519, 116-129.

# CONFERENCES

SECAT'2015 – Catálisis, confluencia interdisciplinary: modelos, catalizadores y reactores, Barcelona (Spain) – July 2015

Oral presentation contribution: "Chalcone Epoxidation Using *In-situ* Generated Hydrogen Peroxide from $H_2$ and $O_2$ Under Very Mild Conditions"

Dana-Georgiana Crivoi, Veronica Pinos, Francesc Medina, Anton Dafinov

Japan-Spain Joint Symposium on Heterogeneous Catalysis, Tarragona (Spain) – June 2015

Poster contribution: "Multifunctional Bio-inspired Catalysis for the One-pot Synthesis of Epoxy-chalcones"

Dana-Georgiana Crivoi, Anna Segarra, Francesc Medina

2nd International Conference on Bioinspired and Biobased Chemistry & Materials, Nice (France) – October 2014

Oral presentation contribution: "Mechanistic Study of the Juliá-Colonna Epoxidation Reaction Catalysed by Oligo-L-Leucine using Quartz Crystal Microbalance with Dissipation"

Deborah Wakeham, Dana-Georgiana Crivoi, Francesc Medina, Anna Segarra, Mark W. Rutland

11th European Congress on Catalysis, Lyon (France) – September 2013

Oral presentation and poster contribution: "Multifunctional Bio-inspired Catalysis for the One-pot Synthesis of Epoxy-chalcones"

Dana-Georgiana Crivoi, Anna Segarra, Francesc Medina

10th Congress on Catalysis Applied to Fine Chemicals, Turku (Finland) – June 2013

Poster contribution: "Multifunctional Bio-inspired Catalysis for the One-pot Synthesis of Epoxy-chalcones"

Dana-Georgiana Crivoi, Anna Segarra, Francesc Medina

COST - European Cooperation in Science and Technology, Amsterdam (Holland) – April 2013

Poster contribution: "Multifunctional Bio-inspired Nanohybrid Catalysts: One-pot Claisen-Schmidt Condensation/Julià-Colonna Epoxidation Reaction"

Dana-Georgiana Crivoi, Anna Segarra, Francesc Medina

1st International Conference on Bioinspired and Biobased Chemistry & Materials, Nice (France) – October 2012

Poster contribution: "One-pot Synthesis of Epoxy-chalcone Catalysed by Poly-L-leucine Immobilized into Hydrotalcite"

Dana-Georgiana Crivoi, Anna Segarra, Francesc Medina

## List of Publications and Conferences

# CURRICULUM VITAE

Tarragona (Spain), 2016

Name: DANA-GEORGIANA CRIVOI

Date of Birth: 09/10/1985

Place of Birth: RÂMNICU-VÂLCEA, ROMANIA

Nationality: ROMANIAN

## Education

**October 2011 – Present:** **PhD Chemical Engineering**

Departament d´Enginyeria Química, Escola Tècnica Superior d´Enginyeria Química, Campus Sescelades, Universitat Rovira i Virgili, Av. Països Catalans 26, 43007 Tarragona, Spain

▪ *Enantioselective synthesis, heterogeneous catalysis, hybrid materials*

Scholarships:

- "Rovira i Virgili" University Scholarship
- FPU - Spanish Ministry of Education, Culture and Sports

**October 2009 – June 2011:** **Master Degree**

"Politehnica" University of Bucharest – Faculty of Applied Chemistry and Material Science, "Polizu" Campus, 1-7, Polizu Street, Sector 1, Bucharest, 011061, Romania

▪ *Pharmaceutical Products and Cosmetics – Toxicology, Drugs, Enzymes, Pharmaceutical Technology, Natural Ingredients*

Final evaluation: 95/100 Valedictorian

**October 2004 - June 2009:** **Engineering Degree**

"Politehnica" University of Bucharest – Faculty of Engineering in Foreign Languages – English Stream, 313, Splaiul Independentei, Bucharest, 060042, Romania

▪ *Chemical Engineering –Organic Chemistry, Inorganic Chemistry, Drugs, Analytical Chemistry, Chemical Engineering, Biochemistry, Organic Chemistry Technology*

Final evaluation: 100/100 Valedictorian

# Work Experience

**March 2013 – January 2016:** **Teaching Assistant**

Departament d´Enginyeria Química, Escola Tècnica Superior d´Enginyeria Química, Campus Sescelades, Universitat Rovira i Virgili, Av. Països Catalans 26, 43007 Tarragona, Spain

- *Unit Operation Laboratory (Laboratori integrat d'operaciones unitaries)*
- *Chemical Products and Processes (Procesos y Productos Quimicos)*

**November 2010 - August 2011:** **Trainer**

Avantaj Consulting SRL, 8-12, Serg. Nutu Ion Street, Sector 5, Bucharest - Romania

- *Web Design – HTML, CSS and FLASH*

**March 2008 - August 2011:** **Research Assistant**

Research Centre of Organic Chemistry "Costin D. Nenitescu" of Romanian Academy 202B, Splaiul Independentei, Sector 6, 711441 Bucharest - Romania

- *Organic synthesis and NMR analysis*

# Seminars and Courses

- 2016, Tarragona (Spain) – English Grammar and Punctuation, Online Course, COURSERA
- 2014, Tarragona (Spain) - Sistemas de conducción de fluidos seguros y eficientes Swagelok Iberica
- 2013, Tarragona (Spain) - Curso de formacion Micromimetrics AUTOCHEM II 2920
- 2013, Jarandilla de la Vera (Spain) - Caracterización químico física de la superficie de los solidos
- 2013, Tarragona (Spain) - Curso de formacion UV-Visible JASCO V-630
- 2012, Tarragona (Spain) - Writing in the Sciences, Online Course, COURSERA
- 2012, Tarragona (Spain) - Learn to Program: The Fundamentals, Online Course, COURSERA
- 2012, Tarragona (Spain) - Curso de aptitude preventive, "Rovira i Virgili" University
- 2006-2009, Bucharest (Romania) - Psychological and Pedagogical Courses at "Politehnica" University of Bucharest
- 2006, Bucharest (Romania) - Leadership and communication, CODECS SA

## Research Stage

- March 2013 - Under the supervision of Prof. Dr. Mark Rutland, Surface and Corrosion Science, Department of Chemistry, KTH Royal Institute of Technology, Stockholm, Sweden

## Research Projects

- 2014-2016. 2014SGR1640: Grupo consolidado MEtA - Enginyeria dels materials i les seves aplicacions (Materials engineering and their applications). AGAUR (Generalitat de Catalunya). IP: F. Medina.
- 2014-2015 - EUIN2013-50984: AD-CO2CHEM - Acción Europa investigación: Convirtiendo $CO_2$ en productos químicos (Converting $CO_2$ in chemical products). Ministerio de Economía y Competitividad (Gobierno de España). IP: A.M. Segarra.
- 2005-2009. WP2 "Selection of objective green molecules and Solvsafe green alternatives for coatings" Programme (FP6/2005-2009). European Union Sixth Framework.

## Publications

"Highly selective multifunctional nanohybrid catalysts for the one-pot synthesis of α,β-epoxy-chalcones" Dana-Georgiana Crivoi, Anna Segarra, Francesc Medina, *Journal of Catalysis*, **2016**, 334, 120-128.

"*In-situ* study of substrate – catalyst interactions in a Juliá–Colonna epoxidation using quartz crystal microbalance with dissipation" Deborah Wakeham, Dana-Georgiana Crivoi, Francesc Medina, Anna Segarra, Mark W. Rutland, *Journal of Colloid and Interface Science,* **2016**, 263-268.

"New tuneable catalytic membrane reactor for various reactions in aqueous media" Veronica Pinos, Dana-Georgiana Crivoi, Francesc Medina, Jesus E. Sueirs, Anton Dafinov, *ChemistrySelect*, **2016**, 1, 124-126.

"Bio-nanohybrid catalysts based on L-leucine immobilized in hydrotalcite and their activity in aldol reaction" Dana-Georgiana Crivoi, Ronald-Alexander Miranda, Elisabetta Finocchio, Jordi Llorca, Gianguido Ramis, Jesús E. Sueiras, Anna Segarra, Francisco Medina, *Applied Catalysis A: General*, **2016**, 519, 116-129.

# Conferences

SECAT'2015 – Catálisis, confluencia interdisciplinary: modelos, catalizadores y reactores, Barcelona (Spain) – July 2015

Oral presentation contribution: "Chalcone Epoxidation Using *In-situ* Generated Hydrogen Peroxide from $H_2$ and $O_2$ Under Very Mild Conditions"

Dana-Georgiana Crivoi, Veronica Pinos, Francesc Medina, Anton Dafinov

Japan-Spain Joint Symposium on Heterogeneous Catalysis, Tarragona (Spain) – June 2015

Poster contribution: "Multifunctional Bio-inspired Catalysis for the One-pot Synthesis of Epoxy-chalcones"

Dana-Georgiana Crivoi, Anna Segarra, Francesc Medina

2nd International Conference on Bioinspired and Biobased Chemistry & Materials, Nice (France) – October 2014

Oral presentation contribution: "Mechanistic Study of the Juliá-Colonna Epoxidation Reaction Catalysed by Oligo-L-Leucine using Quartz Crystal Microbalance with Dissipation"

Deborah Wakeham, Dana-Georgiana Crivoi, Francesc Medina, Anna Segarra, Mark W. Rutland

11th European Congress on Catalysis, Lyon (France) – September 2013

Oral presentation and poster contribution: "Multifunctional Bio-inspired Catalysis for the One-pot Synthesis of Epoxy-chalcones"

Dana-Georgiana Crivoi, Anna Segarra, Francesc Medina

10th Congress on Catalysis Applied to Fine Chemicals, Turku (Finland) – June 2013

Poster contribution: "Multifunctional Bio-inspired Catalysis for the One-pot Synthesis of Epoxy-chalcones"

Dana-Georgiana Crivoi, Anna Segarra, Francesc Medina

COST - European Cooperation in Science and Technology, Amsterdam (Holland) – April 2013

Poster contribution: "Multifunctional Bio-inspired Nanohybrid Catalysts: One-pot Claisen-Schmidt Condensation/Julià-Colonna Epoxidation Reaction"

Dana-Georgiana Crivoi, Anna Segarra, Francesc Medina

1st International Conference on Bioinspired and Biobased Chemistry & Materials, Nice (France) – October 2012

Poster contribution: "One-pot Synthesis of Epoxy-chalcone Catalysed by Poly-L-leucine Immobilized into Hydrotalcite"

Dana-Georgiana Crivoi, Anna Segarra, Francesc Medina

10. Frühjahrssymposium: 10th Young Scientists Conference on Chemistry, Rostock (Germany) – March 2008

Oral presentation contribution: "Nanostructured Microemulsion System for Trace Analysis of the Heavy Metals – Mercury Ion-"

Dana-Georgiana Crivoi, Alina Murariu, Maria Mihaly

## Honours and Awards

- Valedictorian award – Engineering Degree, "Politehnica" University of Bucharest – Faculty of Engineering in Foreign Language – English Stream, 2009
- Mention at the Organic Chemistry Section - The National Students Conference at "Politehnica" University of Bucharest, Bucharest, Romania, 2009
- Mention - The International Conference "Students for students", Cluj, Romania, 2008
- Second prize at the Mathematics-Physics Section - The National Students Conference "Student, Science, Society", Petrosani, Romania, 2007
- Special prize at the Inorganic Chemistry Section - The National Students Conference at "Politehnica" University of Bucharest, Bucharest, Romania, 2007
- Special prize - The International Conference "Students for students", Cluj, Romania, 2007
- Mention at the Inorganic Chemistry Section - The National Students Conference at "Politehnica" University of Bucharest, Bucharest, Romania, 2006
- First Prize at the Mathematic Section - The National Students Conference at "Politehnica" University of Bucharest, Bucharest, Romania, 2005
- Mention at the Inorganic Chemistry Section - The National Students Conference at "Politehnica" University of Bucharest, Bucharest, Romania, 2005

UNIVERSITAT ROVIRA I VIRGILI
HYBRID MATERIALS: DISCOVERING PROPERTIES AND MECHANISMS
Dana Georgiana Crivoi

UNIVERSITAT ROVIRA I VIRGILI
HYBRID MATERIALS: DISCOVERING PROPERTIES AND MECHANISMS
Dana Georgiana Crivoi